Investigation of a solvent-free continuous process to produce pharmaceutical co-crystals

Understanding and developing solvent-free continuous cocrystallisation (SFCC) through study of co-crystal formation under the application of heat, model shear and twin screw extrusion, including development of a near infrared spectroscopy partial least squares quantification method

Clive John WOOD

Submitted for the degree of Doctor of Philosophy

School of Life Sciences

University of Bradford

2016

I Abstract

Keywords: hot melt extrusion, co-crystal, NIR, model shear, twin screw extrusion, quantification, partial least squares, solvent-free, continuous cocrystallisation.

This project utilised a novel solvent-free continuous cocrystallisation (SFCC) method to manufacture pharmaceutical co-crystals. The objectives were to optimize the process towards achieving high co-crystal yields and to understand the behaviour of co-crystals under different conditions. Particular attention was paid to the development of near infrared (NIR) spectroscopy as a process analytical technology (PAT).

Twin screw, hot melt extrusion was the base technique of the SFCC process. Changing parameters such as temperature, screw speed and screw geometry was important for improving the co-crystal yield. The level of mixing and shear was directly influenced by the screw geometry, whilst the screw speed was an important parameter for controlling the residence time of the material during hot melt extrusion. Ibuprofen – nicotinamide 1:1 co-crystals and carbamazepine – nicotinamide 1:1 co-crystals were successfully manufactured using the SFCC method.

Characterisation techniques were important for this project, and NIR spectroscopy proved to be a convenient, accurate analytical technique for identifying the formation of co-crystals along the extruder barrel. Separate thermal and model shear deformation studies were also carried out to determine the effect of temperature and shear on co-crystal formation for several different pharmaceutical co-crystal pairs.

Finally, NIR spectroscopy was used to create two partial least squares regression models, for predicting the 1:1 co-crystal yield of ibuprofen – nicotinamide and carbamazepine – nicotinamide, when in a powder mixture with the respective pure API. It is believed that the prediction models created in this project can be used to facilitate future in-line PAT studies of pharmaceutical co-crystals during different manufacturing processes.

II Acknowledgements

The past 4 years have been tremendously exciting and I am honoured to have been part of a wonderful research team at the University of Bradford. This multidisciplinary project was part of a collaboration between the Institute of Pharmaceutical Innovation (IPI) and the Interdisciplinary Research Centre (IRC) and was funded by the Engineering and Physical Sciences Research Council (EPSRC). This project would not have been possible without my supervisors Dr Adrian Kelly, Professor Anant Paradkar and Dr Tim Gough. I am very grateful they provided me with this opportunity.

Dr Adrian Kelly has consistently supported me throughout my studies and has guided me through this project. His expertise in hot melt extrusion and other technologies was crucial for the success of this project. Adrian was also an important mentor for helping me to develop the manuscript for the publication from this study and he provided support and feedback whenever it was required.

Dr Anant Paradkar has been an inspirational teacher who has guided me and has always made me realise my potential. Anant has provided me with the ability to see beyond the confines of my project and to comprehend the real world value of the research conducted under his guidance. His determined pursuit for advancement in pharmaceutical engineering research provided a strong background for this project.

Dr Tim Gough taught me skills that were vital for this project and was always there to show me new equipment in the labs and to provide training on many different instruments. Tim regularly provided critical analysis of my work in

order to find opportunities for improvements to be made. The two excursions to Diamond Light Source, UK, and the European Synchrotron Radiation Facility, France, with Adrian and Tim during my 4 years was a particular highlight for me during my time at the university.

Sheelagh Halsey and Rod Bottom from ThermoScientific UK provided help and insight with the NIR studies; their expertise was invaluable. Dr Chaitrali Kulkarni, who was a postdoctoral researcher at the University, helped me with my project, including the many practical experiments which we performed together, and was a great mentor. Fellow student Abdolati Alwati helped me enormously during my PhD and was always great fun to be around.

I would like to thank Sophie who has been more than understanding and has always believed in me. Her love has guided me and she has spurred me on every step of the way. Starting our very own family during my studies came with immense joy but also presented many difficulties. Sophie has become the most incredible mother to our amazing son and I cannot imagine my life without them.

My parents have supported me throughout my life and they have always encouraged me to stay true to myself and to be happy. I am truly grateful for their guidance, honesty, and the sacrifices they have made on my behalf. Finally, my family and friends have always been there to support me and I am very grateful for their continued love and support.

III Abbreviations

SFCC	Solvent-free continuous cocrystallisation
API	Active pharmaceutical ingredient
CBZ	Carbamazepine
NIC	Nicotinamide
IBU	Ibuprofen
PM	Physical mixture
CC	Co-crystal
FDA	Food and drug administration
CDER	Centre for drug evaluation and research
NCE	New chemical entity
HME	Hot melt extrusion
EPSRC	Engineering and physical sciences research council
SEM	Scanning electron microscopy
DSC	Differential scanning calorimetry
NIR	Near infrared spectroscopy
PXRD	Powder X-ray diffraction
APS	Academy of pharmaceutical sciences
BACG	British association for crystal growth

SNV	Standard normal variate
SGS	Savitzky-Golay smoothing
NS	Norris smoothing
PLS	Partial least squares
IQPC	The international quality and productivity centre
PAT	Process analytical technology/tool
QbD	Quality by design
R&D	Research and development
HPLC	High performance liquid chromatography
USPC	The United States pharmacopeial convention
RMSEC	Root mean square error of calibration
RMSEP	Root mean square error of prediction
RMSECV	Root mean square error of cross validation
R^2	Correlation coefficient

IV Figure index

V Table index

VI List of publications

Wood, C., A. Alwati, S. Halsey, T. Gough, E. Brown, A. Kelly and A. Paradkar (2016). “Near infra red spectroscopy as a multivariate process analytical tool for predicting pharmaceutical co-crystal concentration.” Journal of Pharmaceutical and Biomedical Analysis **129**: 172-181. DOI: 10.1016/j.jpba.2016.06.010.

Kulkarni, C., C. Wood, A. Kelly, T. Gough, N. Blagden and A. Paradkar (2015). “Stoichiometric Control of Co-Crystal Formation by Solvent Free Continuous Co-Crystallisation (SFCC).” Crystal Growth & Design **15**(12): 5648-5651. DOI: 10.1021/acs.cgd.5b00806.

Table of contents

CHAPTER 1 INTRODUCTION

The invention of high-throughput screening of therapeutically active ingredients has led to an increase in the number of poorly soluble APIs by approximately 25-40% since it has been introduced (Maniruzzaman et al. 2013). Additionally, 70% of new chemical entities (NCE's), that are yet to reach the market, are poorly soluble (Sanphui et al. 2012). The solubility of an API is critical for achieving acceptable, controlled bioavailability when a drug is administered to a patient. However, it is not commonplace to find an API with relatively good aqueous solubility, so instead, a large proportion of pharmaceutical research is now focused on modifying existing APIs to improve their solubility and other important physico-chemical properties such as stability, dissolution rate, bioavailability and compressibility.

The crystal structure, morphology, and particle size are all important factors that can have a large influence on an APIs performance. Different crystal forms of an API generally affect the physico-chemical properties and stability, whereas the crystal morphology and particle size are more likely to affect the dosage form used and the manufacturing stage (Stieger and Liebenberg 2012). Entropy, enthalpy, non-covalent interactions (Hydrogen bonding, Van der Waals interactions, π-π stacking and electrostatic interactions) and molecular assemblies are all determining factors for the different crystal forms an API can achieve (Rodríguez-Spong et al. 2004). The thermodynamics and kinetics of a system ultimately dictate the preferred crystal form and its stability under specified conditions.

Well known alternative API crystal forms include polymorphs (Llinàs and Goodman 2008), salts (Banerjee et al. 2005), solvates and hydrates (Douillet et al. 2012). Pharmaceutical co-crystals, consisting of an API and a co-

former, are relatively new crystal forms that can be utilised for API solubility enhancement (McNamara et al. 2006). There are several published methods for synthesizing co-crystals including solution crystallisation (Gagniere et al. 2009), slow evaporation from solution (Weyna et al. 2009), solvent drop grinding (Weyna et al. 2009), neat grinding (Sanphui et al. 2012), slurry crystallisation (Takata et al. 2008), ultrasound assisted cocrystallisation (Aher et al. 2010) and hot melt extrusion (Dhumal et al. 2010).

Hot melt extrusion (HME) is a well-established manufacturing technique; however, its use in pharmaceutical research is relatively new. Typically, there is no requirement to use a solvent with this technique and it can be easily scaled depending on the quantities that are desired. It can successfully achieve cocrystallisation of an API and co-former (Dhumal et al. 2010) and can deliver continuous crystallisation which is now highly sought after in the pharmaceutical industry.

This project utilised HME as a solvent-free continuous cocrystallisation (SFCC) technique for the formation of pharmaceutical co-crystals. Parameters including temperature, screw speed and screw configuration were explored to achieve the highest co-crystal purity possible and the extrudates were characterized using several different analytical techniques. The project was designed to fundamentally understand the extrusion process, including investigating the mechanisms of co-crystal formation using combinations of model shear deformation experiments. Additionally, near infrared (NIR) spectroscopy was used to predict co-crystal purity using partial least squares linear regression. ThermoFisher Scientific provided insight and knowledge for creating the co-crystal prediction models.

This project is part of a grant awarded to the University of Bradford by the Engineering and Physical Sciences Research Council (EPSRC) and is supported by Bristol-Myers Squibb Company, ThermoFisher Scientific and Diamond Light Source Ltd. It was awarded for the development of a continuous method of co-crystal formation.

CHAPTER 2 LITERATURE REVIEW AND BACKGROUND

2.1 The current state of pharmaceutical research

Pharmaceutical research, whether undertaken by private companies or by publicly funded institutions, is constantly evolving with the aim of becoming more efficient. The current industrial landscape has favoured alliances between companies, and partnerships between companies and institutions (DiMasi et al. 2016), to increase knowledge transfer and to outsource specific research.

Whilst the pharmaceutical sector has been pushing for efficiency, the number of targets for therapeutic agents has significantly increased due to the molecular makeup of diseases being uncovered by innovative advances in technology. This has led to a fall in productivity attributed to diminishing returns in the “knowledge production function” (Pammolli et al. 2011).

It is possible, that in the past, research and development (R&D) has consumed the easier therapeutic targets (Evenson 1993). However, there is little doubt that new research prospects cause a net increase in the complexity of current R&D. The rising “burden of knowledge” has economic implications, but it can be overcome by knowledge transfer and efficient practices (Jones 2009).

Thorough assessments of the continuing technological advances made by the pharmaceutical sector are increasingly being carried out to evaluate the therapeutic merits of new APIs (Pammolli et al. 2011). Considering recent reviews of the value of the novelty of APIs and the associated financial returns for pharmaceutical firms, it has come to light that directing R&D towards novel targets currently has a high risk of failure and lower returns

compared to R&D which focuses on improving known APIs or formulations (Ma and Zemmel 2002). The total risk-adjusted costs of R&D for a “high-novelty approach” could be 40% higher than a “low-novelty approach”. Therefore it is vital for the pharmaceutical industry to head towards significant improvements in processes and technologies in order to decrease the risks involved and improve returns (Ma and Zemmel 2002).

A recent study conducted in 2016 investigated the R&D costs of 106 new drugs from 10 different biopharmaceutical companies (DiMasi et al. 2016). The study showed that the most recent estimate of the “average out-of-pocket cost per approved new compound” was $1395 million, and when adding the estimated post-approval R&D costs, this figure rose to $2870 million.

Any effective, proven innovation to pharmaceutical science, processes or manufacturing methods can have an impact on the R&D costs and the general efficiency of current R&D practises.

2.2 Crystal structures of APIs

Crystal engineering has been an important part of pharmaceutical R&D and can provide researchers with many directions for their research to explore. In the early developmental stages of drug compounds, increasing attention is being paid to material properties, including the effect of different crystal forms (Peterson et al. 2006). APIs are intrinsically valuable materials and crystal engineering is one way to realise their full potential (Almarsson and Zaworotko 2004).

APIs with poor properties, such as poor solubility, are somewhat responsible for the drop in R&D output since the early 1990s (Gardner et al. 2004). Additionally, the physical properties often cause new drug approvals to be delayed by regulatory bodies (CDER 2007). Therefore it is essential for pharmaceutical companies to explore and understand API crystal forms and their inherent physical properties.

Understanding crystal structures was important for this project as it was centred on the knowledge of how different crystal forms can influence the physico-chemical properties of an API. In the pharmaceutical industry, the crystal structure is a fundamental factor in the commercial success or failure of an API. Both the intermolecular and intramolecular interactions are important if one wants to manipulate API properties. The enhancement of the physico-chemical properties of an API is common practice for pharmaceutical companies who are looking to improve solubility, stability and bioavailability.

Crystals have long-range order and have repeating molecular patterns. Well known API crystal forms include polymorphs (Llinàs and Goodman 2008), salts (Banerjee et al. 2005), solvates and hydrates (Douillet et al. 2012).

Polymorphs are crystalline structures that have different arrangements and conformations of the molecules within the crystal lattice. They generally have different melting points and crystal habits. Polymorphism denotes a crystal system where a substance can exist with different unit cells whilst having the exact same elemental composition. Each unique polymorph can exhibit different physico-chemical properties to each other. This is because of

differences in size, morphology, symmetry, number of molecules within the unit cell, packing, and void volumes (Brittain 2009).

Polymorphs have different lattice energies (Enthalpies) and this causes them to possess different physico-chemical properties such as solubility. To be soluble, the free energy of solvation must exceed the lattice free energy of the solid plus the free energy of cavity formation in the solvent for the solvation process to be spontaneous. The enthalpy and entropy change determines the ostwald free energy change, therefore the difference in the lattice energies must imply that the solubility of the crystal forms are different. An unstable polymorph has an increased solubility due to an increase in the lattice energy (Brittain 2009).

A study conducted in 2000 demonstrates the differences in physico-chemical properties polymorphs can have. Solubility tests of carbamazepine forms I, III and dihydrate found that their intrinsic dissolution rates were 61.8, 67.4 and 41.8 µg/cm^2/min using a JP13 1st fluid dissolution medium at 37°C and their solubilities were 460.2, 501.9 and 311.1 µg/mL respectively.

When a substance consists of sufficiently basic and acidic components, it can form a salt. Salt formation involves a proton-transfer or a neutralization reaction (Berge et al. 1977). A pharmaceutical salt is formed when an API forms a sufficiently strong ionic interaction with an oppositely charged ionic molecule (Kumar et al. 2007). Charged ionic groups in the API and counterion molecule generate an intermolecular coulombic force of attraction (Bhattachar et al. 2006).

It is estimated that over half of the approved APIs in the United States of America are pharmaceutical salts (Saal and Becker 2013). They can possess good aqueous solubility compared to co-crystals as described by a study conducted in 2005 (Bhatt et al. 2005) where saccharin was used as a weak acid and was able to protonate different APIs. However, pharmaceutical salts can suffer from toxicological problems such as changes in the pharmacokinetics compared to the API on its own which ultimately leads to different toxicokinetics, and problems can be caused by the counterion itself (Saal and Becker 2013). Typically, for newly developed APIs, the toxicology of the salt forms are not known. The time required to solve this issue is inevitably a hindrance to its development.

Solvates are sometimes considered as pseudopolymorphs because they are different crystalline forms of the API with the inclusion of a solvent within the crystal lattice (Stoichiometric or non-stoichiometric) (Chadha et al. 2010). When the solvent is water, the crystal form is called a hydrate. Approximately one in three APIs can exist in a hydrate form (Breimer 1980). Both solvates and hydrates can be useful when they are thermodynamically stable as the solvate form can enhance the solubility, stability and bioavailability of the API (Sheth and Grant 2005, De Armas et al. 2007).

Solvent molecules can interact with crystalline materials in various ways. These include liquid inclusion, surface adsorption, absorption in disordered regions and as part of the crystal structure itself. Figure 2.1 illustrates these interactions. The majority of these associations are generally considered as nuisances when trying to develop a stable crystalline form and solvates are rarely selected for development. A solvate can only be selected for

development by a pharmaceutical company if it is stable and has a lower than tolerated potential daily exposure of the solvent to the patient (Douillet et al. 2012).

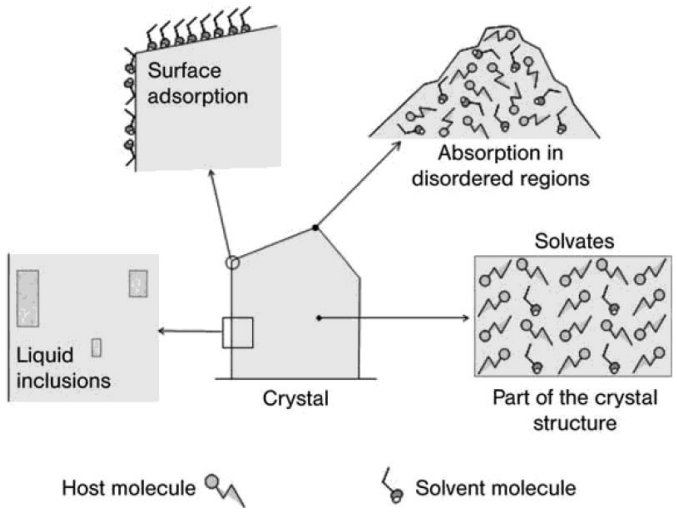

Figure 2.1 An illustration of different solvent interactions with a crystal (Hilfiker 2006).

If there is no long range order in a solid phase, then the substance is referred to as an amorphous material (Mandic 2012). Typically, amorphous solids have no molecular packing or well-defined molecular conformations. There are some desirable properties of amorphous solids, such as high solubility, high dissolution rates and they can sometimes have better compression characteristics than their alternative crystal forms (Yu 2001). Past studies have even treated the amorphous form of an API as a polymorph of the crystalline forms (Haleblian and McCrone 1969). The downside to amorphous solids, is they can be highly hygroscopic and they are generally metastable forms which suffer from poor kinetic stability (Mandic 2012).

Crystal engineering has rapidly evolved and is now seen as synonymous with supramolecular synthesis (Vishweshwar et al. 2006). Multi-component crystalline systems assemble through non-covalent forces and when they form a single crystalline phase, they are referred to as co-crystals (Rodríguez-Spong et al. 2004).

2.3 Co-crystal definitions, nomenclature

Co-crystals can be described as a crystalline phase with multiple distinct molecular constituents that are normally linked by intermolecular bonds. Historically, co-crystals have been referred to as molecular complexes (Blagden et al. 2007, Aitipamula et al. 2012). There are numerous published definitions to help distinguish co-crystals from polymorphs, salts, hydrates, solvates and amorphous materials. They are discussed in this section along with the nomenclature.

The International Quality and Productivity Centre (IQPC) held a meeting in Amsterdam in 2006 which featured intellectual property lawyers, university academics and individuals from international pharmaceutical companies. The purpose was to establish a definition for co-crystals with their intellectual property potential in mind. The end result was the following definition: “crystalline entities with at least two different components constituting the unit cell and interacting by hydrogen bonds”. Additional appendices were required to state that co-crystals are not “salts where the strength of the interaction is so strong that the linkage is between two oppositely-charged ions” and that “cocrystallisation is different from coprecipitation, eutectic

formation, solid solution, or dispersion" (Lara-Ochoa and Espinosa-Perez 2007).

Zaworotko presented a different co-crystal definition for more practical uses. The definition was: "A co-crystal is a multiple component crystal in which all components are solid under ambient conditions when in their pure form. These components consist of a target molecule or ion and a molecular co-crystal former(s); when in a co-crystal, they coexist at the molecular level within a single crystal" (Shan and Zaworotko 2008). This definition was more detailed than the one produced by the IQPC and it served more purpose in scientific research as opposed to patent law.

An interesting proposal by Lara-Ochoa (Lara-Ochoa and Espinosa-Pérez 2007) expressed the need for a definition which describes the type of interaction stabilising the co-crystal. They proposed the following definition: "A crystal constituted by heterosynthons, stabilized by hydrogen bonds or other types of non-valency intermolecular interactions, and in which all the component synthons are solid under ambient conditions, when in their pure form."

In 2013, the Food and Drug Administration (FDA) collaborated with the United States Department of Health and Human services and the Center for Drug Evaluation and Research (CDER) to publish the Regulatory Classification of Pharmaceutical Co-Crystals – Guidance for Industry (FDA 2013). The FDA approved definition for a co-crystal was as follows: 'Crystalline material composed of two or more molecules within the same crystal lattice'. The definition for a pharmaceutical co-crystal was 'a

dissociable “API-excipient” molecular complex, with a neutral guest compound being the excipient’ (Brittain 2013).

Co-crystal nomenclature has also been debated over recent years. Desiraju has stated that issues with the nomenclature of a new subject are a necessary evil which helps to fine-tune what is accurate and what needs to be discarded. In an article published in *CrystEngComm* in 2003 (Desiraju 2003), Desiraju argued that the word ‘crystal’ is too important and too meaningful to be used in this context however he conceded that the term co-crystal has become very popular and may well be used regardless of its controversial nature. The term ‘molecular-complex’ was thought to be more appropriate because the term ‘co-crystal’ implied that the structure has commonalities between its crystal structure and that of the crystal structure of the individual components.

In a response to Desiraju, Dunitz disputed the ‘molecular-complex’ term and reasoned that it had too broad a meaning just as how Desiraju described the word ‘crystal’ (Dunitz 2003). Dunitz argued that the term ‘co-crystal’ had good reasons to be popular and that it aptly describes a crystal containing more than one single component.

Bond (2007) suggested that both Desiraju and Dunitz were well intentioned however missed the point about the fact that ‘co-crystal’ should be nothing more than a synonym and the term ‘multi-component molecular crystal’ was a more accurate term to use. However, he acknowledged that the term ‘co-crystal’ would be difficult to displace, considering its popularity.

Various other authors have entered into the co-crystal nomenclature debate in recent years (Zukerman-Schpector and Tiekink 2008, Almarsson et al. 2012, Kelley et al. 2013).

This project was centred on pharmaceutical co-crystals; therefore it was necessary to distinguish co-crystals from other pharmaceutical solid forms. Figure 2.2 illustrates the differences between each solid form in terms of their components.

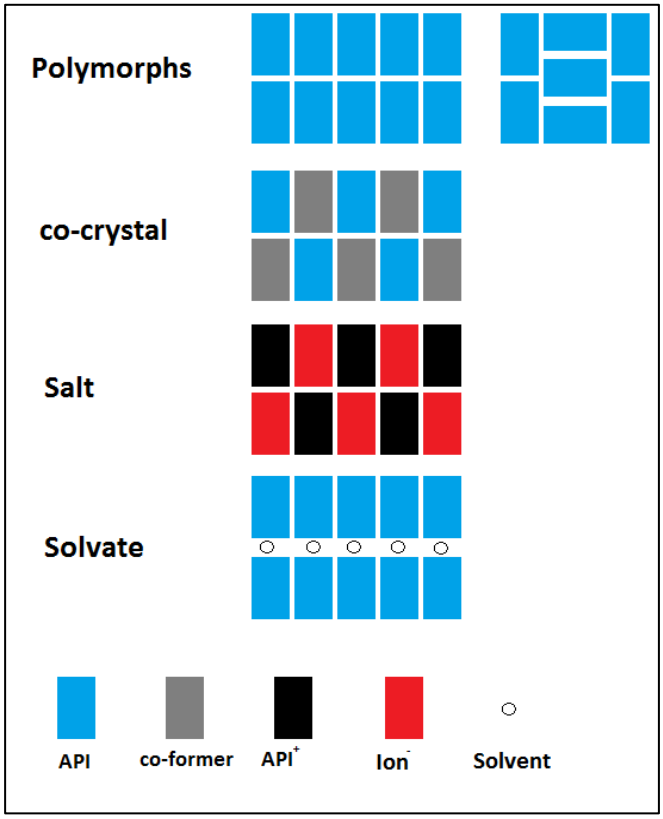

Figure 2.2 A diagram showing the fundamental differences between polymorphs, co-crystals, salts and solvates/hydrates.

A total of 46 scientists working in the field of pharmaceutical co-crystals published an article in 2012 (Aitipamula et al. 2012) to classify co-crystals in pharmaceutical sciences from a regulatory perspective. Figure 2.3 was taken

from this study to highlight the difficulties involved in defining multi-component solid forms. The different forms can overlap with one another and each form can exhibit polymorphism. This was an effective way of describing the complexity of solid forms.

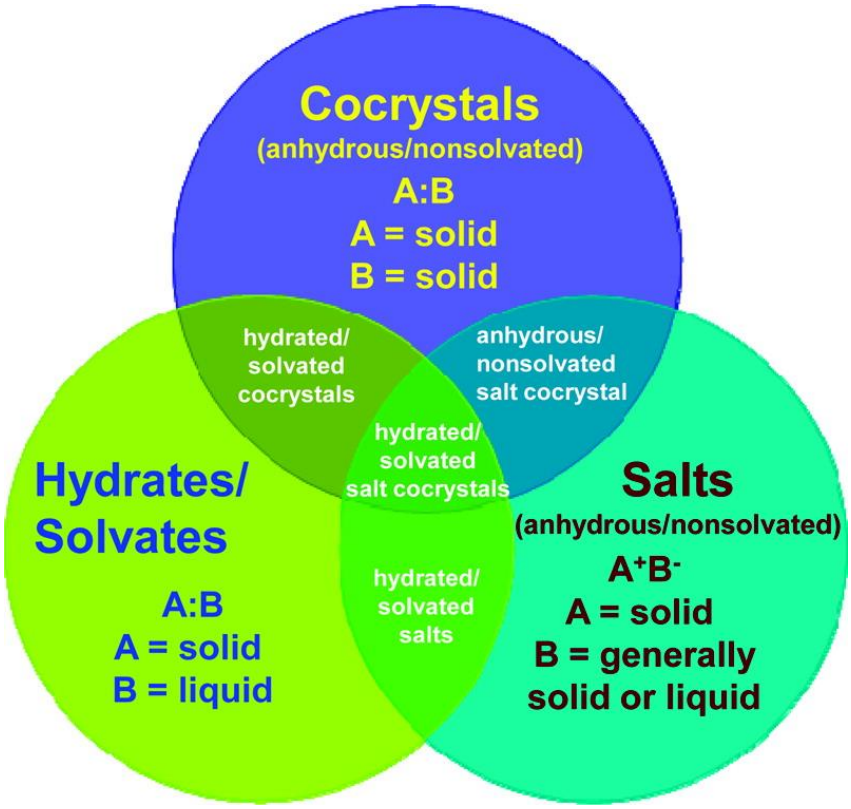

Figure 2.3 The classification of multi-component solid forms. They can overlap with one another and they can exhibit polymorphism (Aitipamula et al. 2012).

2.4 Co-crystal design

Weak intermolecular interactions can play an important role in controlling material properties because they can provide alternative crystal forms, and different forms can exhibit different solubilities, crystal morphologies and other important properties. Carefully designed systems can achieve

favourable, complimentary hydrogen bonding between the molecules. However, such systems can also form hydrogen-bonded molecular aggregates, which are also known as supramolecular assemblies. These aggregates/assemblies can enhance critical physico-chemical properties of pharmaceutical APIs, such as solubility and stability, and are therefore a key part of designing a co-crystal.

Etter (1991) described some general rules when choosing suitable hydrogen-bonding components in organic chemistry. Below is a summary of these rules:

- All good proton donors and acceptors are used in hydrogen bonding

- The best hydrogen bond donor and the best hydrogen bond acceptor will prefer to hydrogen bond with one another

Different hydrogen bonded synthons can be created by the formation of hydrogen bonds between different molecules. Figure 2.4 shows some examples of these synthons. The synthons can be classified as homosynthons or heterosynthons depending on the arrangement of the functional groups involved in the bonding. Homosynthons have the same or similar interacting functional groups whereas heterosynthons have different interacting functional groups. For example, an amide-amide interaction is a homosynthon and an acid-amide is a heterosynthon.

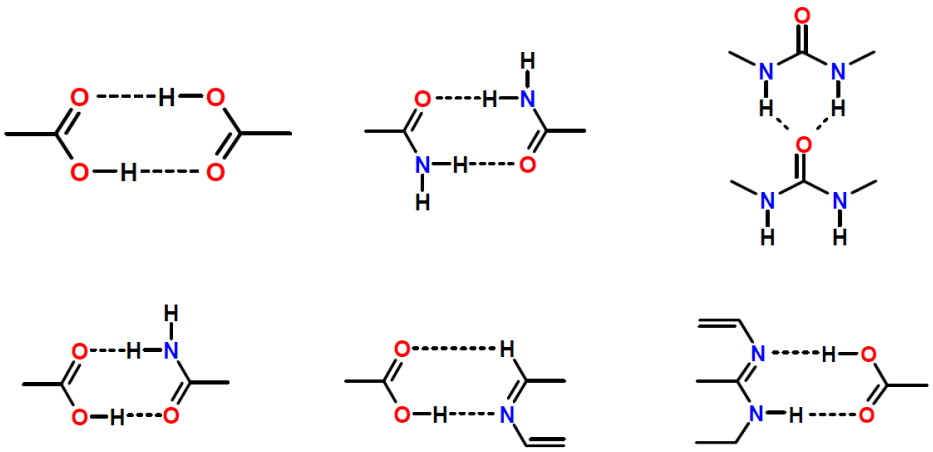

Figure 2.4 Common hydrogen bond synthons found in supramolecular assemblies.

In multi component co-crystals, homosynthons are the most common synthon. It should be noted that heterosynthons can be formed in both a single component crystal and a multi component co-crystal. The interacting molecules that form a synthon can be called homomers or heteromers to describe the type of molecular aggregate they have formed. If both molecules are the same then the aggregate is called a homomer, alternatively, a heteromer aggregate forms a multi component co-crystal.

Multiple hydrogen bonding possibilities, dipoles, ionic states and steric or conformational limitations can cause problems when trying to model co-crystals and can cause conflict with the principles already discussed (Deshpande et al. 2012). Complicated systems will always have some exceptions to the guidelines. Halogen bonds have also been used in co-crystal design and can even be used in combination with hydrogen bonds (Aakeröy et al. 2008). However, heteromeric NH…O, OH…O and NH…N hydrogen-bonding remains the primary method for designing and synthesizing co-crystals (Wood et al. 2014).

2.5 Mechanisms of co-crystal formation

To understand the fundamentals of co-crystal behaviour and discipline, the mechanisms which have been proposed for their formation were reviewed. There are four methods of co-crystal formation found in the literature. These include the reaction crystallisation method, the eutectic and vapour phase method, the deliquescence method and the thermal fusion method.

The reaction crystallisation method proposes that the chemical potential is the main driving force of crystallisation which allows for the rapid and effective formation of co-crystals under ambient conditions. The theory states that the difference between the chemical potential at equilibrium and at a supersaturated state is an important marker. It can predict if cocrystallisation will spontaneously occur or not.

At equilibrium, the sum of a co-crystal component's chemical potentials (Or molar free energies) is equal to that of the solution. The molar free energy of a co-crystal A_mB_n in equilibrium with the solution phase is given by equation 2.1:

$$\mathbf{G_{AmBn} = G_{solution} = mG^{L}_{A} + nG^{L}_{B} = m\mu_A + n\mu_B} \qquad \textbf{(Eq. 2.1)}$$

Equation 2.2 describes the chemical potential (each component has the activity a_i):

$$\mathbf{\mu_i = \mu^{0}_{i} + RTlna_i} \qquad \textbf{(Eq. 2.2)}$$

where μ^0_i is the chemical potential of the reference state for i.

Combining equations 2.1 and 2.2 gives equation 2.3 and 2.4:

$$\Delta G_{AmBn} = \Delta G_{solution} = RT(m\ln a_A + n\ln a_B) \quad \textbf{(Eq. 2.3)}$$

$$\exp(\Delta G_{AmBn} / RT) = (a_A)^m(a_B)^n = K_{sp} \quad \textbf{(Eq. 2.4)}$$

Where K_{sp} is the solubility product of the co-crystal.

Another part of this theory relies on the solubility phase diagram for the crystal, A, and the co-crystal, AB. Figure 2.5 shows an example of a co-crystal solubility phase diagram.

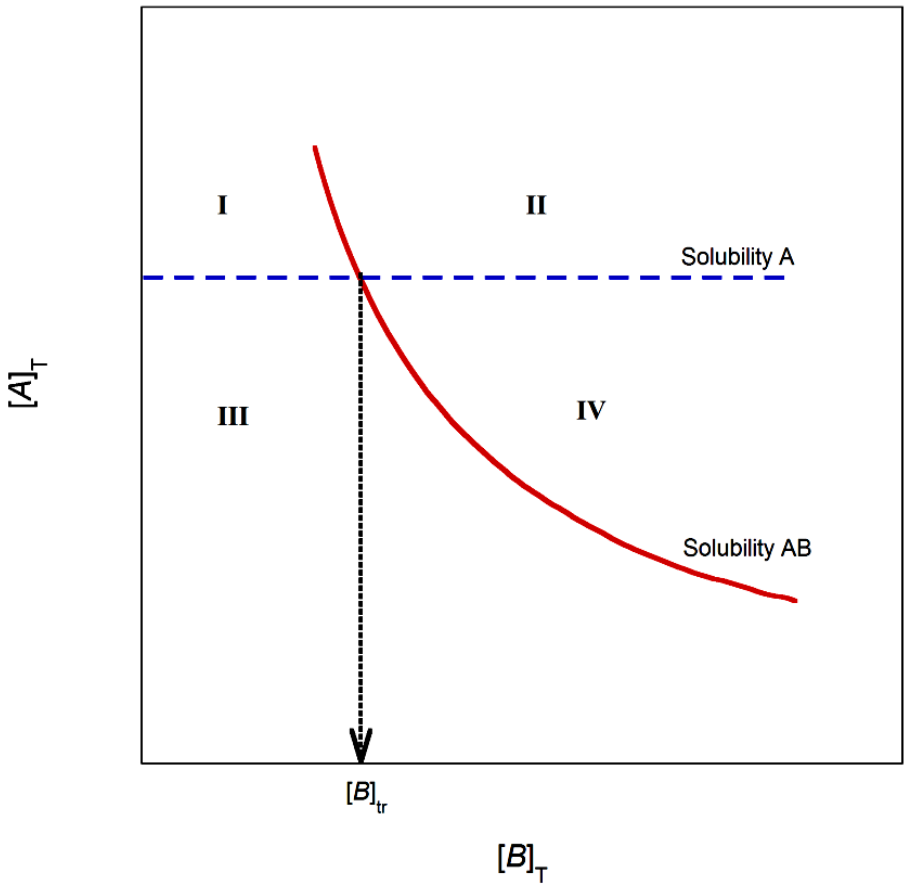

Figure 2.5 Solubility phase diagram of components A and B and co-crystal AB. The subscript 'T' is total concentration and $[B]_{tr}$ is the transition concentration. The four different regions are labelled I-IV (Nehm et al. 2006).

The solubility phase diagram in figure 2.5 has four labelled phase regions I, II, III and IV. Region I describes the area where the solution is supersaturated with respect to A and under saturated with respect to AB, therefore any AB crystals will spontaneously transform into form A crystals in this region. Region II describes a region where the solution is supersaturated with respect to both forms A and AB; this is where AB will precipitate out of the solution as it is the most thermodynamically stable phase. In region III, both A and AB are undersaturated in the solution, and no phase will precipitate out of the solution. Finally, in region IV, the solution is supersaturated with respect to AB and undersaturated with respect to A, therefore form A will transform to crystalline form AB.

There were some assumptions required for interpreting the solubility phase diagram in figure 2.5. It was assumed that B was more soluble than A; AB was more soluble than A in a stoichiometric solution, no complexation or ionization of the components takes place in the solution, and the solubility of A is independent of the concentration of B in the solution.

A crucial part of the phase diagram shown in figure 2.5 was the point where the solubility of the drug A and co-crystal AB intersected. This was the eutectic point and the co-crystal solubility can be calculated from this point using the concentrations of the drug and co-former (Nehm et al. 2006).

In 2006, a research group proposed that when the co-crystal form is added to a solution in excess of the stoichiometric composition, it reduces the solubility of the co-crystal (Rodríguez-Hornedo et al. 2006). It was explained by considering the equilibrium equation of the reaction of a binary co-crystal

when dissociating in a solution of its API and co-former. The equilibrium constant for this reaction is proportional to the thermodynamic activity product of the API and co-former. The co-crystal solubility can therefore be predicted by the solubility product if the activity of the solid is constant or equal to 1.

The reaction theory proposes that cocrystallisation in solid-liquid systems is initiated by the effect of nonstoichiometric concentrations of the co-crystal components causing the reduction of the solubility of the co-crystal to be crystallised (Rodríguez-Hornedo et al. 2006).

The second proposed mechanism for cocrystallisation was the eutectic and vapour phase theory. This theory sets out to explain why, during processes such as mechanical grinding of an API and co-former, the reactants can melt to form the co-crystal form at temperatures below the individual melting points of the components (Chadwick et al. 2007). It is unknown exactly what the cause of this phenomenon is however it has been suggested that vapour diffusion could provide a mass transfer mechanism because kinetic data has shown that the reaction is diffusion controlled (Rastogi et al. 1962). It has also been proposed that additional degrees of freedom, the enhancing of molecular collisions and the formation of co-crystal seeds play an important role when a study was conducted where the rate of cocrystallisation was significantly increased upon the addition on small amounts of solvent (Shan et al. 2002)

Another proposal for the eutectic effect was that if the crystal lattice of each component allows for long-range anisotropic molecular migrations, the

molecules can undergo gas-solid, solid-solid, thermal, photochemical and catalysed reactions (Kaupp 2003).

With regards to the mechanical grinding technique in particular, the eutectic effect was explained by the mechanical act of grinding causing a high interfacial area between the initial solid phases where a liquid phase can form. Additional grinding and shear experienced by the material then facilitated contact between the liquid and solid phases which caused nucleation and growth of the co-crystal phase (Chadwick et al. 2007).

Thirdly, the deliquescence mediated cocrystallisation method has been proposed for describing the formation of co-crystals in a solution. It is based on the deliquescent and hydroscopic properties of the co-crystal components. The proposed process is displayed in the diagram in figure 2.6. Examples of such components include sucrose, fructose and citric acid (Jayasankar et al. 2007). The deliquescent material absorbs moisture at a characteristic relative humidity. This causes it to dissolve and coat the surrounding particles with the solution. Finally, solution-mediated cocrystallisation occurs if two or more co-crystal components are in close proximity with each other.

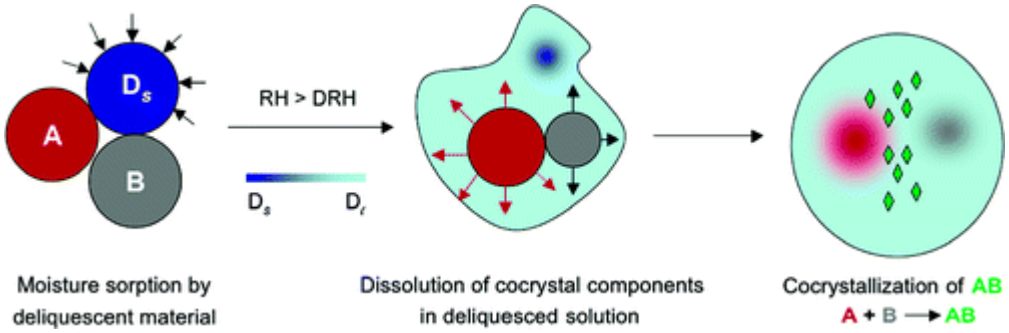

Figure 2.6 A diagram of moisture sorption by a deliquescent material, D_s, dissolution of co-crystal components, and cocrystallisation of the components A and B (Jayasankar et al. 2007).

The driving force for solid blends containing deliquescent materials depends on the rate of moisture sorption, the dissolution rate of the co-crystal components, and the supersaturation of those components in the solution phase. It was demonstrated that moisture can generate co-crystals when exposed to deliquescent conditions.

The thermal fusion method for cocrystallisation describes the use of temperature alone for forming co-crystals and was first described by Lehmann (1888). It is a useful technique for studying the thermal behaviour of co-crystals and their individual components. The mixed fusion Kofler method, as it is now known, has been utilised by researchers to visualise the formation of a co-crystal when the two components meet on a glass slide (Berry et al. 2008). The basic methodology of the Kofler method is illustrated in figure 2.7. The highest melting point component, A, is melted and re-crystallised, next, the lower melting point component B is heated and allowed to melt and is brought into contact with component A to create a zone of mixing, where cocrystallisation can occur.

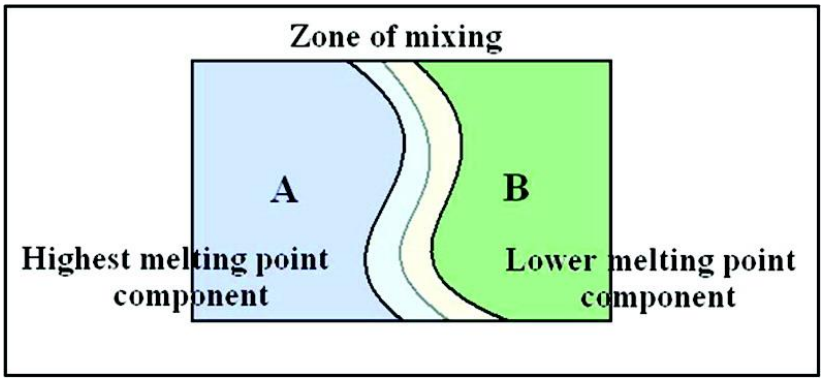

Figure 2.7 A diagram of the mixed fusion Kofler method showing two components (A and B) coming in contact with each other to form a zone of mixing. Cocrystallisation can occur in this mixing zone (Berry et al. 2008).

When combined with any kind of microscopy which has heating capabilities, the mixed fusion Kofler method is a powerful technique which can probe crystal properties and morphology under heating and when in contact with a co-former. The differential scanning calorimetry technique can also be used to accurately characterise the changes a material is experiencing upon heating under set conditions. The method involves heating small quantities of the appropriate stoichiometric amounts of the co-crystal components in the DSC pan up to a temperature which causes cocrystallisation to occur.

2.6 Co-crystal preparation techniques

There are a large number of reported methods for co-crystal synthesis. It is not easy to design a co-crystal that will be successful because a heteromeric system will only form if it is the most thermodynamically stable system (Providing the kinetics allow the transition) when compared to the homomeric

systems (Vishweshwar et al. 2006, Blagden et al. 2007). Intermolecular bonding is the key for the successful synthesis of co-crystals.

Reported methods for the preparation of co-crystals include: solution crystallisation or solution mediated phase transformation (Leyssens et al. 2014), solution evaporation (Weyna et al. 2009), solid-state grinding, liquid assisted grinding, polymer assisted grinding (Hasa et al. 2015), solvent-drop grinding (Trask et al. 2004), hot stage microscopy (Berry et al. 2008), hot melt extrusion (Moradiya et al. 2014), spray drying (Patil et al. 2014), freeze drying (Eddleston et al. 2013) and ultrasound assisted cocrystallisation (Kaur Bhangu et al. 2016). Hot melt extrusion is an increasingly popular cocrystallisation technique which will be discussed in more detail in the next section.

2.7 Hot melt extrusion

Hot melt extrusion formed a large part of this project. The technology surrounding extrusion and a general background review are presented in sub-section 2.71. The use of extrusion technology for manufacturing pharmaceutical co-crystals is also discussed in sub-section 2.72.

2.71 Background

Hot melt extrusion was originally developed for processing foods and plastics and rubber (Breitenbach 2002, Chokshi and Zia 2010). There are two main types: single screw and twin screw. For both single and twin screw designs, granules or powder is fed into the screw typically using a hopper. The material is then conveyed along the barrel where it is heated and subjected

to pressure and shear depending on the screw configuration and processing conditions. In most extruders, the depth of the screw flight is reduced to increase the pressure for compacting the material as it travels along the screw. At the end of the barrel, the material passes through a die which moulds it into a chosen shape (Crawford 1981). Extrusion technology was significantly developed towards the end of the 19th century to provide a continuous process for producing polymers of uniform shape and size (White et al. 2003).

Most commercial extruders are now built with a modular design to make it easier to modify the extruder with attachments, to achieve better control, to facilitate maintenance and to allow for in-line process analytical technology (PAT) tools for analysing the process (Chokshi and Zia 2010). Single screw extrusion uses a single screw housed within the barrel; alternatively, twin screw extrusion uses two complimentary screws. The screws can be custom made to provide a certain level of mixing, shear and conveying.

Screw design and configuration plays an important role in extrusion. The configuration can influence the mixing intensity, shear and how the material is conveyed along the barrel. The modification of screw configurations also allows the extruder to perform functions such as mixing, blending and dissolution (Breitenbach 2002). In figure 2.8, photographs of the most common screw operations that can be used are shown from a 16 mm co-rotating twin screw extruder (Pharmalab, Thermo Scientific, UK). There can be forward conveying, staggered mixing, dispersive mixing and discharge screw functionalities.

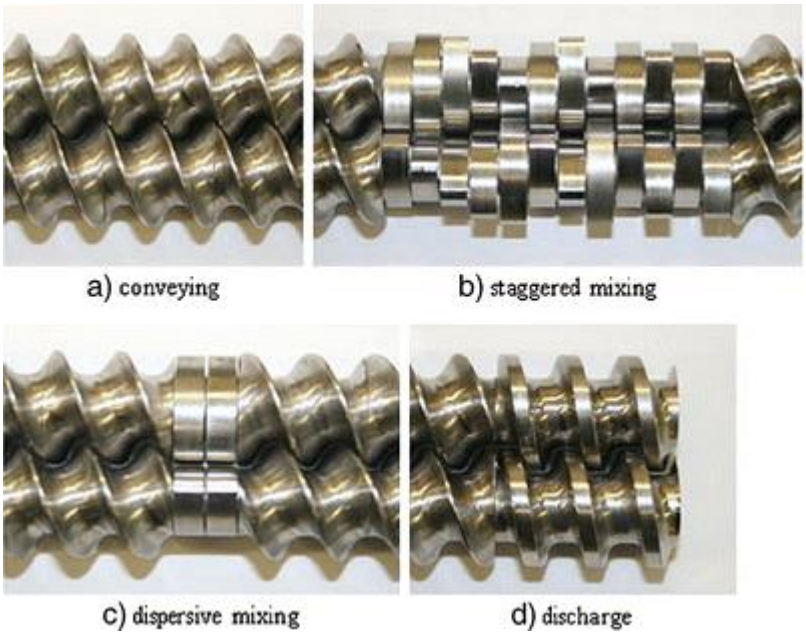

Figure 2.8 Four different screw operations used in twin screw extrusion (Dhumal et al. 2010).

The sequence of screw components along the barrel is called a screw configuration. For the Pharmalab extruder, mixing components can be placed at 0°, 30°, 60° and 90° to each other. However, other extruder models can have different mixing components which are tailored for specific needs, for example, reverse mixing elements for increasing the pressure (Whelan and Dunning 1988, Ghebre-Selassie and Martin 2003). In general, when the mixing components are at 0° to each other, this allows for dispersive mixing of the material. At 30°, 60°, and 90°, the mixing components allow staggered mixing. The mixing components can also be positioned to create reverse flow which creates higher shear experienced by the material in the barrel.

The forward conveying screw elements are important as they convey the material along the extruder barrel, through zones which are set at different temperatures. They also deliver the material to the mixing zones, depending

on the screw configuration, and provide a net forwarding pressure. The mixing elements promote either dispersive or distributive (Staggered) mixing. Dispersive mixing is primarily used for breaking down aggregates and normally has a longer length mixing zone compared to distributive mixing. Dispersive mixing can hold the material in a pressure trap, for a certain period of time, which squeezes, elongates, and shears the material.

Alternatively, distributive mixing regions are designed to separate the material into smaller units. Distributive mixing zones can be further sub-classified due to their directional trait; they can forward convey, reverse convey or be completely neutral. This directional trait is determined by the angles at which the individual kneading elements are placed to one another and whether the element is in the clockwise or anticlockwise direction compared to the one before it. For example, if the kneading elements were positioned at 30° to each other in a clockwise direction, and the screw is rotated in a clockwise direction, this would be a distributive, forward conveying mixing zone. If the kneading elements are positioned at 90° to one another, this would create a neutral, distributive mixing zone. If the kneading elements were at 30° in an anticlockwise direction, and the screw is still spun in a clockwise direction, this would be a reverse, distributive mixing zone. When positioned at 0° to each other, this is a neutral mixing zone, and is exactly the same as a dispersive mixing zone.

Single-screw extruders were developed for injection moulding of polymers and food and are used primarily as a melting device (Eitzlmayr et al. 2014). For highly viscous materials, and for specialised mixing capabilities, twin screw extrusion is preferred. In twin screw extrusion, two screws are

involved. In the majority of cases, the screws are made to be identical to each other in terms of their configuration. Mixing zones cannot be positioned at different points along each screw, they must both have the mixing zones at the same position, otherwise the screws will not complement each other geometrically (Ghebre-Selassie and Martin 2003).

Twin screw extruders can have either co-rotating screws, which rotate in the same direction, or counter-rotating screws, which rotate in opposite directions to one another. Counter-rotating screws offer good material conveying and provide high shear because the material is squeezed through the small gap between the screws, however this can cause air entrapment, high pressures and can only be operated at slow speeds (Lim and White 1994). If the pressure increases between the two screws, this can cause barrel wall scraping by the screws, and ultimately damage to the extruder.

Co-rotating screws usually have an intermeshing design. Figure 2.9 illustrates a forward conveying screw zone where both screws are intermeshing. This intermeshing design allows the screws to self-wipe as they rotate which is very useful as the screws can self-clean themselves and they don't allow material to build up within the extruder barrel. Co-rotating screws can be operated at much higher screw speeds than counter-rotating screws and they do not suffer from mechanical wearing as much as counter-rotating screws because they do not experience an outward pushing effect from a build-up of pressure between the screws. Co-rotational screw configurations are much more flexible than those for counter-rotating screws and they can be specifically tailored for a desired effect, such as intense mixing (Ghebre-Selassie and Martin 2003). Another advantage of a co-

rotating, intermeshing, twin screw extruder is the material has a minimised residence time within the extruder whilst achieving the desired operations such as conveying, melting and sufficient mixing.

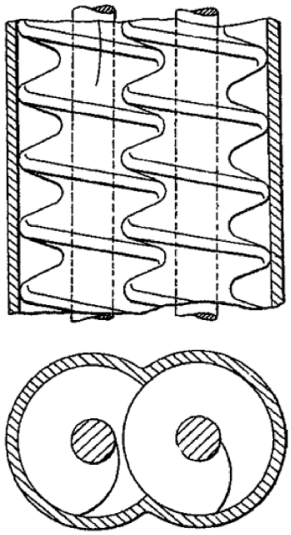

Figure 2.9 An illustration of an intermeshing co-rotating twin screw from two different angles (Ghebre-Selassie and Martin 2003).

Due to the inherent nature of the self-wiping screws in twin screw extruders, emphasis has been put on the solvent-free extrusion capabilities in recent years (Kleinebudde 2011, Eitzlmayr et al. 2014). Solvent-free extrusion is important as it is seen as being more environmentally friendly (Dhumal et al. 2010) and there are no issues regarding solvents needing to be evaporated in post-processing stages (Krause et al. 2009).

Variable-speed drives are used to turn the extruder screws. The gearing controls the speed, in rotations per minute (rpm), and in a twin screw extruder, the distribution gear absorbs any load from the screws and maintains the angular timing of the screws. The length to diameter ratio is an important term, and is simply the length of the screw divided by the diameter

of the screw. Intermeshing twin screw extruders can have an L/D ratio of up to approximately 60:1 and non-intermeshing twin screw extruders can achieve 100:1 or longer because there are no intermesh clearance constraints. A single screw extruder would normally have an L/D ratio of 36:1 or shorter (Ghebre-Sellassie and Martin 2007). The outer diameter (OD) refers to the full diameter of each screw and the inside diameter (ID) refers to the OD minus the depth of flight. The OD/ID ratio is important because it is used to calculate the free volume within an extruder when added to the space between the screws and the gaps between the screw and barrel wall. Therefore, the flight of depth is critical for achieving the perfect balance between the free volume and the torque. The transfer of energy that the material is exposed to by the extruder is directly impacted by this balance. Finally, residence time of material within the extruder barrel can directly affect the properties of the material; the residence time can vary significantly depending on the extrusion conditions.

Computer modelling of the extrusion process has always been a goal for extrusion science and extruder manufacturing companies (Tayeb et al. 1989). Recent efforts have focused on 1D modelling as it has the power to provide crucial data about flow and stress on the extruder components and also for determining mixing modes and rates (Eitzlmayr and Khinast 2015). There are limitations to the modelling, as authors admit that a 3D model would be preferred, however this would require more computational effort (Eitzlmayr et al. 2014).

In the last decade, hot melt extrusion technology has evolved and a transition has been made to pharmaceutical science (Crowley et al. 2007).

Hot melt extrusion can be used to prepare pharmaceutical delivery systems, including granules (Gryczke et al. 2011), pellets (Bialleck and Rein 2011, Roblegg et al. 2011), sustained release (Almeida et al. 2011, Vithani et al. 2013) and rapid release (Perissutti et al. 2002) dosage matrices and many other devices. The technology can also be utilised for polymorphic transformation of APIs (Kulkarni et al. 2013, Kulkarni et al. 2015).

2.72 Extruding co-crystal pairs

Pharmaceutical co-crystals can be prepared using twin screw, hot melt extrusion when subjected to the correct conditions (Temperature, shear, residence time and sufficient mixing) (Dhumal et al. 2010) without the use of binders, polymers or solvents.

As discussed in section 2.5, the right conditions are required for cocrystallisation to be spontaneous. The conditions must thermodynamically favour co-crystal formation. Hot melt extrusion technology provides a process where the temperature, pressure, shear and mixing intensity amongst other parameters can be accurately controlled. Adjusting these parameters, allows for the process to be optimised to favour a certain reaction, transformation or other desired effects. An advantage of using extrusion is that no solvent is needed to facilitate the conversion to co-crystal (Dhumal et al. 2010) and is thus considered a green technology.

Ibuprofen – nicotinamide co-crystals were made using twin screw, hot melt extrusion by Dhumal et al. (2010). Ibuprofen and nicotinamide were blended and sufficiently mixed in a 1:1 molar ratio before being loaded into a gravimetric twin-screw feeder. The feeder fed the materials into the

Pharmalab 16 mm co-rotating twin screw extruder (40:1 L/D) (Thermo Scientific, UK) which was operated without a die. Their study found that a long residence time was important for increasing the 1:1 co-crystal yield. The residence time of the material was controlled by the screw speed; 20 rpm, 30 rpm and 40 rpm. Equally as important was the temperature; if situated above the eutectic point of the two raw materials a good co-crystal yield was obtained. The most effective temperature profile involved heating the material from 25 to 90°C from zone 2 to zone 7 of the extruder barrel. The maximum temperature of 90°C was situated where the main mixing zone of the screw was positioned. Finally, at zone 10, the temperature was reduced to 80°C. The effectiveness of this temperature profile relied on the temperature being adequately above the eutectic point of the raw materials to cause partial melting, without causing any degradation. Finally, the screw geometry played an important role in forming the co-crystals. The group used three different configurations: low shear, medium shear and high shear. This nomenclature relates to the number, length and type of mixing zones that were positioned along the screws with the low shear screws having no mixing zones, and the high shear screws having five separate mixing zones. Overall, the team were able to prove that all three parameters, residence time, temperature and screw geometry, were important for controlling the co-crystal yield using twin screw extrusion.

Similarly, four case studies were undertaken by Daurio et al. (2011) to see whether twin screw, hot melt extrusion could be used for manufacturing co-crystals. The co-crystal systems they investigated were caffeine – oxalic acid, nicotinamide – trans cinnamic acid, carbamazepine – saccharin and

theophylline – citric acid. The extruder they used for their experiments was a Prism Pharmalab 16 mm twin screw extruder (25:1 L/D). It has three controlled temperature zones along the barrel and an additional temperature control for the die. However, the die was not needed and was therefore disconnected for the study. The screw geometry they used was designed to be a high shear, high mixing operation, with alternating forward conveying and 90° mixing zones along the full length of each screw.

For the caffeine – oxalic acid system, Daurio et al. (2011) blended and mixed the material in a 2:1 molar ratio. To study the effect of mixing, the material was extruded using two screw geometries; one solely consisting of forward mixing elements, the other as described in the paragraph above, high mixing. No 2:1 co-crystals formed when applying the forward conveying screw, however, when using the mixing screw, the co-crystal formed at 25°C and 75°C. The authors stated that the eutectic formation may not be the mechanism controlling co-crystal formation in this co-crystal system. Next, the team collected samples from the beginning, middle and end of the extruder barrel and analysed them using PXRD. They found a metastable caffeine – oxalic acid co-crystal polymorph situated in the middle of the barrel. Finally, they studied the effect of material residence time on co-crystal formation. The screw speed was set to 25, 50, 75, 100 and 250 rpm and from looking at the PXRD patterns, they determined that the slowest screw speed was the optimal setting for co-crystal formation. However, they noted that residence time did not play a significant role in increasing co-crystal formation because it was only at 250 rpm were they found incomplete co-crystal formation.

Concerning the nicotinamide – trans cinnamic acid co-crystal system, Daurio et al. (2011) blended and mixed the components in a 1:1 molar ratio. The first study they conducted involved investigating the effect of temperature on co-crystal formation by extruding the physical mixture at 75 rpm with temperatures of 80, 90, 100 and 110°C. Only at 110°C was full co-crystal conversion achieved. At 120°C, the large amount of torque suffered by the extruder precluded the run. The authors state that for this co-crystal system, eutectic formation is involved.

For the carbamazepine – saccharin co-crystal system, Daurio et al. (2011) blended and mixed the raw materials in a 1:1 molar ratio. Extrusion was carried out at 50°C and 190°C using a screw speed of 25 rpm. Near complete co-crystal formation (97%) was only observed in the sample processed at 190°C. They chose 190°C because this is very close to the melting point of carbamazepine. To investigate the effect of the presence of water during extrusion of the material, the team decided to add approximately 5 mL of water to 10.4 g of 1:1 physical mixture of anhydrous carbamazepine and saccharin and then extruded this at 100°C. 100°C was chosen to rid the end product of water. For this sample, an 87% co-crystal yield was achieved. The authors suggest that this method could be more optimized to increase the co-crystal yield and recommend that using hydrated starting materials could also have a similar effect. Finally, the researchers tried to make form II of the 1:1 co-crystal by adding ethanol during extrusion. However, they were only able to produce form I. This proves that by utilizing the effect of catalytic solvents during extrusion, they

were able to lower the processing temperatures required for formation of the form I co-crystal.

A theophylline – citric acid system was also studied by Daurio et al. (2011) using twin screw extrusion. They blended and mixed the anhydrous and monohydrated forms of the materials in 1:1 molar ratios ready for extrusion. The experiment details are shown in table 2.1. Both the hydrated and anhydrous co-crystals were formed using different combinations of the starting components. At the high temperature, the anhydrous co-crystals were formed, as was expected, regardless of the starting components. They concluded that when extrusion was carried out at 20°C, water resided within the crystal lattice of the co-crystal, however, in the case of 50°C, the water aided the formation of the anhydrous co-crystal. Similarly, the water aided the formation of the anhydrous co-crystal at 153°C but was unable to help the material to reach full conversion due to evaporation. An additional ethanol assisted run, concluded that the anhydrous co-crystal was formed.

Table 2.1 Outcome of twin screw extrusion experiments performed with theophylline – citric acid system (Daurio et al. 2011). A: anhydrous, M: monohydrate, AC: anhydrous co-crystal, HC: hydrated co-crystal.

#	Theophylline	Citric acid	Type of extrusion	Temperature (°C)	Product
1	A	A	Neat	153	AC + unreacted
2	A	M	Neat	153	AC + unreacted
3	M	A	Neat	153	AC + unreacted
4	A	M	Neat	50	AC
5	A	A	Ethanol-assisted	20	AC
6	A	M	Neat	20	HC
7	A	M	Water-assisted	20	HC

In 2010, Medina et al. (2010) attempted using twin screw extrusion to manufacture 2:1 caffeine – oxalic acid and 1:1 AMG 517 – sorbic acid co-crystals. The appropriate stoichiometric blends of the starting materials were fed into a ThermoScientific Pharmalab 16 mm co-rotating twin screw extruder for processing. For both systems, a high intensity mixing screw geometry was used. The temperature used for the caffeine – oxalic acid system was 75°C for each temperature controlled zone along the extruder barrel and the screw speed was set at 100 rpm. For the AMG 517 – sorbic acid system, the temperature was 115°C throughout the barrel, and the screw speed was 25 rpm. No die was used for both systems and a forward

conveying screw featuring no mixing elements was used as a control. PXRD confirmed that both co-crystals were successfully manufactured using the aforementioned settings and when the control conditions were employed, no co-crystals were formed in either system. The authors conclude the results by stating that efficient mixing and close material packing during twin screw extrusion are critical for providing surface contact between the raw components and thus, facilitating co-crystal formation.

Kulkarni et al. (Kulkarni et al. 2015) presented a study where the stoichiometry of the caffeine – maleic acid co-crystal was controlled using twin screw, hot melt extrusion. The team used a ThermoScientific Pharmalab 16 mm co-rotating twin screw extruder (40:1 L/D). The findings are presented in figure 2.10.

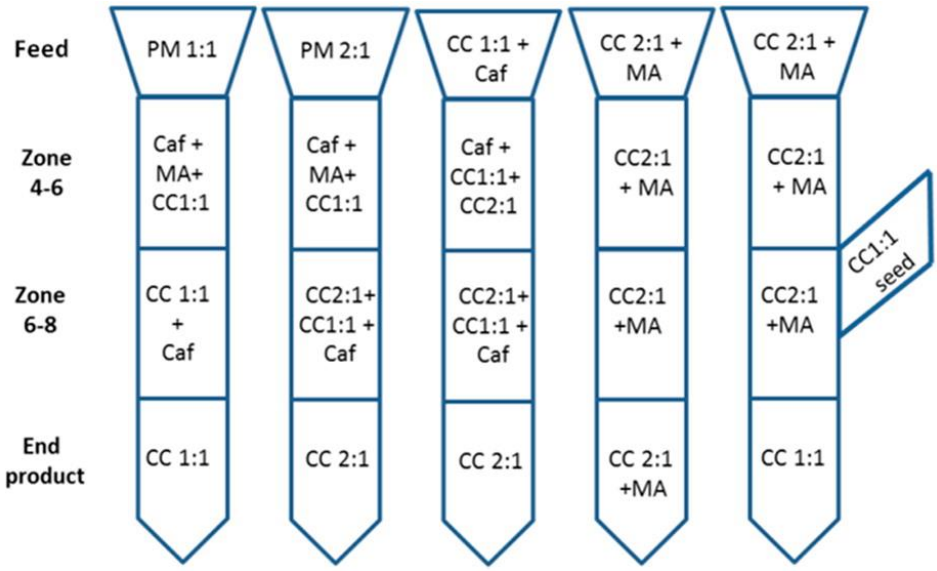

Figure 2.10 Schematic representation of caffeine – maleic acid co-crystal formation using SFCC (Kulkarni et al. 2015).

The findings from the study confirmed that hot melt extrusion was able to successfully form 2:1 caffeine – maleic acid co-crystals where other

crystallisation techniques had failed. The extrusion process was also capable of converting the 1:1 co-crystals into 2:1 co-crystals and conversion from 2:1 to 1:1 was achieved by seeding with the phase pure 1:1 co-crystal (15% w/w) at zone 6 of the extruder barrel.

In this section, many examples of cocrystallisation via hot melt extrusion were presented. It is an increasingly popular technique which has great potential for the pharmaceutical sector as a whole.

2.8 Applications of co-crystals

Pharmaceutical co-crystals have been celebrated for their ability to improve the physicochemical properties of an API without disrupting the functionality of the API molecule itself (Schultheiss and Newman 2009). Highly symmetrical, rigid, low molecular weight molecules which can form strong intermolecular interactions have a high probability of being able to cocrystallise with suitable co-formers (Stahly 2007). Co-crystals are "underutilised solids that greatly expand the possibilities for finding a developable solid form of an API" according to Stahly (2007).

In the current literature, there are many examples where cocrystallisation has provided a means of improving API solubility and dissolution rates. Chow et al. (2012) reported that 1:1 ibuprofen – nicotinamide co-crystals and 1:1 flurbiprofen – nicotinamide co-crystals can have improved tableting behaviour, hygroscopicity and dissolution performance compared to ibuprofen and flurbiprofen on their own. Similarly, Yan et al. (2012) reported that cocrystallising agomelatine with glycolic acid, isonicotinamide, methyl-4-

hydroxybenzoate and urea improves the APIs aqueous solubility compared to agomelatine form I and II.

A large study was conducted by Good and Rodriguez-Hornedo (2009) to compare the solubilities of the API and co-formers to their co-crystal forms. Their findings are shown in table 2.2. For some co-crystal forms, the co-crystal solubilities were lower than the solubility of the API on its own. The research team found that the co-crystal solubility increased with the solubility of the components. They also found that if the co-former solubility is approximately 10-fold higher than the API, this generally leads to a co-crystal form which has a higher solubility than the API.

Table 2.2 Component solubilities and co-crystal solubilities (Good and Rodríguez-Hornedo 2009).

Co-crystal (drug – co-former)	***A*:*B* co-crystal stoichiometry (drug − co-former)**	**Solvent**	$S_{\text{co-former}}$ **(M)**	S_{drug} **(M)**	**Co-crystal solubility (M)**
CBZ-MLN	2:1	water	$1.5 \times 10^{+1}$	4.6×10^{-4}	5.9×10^{-3}
CBZ-GTA	1:1	water	$1.0 \times 10^{+1}$	4.6×10^{-4}	5.4×10^{-2}
CBZ-NCT	1:1	water	7.5×10^{0}	4.6×10^{-4}	7.0×10^{-2}
THP-NCT	1:1	water	7.5×10^{0}	3.1×10^{-2}	4.5×10^{-1}
CBZ-OXA	2:1	water	1.3×10^{0}	4.6×10^{-4}	1.3×10^{-3}
CBZ-SUC	2:1	water	5.4×10^{-1}	4.6×10^{-4}	1.2×10^{-3}
CBZ-SAC	1:1	water	1.8×10^{-2}	4.6×10^{-4}	1.2×10^{-3}

CAF-SLC	1:1	water	1.4×10^{-2}	1.1×10^{-1}	2.9×10^{-2}
THP-SLC	1:1	water	1.4×10^{-2}	3.1×10^{-2}	1.3×10^{-2}
CBZ-SLC	1:1	water	1.4×10^{-2}	4.6×10^{-4}	9.1×10^{-4}
CBZ-GTA	1:1	IPA	3.6×10^{0}	5.0×10^{-2}	2.2×10^{-1}
THP-NCT	1:1	IPA	6.3×10^{-1}	3.0×10^{-3}	4.8×10^{-2}
CBZ-NCT	1:1	IPA	6.3×10^{-1}	5.0×10^{-2}	6.1×10^{-2}
CBZ-SAC	1:1	IPA	1.6×10^{-1}	5.0×10^{-2}	2.0×10^{-2}
CBZ-SUC	2:1	IPA	5.5×10^{-1}	5.0×10^{-2}	8.8×10^{-3}
CBZ-GTA	1:1	EtOH	2.8×10^{0}	1.4×10^{-1}	3.1×10^{-1}
THP-NCT	1:1	EtOH	1.1×10^{0}	1.8×10^{-2}	7.6×10^{-2}
CBZ-NCT	1:1	EtOH	1.1×10^{0}	1.4×10^{-1}	1.5×10^{-1}
CBZ-SAC	1:1	EtOH	2.4×10^{-1}	1.4×10^{-1}	6.5×10^{-2}
CBZ-SUC	2:1	EtOH	8.1×10^{-1}	1.4×10^{-1}	4.5×10^{-2}
CBZ-GTA	1:1	EtOAc	1.0×10^{0}	4.9×10^{-2}	9.4×10^{-2}
CBZ-SAC	1:1	EtOAc	1.8×10^{-1}	4.9×10^{-2}	5.0×10^{-2}
THP-NCT	1:1	EtOAc	1.1×10^{-1}	6.2×10^{-3}	1.4×10^{-2}
CBZ-NCT	1:1	EtOAc	1.1×10^{-1}	4.9×10^{-2}	2.6×10^{-2}
CBZ-SUC	2:1	EtOAc	4.6×10^{-2}	4.9×10^{-2}	2.0×10^{-3}

The solubility of a co-crystal is thought to be determined by the strength of the crystal lattice and the solubility of the individual components (Thakuria et al. 2013). Therefore, one can theoretically alter the solubility of an API by cocrystallisation with a carefully selected co-former, as evidenced in table 2.2. The co-crystal lattice strength/energy has complete control of the solubility when in solvents with a small resistance to solvation or in an ideal

solution where solvent-solute interactions equal those of solvent-solvent interactions. However, drug hydrophobicity plays a major role in determining the aqueous solubility of the co-crystal (Lu et al. 2008). Co-crystals which involve hydrophobic components can have reduced solubilities compared to what would be expected if the solubility was solely calculated from the lattice energy.

Approximately 40% of marketed drugs have low solubility and up to 90% may not make it to market due to solubility issues (Thayer 2010). The data in table 2.3 highlights this problem. Over the past decade, there have been many patent application filings for pharmaceutical co-crystals which possess improved solubility and stability (Miroshnyk et al. 2009). It is clear that co-crystal forms can provide a route for the enhancement of the solubility of APIs and they offer a new hope for poorly soluble drugs.

Table 2.3 Drugs on the market and in the R&D pipeline and their Biopharmaceutics Classification System class (Thayer 2010).

BCS class	Solubility	Permeability	% Drugs on market	% Drugs in R&D pipeline
I	High	High	35	5-10
II	Low	High	30	60-70
III	High	Low	25	5-10
IV	low	low	10	10-20

Cocrystallisation has also been proven as a viable technique for modifying the melting point and thermal stability of APIs (Thakuria et al. 2013). Vishweshwar et al. (2003) reported that the melting point of isonicotinamide

– aliphatic dicarboxylic acid co-crystals exhibited a similar trend to that of the pure co-formers. As they changed the number of diacids from odd to even, the melting point increased. Bond (2006) observed a similar trend with the melting point when studying 2:1 n-alkyl carboxylic acid – pyrazine co-crystals and comparing with the melting point of the pure n-alkyl carboxylic acids. The melting point of the co-formers increased from 285 to 315 Kelvin as the chain length was extended from C1 to C13, while the co-crystal forms had the opposite effect on the melting temperature. Finally, Trask et al. (2005) were able to improve the hydration stability of caffeine by cocrystallising the API with oxalic acid. They achieved “complete stability to humidity over a period of several weeks”.

2.9 NIR spectroscopy

Near infrared spectroscopy played a key role in this study. It was utilised due to its ability to characterise materials in a practical and rapid way. In this section, the background of NIR is discussed along with the PAT applications of this technology.

2.91 Background

The near infrared region of the electromagnetic spectrum is defined as the wavenumber range of 12820 – 3959 cm^{-1} by the American Society of Testing and Materials (ASTM) (ASTM 2012). The earliest reported use of NIR spectroscopy as an analytical tool was in the 1950s. Following the invention of computers that were capable of processing NIR spectra, the technique was expanded and became increasingly popular in various scientific fields (Blanco and Villarroya 2002).

NIR spectroscopy can provide spectra for solid and liquid samples without any pre-treatment of the samples being required (Blanco and Villarroya 2002). It can be used in-line with continuous technologies and it is a rapid technique which can provide multivariate qualitative (Blanco et al. 1998), quantitative (Long 2009), physical and chemical (Reich 2005).

Absorption bands in the NIR spectrum mainly correspond to overtone bands and combination bands of fundamental molecular vibrations. One of the simplest ways of describing the vibration of molecules is by using the harmonic oscillator model (Eq. 2.5) which calculates the energy of the different equally spaced energy levels (Blanco and Villarroya 2002).

$$\boldsymbol{E_{vib}} = \left(\boldsymbol{u} + \frac{\mathbf{1}}{\mathbf{2}}\right) \frac{\boldsymbol{h}}{\mathbf{2}\boldsymbol{\pi}} \sqrt{\frac{\boldsymbol{k}}{\boldsymbol{\mu}}} \qquad \textbf{(Eq. 2.5)}$$

Where u is the vibrational quantum number, μ is the reduced mass of the bonding atoms, and Planck's constant h and the force constant k are used. The harmonic oscillator model only allows transitions between consecutive energy levels which cause the dipole moment to change (Eq. 2.6) (Blanco and Villarroya 2002).

$$\Delta\boldsymbol{E_{vib}} = \Delta\boldsymbol{E_{rad}} = \boldsymbol{hv} \qquad \textbf{(Eq. 2.6)}$$

Where v is the fundamental vibrational frequency of the bond (Which produces an absorption band in the mid IR region). The harmonic oscillator model does not take into account the coulombic repulsion between atoms or even the dissociation of molecular bonds, and therefore it is not an accurate representation of the behaviour of real molecules. Molecular behaviour can be described more accurately by an anharmonic oscillator model. This is

because the energy curve of an oscillating molecule is affected by intramolecular interactions, and therefore the equilibrium position vibrations are non-symmetric. The energy levels are not equally spaced in the anharmonic model (Eq. 2.7) (Blanco and Villarroya 2002).

$$\Delta E_{vib} = hv\,[1 - (2u + \Delta u + 1)y] \qquad \textbf{(Eq. 2.7)}$$

The difference between the energy levels decreases with increasing vibrational quantum number, u. Where y is the anharmonicity factor. The anharmonic nature of the transitions between molecular vibrational energy states gives rise to overtone absorption bands situated at multiples of the fundamental vibrational frequencies.

Combination absorption bands are produced by polyatomic molecules where more than one vibrational mode can interfere with each other and cause simultaneous energy changes. Overtone bands are typically located between 12820 and 5000 cm^{-1} (Wavenumber). Combination bands are typically located between 5263 and 4000 cm^{-1} (Wavenumber) (Blanco and Villarroya 2002).

As the hydrogen atom is the lightest, it exhibits the largest vibrations and the most exaggerated anharmonic behaviour. Common absorption bands that occur in the NIR region are usually overtones and combinations of vibrations of the following functional groups: -CH, -OH, -NH and -SH (Reich 2005). Absorption bands for C=O, C-C and C-Cl are produced in the spectrum but are notably weaker. The frequency and intensity of NIR absorption bands are directly affected by anharmonicity and Fermi resonance.

When two NIR absorption bands of a molecule, which have the same frequency due to possessing a similar energy, do not overlay and sum up with one another but instead split into two peaks of higher and lower frequencies, this is called Fermi resonance (Fermi 1931). Intermolecular hydrogen bonding and dipole interactions must also be considered because they too can alter the vibrational energy states, causing existing absorption bands to shift or creating new ones.

Hydrogen bonding has the same effect of increasing the mass of the vibrating hydrogen atom. This leads to a reduction of mechanical anharmonicity of the hydrogen bond vibration and therefore leads to a reduced absorption intensity of the resulting NIR band (Siesler 2008). This phenomenon is important to this study because hydrogen bonding plays an essential role in forming co-crystals. In conclusion, crystal phases can be successfully determined by using NIR spectroscopy, and small changes to the molecular structure can be observed.

2.92 PAT applications

One of the aims of this study was to develop a co-crystal yield prediction model using NIR. The hope was to gather and analyse spectral data which could provide important co-crystal information. The findings of this model could then eventually be used for future in-line NIR monitoring of pharmaceutical co-crystal manufacturing techniques such as hot melt extrusion. NIR spectroscopy provided an accurate characterisation technique which could be used to reach this goal due to its inherent advantages over other methods as discussed in section 2.91.

NIR spectroscopy has important implications for PAT tools. In 2004, the US Food and Drug Administration (FDA) published a PAT guidance document called “PAT – A Framework for Innovative Pharmaceutical Development, Manufacturing, and Quality Assurance” (Afnan 2004). It was designed to encourage the voluntary development and implementation of innovative technologies in the pharmaceutical sector which are effective and efficient. The report recommended using analytical techniques to help understand manufacturing processes to ensure quality and consistency.

In 2008, a conference on harmonisation was held in Geneva, Switzerland where it was concluded that PAT tools were an opportunity for more flexible regulatory approaches for pharmaceuticals (ICH 2008a). The conference also encouraged the use of quality by design (QbD) which encompasses PAT tools (ICH 2008b).

The PAT approach involves understanding a process or technique combined with the analysis and monitoring of the process, usually in real-time. The objective is to guarantee acceptable final product quality using a defined methodology. It allows research groups to control, adapt and fix processes more quickly and efficiently instead of only analysing the end product and making their decisions from further down the line (Read et al. 2010).

Kelly et al. (Kelly et al. 2012) demonstrated in 2012 that NIR can be used as an in-line PAT tool during the formation of ibuprofen - nicotinamide co-crystals using hot melt extrusion. The team were able to identify key band shifts and band formations relating to the co-crystal form; particularly in the region 5200-4700 cm^{-1}, when comparing the spectra of processed samples

to the 1:1 physical mixture of the starting components. Similarly, Moradiya et al. (2014) used NIR for in-line characterisation during the HME of carbamazepine - cinnamic acid co-crystals allowing for the determination of the position along the extruder barrel where co-crystal formation commenced by identifying key NIR band shifting.

A case study, in 2014, using furosemide - adenine co-crystals was used to demonstrate a chemometric assisted NIR spectral analysis method with principal component analysis (PCA) which was able to pinpoint cocrystallisation nucleation and solvent evaporation events during a solvent evaporation method (Sarraguça et al. 2014). From this case study, further studies were conducted by Sarraguça et al. where they monitored cocrystallisation using NIR spectroscopy for furosemide - nicotinamide and furosemide - *p*-aminobenzioc acid co-crystals during a solvent evaporation technique (Sarraguça et al. 2015, Sarraguça et al. 2015). Carbamazepine - saccharin co-crystals (Lee et al. 2015) and indomethacin - saccharin co-crystals (Chun et al. 2014) have also been monitored during antisolvent cocrystallisation using NIR spectroscopy.

CHAPTER 3 MATERIALS AND METHODS

3.1 Materials

Carbamazepine form III (Figure 3.1) was purchased from Sigma Aldrich. It has the chemical formula $C_{15}H_{12}N_2O$ and molecular weight 236.27 g/mol.

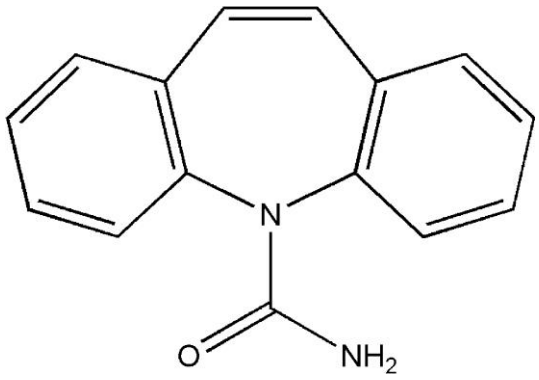

Figure 3.1 Carbamazepine diagram (Kelly and Rodríguez-Hornedo 2009).

Racemic ibuprofen (Figure 3.2) was purchased from Sigma Aldrich. It has the chemical formula $C_{13}H_{18}O_2$ and molecular weight 206.28 g/mol.

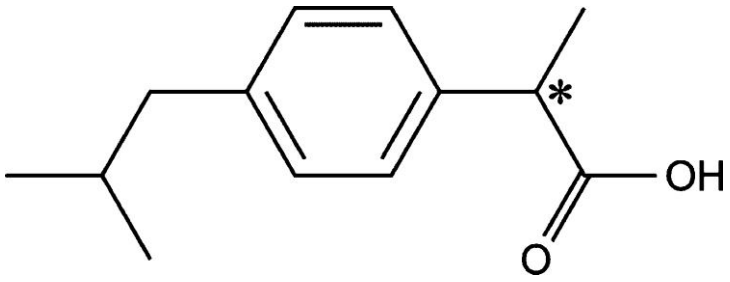

Figure 3.2 Ibuprofen diagram (Williams et al. 2012).

Nicotinamide (Figure 3.3) was purchased from Sigma Aldrich. It has the chemical formula $C_6H_6N_2O$ and molecular weight 122.12 g/mol.

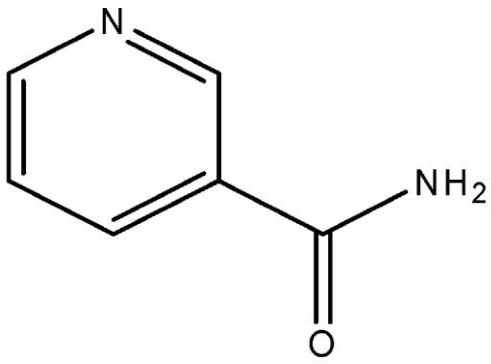

Figure 3.3 Nicotinamide diagram (Chiarella et al. 2007).

Salicylic acid (Figure 3.4) was purchased from Sigma Aldrich. It has the chemical formula $C_7H_6O_3$ and molecular weight 138.12 g/mol.

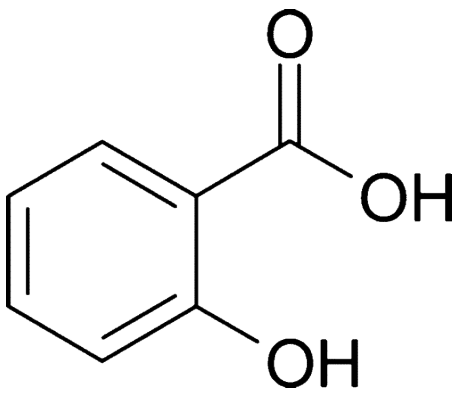

Figure 3.4 Salicylic acid diagram (Nordström and Rasmuson 2006).

Caffeine (Figure 3.5) was purchased from Sigma Aldrich. It has the chemical formula $C_8H_{10}N_4O_2$ and molecular weight 194.19 g/mol.

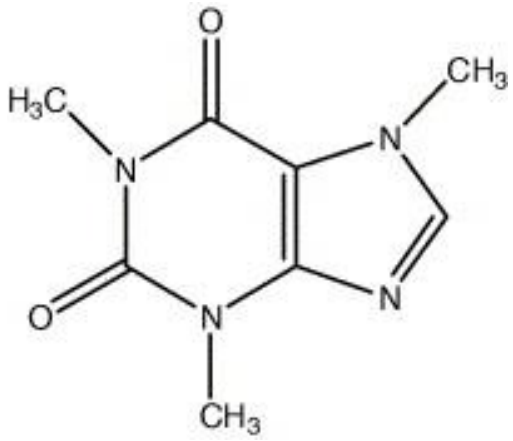

Figure 3.5 Caffeine diagram (Pinto and Diogo 2006).

Maleic acid (Figure 3.6) was purchased from Sigma Aldrich. It has the chemical formula $C_4H_4O_4$ and molecular weight 116.07 g/mol.

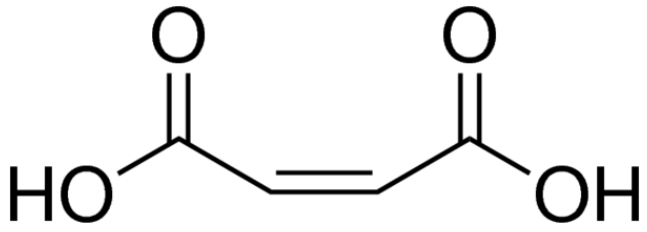

Figure 3.6 Maleic acid diagram (Database 2016).

All the above materials were a minimum of 98% purity. No further purification of the materials was performed. The solvents used for solution crystallisation were ethanol (99% analytical grade) and methanol (99% analytical grade).

3.2 Preparation of ibuprofen – nicotinamide co-crystals

Solvent mediated co-crystallisation was carried out using a microwave reactor (Monowave 300, Anton Paar GmbH, Austria). 1:1 equimolar weights of ibuprofen and nicotinamide, totalling 0.820 g, was mixed with 82 µL of diluted water in a 30 mL capacity glass tube. The temperature was set to

80°C and samples were subjected to microwave irradiation with a holding time of 5 minutes and were then cooled at 10°C/min to 40°C and held for 1 minute. For chapter 6, the preparation of this co-crystal was carried out by the PhD student Abdolati Alwati. The resulting co-crystal molecular structure is shown in figure 3.7.

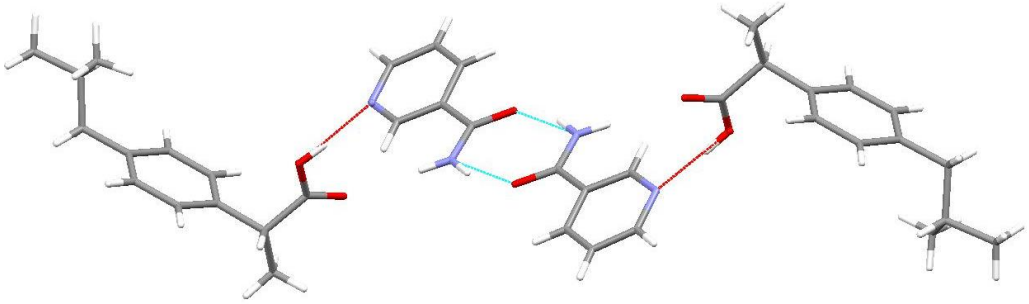

Figure 3.7 1:1 IBU-NIC co-crystal molecular structure. Hydrogen bonding is shown by light blue and red dashed lines. Source: Fleischman et al. (Fleischman et al. 2003) via Cambridge Structural Database (Allen 2002).

The hydrogen bonding patterns are well documented for the 1:1 IBU-NIC co-crystal. The racemic ibuprofen binds to nicotinamide via an acid-pyridine motif, before a pair of dimers come together through an amide-amide motif between the nicotinamide molecules. Finally an amide-acid motif forms between the nicotinamide and the ibuprofen to create a 'supramolecular macrocycle structure' (Blagden et al. 2008).

3.3 Preparation of carbamazepine – nicotinamide co-crystals

Solvent evaporation was carried out based on the method reported by Shayanfar et al. (2014) in 2014. 1:1 equimolar weights of carbamazepine (2.363 g, 0.01 mol) and nicotinamide (1.221 g, 0.01 mol) were dissolved in

20 mL of absolute ethanol. The mixture was gently heated and manually stirred with a glass rod for 30 minutes. The mixture was then left for 72 hours at room temperature to allow for evaporation of the solvent. The resulting co-crystal molecular structure is shown in figure 3.8.

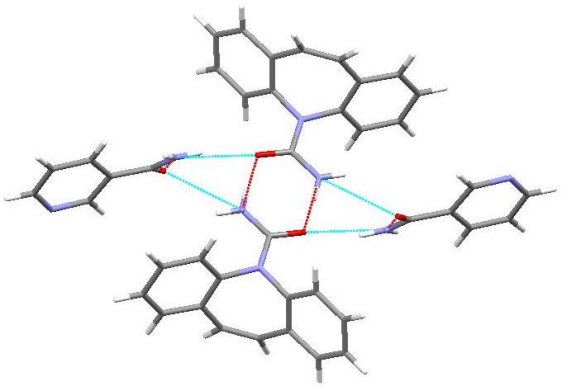

Figure 3.8 1:1 CBZ-NIC co-crystal molecular structure. Hydrogen bonding is shown by light blue and red dashed lines. Source: Berry et al. (Berry et al. 2008) 2008 via Cambridge Structural Database (Allen 2002).

In this 1:1 co-crystal, a translation related hydrogen-bonding pattern exists between the nicotinamide molecules and the carbamazepine molecules. The donors and acceptors of both amide groups are fulfilled but the nitrogen atom within the ring structure of nicotinamide does not form any strong hydrogen bonds. The crystal packing suggests hydrophobic interlocking rows with π…π interactions between the carbamazepine and the nicotinamide rings (Fleischman et al. 2003).

There are reported studies which suggest there are other polymorphic forms of the 1:1 carbamazepine – nicotinamide co-crystal (Seefeldt et al. 2007, Porter III et al. 2008), however these forms are thought to be unstable and

can only form under specially controlled conditions. In this thesis, there was no indication of this alternative polymorphic form when observing the powder X-ray diffraction characterisation of samples.

3.4 Powder X-ray diffraction

X-ray scattering occurs when an X-ray is absorbed by an atom and excites another electron within that atom and the incident energy is then re-irradiated. Coherent scattering (Elastic) occurs when the incident X-ray photon changes direction when it comes into contact with an atom and none of its energy is transferred to an electron. Finally, incoherent scattering is when some energy from the incident X-ray photon is lost when it collides with the atom and the emitted X-ray has a lower energy and becomes out of phase with the incident X-ray. In any case, waves scattering from one or more objects will expand in space until they come in contact with each other, causing constructive or destructive interference. A periodic array of molecules within a crystal that coherently scatter radiation, and as a result cause constructive interference at certain angles, is called diffraction (Giacovazzo 2002).

The diffraction of a crystal phase is unique because the angles of diffraction are directly affected by the periodic arrays within the lattice. Bragg's law explains this phenomenon in figure 3.9. In Bragg's law, the crystallographic planes are described by Miller indices h, k and l. The incident X-rays are monochromatic and in phase with one another and they reflect from different crystallographic planes within the crystal lattice. In figure 3.9, the X-ray that interacts with the lower plane has to travel further than the one above it and

this difference is equal to the wavelength (λ) and causes constructive interference. Similarly, if an X-ray interacted with a third plane, the extra distance travelled will be equal to 2λ (Klug and Alexander 1974).

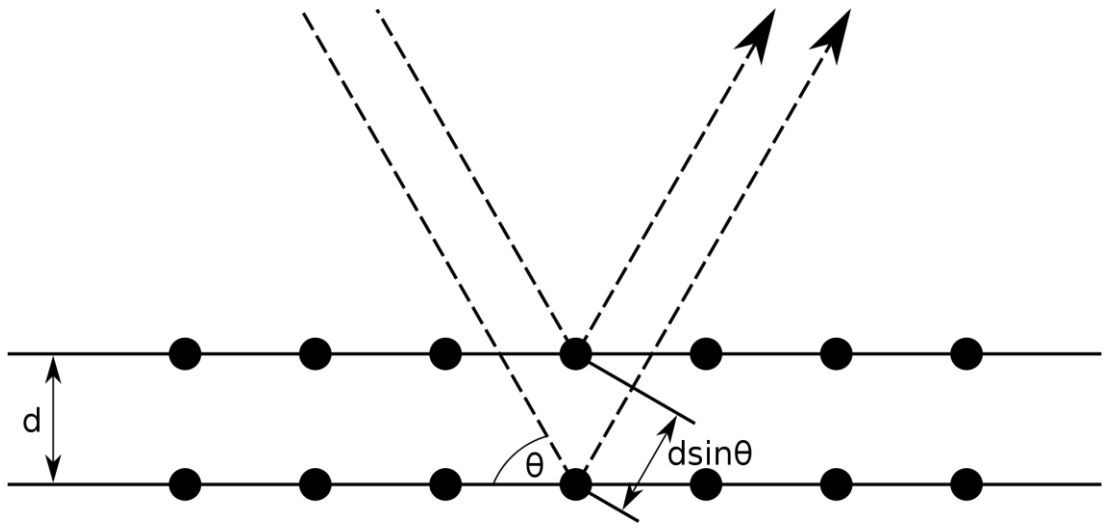

Figure 3.9 Bragg's law analogy. Two crystallographic planes are shown with spacing, d. Also two incident X-rays are drawn to show coherent scattering and their incident angle, theta (θ) (Adapted from (Giacovazzo 2002)).

This theory leads to the Bragg equation (Eq. 3.1):

$$n\lambda = 2d_{hkl}\sin\theta \qquad \textbf{(Eq. 3.1)}$$

Where n is the plane, λ is the wavelength, dhkl is the distance between the planes and θ is the incidence angle of the X-ray beam.

In this study, the crystallinity of the raw and extruded material was determined using a Bruker D8 X-ray diffractometer provided by the Analytical Centre at the University of Bradford. Scans from 2-40° (2θ) with a 0.01° step width and a 1s time count were carried out for most samples using CuKα1 radiation (1.5406 Ang wavelength). The receiving slit was 1° and the

scattering slit, 0.2°. The diffracted X-rays were collected by a detector and were arranged into a 2 dimensional pattern showing the position (2θ) and intensity of each reflection. The composition of the powder was predicted by comparing the obtained peaks to X-ray diffraction data for known molecules.

3.5 Differential scanning calorimetry

Differential thermal analysis involves two thermometers attached by a thermocouple, where one thermometer is used as a reference while the other measures the temperature of a sample. The difference between the temperature of the reference and the sample provides thermal information about the sample (Richardson and Charsley 1998). Differential scanning calorimetry (DSC) measures the difference in the heat flow instead of the difference in temperature and a simple diagram of a DSC arrangement is shown in figure 3.10.

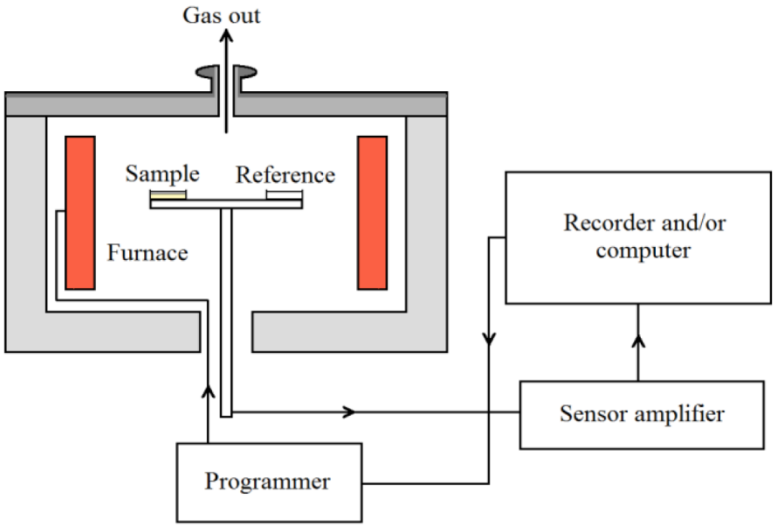

Figure 3.10 A simplified diagram of differential scanning calorimetry.

For all thermal analysis studies, including modulated DSC, samples with a typical mass between 3 mg and 8 mg, were subjected to heating profiles

using a Q2000 Differential Scanning Calorimeter (Thermal Analysis Instruments, UK). The standard heating profile used was a temperature ramp typically starting from 40°C, the end temperature varied depending on the material being analysed. The default heating rate used was 10°C/min unless otherwise specified. As the temperature increased, the heat flow was recorded in mW and was converted to W/g in most cases. This technique was able to accurately determine the melting point of each individual material, as well as obtain the eutectic point for the co-crystal pairs studied.

3.6 Scanning electron microscopy

SEM images were taken using an FEI Quanta 400 Scanning Electron Microscope (Cambridge, UK) under a high vacuum using an acceleration voltage of 20 kV and spot size 3.0. The accompanying software was XTM microscope control software version 2.3. Samples were mounted on aluminium pin-stubs (Agar Scientific, Stansted, UK) using self-adhesive carbon stickers (Agar Scientific) and were coated with a layer of gold approximately 30 nm thick. The stubs were then placed on the SEM stage before being placed under a vacuum. The objective of using scanning electron microscopy was to observe the particle morphology of the individual materials and the co-crystals manufactured using hot melt extrusion and solution crystallisation.

3.7 Model shear deformation

Rheology is the study of the flow and the deformation of matter and in theory, it can be used experimentally to predict and understand the effect of shear stress and shear strain on a material. Quantitative measurements of viscosity

or other rheological values from rheological experiments is only possible if studying suitable materials such as polymers or liquids. In this study, solid pharmaceutical powders were used. So collecting typical rheological data was not possible.

Nonetheless, a rotational rheometer can be used as an instrument which can apply a known amount of shear to a variety of materials, including solid powders. It can also heat and cool the material to a range of temperatures whilst applying the shear.

In order to investigate the effect of shear force on co-crystal formation in this study, model shear deformation experiments, using a rotational rheometer, were designed. Model shear deformation was performed using an Anton Paar MCR rheometer equipped with parallel bottom and top plates (25 mm diameter). The heating and cooling rate used for all samples was 20°C/min. The top temperature was held for 10 minutes to mimic the time the material would spend, on average, inside the extruder barrel during extrusion. Different levels of strain were applied during the heating, hold and cooling of the sample and the direction of shear was set to oscillation mode, therefore, once the strain limit had been reached the direction would reverse. The oscillatory mode was chosen over the continuous mode in an attempt to keep as much of the material in contact with the upper and lower rheometer plates as possible during the applied shear.

For the ibuprofen – nicotinamide pair in chapter 4, the maximum temperatures used were 70, 80 and 90°C with a holding time of 10 minutes.

The strain was set to 0, 25, 50, 75, 100, 200 and 300% and the heating/cooling rate was 20°C/min.

By varying the temperature at which shear is applied to the material, and by changing the strain limit, the effect of both parameters on the co-crystal yield can be discovered. The results can then be compared to what is observed when using hot melt extrusion and can be used to determine the effect of shear on co-crystal formation.

3.8 Twin screw, hot melt extrusion

The hot melt extrusion technique provided a base technology for continuous cocrystallisation. A 16 mm co-rotating twin screw extruder (Pharmalab, Thermo Scientific, UK) with a length-to-diameter ratio of 40:1 was used and was operated without a die. The die was not necessary when extruding the powder materials because under high temperatures, the die can clog up and can prevent the material from being extruded. The powder materials were fed into the extruder at an approximate rate of 0.2 Kg/h by hand into a feeding funnel. Typically, 10-20 g of material was used per extrusion run. Several different temperature profiles, screw geometries and screw speeds were used to improve the co-crystal yield and were designed around the thermal data gathered for the subject materials.

3.81 Temperature profiles

Table 3.1 displays the temperature profiles used during hot melt extrusion of all materials in this study. The temperature codes indicate the maximum temperature achieved along the extruder barrel, for example, T140 describes

the temperature profile which started at 25°C at zone 2, reached 140°C at zone 7-8 and ended on 125°C at zone 10. For this project, the maximum temperature for each profile was positioned at zone 7 and zone 8 to allow for gradual heating from zone 2, whilst allowing for a slight decrease in the temperature towards the end of the extruder barrel.

Table 3.1 Temperature profiles for hot melt extrusion. Each zone represents a controlled heating area along the extruder barrel. The code indicates the maximum temperature.

Code	**Temperature (°C)**								
	Zone 2	Zone 3	Zone 4	Zone 5	Zone 6	Zone 7	Zone 8	Zone 9	Zone 10
T80	25	40	50	70	75	80	80	80	70
T90	25	40	50	75	80	90	90	80	80
T110	25	40	60	85	100	110	110	100	100
T120	25	40	60	85	105	120	120	110	110
T125	25	40	70	90	120	125	125	120	110
T130	25	40	80	110	125	130	130	125	120
T135	25	50	100	120	130	135	135	130	120
T140	25	50	100	125	135	140	140	135	125
T150	25	60	110	135	145	150	150	145	135

A range of temperatures for each co-crystal pair where used to monitor the effect of temperature on the co-crystal yield. The majority of the temperature profiles used were purposely designed to heat the material in the extruder barrel beyond the eutectic point of the system.

3.82 Screw Geometry

There were two screw geometries adopted for this study: screw geometry A and screw geometry B. Images of each screw geometry are shown in figure 3.11. Screw geometry A is a basic design featuring one mixing zone. This mixing zone consists of kneading screw elements angled at 30, 60 or 90° and is designed for mixing the material in the barrel at zone 7 and zone 8. Screw geometry B is a more complex screw geometry. It features three separate mixing zones positioned between zone 5 and zone 8. Screw geometry B provides more mixing capacity than geometry A and it also provides some dispersive mixing zones (0°) as opposed to only staggered mixing in geometry A. The two geometries were chosen to study the effect of different levels of mixing and shear applied to the material as it is conveyed along the extruder barrel. Figure 3.12 displays the individual screw components used to build a screw geometry and a detailed list of the components used to make each screw along with their relative length is shown in table 3.2. Finally, figure 3.13 is an image of the extruder barrel where the individual barrel zones have been labelled in pen.

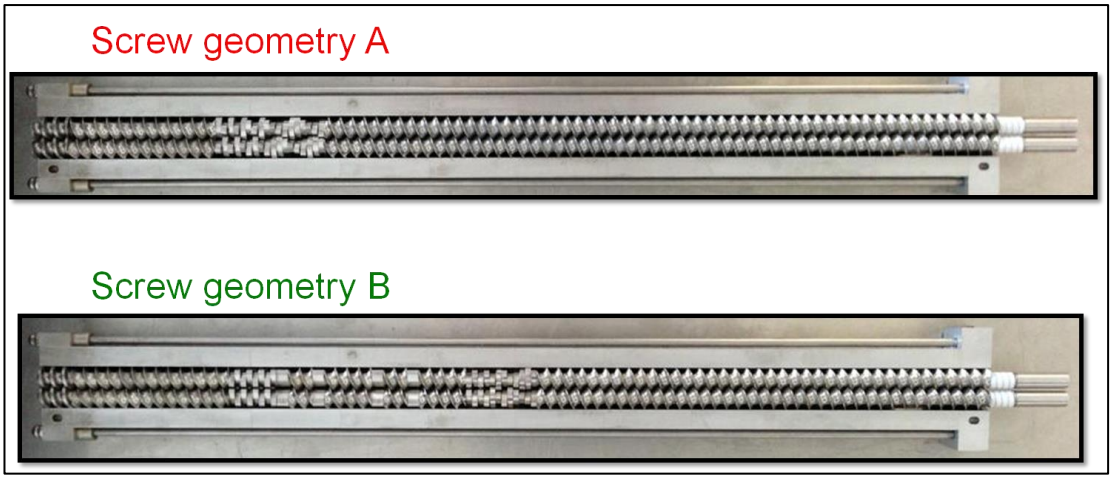

Figure 3.11 Photographs of screw geometry A and B situated in an open extruder barrel.

Figure 3.12 Individual screw components used for screw geometries A and B. Forward conveying screw (Left), broad end kneading component (Centre), narrow end kneading component (Right).

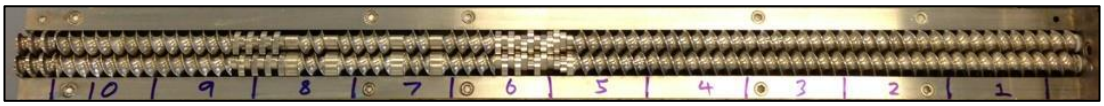

Figure 3.13 Extruder barrel zones marked in pen. Zone 1 is where the material is fed into the barrel.

Table 3.2 A list of screw components in order from zone 1 to zone 10 of the extruder barrel for screw geometries A and B. The relative length of each component is also stated.

Screw Geometry A		Screw Geometry B	
Length (D)	Component	Length (D)	Component
28	Forward conveying	19	Forward conveying
2.25	30° kneading	1	30° kneading
1.25	60° kneading	1	60° kneading
1	90° kneading	1	90° kneading
6	Forward conveying	2	Forward conveying
1.5	Discharge	0.5	0° kneading
		1	Forward conveying
		0.5	0° kneading
		2	Forward conveying
		0.5	0° kneading
		1	Forward conveying
		0.5	0° kneading
		2	90° kneading
		6.5	Forward conveying
		1.5	Discharge

3.83 Screw speed

The Pharmalab twin screw extruder can achieve speeds in excess of 200 rpm, however for this study, a long residence time for the material was key for cocrystallisation, thus only slow speeds were used. Screw speeds of 10, 20 and 30 rpm were chosen. A screw speed of 10 rpm provided a long residence time of the material in the extruder barrel, whereas the screw speed of 30 rpm provided increased shear intensity but a shorter residence

time. Different screw speeds were used to work out how the compromise between residence time and shear intensity effects the co-crystal yield.

3.9 Near infrared spectroscopy

A powerful characterisation technique was required for many different experiments throughout this study. NIR provided an accurate characterisation technique which could meet this goal. Off-line NIR spectra were collected using an Antaris II NIR spectrometer (Thermo Scientific, UK). Scans were carried out over the wavenumber range 4000-10,000 cm^{-1} (2500-1000 nm wavelength) using the RESULT software by Thermo Scientific. Each scan provided an average of 32 individual spectra taken with a resolution of 8 cm^{-1}. The material was loaded into a glass vial and placed on top of the glass window on the spectrometer. NIR was mainly used for characterisation purposes in chapters 4 and 5. However, it also provided an accurate way of predicting the co-crystal yield in the samples in chapter 6.

The prediction models created in chapter 6 were made by using the NIR spectra of standard samples. For the ibuprofen – nicotinamide pair, a PLS regression model was designed using a set of standard samples consisting of a mixture of 1:1 IBU-NIC co-crystal and pure ibuprofen. The PLS model for the carbamazepine – nicotinamide pair was designed using a set of standard samples consisting of a mixture of 1:1 CBZ-NIC co-crystal and pure carbamazepine. The pure co-crystals used for the calibration and validation samples were made using the methods described in sections 3.2 and 3.3. The validation samples were made from a separate batch of co-crystal to the calibration samples for both co-crystal pairs, they were not used to create the

PLS models, but they were used to validate the models. The concentration of the calibration samples ranged from pure ibuprofen/carbamazepine (0%) to 100% 1:1 co-crystal with standards made at concentrations of 5% increments in between, totalling 20 calibration samples. Validation samples were made at the following concentrations: 2.5, 7.5, 12.5, 17.5, 27.5, 37.5, 52.5, 62.5, 72.5 and 92.5% 1:1 co-crystal, totalling 10 validation samples.

CHAPTER 4 UNDERSTANDING CO-CRYSTAL FORMATION

This chapter was designed to focus on the fundamental characteristics of co-crystal formation for several different co-crystal pairs. It was vital to understand the behaviour of the physical mixtures and the co-crystal forms because this would provide important data to cross reference with the extrusion experiments in chapter 5 and future work.

The chapter focuses on a range of characterisation techniques such as DSC, modulated DSC, light microscopy equipped with a hot stage and a shear cell mounts, and rheometry. Several different pharmaceutical pairs were chosen for investigation. All were previously known to form stable co-crystals. The following pairs that were investigated were ibuprofen – nicotinamide, carbamazepine – nicotinamide, nicotinamide – salicylic acid and caffeine – maleic acid. The pharmaceutical pairs were chosen according to their availability at the time and their pharmaceutical importance, particularly ibuprofen – nicotinamide and carbamazepine – nicotinamide.

The knowledge gathered from the ibuprofen – nicotinamide and carbamazepine – nicotinamide studies was used to guide the extrusion experiments carried out in chapter 5, the thermal data was particularly important for designing the extrusion experiments.

4.1 Carbamazepine – nicotinamide thermal analysis

Standard DSC ramps of carbamazepine and nicotinamide were carried out at two different heating rates of 5°C/minute and 10°C/minute. The resulting thermograms for carbamazepine are shown in figure 4.1.

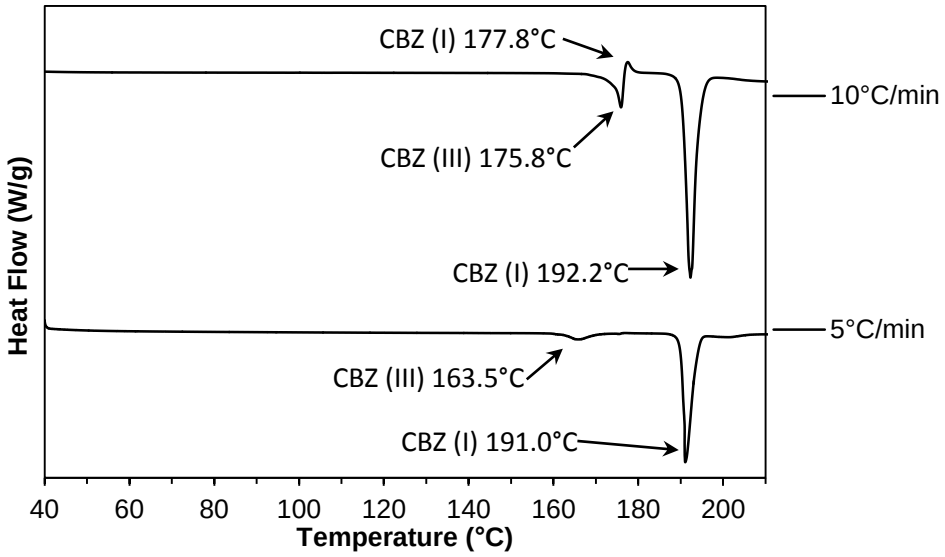

Figure 4.1 DSC thermograms of carbamazepine (Form III) using heating ramps of 5°C and 10°C per minute.

The thermograms display the difference in the behavior of carbamazepine between the two heating rates. The 5°C/min thermogram had a broad endothermic peak at 163.5°C (T_m CBZ (III)) followed by a sharp endothermic peak at 191.0°C (T_m CBZ (I)). The 10°C/min thermogram had an endothermic peak at 175.8°C (T_m CBZ (III)) immediately followed by a small exothermic peak at 177.8°C (Crystallisation of CBZ (I)) and then displays a sharp endothermic peak at 192.2°C (T_m CBZ (I)). The standard DSC ramps for nicotinamide are shown in figure 4.2.

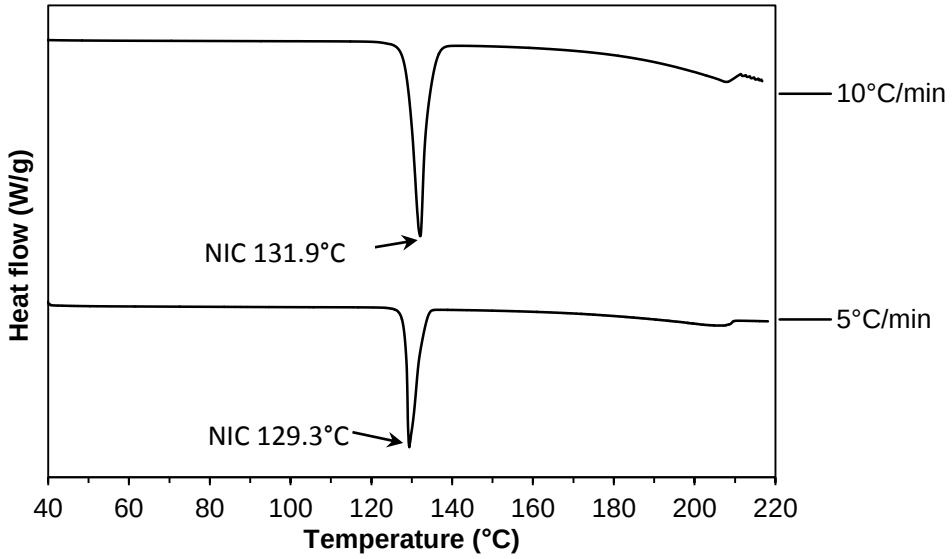

Figure 4.2 DSC thermograms of nicotinamide using heating ramps of 5°C and 10°C per minute.

For nicotinamide, the thermograms show very little difference when using the two heating rates of 5°C and 10°C per minute. The 5°C/min thermogram has an endothermic peak at 129.3°C (T_m NIC) and the 10°C/min thermogram has an endothermic peak at 131.9°C (T_m NIC).

The impact of the heating rate on the melting temperature of carbamazepine is important because the melting point is significantly reduced under slower heating rates. Therefore slower heating rates could improve thermal manufacturing methods of materials where carbamazepine is present because they could allow for processing at lower temperatures. Processing materials at lower temperatures has many benefits including reduced energy consumption, however it may also prevent decomposition of pharmaceutical materials which is very important if materials are to meet acceptable standards for market.

4.2 Carbamazepine – nicotinamide modulated DSC

Modulated DSC is a technique where the temperature is modulated compared to a normal linear temperature profile. The technique can locate and distinguish reversible and non-reversible melting and crystallisation events. It also provides a more realistic melting point by delivering improved accuracy and sensitivity compared to conventional DSC (Reading, Luget et al. 1994).

Modulated DSC was used to analyse carbamazepine – nicotinamide physical mixture samples with the following molar ratios: 1:9, 2:8, 3:7, 4:6, 5:5, 6:4, 7:3, 8:2 and 9:1. A standard heating rate of 5°C/min was used with a set modulation of 2°C every 60 seconds. The resulting thermograms are shown in figure 4.3.

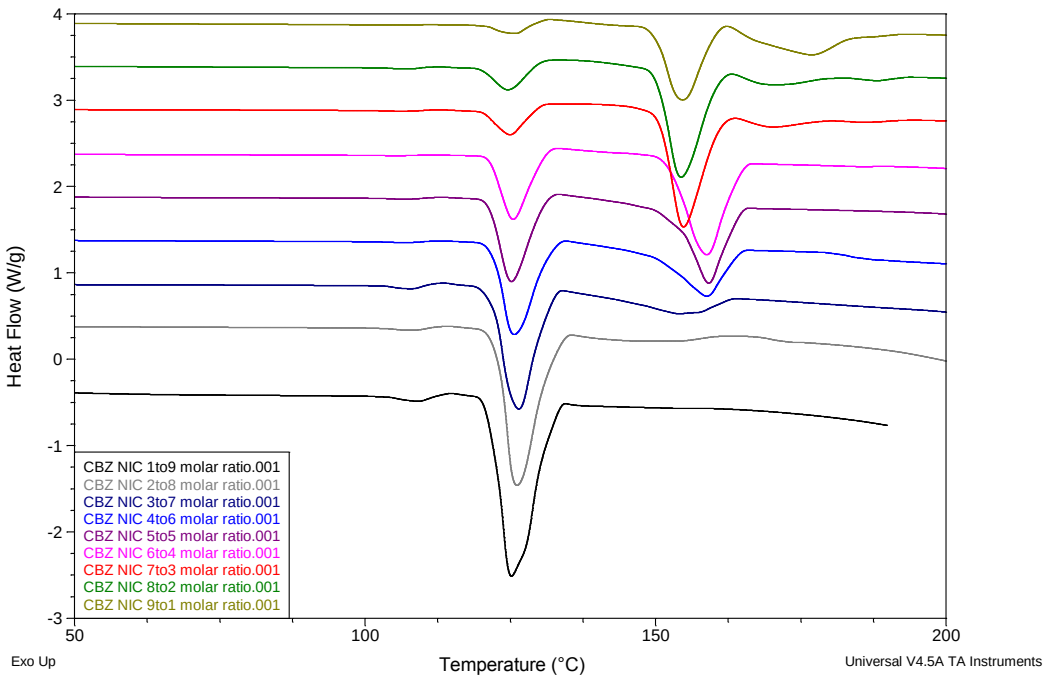

Figure 4.3 Modulated DSC thermograms of carbamazepine – nicotinamide physical mixtures at different molar ratios.

The endothermic and exothermic peak and onset temperatures are shown in table 4.1 along with the integrated energies.

Table 4.1 Endothermic and exothermic events with the corresponding onset and peak temperatures and the integrated energies.

CBZ - NIC molar ratio	First endotherm			Second endotherm			Third endotherm		
	Onset (°C)	Peak (°C)	Energy (J/g)	Onset (°C)	Peak (°C)	Energy (J/g)	Onset (°C)	Peak (°C)	Energy (J/g)
1 to 9	104.1	109.1	3.13	121.8	124.1	168.40			
2 to 8	103.8	108.1	1.26	122.9	126.1	139.70			
3 to 7	103.4	107.8	1.71	122.0	126.4	106.90	143.3	154.0	26.89
4 to 6	102.9	106.3	0.47	122.1	125.6	81.92	150.0	158.8	55.65
5 to 5	102.9	106.5	0.63	121.3	125.1	68.65	153.4	159.1	71.77
6 to 4	102.1	105.7	0.17	121.3	125.5	52.00	152.7	158.7	99.11
7 to 3	103.7	106.3	0.26	120.2	125.0	20.48	150.8	154.7	98.90
8 to 2	103.5	107.2	0.49	120.0	124.7	20.23	150.3	154.3	94.57
9 to 1	102.4	106.1	0.09	120.4	125.9	9.96	149.9	154.6	68.60

The results from the modulated DSC experiment firstly show that the relatively small endothermic peak between 105°C and 109°C has a higher integrated energy for the physical mixture ratios of 3:7, 2:8 and 1:9, compared to the ratios of 4:6, 5:5, 6:4. 7:3, 8:2 and 9:1. This suggests this endothermic event is affected by higher concentrations of nicotinamide. The second endothermic peak between 124°C and 126°C significantly increases in the integrated energy as the amount of nicotinamide is increased. This would make sense as this melting endotherm is the eutectic melting point which is thought to be heavily influenced by nicotinamide which has the lower melting point of the two components. The third endotherm between

154°C and 159°C experiences a shift towards a lower melting temperature from the ratio of 6:4 to the ratio of 7:3. This significant shift is caused by a higher concentration of carbamazepine. The modulated DSC technique provided important thermal data for the carbamazepine – nicotinamide pair.

There is an additional endothermic event experienced for the ratios of 7:3, 8:2 and 9:1 between 170-190°C. This could be due to excess carbamazepine which has transformed into carbamazepine form I and subsequently melted.

4.3 Carbamazepine – nicotinamide phase diagram

Following on from the modulated DSC data gathered in section 4.2, a simple carbamazepine – nicotinamide binary phase diagram was created using modulated DSC data. The eutectic melting point, 1:1 co-crystal melting point and carbamazepine form I melting point for each mol fraction of carbamazepine are plotted in figure 4.4. Also included in the graph are the melting points for pure carbamazepine (Form III and form I) and nicotinamide.

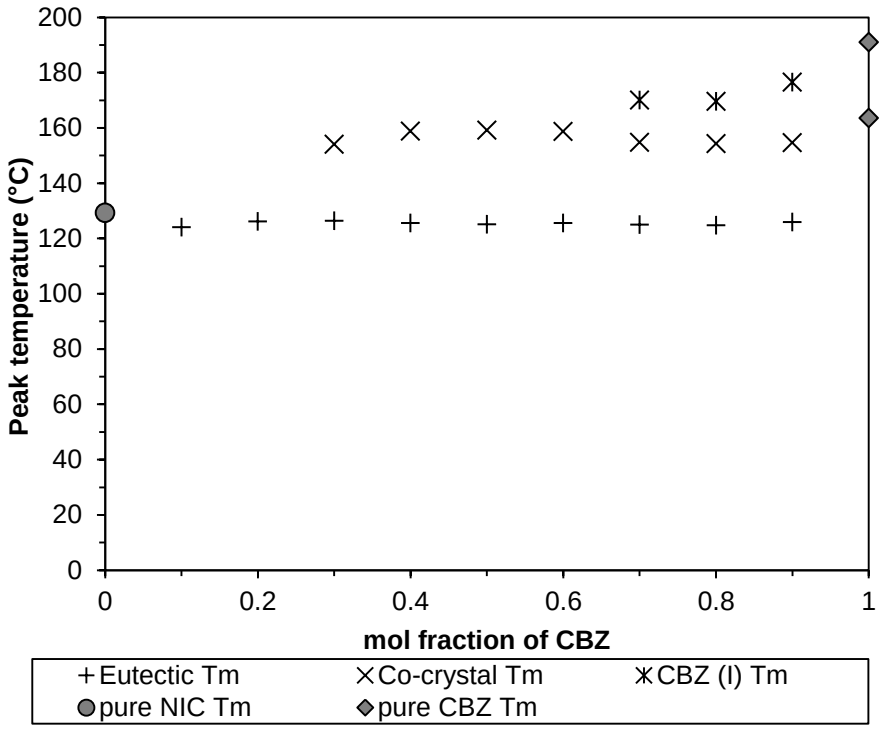

Figure 4.4 Modulated DSC melting temperatures for 1:1 physical mixture (Eutectic), 1:1 co-crystal and carbamazepine form I plotted for each mol fraction of carbamazepine.

The eutectic, 1:1 co-crystal and carbamazepine form I integrated melting peak energies are plotted in figure 4.5. The integrated energies are directly influenced by the amount of material associated with each peak, so a larger integrated energy suggests a larger amount of material has undergone a transformation at that particular temperature.

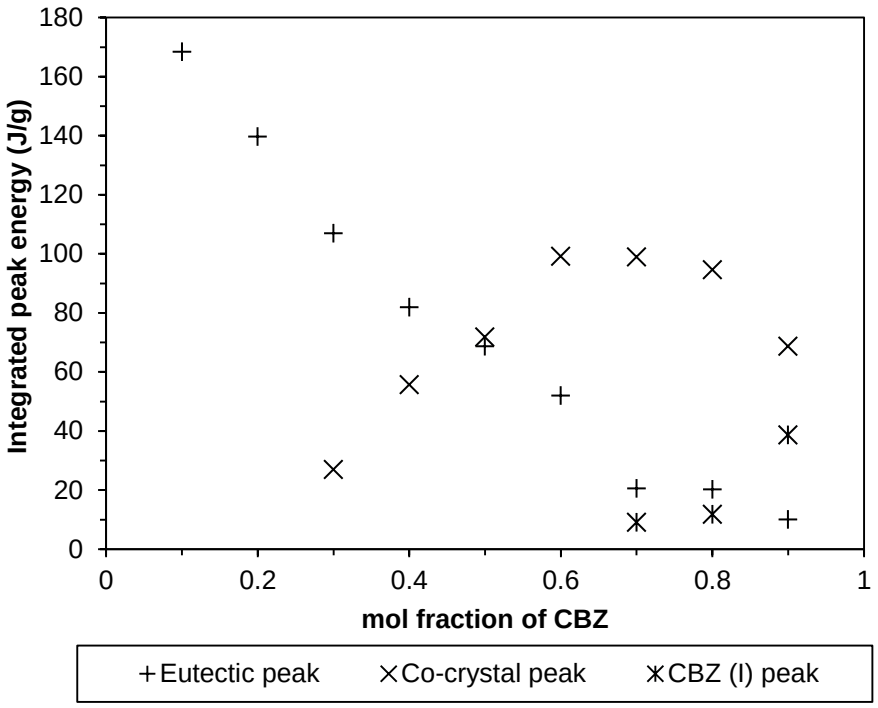

Figure 4.5 Modulated DSC integrated melting peak energies for 1:1 physical mixture (Eutectic), 1:1 co-crystal and carbamazepine form I plotted for each mol fraction of carbamazepine.

The energies in figure 4.5 confirm that as the mol fraction of carbamazepine is increased, the integrated energy for the eutectic melting peak reduces. The integrated energy for the 1:1 co-crystal melting peak increases with the mol fraction of carbamazepine before reducing from 0.7 to 0.9 mol fraction of carbamazepine due to an increased amount of carbamazepine form I.

Using the endotherm melting temperatures, a simple binary phase diagram according to the mol fraction of carbamazepine was constructed and is shown in figure 4.6. The phase diagram indicates the eutectic temperatures and each phase was labelled according to the DSC data. The curves have

not been calculated but are simply a prediction of where the real curves would lie.

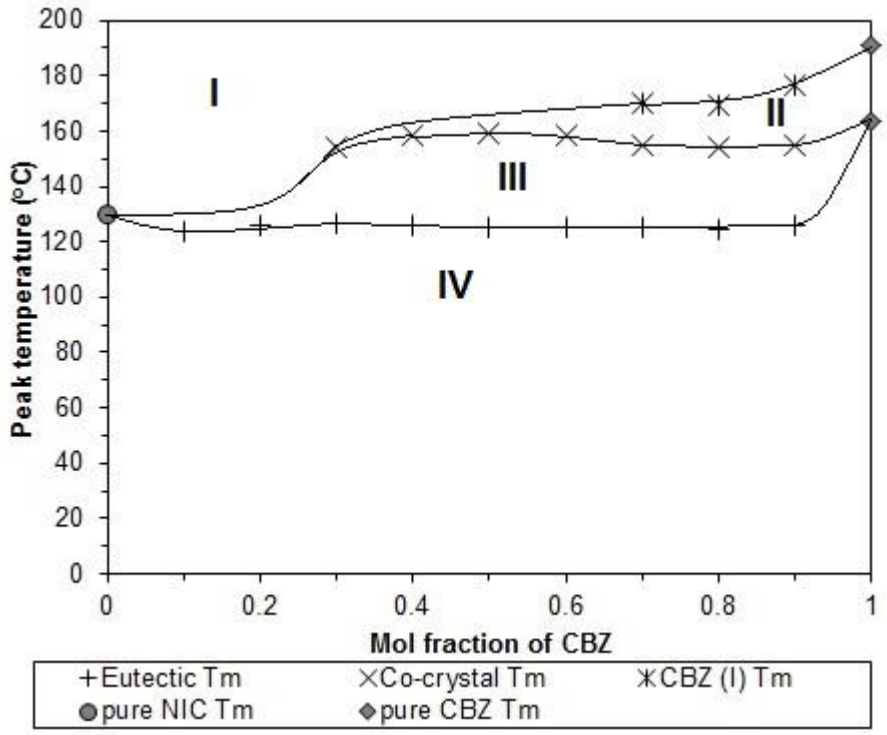

Figure 4.6 A simple carbamazepine – nicotinamide binary phase diagram plotted using the modulated DSC data.

Phase I is where the material has experienced a full melt. Phase II is where solid carbamazepine form I is present plus the liquid phase. Phase III is where the co-crystal forms after the eutectic melting of the physical mixture. Phase IV is the solid physical mixture of carbamazepine and nicotinamide. It is interesting to note that the eutectic melting temperature is slightly raised between 0.4 and 0.6 mol fraction of carbamazepine.

4.4 Model shear deformation studies

4.41 Introduction

An integral part of this project was to understand the effect of shear on co-crystal formation. Shear force is experienced by materials as they are extruded using twin screw extrusion. Therefore it was vital to understand the behaviour of co-crystal formation under shear using several different techniques.

An initial hot stage microscopy technique was used to explore the hot stage equipment and to view individual ibuprofen and nicotinamide crystals and their co-crystal form. This experiment provided an opportunity to set up the light microscope and hot stage, and to gain knowledge for using the equipment.

Secondly, an amorphous experiment was conducted using DSC and the hot stage in conjunction with each other. This was done to provide visual evidence of the material to support the DSC data and to learn how the hot stage performed, compared to the DSC technique.

A shear cell investigation was carried out, supported by light microscopy, of three different pharmaceutical pairs. Followed by an in-depth rheometry study into the effect of temperature and shear on the ibuprofen – nicotinamide pair.

4.42 Ibuprofen – nicotinamide Kofler method

The Kofler method (Or thermal fusion method) is a basic technique which is described in section 2.5. It can provide critical information about the crystal

form and morphology of materials, including co-crystals, and it can give further insight into the thermal behaviour of the materials.

In this section, the Kofler method was performed using the ibuprofen – nicotinamide pair. Figure 4.7 shows the bright field microscopy image of the resulting experiment. The image shows re-crystallised nicotinamide (Left) and carbamazepine (Right) with a central mixing zone where co-crystal needles have formed.

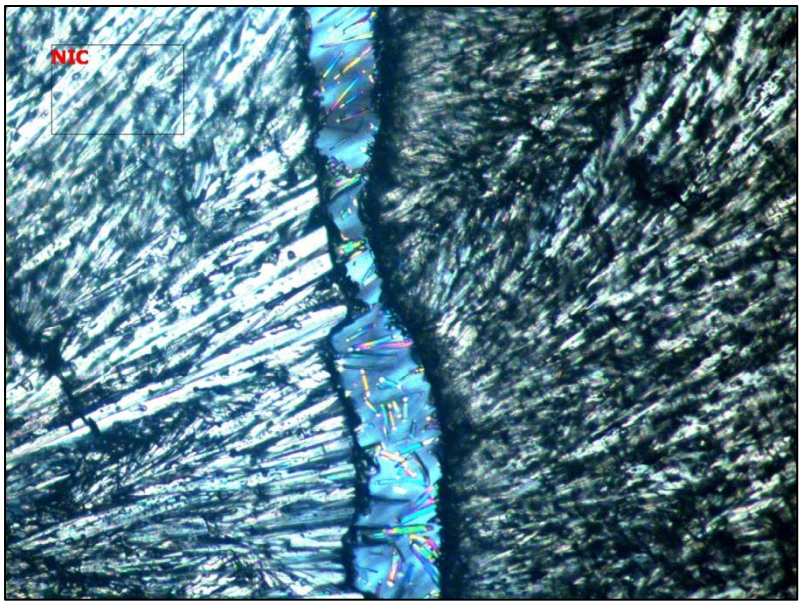

Figure 4.7 Light microscope image of the Kofler method using ibuprofen and nicotinamide.

This simple technique allowed for a first observation of the 1:1 carbamazepine – nicotinamide co-crystal under the light microscope. The co-crystal forms thin needle shaped crystals which coincides with the reported crystal morphology (Seefeldt et al. 2007, Qiao et al. 2013).

4.43 Carbamazepine – nicotinamide amorphous study

In this section, a small study was conducted for the carbamazepine – nicotinamide pair. The 1:1 physical mixture was subjected to a heat-cool-heat DSC method. Then, the exact same method was performed on a Linkam hot stage where bright field and polarised light microscopy images of the sample could be collected. The heating method that was utilised was as follows.

1. 40°C → 200°C (5°C/min)
2. Isothermal for 1 minute at 200°C
3. 200°C → 10^{o}C (20°C/min)
4. Isothermal for 5 minutes at 10°C
5. 10°C → 50°C (5°C/min, isothermal for 60 minutes)
6. 50°C → 220°C (5°C/min)

The heating method was designed to fully melt the physical mixture, then to rapidly cool at 20°C per minute to quench the material, then to heat the material to 50°C to observe any crystallisation or cocrystallisation and finally a standard heating ramp to determine the crystal that had formed. The DSC thermogram for this experiment is shown in figure 4.8. The endothermic and exothermic peak and onset temperatures are shown in table 4.2 along with the integrated energies.

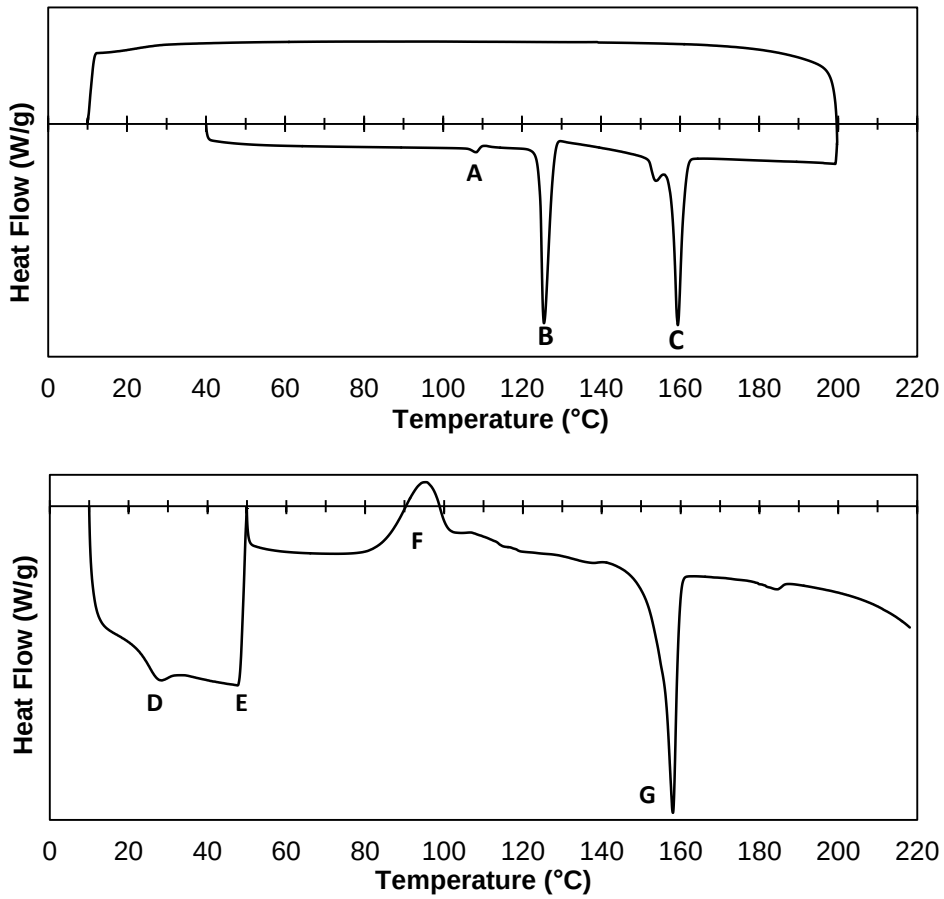

Figure 4.8 A DSC thermogram of 1:1 carbamazepine – nicotinamide physical mixture using a heat-cool-heat method. Important events are labelled A to G.

Table 4.2 Endothermic and exothermic events with the corresponding onset and peak temperatures and the integrated energies.

Event	Onset temperature (°C)	Peak temperature (°C)	Energy (J/g)
A	106.6	108.3	0.78
B	124.4	125.6	64.12
C	157.8	159.4	76.48
D	24.6	27.7	1.00
E	49.6	50.0	2.24
F	85.3	94.7	41.68
G	154.9	158.0	79.37

The bright field and polarised microscopy images taken at specific temperatures are displayed in figures 4.9 and 4.10 to provide visual evidence of the changes the material underwent.

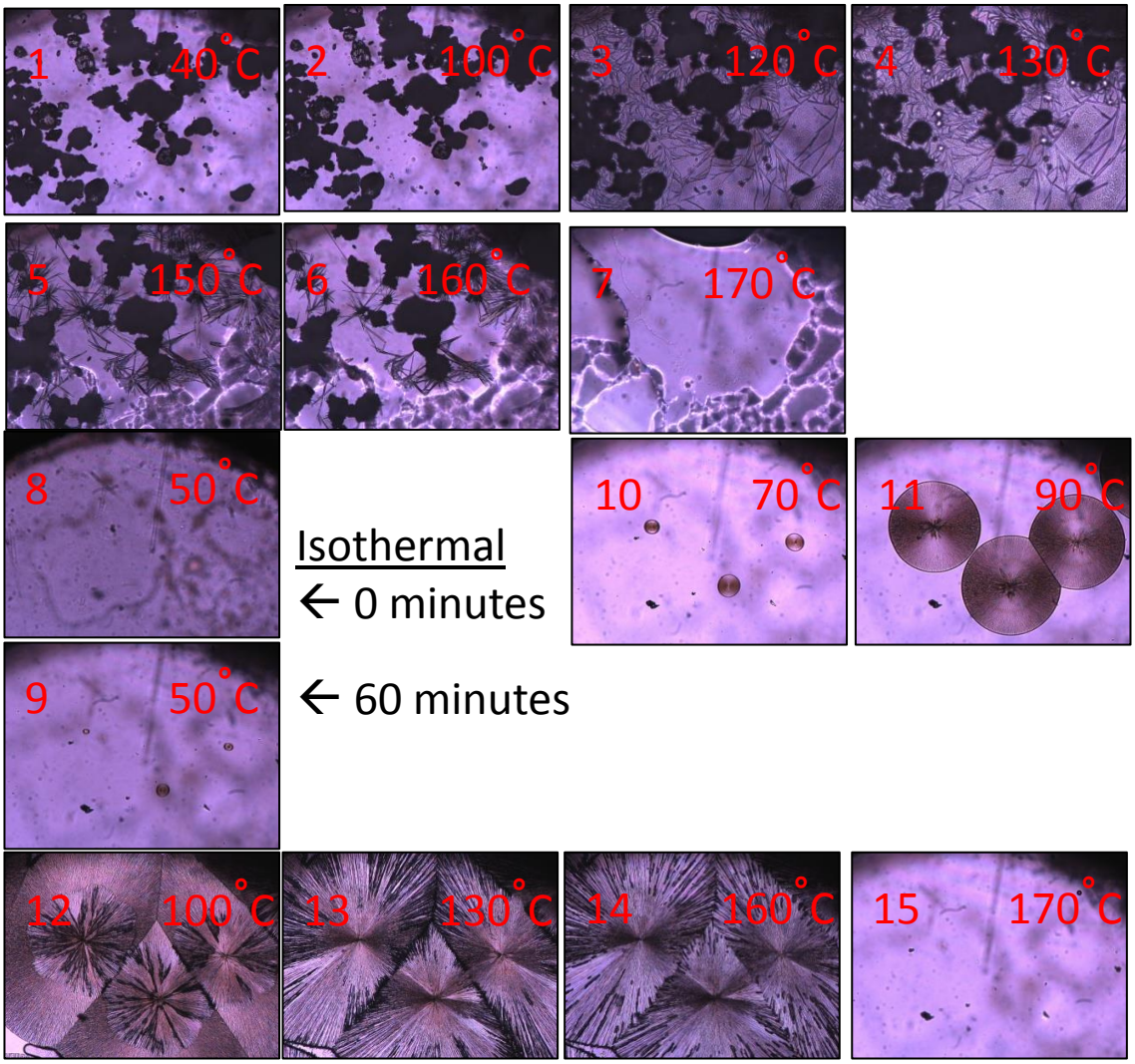

Figure 4.9 Bright field light microscopy images of 1:1 carbamazepine – nicotinamide physical mixture using a heat-cool-heat method.

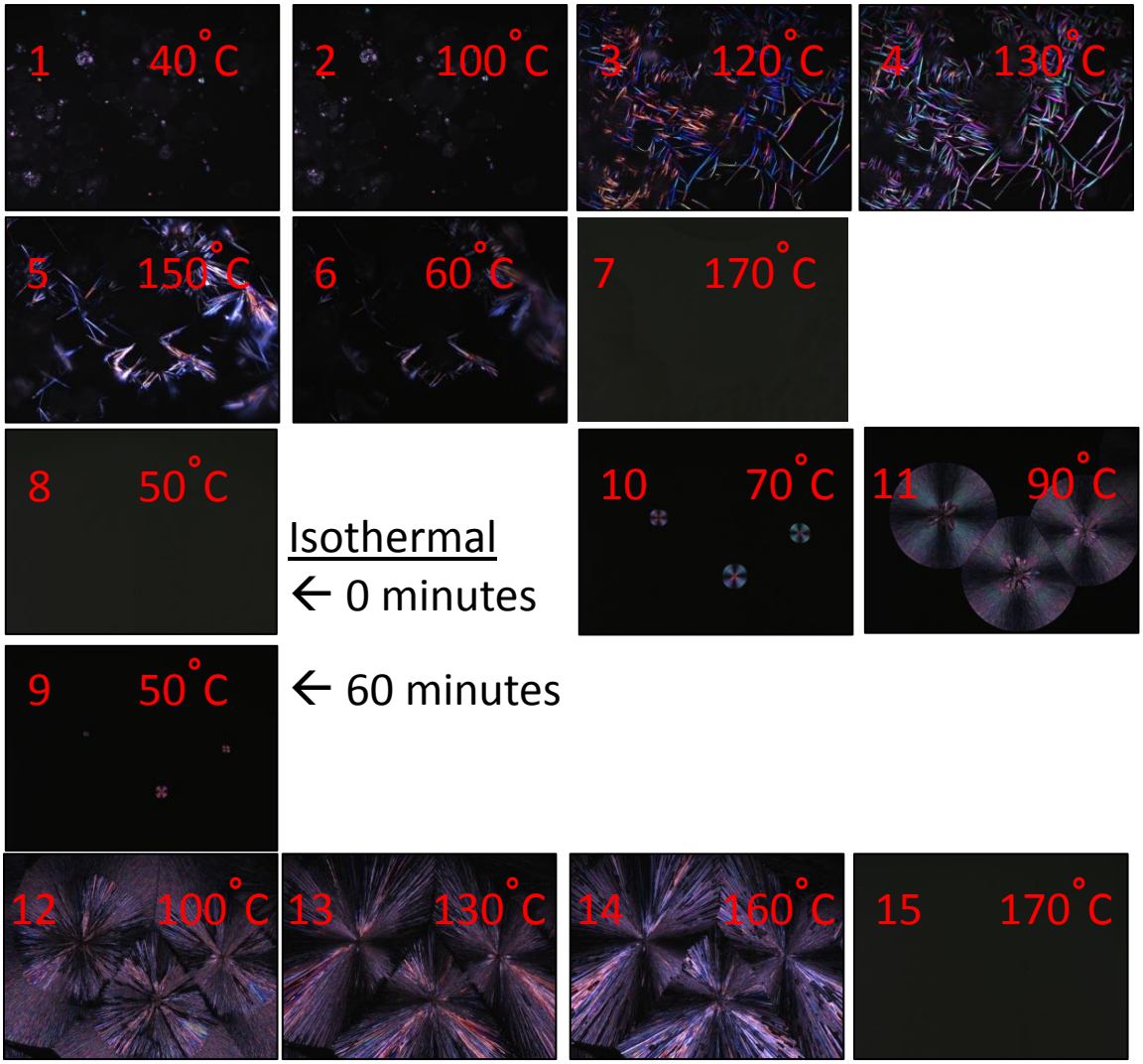

Figure 4.10 Polarised light microscopy images of 1:1 carbamazepine – nicotinamide physical mixture using a heat-cool-heat method.

The microscope images confirm the changes the sample underwent during the employed thermal program. Firstly, the powder was heated through event A where a crystal form appeared. At event B the nicotinamide crystals melted and subsequent cocrystallisation occurred. Event C marks the melting of the remaining carbamazepine and co-crystal immediately after. It is unclear from the images what takes place at event D because no solid phase was observed before or after, the event may be caused by short range order

within the amorphous phase relaxing and molecules moving further apart upon heating.

During the isothermal period where event E is situated, three separate crystal seeds form. This crystal form then proceeds to grow as the temperature is increased. At event F, another crystal form is observed within the initial crystal, and eventually takes over the initial crystal to become the thermodynamically preferred crystal form at temperatures above 94.7°C. The melting point of this crystal form, event G, has a similar melting temperature to the 1:1 co-crystal.

The results from this study directly match those conducted by Seefelt et al. (2007). They observed a birefringent crystal forming from the amorphous phase which is then transformed into another crystal form. The researchers provided evidence from several characterization techniques which confirmed the first crystal form is an intermediate co-crystal form which they referred to as CBZ-NCT (Form II). They concluded that a relatively slow heating rate increases the chance of forming the intermediate co-crystal phase compared to forming the individual components.

4.44 Shear cell investigation

The shear cell (Linkam Scientific) was another technology which was utilised in this study. It provided the combined capability of applying rotational shear and hot stage microscopy. Three different co-crystal pairs were chosen for the study; ibuprofen – nicotinamide, nicotinamide – salicylic acid and caffeine – maleic acid. The main reason these co-crystal pairs were chosen was to link up with synchrotron studies that were planned by our research team. The

data gathered from the ibuprofen – nicotinamide study was beneficial for other sections and chapters in this project. Characterisation of the samples was performed using PXRD and light microscopy images were collected at various stages during each run.

4.441 Ibuprofen – nicotinamide

For the ibuprofen – nicotinamide pair, a gap size of 50 µm and rotary velocity of 5 rad/s were used. For both runs that were carried out, the 1:1 physical mixture was heated from RT to 85/90°C at 5°C/min. It was held at 85/90°C for 10 minutes before shear was applied to ensure the material had reached the desired temperature. The shear was applied in 1 minute long bursts for a total of 8 minutes of shear. The sample was then cooled to RT at 5°C/min.

The PXRD spectra of the samples are shown in figure 4.11 along with the 1:1 physical mixture and co-crystal spectra for the ibuprofen – nicotinamide pair.

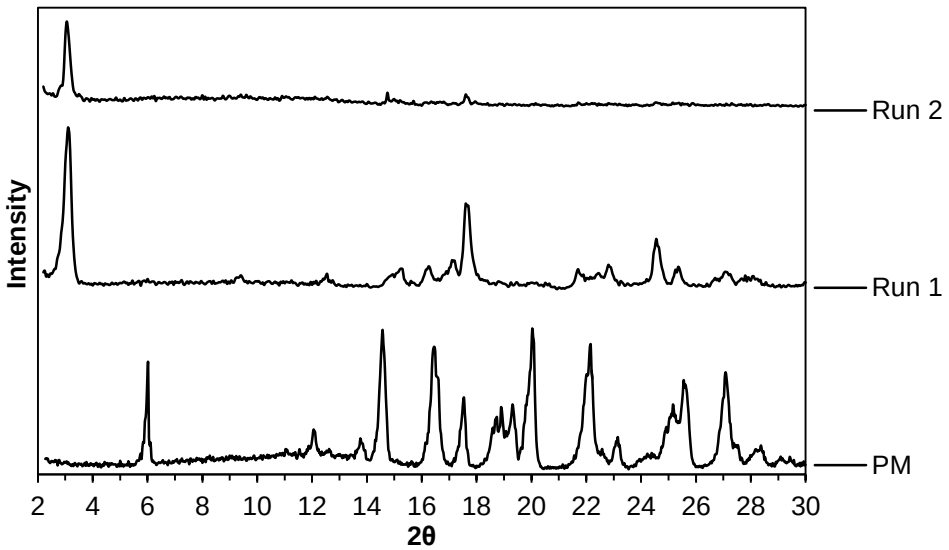

Figure 4.11 PXRD spectra of 1:1 ibuprofen – nicotinamide physical mixture (PM) and the samples for T_{max} 85°C (Run 1) and T_{max} 90°C (Run 2).

The study by Kelly et al. (Kelly et al. 2012) was used as a guide for identifying the 1:1 co-crystal peaks. The sample for run 1 which reached 85°C produced a 1:1 co-crystal spectrum, showing the standard co-crystal peaks at 3.1°, 9.3° and 12.45° (2θ). The sample for run 2 which reached 90°C had the 1:1 co-crystal peak at 3.1° (2θ), however the other 1:1 co-crystal peaks were largely missing, suggesting that some of the powder had potentially become amorphous when subjected to the higher temperature.

Light microscopy images were collected throughout the two runs and are showing in figures A.1 and A.2 in appendix A. It was difficult to determine exactly when co-crystal formation initiated for run 1, however the images suggest a large proportion of the final co-crystal crystallised upon cooling, after the shear had been applied. The sample for run 2 exhibited significant melting when the temperature reached 85°C and above, with a small number of co-crystals visible before shear was applied. After shearing and then cooling, the images for the sample for run 2 indicated that an amorphous phase had formed, again with some short co-crystal needles visible.

4.442 Nicotinamide – salicylic acid

For the nicotinamide – salicylic acid pair, a gap size of 50 µm and rotary velocity of 5 rad/s were used. For the experiments that were carried out, the 1:1 physical mixture was heated from RT to 115/120°C at 5°C/min. It was held at 115/120°C for 10 minutes before shear was applied to ensure the

material had reached the desired temperature. The shear was applied in 1 minute long bursts for a total of 8 minutes of shear. The sample was then cooled to RT at 5°C/min. A third experiment was also conducted using the same conditions as the second run, but instead, a faster rotary velocity of 10 rad/s was used.

The PXRD spectra of the samples and their physical mixture are shown below in figure 4.12.

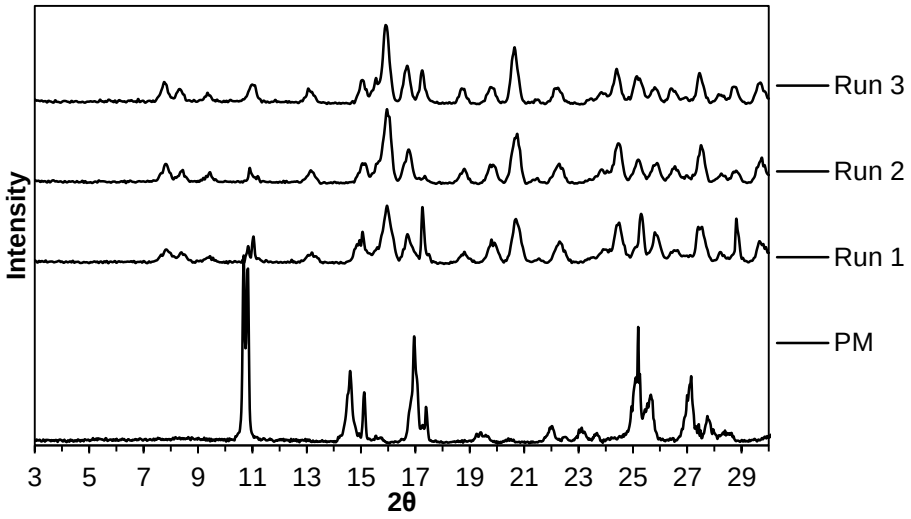

Figure 4.12 PXRD spectra of 1:1 nicotinamide – salicylic acid physical mixture (PM) and the samples for T_{max} 115°C (Run 1), T_{max} 120°C (Run 2) and T_{max} 120°C 10 rad/sec (Run 3).

The reported PXRD peaks for 1:1 nicotinamide – salicylic acid are 7.4°, 8.4° and 9.4° (2θ) (Berry et al. 2008). These peaks are present for all three runs completed for this co-crystal pair using the shear cell. Although the co-crystal was present in all samples, there was also some remaining salicylic acid. It was difficult to determine the co-crystal purity because the spectra for all runs exhibited relatively small diffraction peaks. The salicylic acid peak at

10.8° (2θ) was present for all samples. There were very few differences between the spectra for run 2 and 3, however the peaks at approximately 17.3° (2θ) was much more prominent in the spectra for the sample of run 3. This peak is also associated with salicylic acid. This may suggest that a faster rotational velocity does not necessarily increase the extent of mixing of the material, or indeed promote further cocrystallisation.

Light microscopy images were collected for the samples for all three runs and are shown in figures A.3, A.4 and A.5 in appendix A. The sample for run 1 exhibited co-crystal formation upon the application of shear and after 8 minutes of applied shear, a significant amount of co-crystals could be viewed. There were issues with the images that were collected after any amount of shear had been applied for runs 2 and 3 because the resulting material was opaque. This may have been caused by the agglomeration of cocrystallised particles at the higher temperature of 120°C when shear was applied. The images collected during the isothermal period at 120°C for runs 2 and 3 indicated the formation of some co-crystals had begun during this stage. This was interesting because 120°C is well below the melting points for salicylic acid (159.83°C) (Elbagerma et al. 2010) and nicotinamide (132.1°C).

4.443 Caffeine – maleic acid

For the caffeine – maleic acid pair, a gap size of 50 µm and rotary velocity of 5 rad/s were used. For the experiments that were carried out, the 1:1 physical mixture was heated from RT to 90/100/110°C at 5°C/min. It was held at 90/100/110°C for 10 minutes before shear was applied to ensure the material had reached the desired temperature. The shear was applied in 1

minute long bursts for a total of 8 minutes of shear. The sample was then cooled to RT at 5°C/min. For some of the runs, the shear direction was alternated for each 1 minute burst of shear. Additionally, for run 5, the 2:1 physical mixture was used. The PXRD spectra of the samples and their physical mixture are shown below in figure 4.13.

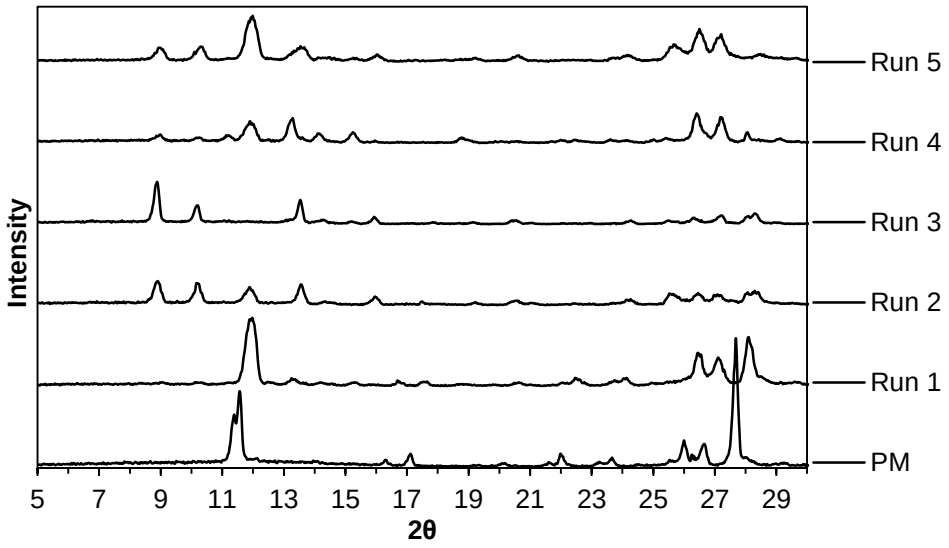

Figure 4.13 PXRD spectra of 1:1 caffeine – maleic acid physical mixture (PM) and the samples for T_{max} 90°C (Run 1), T_{max} 100°C (Run 2) T_{max} 100°C with alternating shear direction (Run 3), T_{max} 110°C (Run 4) and 2:1 PM initial material T_{max} 100°C (Run 5).

The study by Guo et al. (Guo et al. 2009) was used as a guide for identifying 1:1 and 2:1 co-crystal peaks. The PXRD spectra for run 1 indicated that the sample was still mostly 1:1 physical mixture, showing a large caffeine peak at approximately 12° (2θ), however, low intensity 1:1 co-crystal peaks were observed at 13.3°, 14.1° and 15.2° (2θ) also. The spectrum for run 2 exhibited 2:1 co-crystal peaks at 8.9° 10.2° 13.5° and 15.9° (2θ) along with a reduced caffeine peak at 12° (2θ) compared to run 1. The spectrum for run 3

indicates that a high yield of 2:1 co-crystal was obtained, displaying the main 2:1 co-crystal peaks as previously discussed, and an absence of the 12° (2θ) caffeine peak.

The spectrum for run 4 exhibited 1:1 co-crystal peaks at 11.2°, 13.3°, 14.1° and 15.2° (2θ), and 2:1 co-crystal peak at 10.2° (2θ). The spectrum for run 5 displays 2:1 co-crystal peaks 8.9° 10.2° 13.5° and 15.9° (2θ). Both samples for runs 4 and 5 have residual caffeine, indicated by the peak at 12° (2θ).

The PXRD findings suggest the alternating shear direction method promotes more sufficient mixing and is able to increase the purity of the 2:1 co-crystal form at 100°C compared to the single shear direction method. Additionally, the presence of 1:1 co-crystal in the sample for run 4 was surprising considering the melting point of the 1:1 co-crystal is approximately 104°C (Guo et al. 2009). Run 5, which used the same conditions as run 2, albeit starting with a 2:1 physical mixture, yielded a similar material composition to run 2.

The light microscopy images are shown in figures A.6 to A.10 in appendix A. The images show that needle shaped crystals formed typically after 2 minutes of shear had been applied for all shear cell runs apart from run 1, where it was clear that the bulk material had not undergone any transformations and exhibited a similar morphology to the starting material. The sample for run 3 had a more uniform co-crystal morphology and size compared to the sample for run 2. This strengthens the case that the alternating shear direction promotes good quality mixing. Finally, the sample

for run 4 experienced significantly more melting than the other runs, however this was expected at the higher temperature used.

4.45 Ibuprofen – nicotinamide rheometry investigation

Model shear deformation studies were carried out for the ibuprofen nicotinamide system to show the effect of shear and temperature on 1:1 co-crystal formation. All samples, that were processed using an Anton Paar rheometer, were heated and cooled at a rate of 20°C/min and held at the maximum temperature for 10 minutes to mimic the time the material would spend, on average, inside the extruder barrel during extrusion. Different strain limits were applied during the heating, hold and cooling of the sample and the direction of shear was set to oscillation mode. The shear cell study in the previous section concluded that the oscillating mode provided improved mixing of the material. The oscillation mode was programmed to reverse the direction once a pre-set strain value had been reached. The oscillatory mode was also chosen over the continuous direction mode in an attempt to keep as much of the material in contact with the upper and lower rheometer plates as possible during the applied shear. Both the upper and lower plates were standard parallel plates and unless otherwise specified, the downwards force applied to the material was programmed to stay at 1 N throughout the duration of the experiments.

Figure 4.14 shows PXRD spectra of the 1:1 physical mixture heated and held at 70°C for 10 minutes before being cooled to room temperature. No shear was applied to one of the samples and the others had shear applied with the strain set to 25%, 50%, 75% and 100%. The resulting PXRD spectra indicated that at 70°C and no shear, there are new peaks formed at 14.9°,

16.7°, 17.2° and 24.2° (2θ). These new peaks are associated with the 1:1 co-crystal. When the strain is increased from 25% to 100%, the intensity of the ibuprofen peak at 6° (2θ) decreases and the new peaks at 14.9°, 16.7°, 17.2° and 24.2° (2θ) experience no significant changes in intensity. The 1:1 co-crystal peak situated at 3.1° (2θ) appears at 75% and 100% strain.

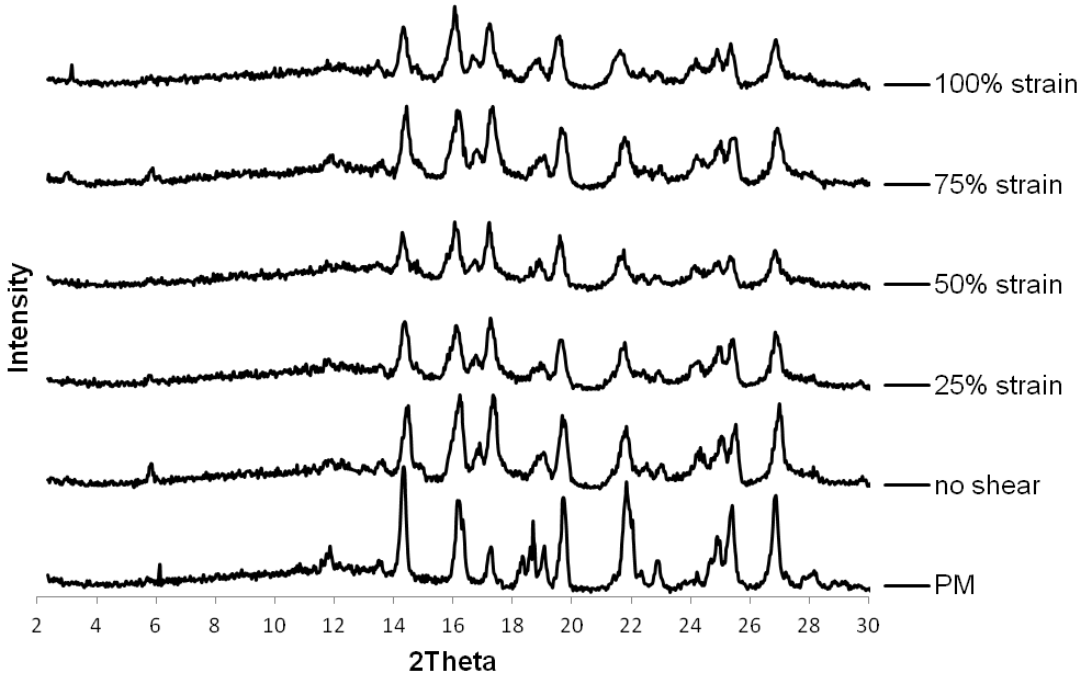

Figure 4.14 PXRD spectra of IBU-NIC 1:1 physical mixture subjected to no shear, 25% strain, 50% strain, 75% strain and 100% strain and held at 70°C for 10 minutes with a heating and cooling rate of 20°C/min. The 1:1 physical mixture spectrum is also shown (PM).

Figure 4.15 shows PXRD spectra of the 1:1 physical mixture heated and held at 80°C for 10 minutes before being cooled to room temperature. No shear was applied to one of the samples and the others had applied strain of 25%, 50%, 75% and 100%. The spectra indicated that at 80°C and no shear, the 1:1 co-crystal peaks are present at 14.9°, 16.7°, 17.2° and 24.2° (2θ). The

1:1 co-crystal peak situated at 3.1° (2θ) had a relatively high intensity for the 50% strain sample. The ibuprofen peak at 6° (2θ) suggested that there was residual ibuprofen present in the majority of the samples, including the sample at 50% strain.

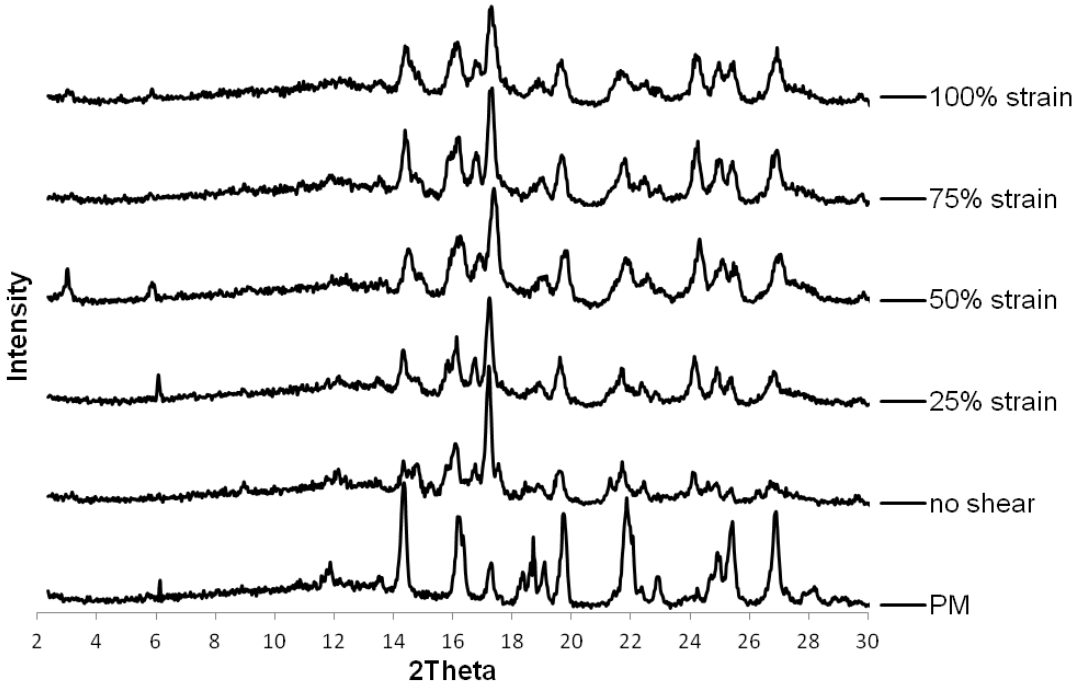

Figure 4.15 PXRD spectra of IBU-NIC 1:1 physical mixture subjected to no shear, 25% strain, 50% strain, 75% strain and 100% strain and held at 80°C for 10 minutes with a heating and cooling rate of 20°C/min. The 1:1 physical mixture spectrum is also shown.

Figure 4.16 shows PXRD spectra of the 1:1 physical mixture heated and held at 90°C for 10 minutes before being cooled to room temperature. No shear was applied to one of the samples and the others had applied strain of 25%, 50%, 75% and 100%. The spectra indicated that 1:1 co-crystal had formed in all the samples. The 1:1 co-crystal peak situated at 3.1° (2θ) appeared at all levels of strain and it had the highest intensity for the 50% strain sample. The

ibuprofen peak at 6° (2θ) was not observed in any samples, however the nicotinamide peak at 14.7° (2θ) can be observed in the majority of the samples suggesting there was some residual nicotinamide.

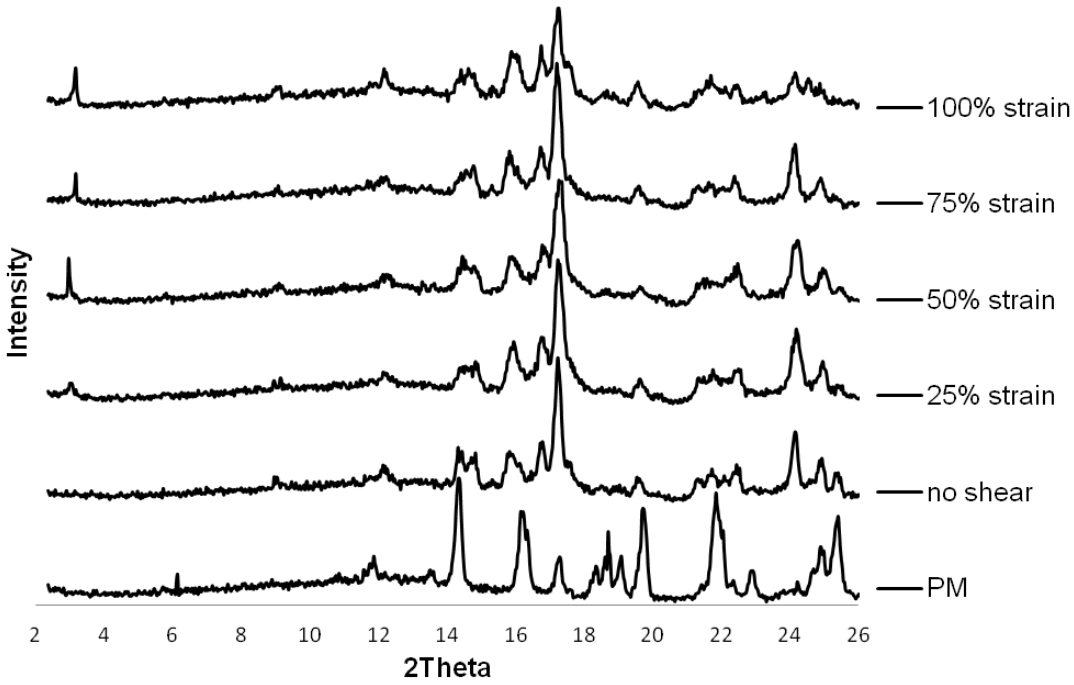

Figure 4.16 PXRD spectra of IBU-NIC 1:1 physical mixture subjected to no shear, 25% strain, 50% strain, 75% strain and 100% strain and held at 90°C for 10 minutes with a heating and cooling rate of 20°C/min. The 1:1 physical mixture spectrum is also shown.

The samples from figures 4.14 to 4.16 above were subjected to DSC analysis. The DSC data is shown in figures 4.17 and 4.18. Thermal analysis of the samples provided another characterisation approach. All samples were heated to 175°C with a standard heating rate of 10°C/min. Figure 4.17 shows the DSC thermograms of the samples which experienced no shear and shear with 25% and 50% strain limits. Figure 4.18 shows the DSC

thermograms of the samples which experienced shear with 75% and 100% strain limits.

The 90°C samples exhibited the largest co-crystal melting peaks situated at approximately 91.1°C compared to samples processed at lower temperatures. This may suggest that 90°C was the optimal temperature for 1:1 co-crystal formation during the model shear deformation experiments, even when no shear was applied. However, for this particular pharmaceutical pair, the 1:1 co-crystal is known to form from the 1:1 physical mixture during a 10°C/min DSC ramp from RT to 200°C. Therefore it is difficult to determine the effect any remaining unreacted ibuprofen or nicotinamide will have on the DSC thermograms, in figures 4.17 and 4.18, because some additional co-crystals could form during the DSC heating. The DSC results show no obvious correlation between the amount of applied strain and the yield of the 1:1 co-crystal.

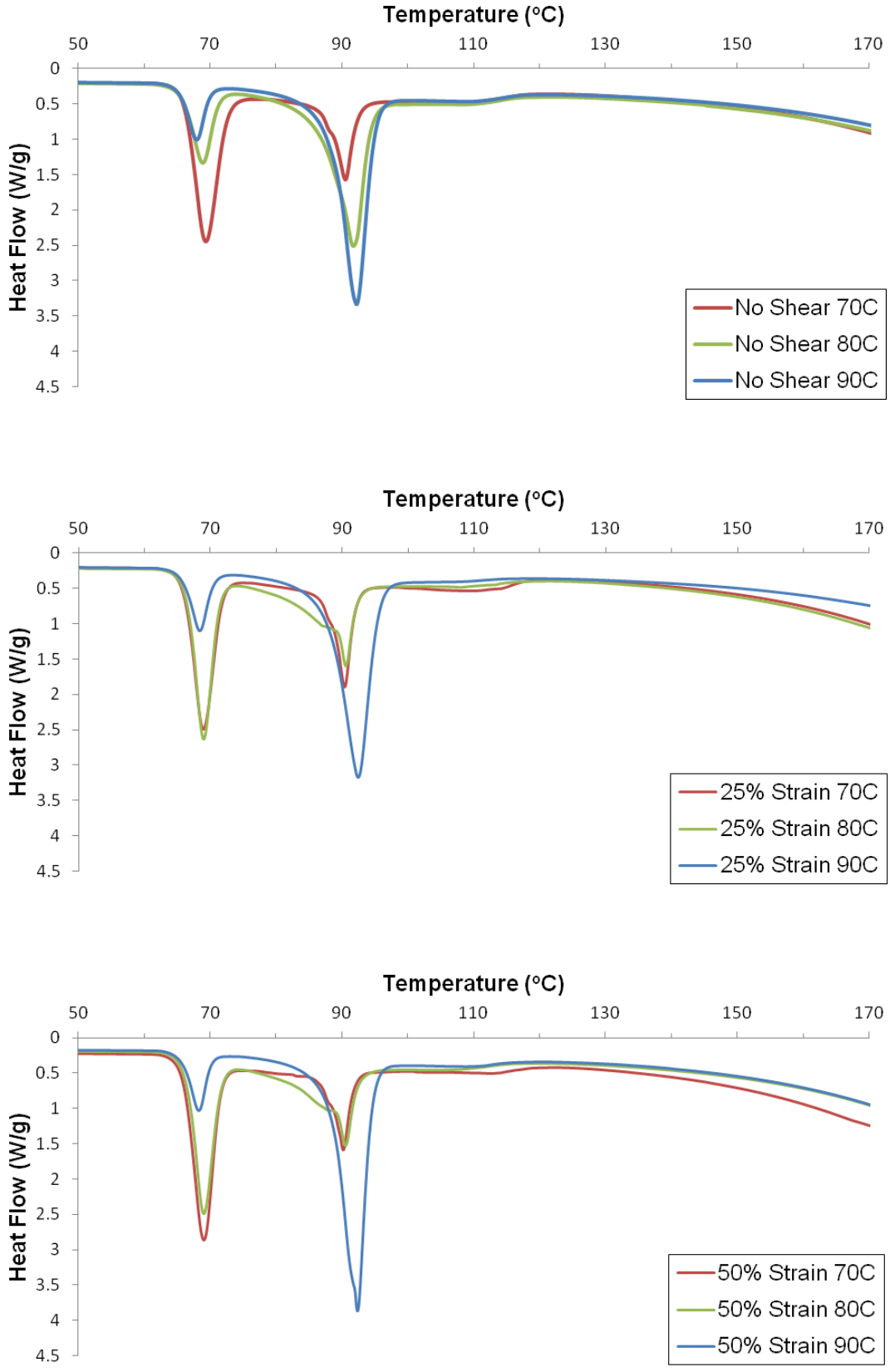

Figure 4.17 DSC thermograms of the model shear deformation samples. Temperatures: 70, 80 and 90°C. Strain: 0, 25 and 50%.

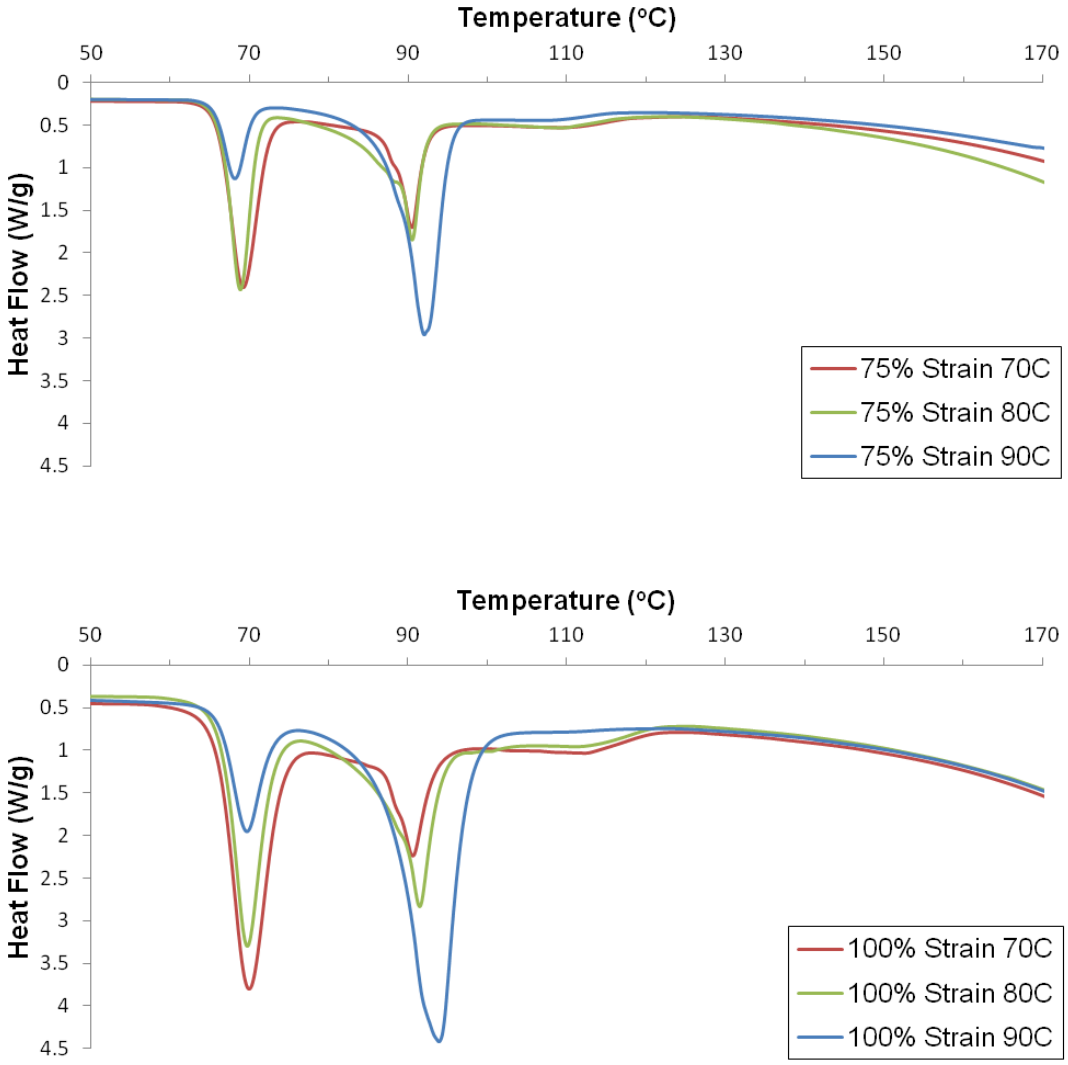

Figure 4.18 DSC thermograms of the model shear deformation samples. Temperatures: 70, 80 and 90°C. Strain: 75 and 100%.

During the application of shear with varying strain limits, contact between the material and the upper and lower rheometer plates was an important factor. Little or no contact can lead to significantly lower levels of shear force that the material experiences during the model rheology method. An additional experiment was carried out where a force of 5 N was applied directly onto each sample during heating, holding and cooling. Each sample was heated to 70°C, 80°C and 90°C with a 25% strain limit for the oscillating shear

mode. The PXRD spectra for these samples are shown in figure 4.19. Both the 1:1 co-crystal peak at 3.1° (2θ) and the ibuprofen peak at 6° (2θ) were present in the 70°C and 80°C samples, however, the 90°C sample spectrum did not show these two peaks. The presence of peaks at 9.3°, 12.4° and 14.7° (2θ) indicated the 90°C sample was a mixture of 1:1 co-crystal and nicotinamide. During this experiment, the rheometer was unable to apply a downward force of 5 N onto the sample at all times, particularly when the material had experienced melting.

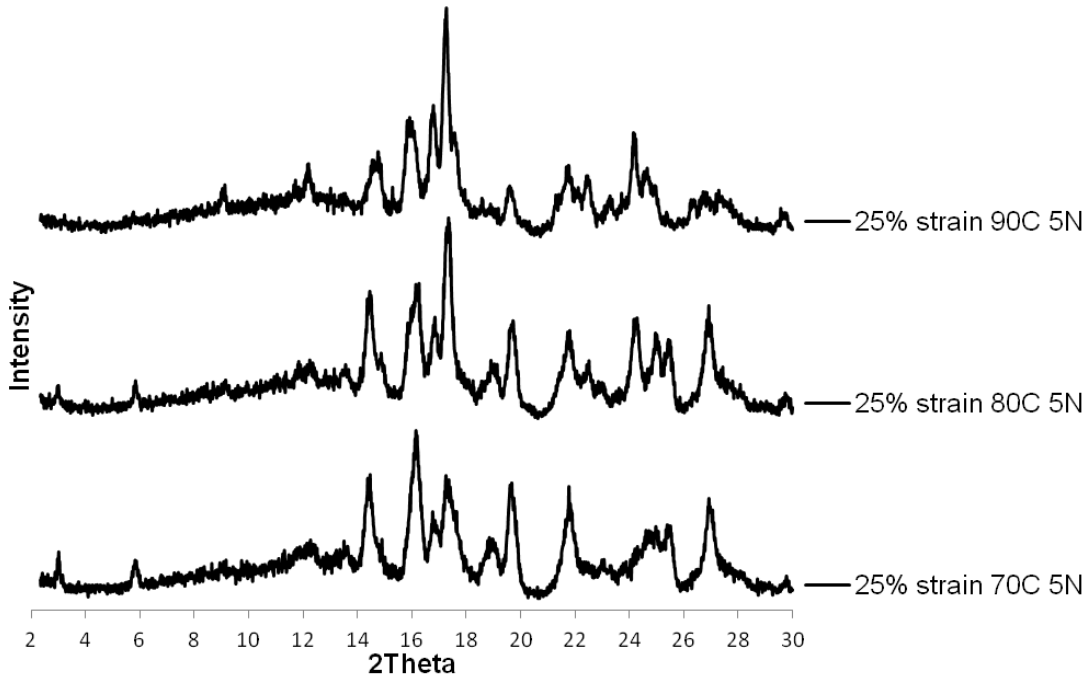

Figure 4.19 PXRD spectra of IBU-NIC 1:1 physical mixture subjected to 25% strain and held at 70°C, 80°C and 90°C for 10 minutes with a heating and cooling rate of 20°C/min and an applied force of 5 N.

In an attempt to increase the 1:1 co-crystal yield, the strain limit was increased to 200% to potentially increase the chance of the carbamazepine and nicotinamide molecules coming into contact with one another. The

samples were run at 70, 75, 80, 85 and 90°C with a force of 1 N applied throughout each experiment. Figure 4.20 shows the PXRD spectra for these samples. All the samples shown in figure 4.20 exhibited the 3.1° (2θ) peak, even at the lowest temperature of 70°C. The 80°C sample produced the highest intensity 1:1 co-crystal peak at 3.1° (2θ) compared to the other samples. The increased yield of the 1:1 co-crystal may have been caused by the larger strain limit providing more efficient mixing. The samples run at 85°C and 90°C exhibited a small 3.1° (2θ) peak compared to the sample at 80°C, this may have been caused by a loss of contact between the material and the rheometer plates as it melted, therefore leading to reduced mixing and shear force experienced by the samples.

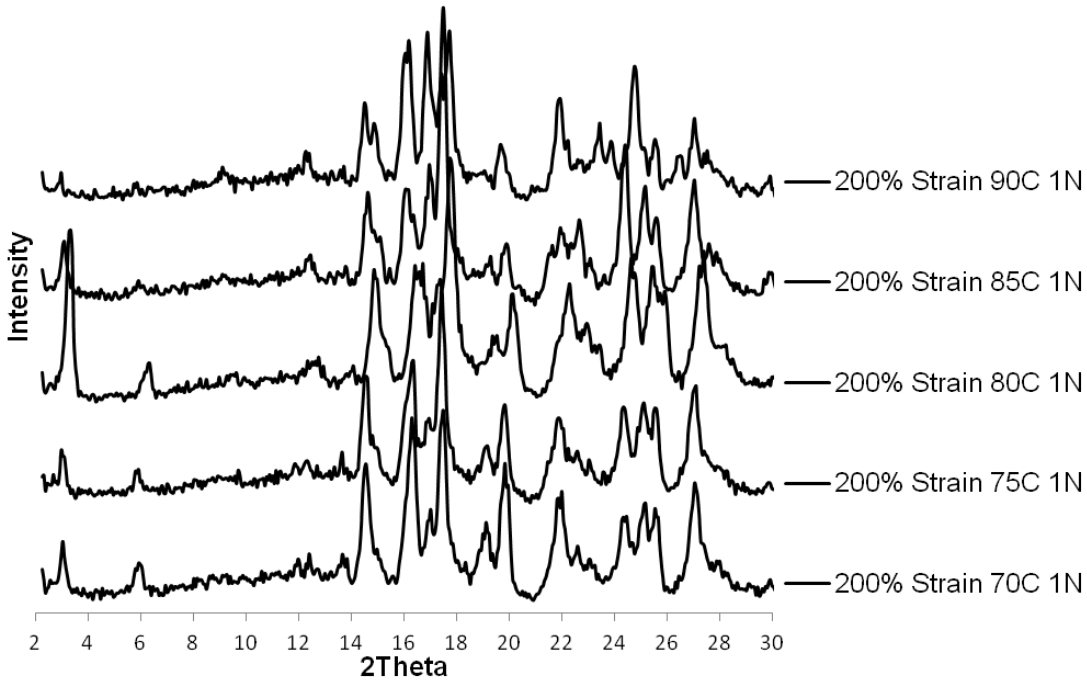

Figure 4.20 PXRD spectra of IBU-NIC 1:1 physical mixture subjected to 200% strain and held at 70°C, 75°C, 80°C, 85°C and 90°C for 10 minutes with a heating and cooling rate of 20°C/min and an applied force of 1 N.

An additional experiment was conducted using a 300% strain limit and the PXRD spectra are shown in figure 4.21. It is unclear whether increasing the strain from 200% to 300% caused the 1:1 co-crystal yield to increase. However, the 80°C sample had an increased intensity 3.1° (2θ) peak compared to the other samples which was a similar result compared to the 200% strain limit experiment.

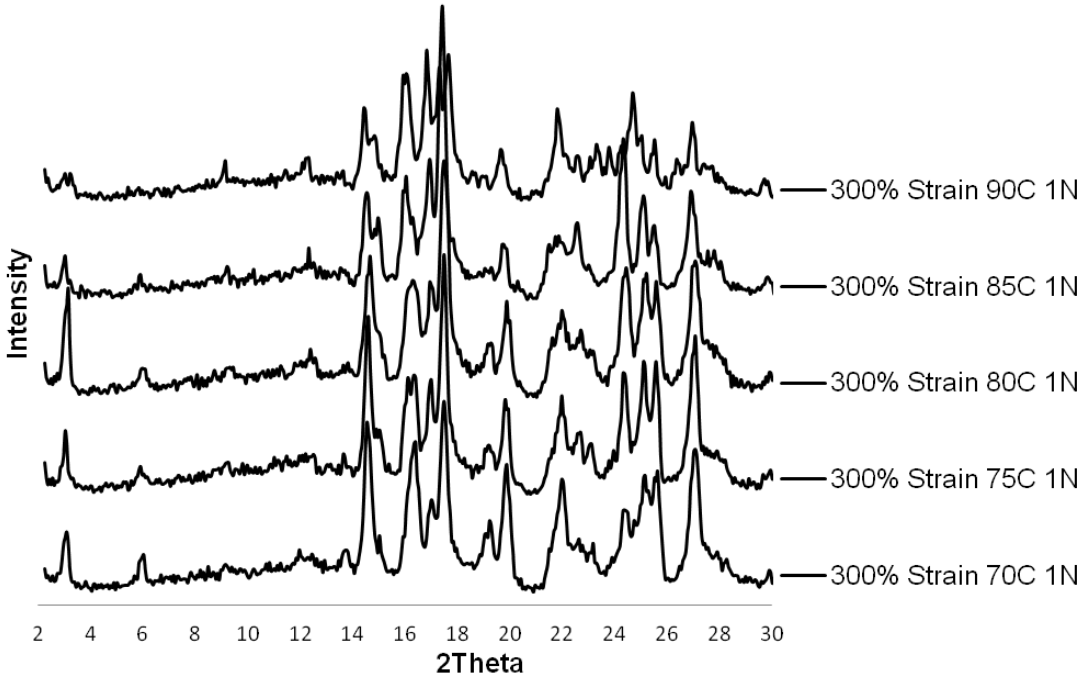

Figure 4.21 PXRD spectra of IBU-NIC 1:1 physical mixture subjected to 300% strain and held at 70°C, 75°C, 80°C, 85°C and 90°C for 10 minutes with a heating and cooling rate of 20°C/min and an applied force of 1 N.

The conclusion from the ibuprofen – nicotinamide model shear deformation study is that shear does have a role in the 1:1 co-crystal formation at 70°C, 80°C and 90°C. However, temperature is the most important factor for cocrystallisation of the ibuprofen – nicotinamide pair.

4.5 Conclusion

This chapter set out to explore the behaviour of pharmaceutical co-crystals under different conditions using a wide array of techniques to probe and characterise the materials. The results show that temperature and shear play different roles in co-crystal formation and in some techniques; the shear force provided a form of mixing to facilitate further cocrystallisation.

The model shear experiments that were carried out provided a unique insight into the behaviour of co-crystal pairs subjected to different quantities of shear force at high temperatures. The shear cell microscope stage is a promising technology that can be used to apply defined amounts of shear force to a small amount of material whilst accurately controlling the temperature. The shear cell provided an enclosed space for the material that was being analysed; this was not the case for the larger scale rheometer where some material could potentially spill over the side of the parallel plates.

Light microscopy was an important characterisation tool, particularly when combined with temperature control capabilities. It provided a key insight into changes and events that occurred to the material during a range of different experiments with a selection of pharmaceutical pairs which are able to form stable co-crystals. Key information was gathered about different crystal forms of the pharmaceutical materials and cocrystallisation was able to be observed in situ in real time.

The thermal behaviour of the physical mixtures of the pharmaceutical pairs in chapter 4 was found to be in conjunction with relevant studies in the literature. The data gathered in this chapter was directly used for designing

the extrusion experiments in chapter 5 and also provided important knowledge, particularly for the carbamazepine – nicotinamide pair.

CHAPTER 5 HOT MELT EXTRUSION OF CO-CRYSTAL PAIRS

Hot melt extrusion of two co-crystal pairs was investigated in this chapter. The ibuprofen – nicotinamide pair was chosen initially because it is a relatively well-understood co-crystal and it has already been proven to cocrystallise during hot melt extrusion (Dhumal et al. 2010). The carbamazepine – nicotinamide pair was also investigated. Carbamazepine – nicotinamide had not been successfully produced by hot melt extrusion so it was selected to be investigated using this method.

A thorough analysis of the extruded samples was carried out in this chapter. This included using X-ray diffraction, differential scanning calorimetry, near infrared spectroscopy and scanning electron microscopy techniques. XRD, DSC and NIR all gave insight into the purity and composition of the extruded samples. SEM provided crucial morphological information and was also used to estimate the size of some extruded particles.

5.1 Ibuprofen – nicotinamide

5.11 Extrusion study

The purity of the individual components was determined using powder X-ray diffraction. The diffraction spectra for ibuprofen, nicotinamide, IBU-NIC 1:1 physical mixture and IBU-NIC 1:1 co-crystal are shown in figure 5.1. The key, standalone ibuprofen peak is situated at 6° (2θ). This can be used to determine whether ibuprofen is present in a sample. Similarly, the peak at 14.7° (2θ) is a distinguishable peak associated with nicotinamide. The co-crystal exhibits a major peak at 3.1° (2θ) and has two more peaks situated at 9.3° and 12.4° (2θ) which can be used to help identify co-crystal present in experimental samples.

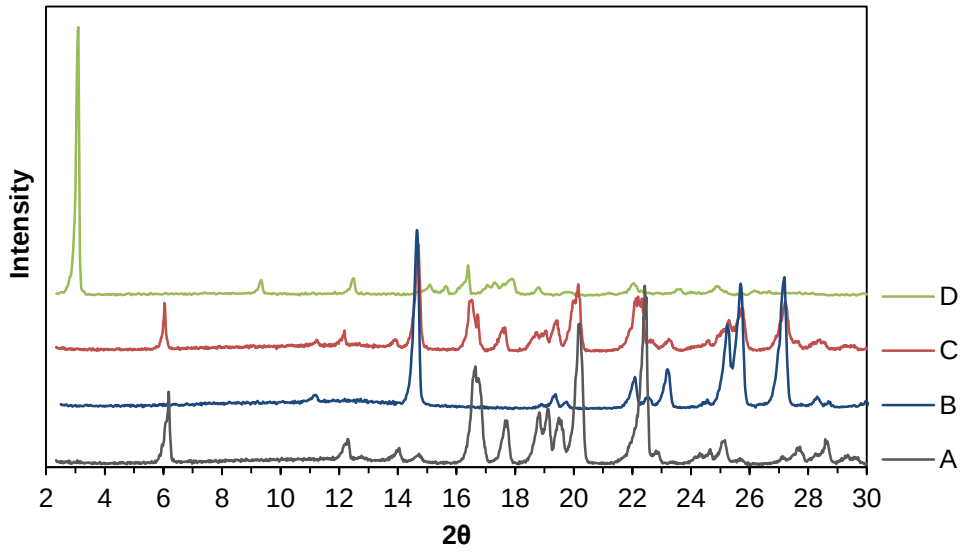

Figure 5.1 PXRD spectra of A. ibuprofen, B. nicotinamide, C. IBU-NIC 1:1 physical mixture and D. IBU-NIC 1:1 co-crystal (Microwave method section 3.2).

Extrusion was carried out using the ibuprofen – nicotinamide system to evaluate if this process can be used for manufacturing the co-crystal. Thermal information about the pair was critical for optimising the temperature of extrusion and for selecting the temperature profiles that were used. Differential scanning calorimetry provided this information and the thermograms for ibuprofen, nicotinamide, IBU-NIC 1:1 physical mixture and IBU-NIC 1:1 co-crystal are shown in figure 5.2. The melting temperatures of ibuprofen and nicotinamide were found to be 78.0°C and 132.1°C respectively. The physical mixture eutectic melting point of the pair was 72.8°C and the co-crystal melting point was 91.1°C.

The thermal data that was gathered from the DSC results was used to decide what temperature profiles were chosen for the HME of ibuprofen – nicotinamide. It is thought that cocrystallisation can occur from the melt

phase of the physical mixture. The physical mixture for ibuprofen – nicotinamide has a eutectic melting point of 72.8°C. So the temperature profiles were based around this temperature and were increased until pure co-crystal was obtained.

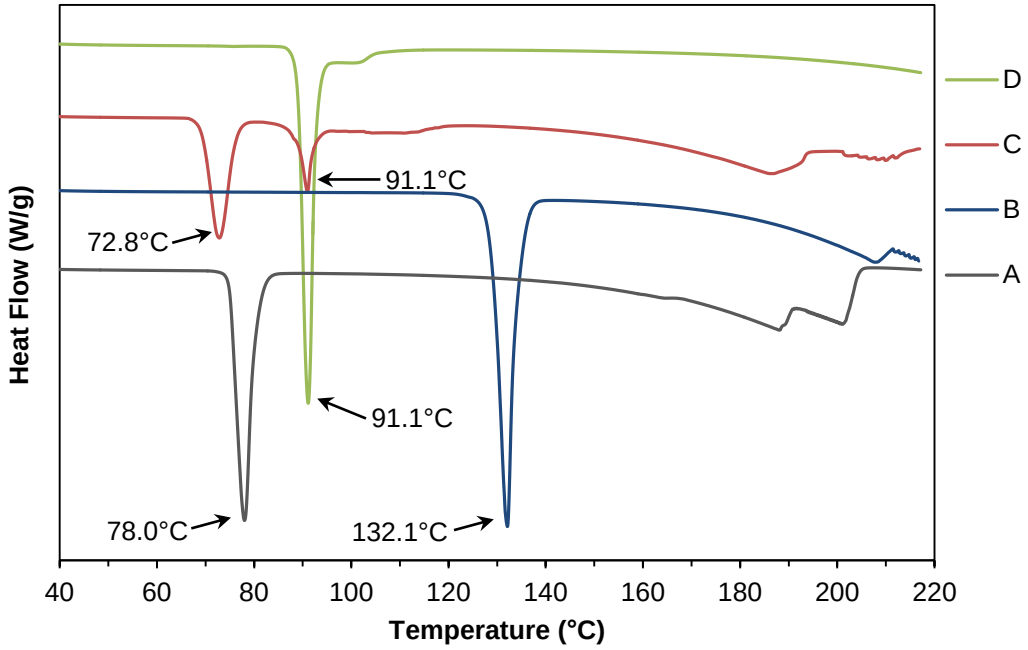

Figure 5.2 DSC thermograms of A. ibuprofen, B. nicotinamide, C. IBU-NIC 1:1 physical mixture and D. IBU-NIC 1:1 co-crystal (Microwave method section 3.2) heated at 10°C/min from 40°C to 220°C.

Extrusion was carried out by feeding a pre-mixed 1:1 physical mixture of ibuprofen and nicotinamide into the first zone of the extruder barrel. The temperature codes of T80 and T90 are the temperature profiles that were used and which are described in section 3.81. The maximum temperatures achieved along the extruder barrel were 80°C for T80 and 90°C for T90. The high shear screw geometry, SGB (Described in section 3.82), was used to provide sufficient mixing and shear which is thought to aid cocrystallisation.

Two screw speeds were selected; 20 rpm and 30 rpm. The 20 rpm screw speed provided a longer residence time and caused the material in the extruder barrel to experience a longer period of thermal exposure whereas the 30 rpm screw speed provided higher shear forces experienced by the material. The extrudates were collected and PXRD spectra of the samples were obtained for investigation purposes. The spectra are shown in figure 5.3 and are stacked to help identify subtle differences. The IBU-NIC 1:1 physical mixture and IBU-NIC 1:1 co-crystal spectra were included to display the peaks of interest.

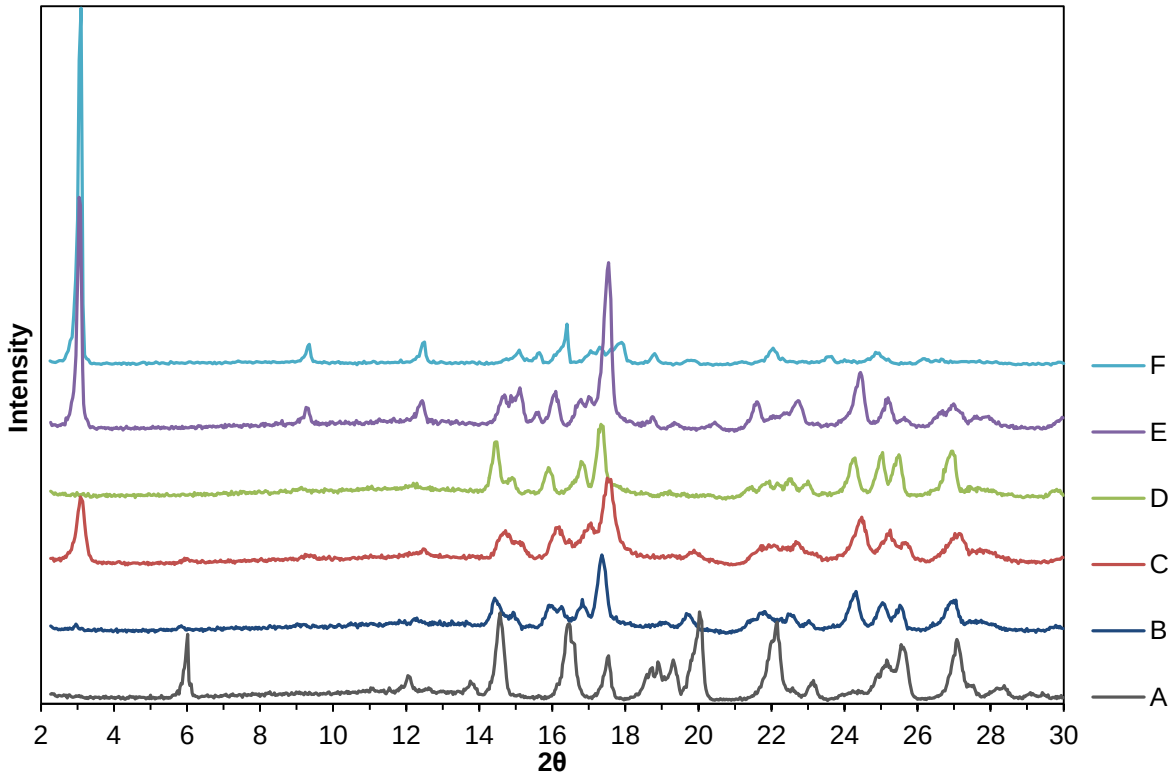

Figure 5.3 PXRD spectra of A. IBU-NIC 1:1 physical mixture, B. extrudate T80 30 rpm, C. extrudate T80 20 rpm, D. extrudate T90 30 rpm, E. extrudate T90 20 rpm, F. IBU-NIC 1:1 co-crystal (Microwave method section 3.2).

The 20 rpm extrudates both exhibited the co-crystal peak situated at 3.1° (2θ), indicating significant cocrystallisation had occurred when using this screw speed. The ibuprofen peak at 6° (2θ) is present in both samples processed using the T80 temperature profile but is absent in the T90 samples. This would suggest that temperature also played a key role in cocrystallisation and ensuring the remaining ibuprofen is able to form the co-crystal. The T90 20 rpm extrudates exhibited all 3 previously mentioned co-crystal peaks at 3.1°, 9.3° and 12.45° (2θ), however it also had the nicotinamide peak situated at 14.7° (2θ) suggesting there was still some remaining nicotinamide.

Extrusion carried out at temperatures higher than 90°C ended in degradation of the powder which formed a light green colour. However, this degradation was not investigated further.

5.12 Seeding study

Seeding of IBU-NIC 1:1 co-crystal was done to determine if it was possible to extrude the co-crystal using a low shear screw geometry (SGA) described in section 3.82. The other conditions for extrusion were T90 temperature profile and a 20 rpm screw speed. The pure 1:1 co-crystal seed was pre-mixed into the physical mixture before being fed into the extruder barrel. The total co-crystal seed added was 15% w/w. The extruded samples were characterised using NIR spectroscopy. The normal spectra for ibuprofen, nicotinamide, 1:1 physical mixture, 1:1 co-crystal and the extruded batch (Original and ground powder) are shown in figure 5.4.

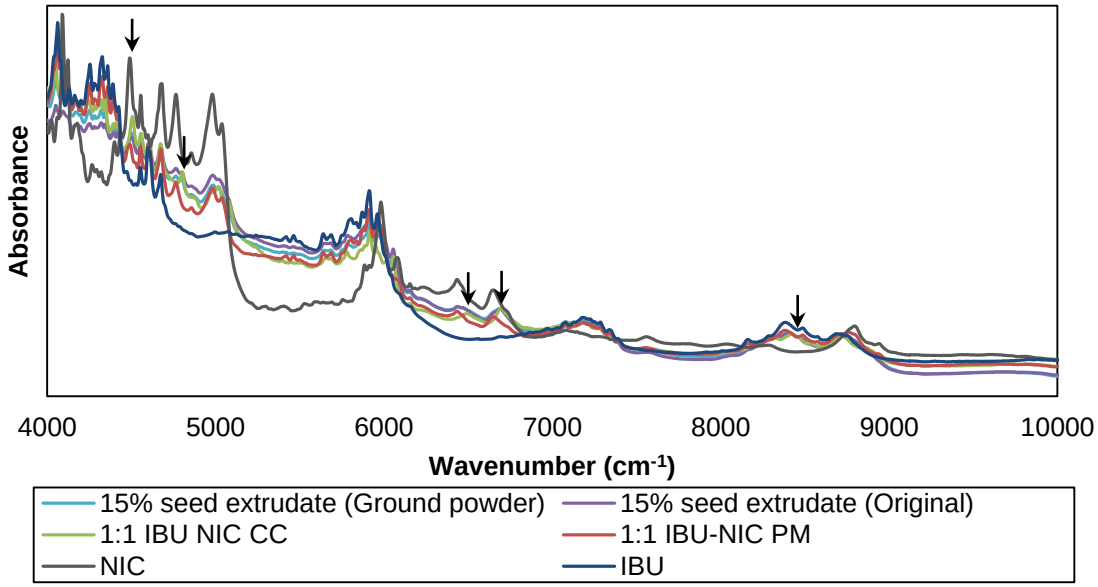

Figure 5.4 NIR spectra of ibuprofen, nicotinamide, 1:1 IBU-NIC physical mixture, 1:1 IBU-NIC co-crystal (Microwave method section 3.2), extrudate T90 20 rpm 15% seed, extrudate T90 20 rpm 15% seed, ground powder. All the spectra shown have been treated with SNV baseline correction.

Each region of the spectra in figure 5.4 was examined. Firstly, the spectra showed that the extruded samples were very similar to the pure co-crystal, exhibiting stand-alone co-crystal bands at approximately 4466, 4794, 6445 6688 and 8451 cm^{-1} (Black arrows in figure 5.4). There was no observed band shifting between the extruded sample and the ground powder version. The ibuprofen band at 6426 cm^{-1} was present in the extruded samples spectra, which suggests there was some residual ibuprofen however this was the only point where the extruded sample spectra deviated from the pure co-crystal spectra. The second derivative spectra were calculated to see if there were any other subtle differences between the extruded sample

and the pure co-crystal. The spectra are shown as 3 separate regions in figure 5.5.

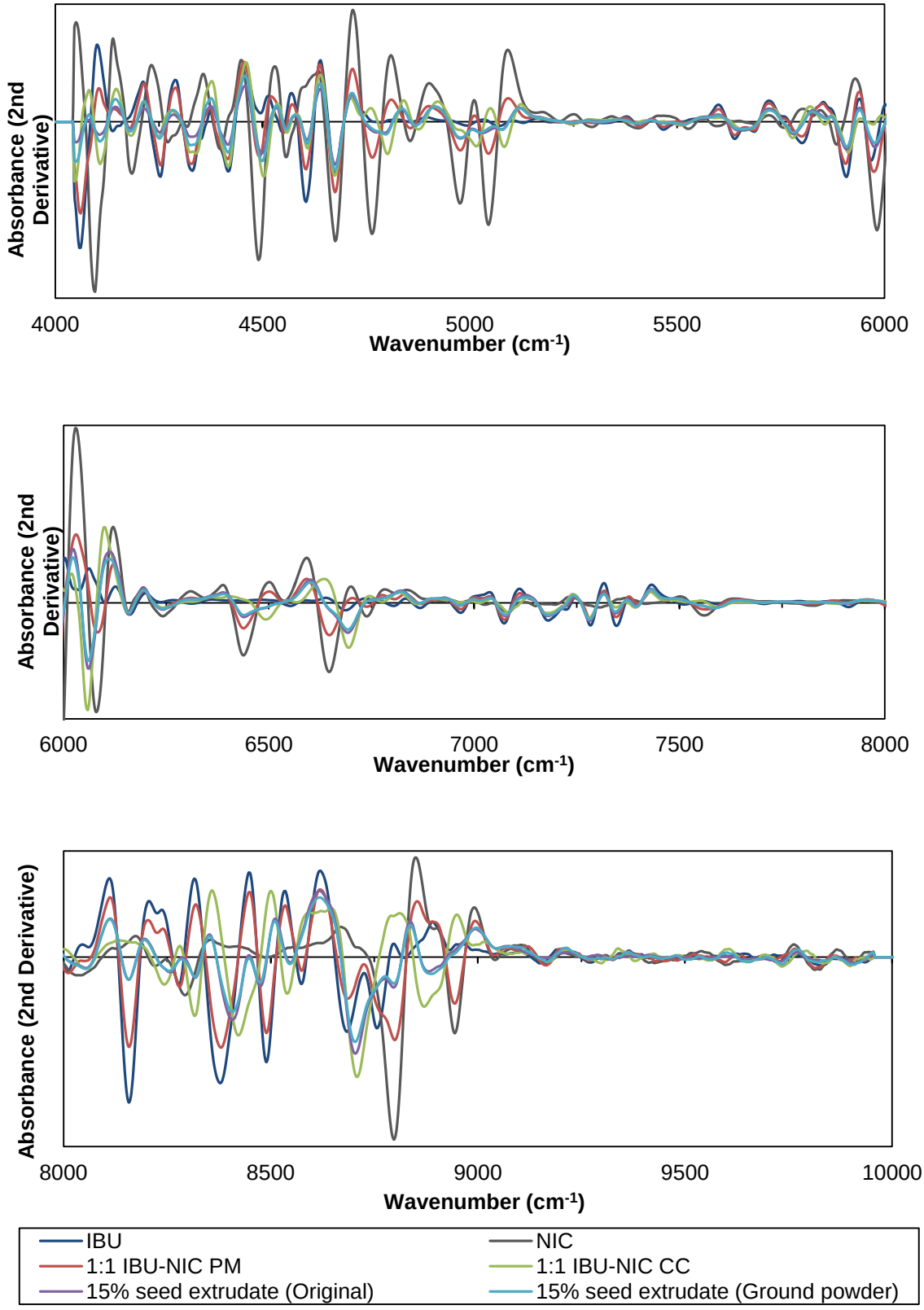

Figure 5.5 Second derivative NIR spectra of ibuprofen, nicotinamide, IBU-NIC 1:1 physical mixture, IBU-NIC 1:1 co-crystal (Microwave method section 3.2), extrudate T90 20 rpm 15% seed, extrudate T90 20 rpm 15% seed, ground powder. All the spectra shown have been treated with SNV baseline correction and Norris smoothing.

The second derivative spectra improved the resolution of the overlapping bands which provided an insight into whether the extruded samples were pure co-crystal as it was able to find small differences in the spectral data. When observing the second derivative spectra, there was no discernible difference between the original extruded sample and the ground powder sample. There are many examples throughout the second derivative NIR spectrum (4000-10000 cm^{-1}) where the extruded samples had bands which aligned with those for the pure co-crystal. However there were a number of extruded sample bands which had experienced a pull towards the ibuprofen spectra. This would suggest that there was a residual amount of ibuprofen in the extruded samples. The presence of ibuprofen in the extruded samples may have been caused by some of the initial (Within the first 10 minutes of extrusion) ibuprofen coating the extruder barrel, which then may have dislodged from the barrel during the extrusion process.

In conclusion, the 1:1 ibuprofen – nicotinamide co-crystal was successfully manufactured by hot melt extrusion. The screw speed was an important factor for co-crystal purity as well as the temperature profile that was used. Interestingly, the highest co-crystal yield was achieved using the temperature profile which provided a maximum temperature which was closest to the melting point of the 1:1 co-crystal. NIR analysis of 1:1 co-crystal seeded

extruded samples suggested that a high co-crystal purity could be achieved when using the low shear screw geometry A.

5.2 Carbamazepine – nicotinamide

A large proportion of the HME investigation was carried out using carbamazepine and nicotinamide with the general objective of producing 1:1 co-crystals. This section includes the initial study, the extruder barrel zone analysis, NIR characterisation and SEM particle analysis.

5.21 Extruder Study

The purity of the individual components was determined using powder X-ray diffraction. The diffraction spectra for carbamazepine, nicotinamide, CBZ-NIC 1:1 physical mixture and CBZ-NIC 1:1 co-crystal are shown in figure 5.6. The more prominent carbamazepine peaks are situated at approximately 12.8°, 14.9° and 15.7° (2θ). They can indicate whether any carbamazepine is present in a sample. Nicotinamide has a peak at 14.7° (2θ) which is useful for identifying nicotinamide in a sample. The co-crystal exhibits three major peaks at 6.6°, 8.8° and 10.2° (2θ) which can be used to reveal if any co-crystal is present in samples.

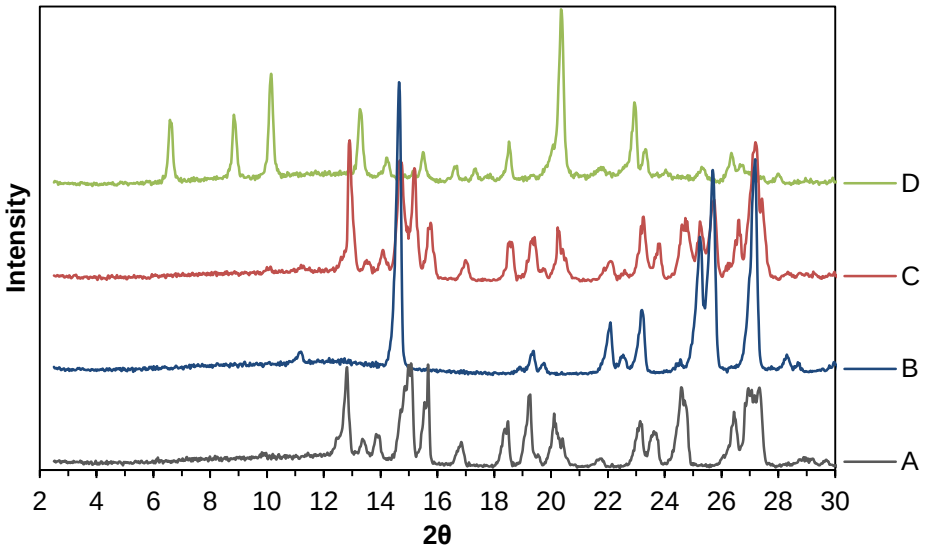

Figure 5.6 PXRD spectra of A. carbamazepine (Form III), B. nicotinamide, C. CBZ-NIC 1:1 physical mixture and D. CBZ-NIC 1:1 co-crystal (Solvent evaporation method section 3.3).

Thermal information about the carbamazepine – nicotinamide pair was important for optimising the temperature of extrusion and for selecting the temperature profiles that were used. Differential scanning calorimetry provided this information and the thermograms for carbamazepine, nicotinamide, CBZ-NIC 1:1 physical mixture and CBZ-NIC 1:1 co-crystal are shown in figure 5.7. The melting temperatures of carbamazepine and nicotinamide were found to be 175.0°C and 132.1°C respectively. The physical mixture eutectic melting point of the pair was 125.8°C and the co-crystal melting point was 162.4°C.

The thermal data that was gathered from the DSC results was used to decide what temperature profiles were chosen for the HME of carbamazepine – nicotinamide. It is thought that cocrystallisation can occur from the melt phase of the physical mixture. The physical mixture for

carbamazepine – nicotinamide has a eutectic melting point of 125.8°C. The temperature profiles for extrusion were based around this eutectic melting point, temperature and other parameters were investigated to increase the co-crystal purity.

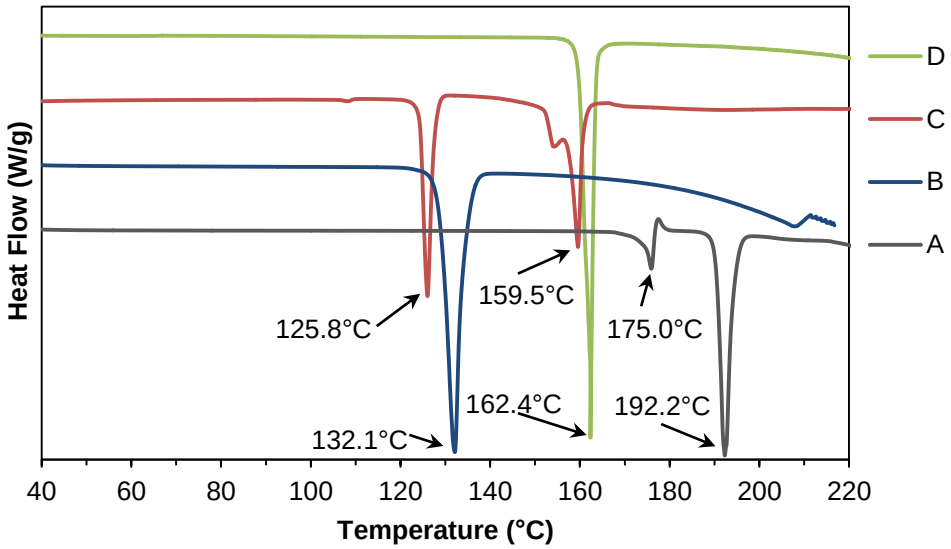

Figure 5.7 DSC thermograms of A. carbamazepine (Form III), B. nicotinamide, C. CBZ-NIC 1:1 physical mixture and D. CBZ-NIC 1:1 co-crystal (Solvent evaporation method section 3.3) heated at 10°C/min from 40°C to 220°C.

Extrusion was carried out by feeding a pre-mixed 1:1 physical mixture of carbamazepine and nicotinamide into the first zone of the extruder barrel. More details of the set-up are found in section 3.8. The temperature codes, such as T140, indicate the temperature profiles that were used and each code is described in section 3.81. The code indicates the maximum temperature achieved along the extruder barrel, so for T140 the maximum temperature was 140°C. Two screw geometries were explored, SGA and SGB (Described in section 3.82). The screw geometries directly influence the

degree of mixing and shear which are thought to aid the cocrystallisation process. Two screw speeds were selected; 20 rpm and 30 rpm. The 20 rpm screw speed provided a longer residence time and caused the material in the extruder barrel to experience a longer period of thermal exposure whereas the 30 rpm screw speed provided higher shear forces experienced by the material.

The first set of extrusion runs were carried out using SGA and a 20 rpm screw speed. The temperature was increased from T125 to T140 with 5°C intervals in between. The extrudates were collected and PXRD spectra of the samples were obtained for investigation purposes. The spectra are shown in figure 5.8 and are stacked to help identify subtle differences. The CBZ-NIC 1:1 physical mixture and CBZ-NIC 1:1 co-crystal spectra were included to display the peaks of interest.

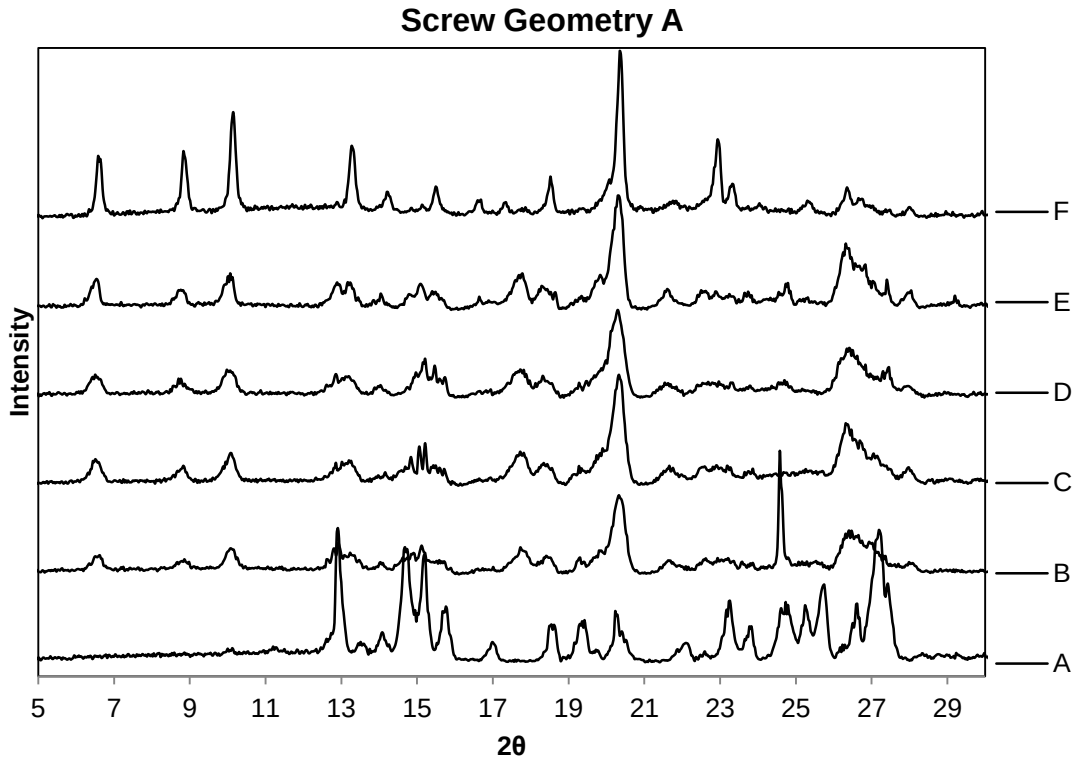

Figure 5.8 PXRD spectra of A. CBZ-NIC 1:1 physical mixture, B. extrudate T125 20 rpm, C. extrudate T130 20 rpm, D. extrudate T135 20 rpm, E. extrudate T140 20 rpm, F. CBZ-NIC 1:1 co-crystal (Solvent evaporation method section 3.3).

The extrudates PXRD spectra, shown in figure 5.8, all exhibited the first three co-crystal peaks situated at 12.8°, 14.9° and 15.7° (2θ), indicating cocrystallisation had occurred when using this screw speed. The carbamazepine peak at 12.8° (2θ) is present in all extruded samples, suggesting there was some pure carbamazepine remaining after extrusion. There were very subtle differences between the spectra for the extruded samples with no significant indications that an increase in temperature has an impact on the co-crystal purity when using 20 rpm screw speed and SGA.

The second set of extrusion runs were carried out using SGB and a screw speed of 20 rpm. The number of different temperature profiles was increased to accommodate the lower temperatures of T110 and T120. The extrudates were collected and PXRD spectra of the samples were obtained and are shown in figure 5.9 and are stacked to help identify subtle differences. The CBZ-NIC 1:1 physical mixture and CBZ-NIC 1:1 co-crystal spectra were included to display the peaks of interest.

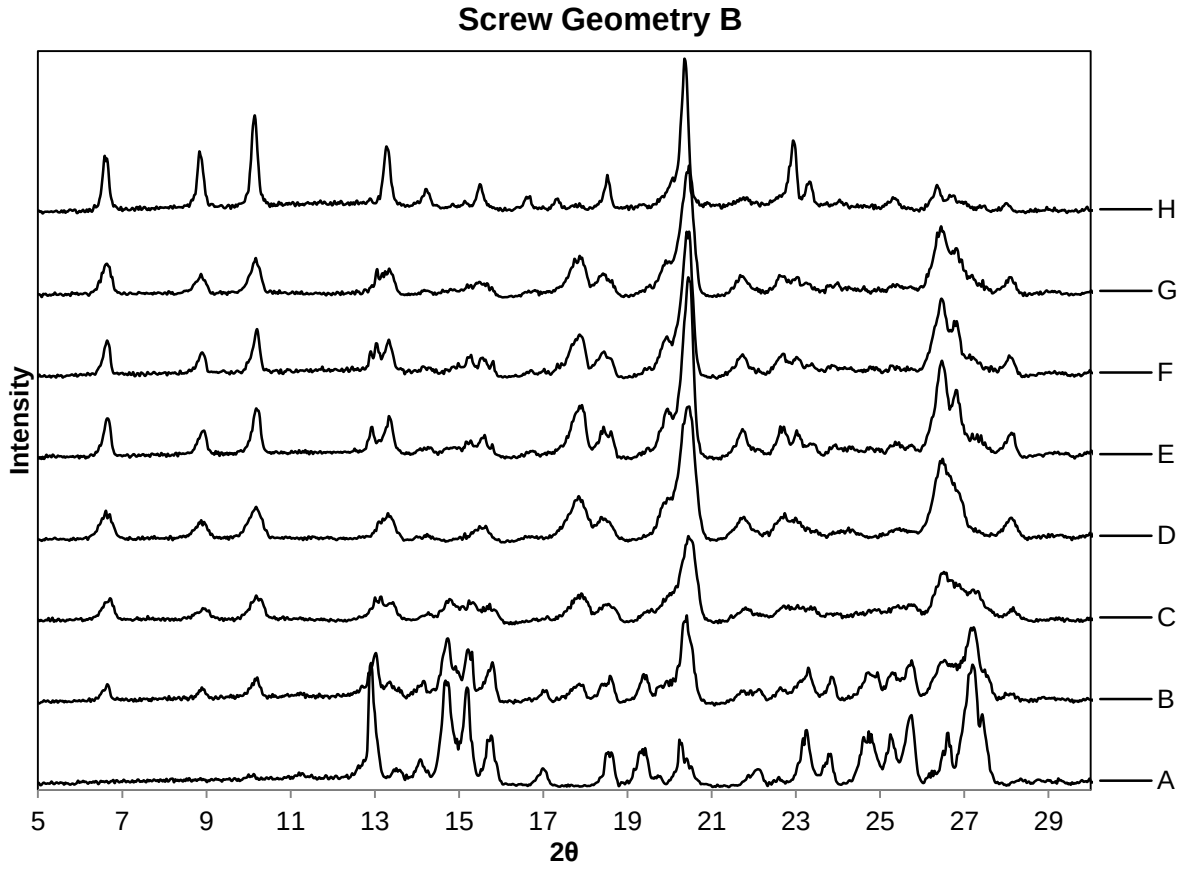

Figure 5.9 PXRD spectra of A. CBZ-NIC 1:1 physical mixture, B. extrudate T110 20 rpm, C. extrudate T120 20 rpm, D. extrudate T125 20 rpm, E. extrudate T130 20 rpm, F. extrudate T135 20 rpm, G. extrudate T140 20 rpm, H. CBZ-NIC 1:1 co-crystal (Solvent evaporation method section 3.3).

The extrudates PXRD spectra, shown in figure 5.9, all exhibited the first three co-crystal peaks situated at 12.8°, 14.9° and 15.7° (2θ), these peaks appear more prominent compared to the extrudates in figure 5.8, particularly for the extruded samples at T130, T135 and T140. The carbamazepine peak at 12.8° (2θ) was present in all extruded samples, suggesting there was some pure carbamazepine remaining after extrusion. The increase in temperature did have a small impact on the co-crystal yield, particularly from T110 through to T130.

Two additional extrusion runs were carried out using the 10 rpm screw speed at T135 and T140 using SGB. The objective was to reduce the screw speed and increase the residence time of the material in the extruder barrel to increase the co-crystal yield. The resulting extruded samples were subjected to PXRD and are shown in figure 5.10 along with the corresponding samples extruded at 20 rpm, the physical mixture and the pure co-crystal.

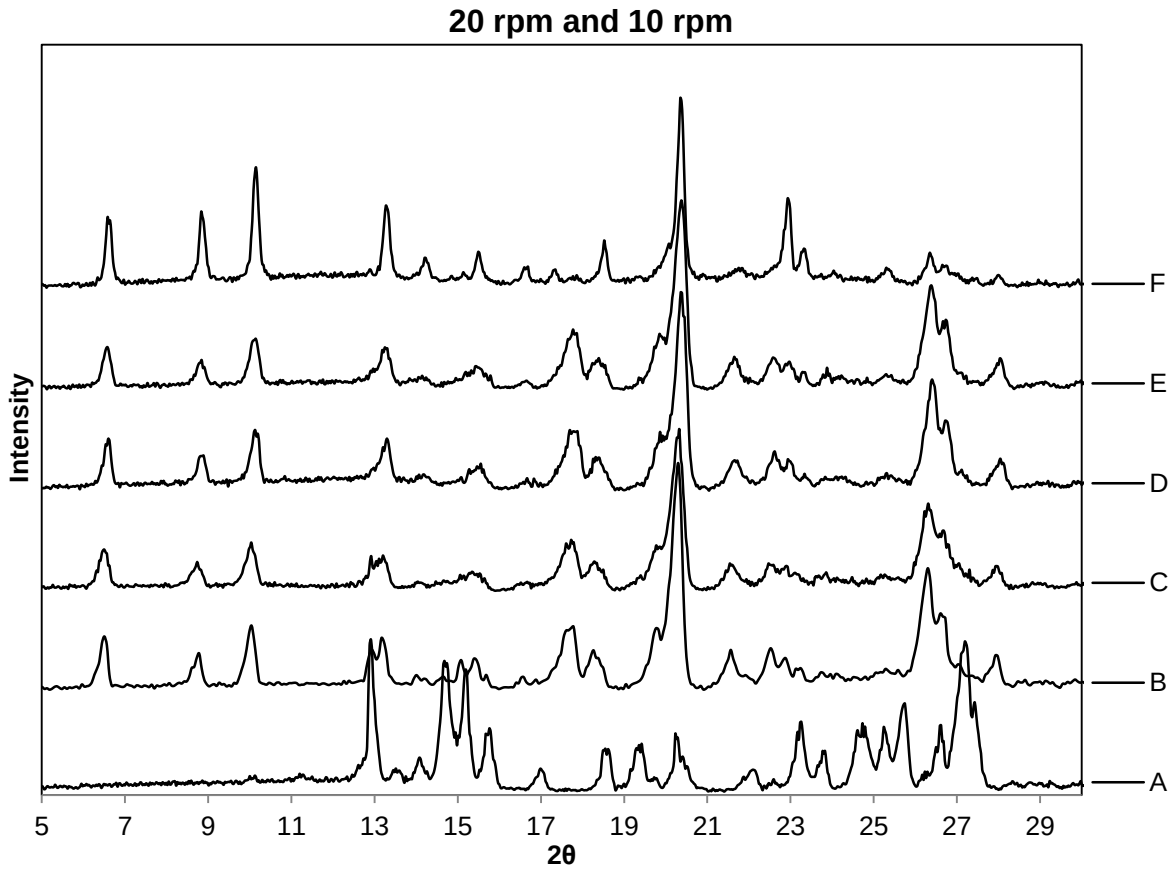

Figure 5.10 PXRD spectra of A. CBZ-NIC 1:1 physical mixture, B. extrudate T135 20 rpm, C. extrudate T140 20 rpm, D. extrudate T135 10 rpm, E. extrudate T140 10 rpm, F. CBZ-NIC 1:1 co-crystal (Solvent evaporation method section 3.3).

The PXRD spectra in figure 5.10 showcase the 20 rpm extrudates (B and C) and the 10 rpm extrudates (D and E). The carbamazepine peak at 12.8° (2θ) had a reduced intensity for the 10 rpm spectra compared to the 20 rpm spectra. This indicated that the increased residence time allowed for more of the remaining carbamazepine to form the co-crystal. From observing the PXRD spectra, the T135 10 rpm SGB extrudate sample had the least amount of remaining carbamazepine and nicotinamide.

In conclusion, the hot melt extrusion technique was able to successfully produce the 1:1 co-crystal of carbamazepine and nicotinamide. With often small differences between the PXRD spectra when comparing the extruded samples it was difficult to determine the true purity. Both screw geometries (SGA and SGB) were able to provide enough shear and mixing for cocrystallisation to occur and the co-crystal yield increased when the temperature was increased from T110 to T130. Samples extruded at higher temperatures between T130 and T140 had very small differences in the PXRD spectra when compared with one another.

The increased residence time that the 10 rpm screw speed provided, enabled further cocrystallisation to take place, which in turn reduced the amount of residual carbamazepine and nicotinamide in the extruded samples. It was observed that under the conditions of T135 10 rpm SGB, the extruded sample had a relatively good co-crystal yield with very low amounts of residual carbamazepine and nicotinamide. This temperature profile reached the maximum temperature of 135°C along the extruder barrel, this was approximately 10°C above the eutectic melting point of the 1:1 physical mixture of carbamazepine and nicotinamide.

5.22 Extruder barrel zone investigation

To further understand cocrystallisation via hot melt extrusion, it was necessary to explore where along the extruder barrel cocrystallisation was occurring. The extruder barrel zone investigation was carried out for the carbamazepine – nicotinamide pair. A series of extrusion runs, carried out at different temperatures and screw speeds, were selected according to the

results from section 5.21. Each extrusion run was allowed to mature for 10 minutes before the extruder was switched off. This was done to ensure that the extruder barrel was as full as possible with the pre-mixed carbamazepine – nicotinamide physical mixture and to make sure the process had reached full maturity regarding cocrystallisation. Samples were immediately collected from along the barrel and PXRD analysis was carried out. It is important to note that zone 1 of the extruder barrel is behind where the pre-mixed physical mixture is fed into the extruder, therefore there was no point of collecting the zone 1 sample as it is irrelevant to the extrusion process.

Initially, a test extrusion run was carried out to determine if it was possible to collect the samples from the extruder barrel. It was difficult to locate exactly where each zone began and finished along the extruder barrel when the barrel was full of material, this test run also highlighted concerns about handling the material next to a high temperature extruder barrel. Due to an issue with locating the barrel zones between zone 2 and zone 6, the samples from these zones were discarded. Figure 5.11 shows the PXRD spectra from this test run which was carried out under the conditions of temperature profile T130, screw geometry B and 20 rpm screw speed.

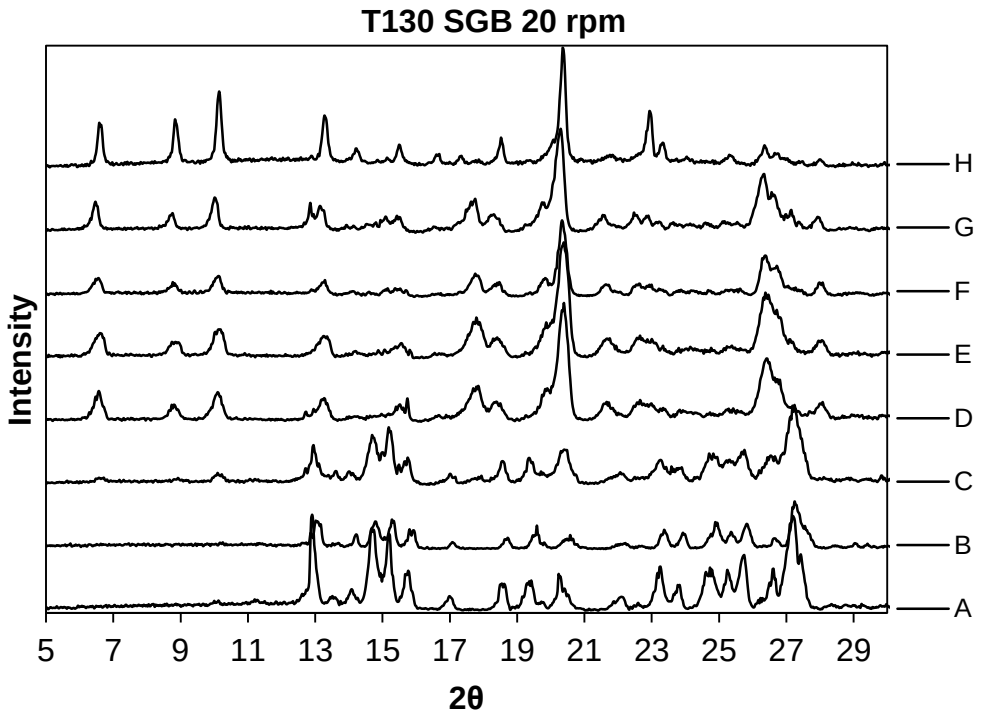

Figure 5.11 PXRD spectra of A. CBZ-NIC 1:1 physical mixture, B. zone 2 sample, C. zone 6 sample, D. zone 7 sample, E. zone 8 sample, F. zone 9 sample, G. extrudate sample, H. CBZ-NIC 1:1 co-crystal (Solvent evaporation method section 3.3).

The PXRD spectra in figure 5.11 indicated that cocrystallisation had occurred by at least zone 6 of the extruder barrel. There was remaining carbamazepine in the samples from zones 2, 6 and 7 and also in the extruded sample. The temperature of the extruder barrel at zone 6 was set to 125°C. The eutectic point of the carbamazepine – nicotinamide physical mixture is 125.8°C. This may suggest that the eutectic point plays an important role in the cocrystallisation process. However, to explore this, samples from each extruder barrel zone would be required.

The issue regarding locating the extruder barrel zones was solved by marking the start of each zone on the side of the extruder barrel. This did not

interfere with the extrusion process and provided a simple way of determining the location of each zone. Two more extrusion runs were carried out under the conditions of screw geometry B, 20 rpm screw speed and temperature codes T135 and T140. Samples were collected from all extruder zones (Zone 2 to the extruded sample). The PXRD spectra are shown in figure 5.12 and figure 5.13 for T135 and T140 respectively.

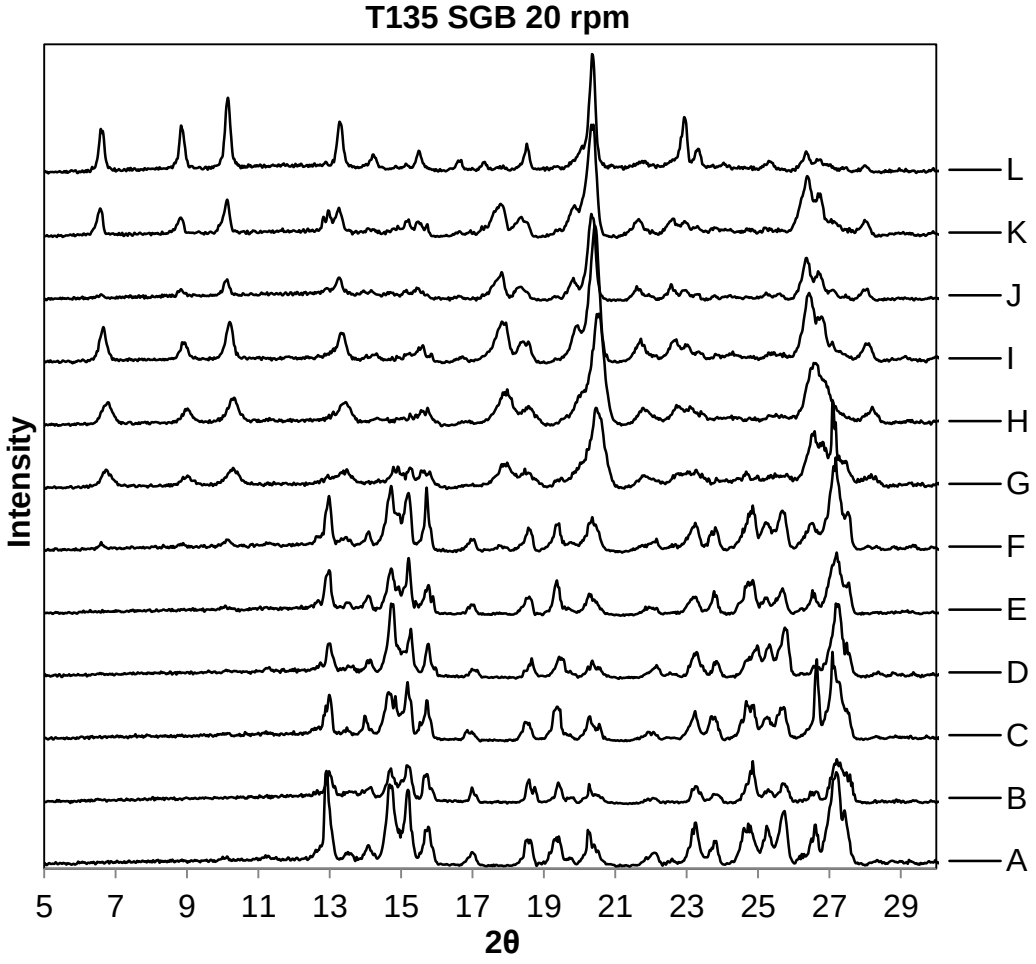

Figure 5.12 PXRD spectra of A. CBZ-NIC 1:1 physical mixture, B. zone 2 sample, C. zone 3 sample, D. zone 4 sample, E. zone 5 sample, F. zone 6 sample, G. zone 7 sample, H. zone 8 sample, I. zone 9 sample, J. zone 10 sample, K. extrudate sample, L. CBZ-NIC 1:1 co-crystal (Solvent evaporation method section 3.3).

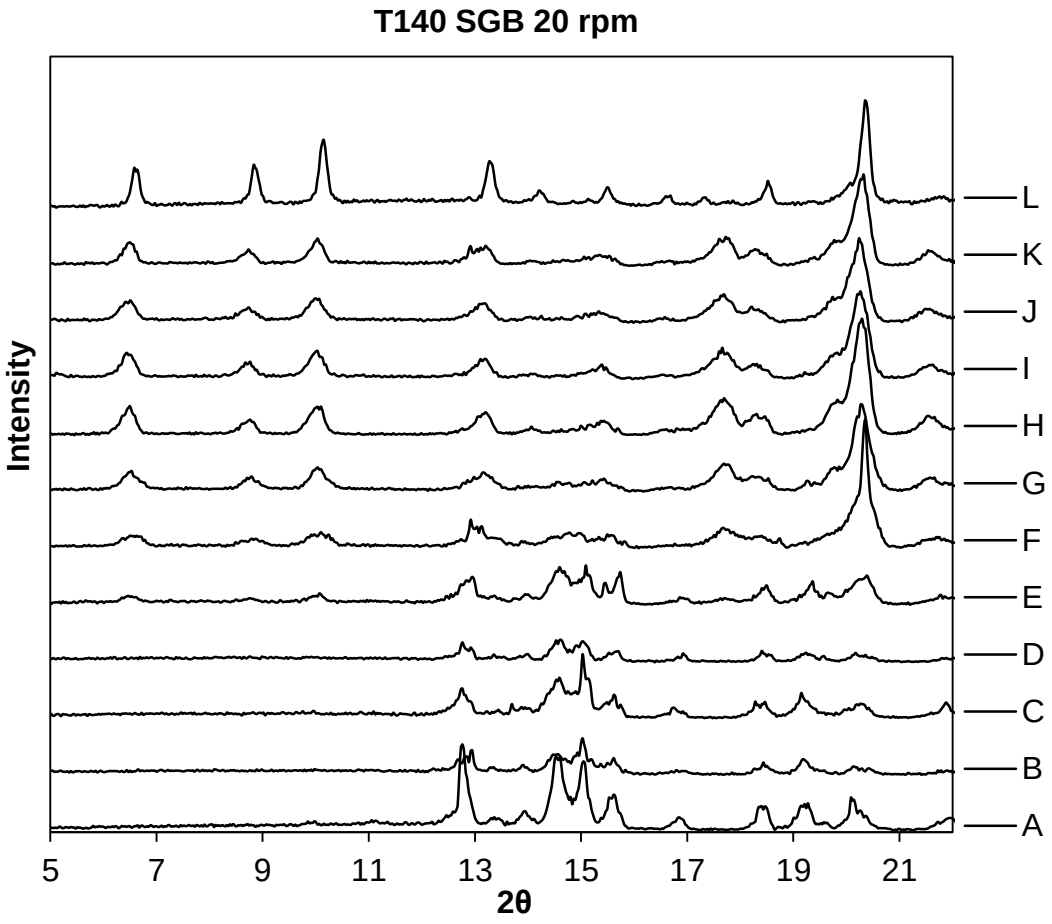

Figure 5.13 PXRD spectra of A. CBZ-NIC 1:1 physical mixture, B. zone 2 sample, C. zone 3 sample, D. zone 4 sample, E. zone 5 sample, F. zone 6 sample, G. zone 7 sample, H. zone 8 sample, I. zone 9 sample, J. zone 10 sample, K. extrudate sample, L. CBZ-NIC 1:1 co-crystal (Solvent evaporation method section 3.3).

For the T135 extrusion run in figure 5.12, the three main co-crystal PXRD peaks appear at zone 6 of the extruder barrel. The temperature of zone 6 for the T135 temperature profile was 130°C, and the temperature of zone 5 was 120°C. For the T140 extrusion run, the PXRD spectra in figure 5.13 indicate that cocrystallisation first occurs at zone 5 of the extruder barrel. For the T140 temperature profile, the temperature of zone 5 is 125°C. Therefore, the

eutectic melting point of the carbamazepine – nicotinamide physical mixture is very important for cocrystallisation of this pair. Although it is unclear from the PXRD spectra which extrusion run produced the best co-crystal yield, the higher temperature of T140 may provide a more optimal environment for cocrystallisation because the co-crystals start to form earlier along the extruder barrel, allowing the co-crystals to form and grow for the remainder of the residence time.

5.23 NIR analysis

An alternative characterisation method was chosen to analyse the extruded material. NIR spectroscopy was believed to provide key molecular information about the material as well as the capability to provide more detail about the co-crystal yield, particularly when chemometric techniques were applied, such as the second derivative. The rapid scanning time for the offline, reflection NIR spectroscopy mode, ensured that the NIR spectra gave a more accurate characterisation of the extruded materials than PXRD, this is because the time it took for PXRD of some samples was several hours, in which time, more co-crystal may have formed.

Firstly, the original and second derivative NIR spectra for carbamazepine, nicotinamide, CBZ-NIC 1:1 physical mixture and the CBZ-NIC 1:1 co-crystal are shown in figure 5.14.

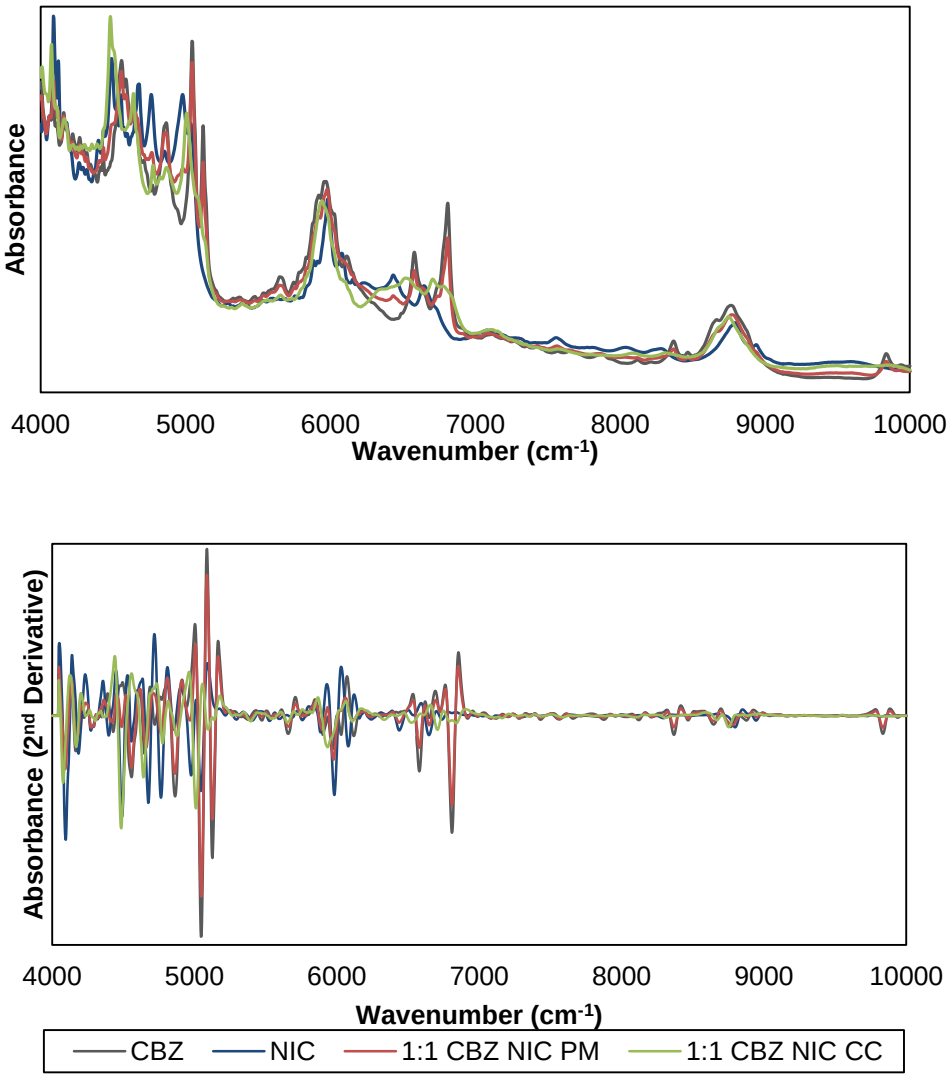

Figure 5.14 Original (Top) and second derivative (Bottom) NIR spectra of carbamazepine (Form III), nicotinamide, CBZ-NIC 1:1 physical mixture and CBZ-NIC 1:1 co-crystal (Solvent evaporation method section 3.3). All the spectra shown have been treated with SNV baseline correction.

Extrusion runs were carried out at different screw speeds of 10 rpm and 20 rpm and with different temperature profiles. Screw geometry B was used for all the runs. The NIR spectra collected from the extruded samples are shown in figure 5.15.

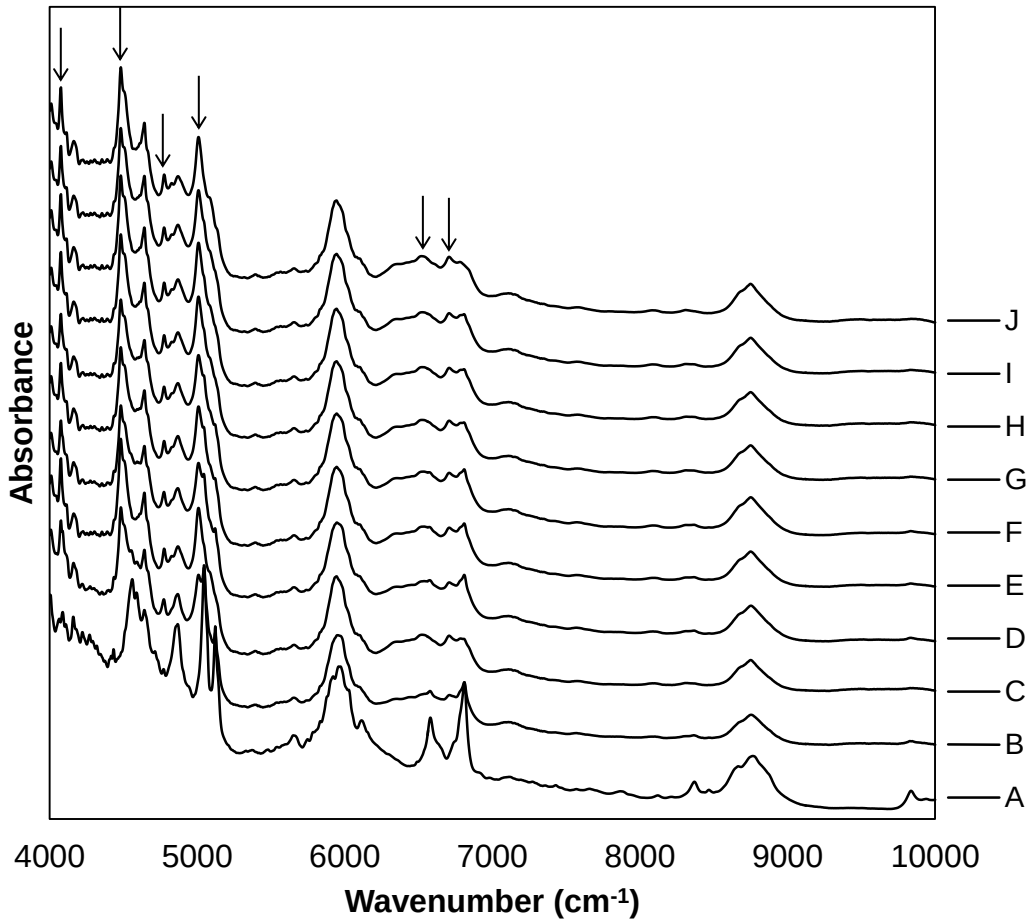

Figure 5.15 Original NIR spectra of A. 1:1 CBZ-NIC physical mixture, B. T120 SGB 20 rpm sample, C. T125 SGB 20 rpm sample, D. T130 SGB 20 rpm sample, E. T135 SGB 20 rpm sample, F. T140 SGB 20 rpm sample, G. T130 SGB 10 rpm sample, H. T135 SGB 10 rpm sample, I. T140 SGB 10 rpm sample, J. 1:1 CBZ-NIC co-crystal (Solvent evaporation method section 3.3).

The NIR spectra of the extruded samples in figure 5.15 show a large reduction of the intensity of the carbamazepine NIR bands situated at 4555, 5045, 5064, 6576, 6807 and 8358 cm^{-1}. The intensity of these bands reduced further when the screw speed was decreased to 10 rpm (Spectra G, H and I). This is a clear indication of the impact the 10 rpm screw speed has

on the co-crystal yield of the extruded samples. The unique co-crystal bands at 4073, 4478, 4771, 5002, 6503, 6680 cm^{-1} are indicated by the black arrows in figure 5.15. The NIR spectra suggest that all extruded samples have a relatively high co-crystal yield, and this yield increased when the screw speed was decreased. To extract more information from the spectra, the second derivative spectra for the extruded samples are shown in figure 5.16.

The second derivative NIR spectra in figure 5.16 have been colour coordinated to orange/red colours for 20 rpm samples and blue/purple colours for 10 rpm samples to make the graphs clearer. The samples processed at 10 rpm have more NIR bands in line with the bands for the 1:1 co-crystal compared to the 20 rpm samples. However, a smaller region was required to observe differences in the spectra of the extruded samples.

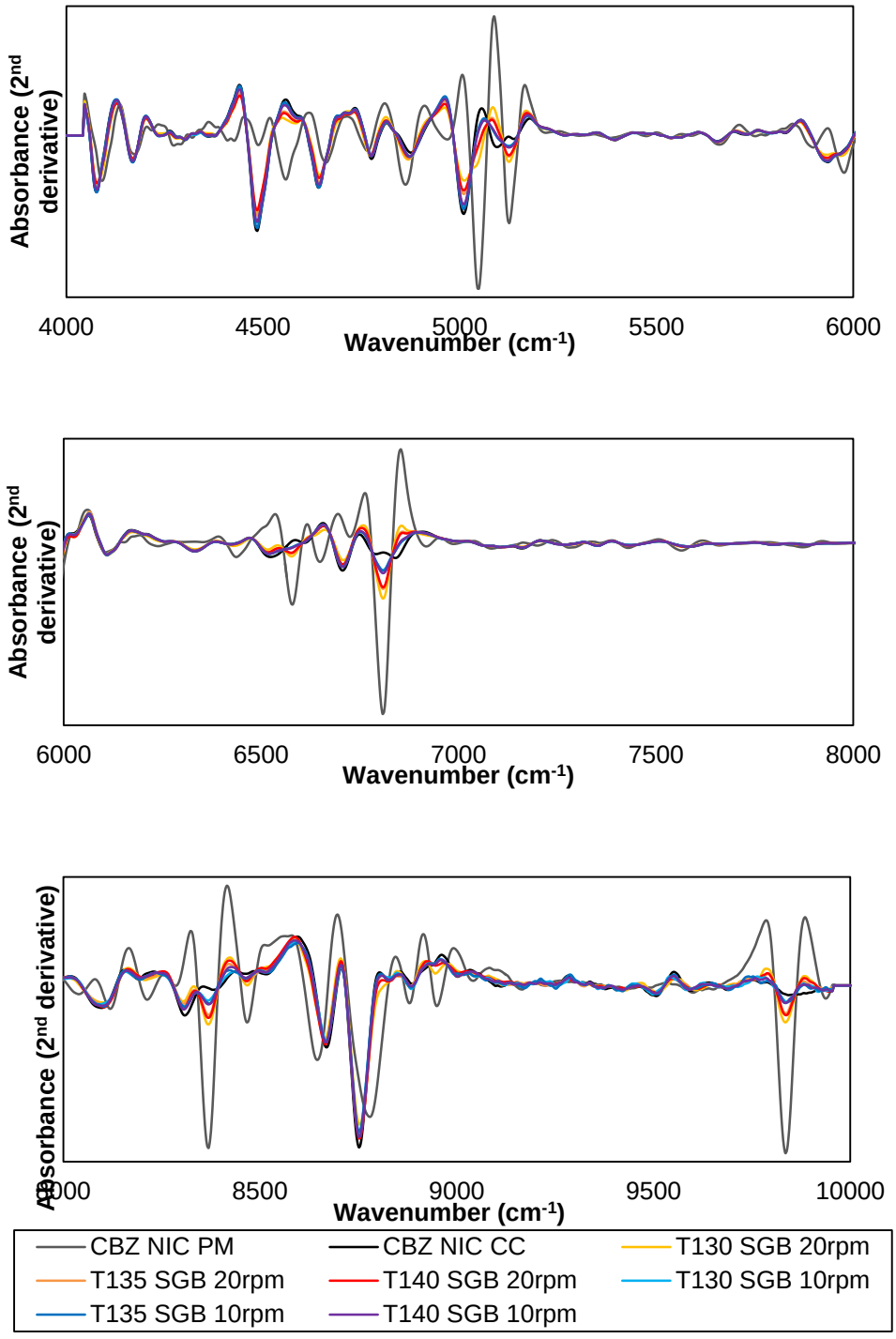

Figure 5.16 Second derivative NIR spectra of 1:1 CBZ-NIC physical mixture, T130 SGB 20 rpm sample, T135 SGB 20 rpm sample, T140 SGB 20 rpm sample, T130 SGB 10 rpm sample, T135 SGB 10 rpm sample, T140 SGB 10 rpm sample, 1:1 CBZ-NIC co-crystal (Solvent evaporation method section 3.3).

Figure 5.17 shows second derivative NIR spectra for the region of 4930 cm^{-1} to 5150 cm^{-1} taken from figure 5.16. This region provided the clearest indication of how the co-crystal yield increased when the samples were processed at a 10 rpm screw speed compared to the 20 rpm.

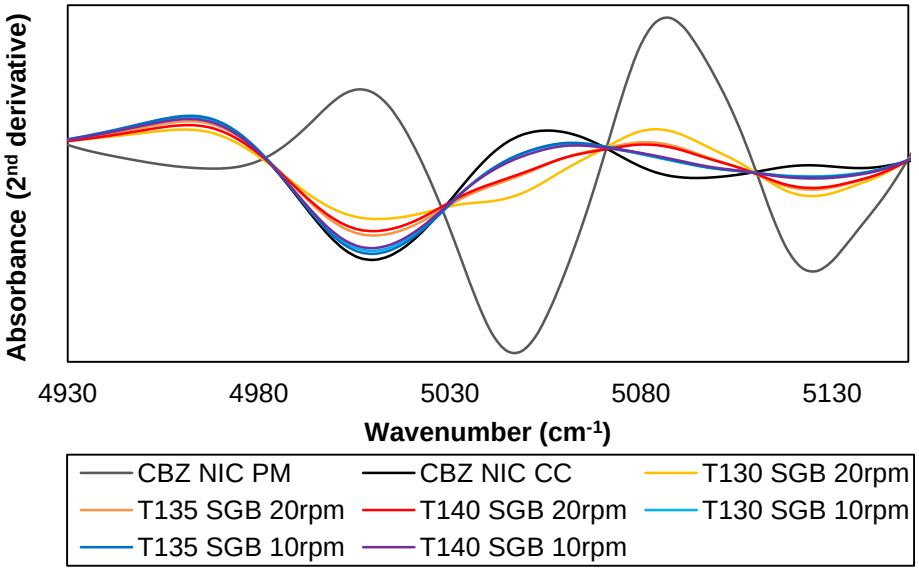

Figure 5.17 Second derivative NIR region 4930 cm^{-1} to 5150 cm^{-1} spectra of 1:1 CBZ-NIC physical mixture, T130 SGB 20 rpm sample, T135 SGB 20 rpm sample, T140 SGB 20 rpm sample, T130 SGB 10 rpm sample, T135 SGB 10 rpm sample, T140 SGB 10 rpm sample, 1:1 CBZ-NIC co-crystal (Solvent evaporation method section 3.3).

NIR spectra were also collected for the extruded samples from the experiments in section 5.22. The original spectra for the extruded samples, taken from the barrel zones and the final extruded sample under the conditions of T135 SGB 20 rpm, T140 SGB 20 rpm and T140 SGB 10 rpm are plotted in figure 5.18. The spectra for all three extrusion runs displayed observable changes in the spectra between zone 5 and zone 8.

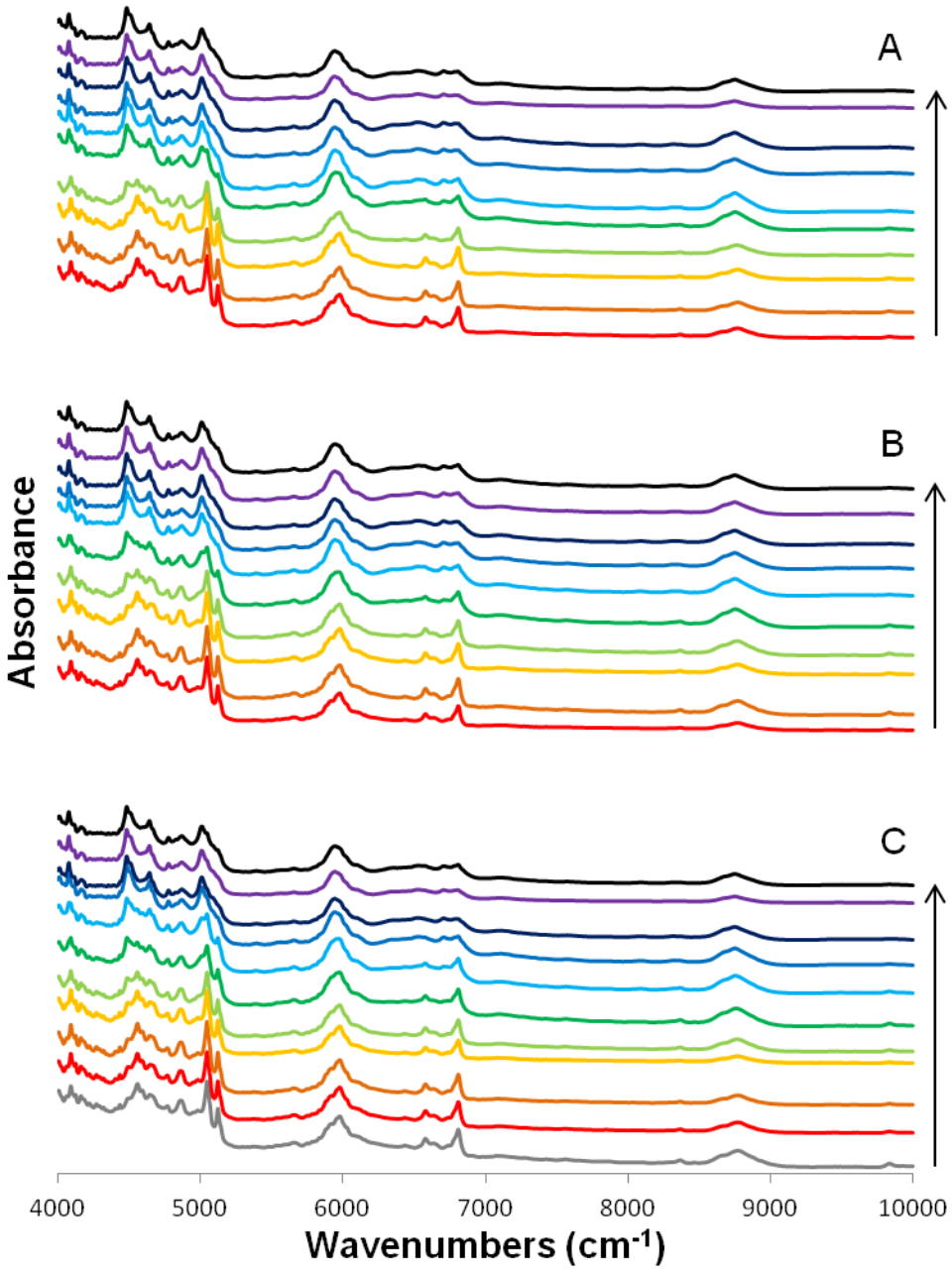

Figure 5.18 NIR spectra of samples taken from along the extruder barrel from zone 2 to the extruded material. A) T140 SGB 10 rpm, B) T140 SGB 20 rpm, C) T135 SGB 20 rpm. The arrows indicate the samples starting at zone 2 and finishing at the extruded material. The 1:1 carbamazepine nicotinamide physical mixture is also included (The grey spectrum).

Between these four zones, carbamazepine bands reduced in intensity, and co-crystal bands significantly increased in intensity. The carbamazepine band at 6807 cm^{-1} indicated the amount of pure carbamazepine left in each sample, this band exhibited a significant reduction in intensity at zone 8 for the T135 SGB 20 rpm run, and at zone 7 for the T140 SGB 20 rpm and 10 rpm runs.

Again, the second derivative spectra were observed to find any small variations between the three extrusion runs. The second derivative spectra are plotted in figure 5.19 for the same samples as viewed in figure 5.18. Four small regions were selected, 5850 to 6000 cm^{-1}, 6780 to 6890 cm^{-1}, 4050 to 4150 cm^{-1} and 4600 to 4700 cm^{-1} which showed clear differences between the second derivative spectra.

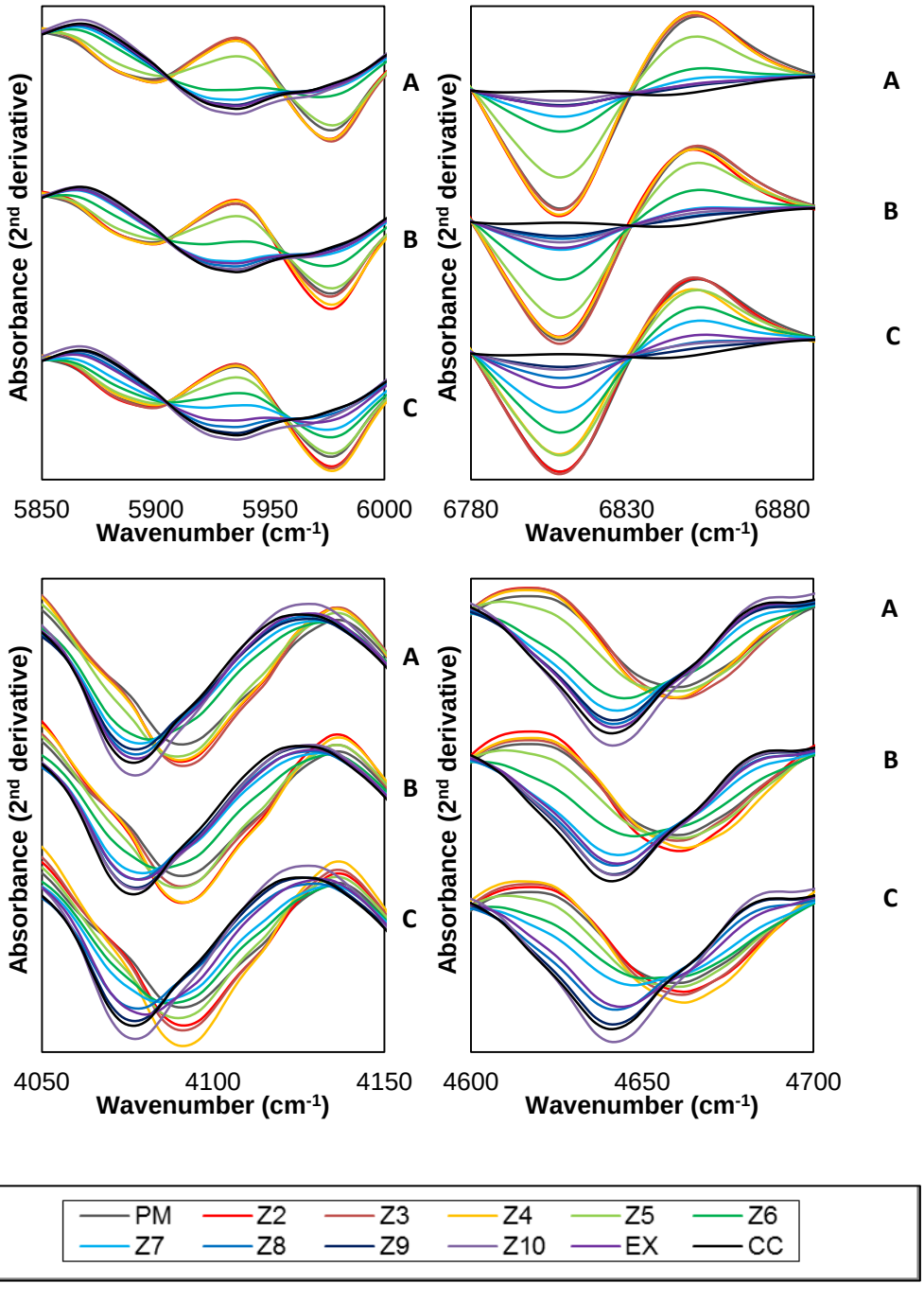

Figure 5.19 Second derivative NIR regions: 5850 to 6000 cm^{-1}, 6780 to 6890 cm^{-1}, 4050 to 4150 cm^{-1} and 4600 to 4700 cm^{-1}. Spectra of 1:1 CBZ-NIC physical mixture, zone 2 to zone 10 and extruded samples and 1:1 CBZ-NIC co-crystal (Solvent evaporation method section 3.3) for three extrusion runs of T140 SGB 10 rpm (A), T140 SGB 20 rpm (B) and T135 SGB 20 rpm (C).

The second derivative spectra in figure 5.19 showed band ‘reversal’ in intensity and also band shifting. The region of 5850 to 6000 cm^{-1} exhibited the bands changing their intensity from positive to negative and vice versa, as the co-crystal yield increased. This was also the case for the region of 6780 to 6890 cm^{-1}. For the regions of 4050 to 4150 cm^{-1} and 4600 to 4700 cm^{-1}, the band at approximately 4092 cm^{-1} shifted to 4077 cm^{-1} and the band at approximately 4663 cm^{-1} shifted to 4640 cm^{-1} with increasing co-crystal yield. The spectra for the samples taken from zone 6 for all three extrusion runs show a greater change in intensity, or greater shift towards the pure co-crystal spectrum, as the temperature profile is increased from T135 to T140, and the screw speed is reduced from 20 rpm to 10 rpm. For the two temperature codes, the increase in temperature at zone 6 of the extruder barrel is from 130°C to 135°C when going from T135 to T140. As the carbamazepine – nicotinamide physical mixture eutectic melting point of 125.8°C is reached earlier along the extruder barrel, as a higher temperature profile is used, the co-crystal begins to form earlier along the barrel.

This section provided a clear insight into the effect of different parameters on co-crystal formation by hot melt extrusion. Samples taken and analysed from along the extruder barrel indicated that the eutectic temperature was an important factor for co-crystal formation as presented by PXRD and NIR characterisation techniques.

5.24 SEM analysis

Scanning electron microscopy (SEM) was an important technique used to support the extrusion chapter. It was viewed as a powerful technique which

can determine particle morphology information including particle size. In this section, SEM was used for analysing pure carbamazepine and nicotinamide, 1:1 carbamazepine nicotinamide physical mixture and 1:1 carbamazepine – nicotinamide co-crystal. Secondly, it was employed for analysing selected carbamazepine nicotinamide extrusion samples.

SEM images of pure carbamazepine and nicotinamide are shown in figure 5.20 at 400X and 200X magnification respectively. The carbamazepine particles ranged from 10 µm to 100 µm in diameter and the nicotinamide particles ranged from 50 µm to 400 µm in diameter.

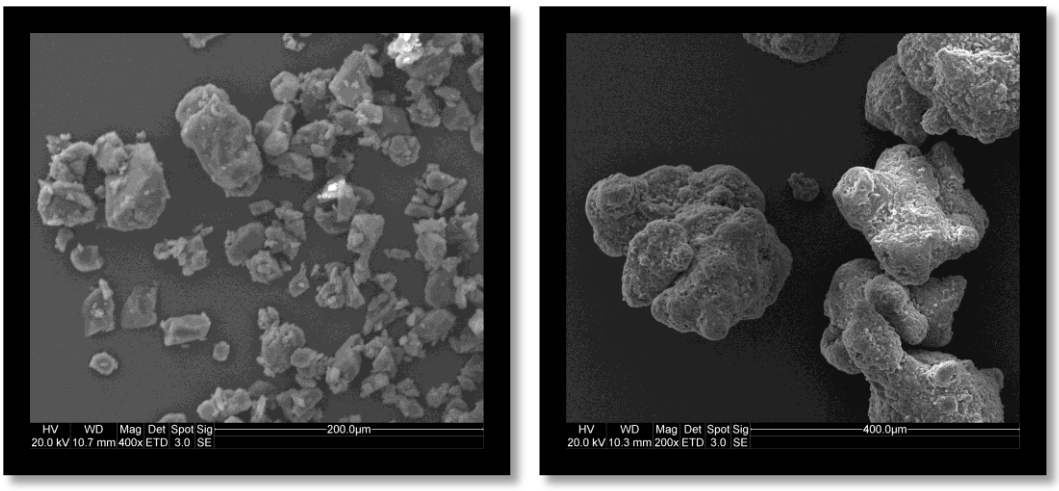

Figure 5.20 SEM image of carbamazepine (Form III) 400X (Left). SEM image of nicotinamide 200X (Right).

The SEM images for the 1:1 carbamazepine nicotinamide physical mixture are shown in figure 5.21. In the 200X image, the contrasting sizes of the carbamazepine and nicotinamide particles can be observed next to one another. Under further magnification of 2000X, carbamazepine particles can be seen coating the nicotinamide particle surface.

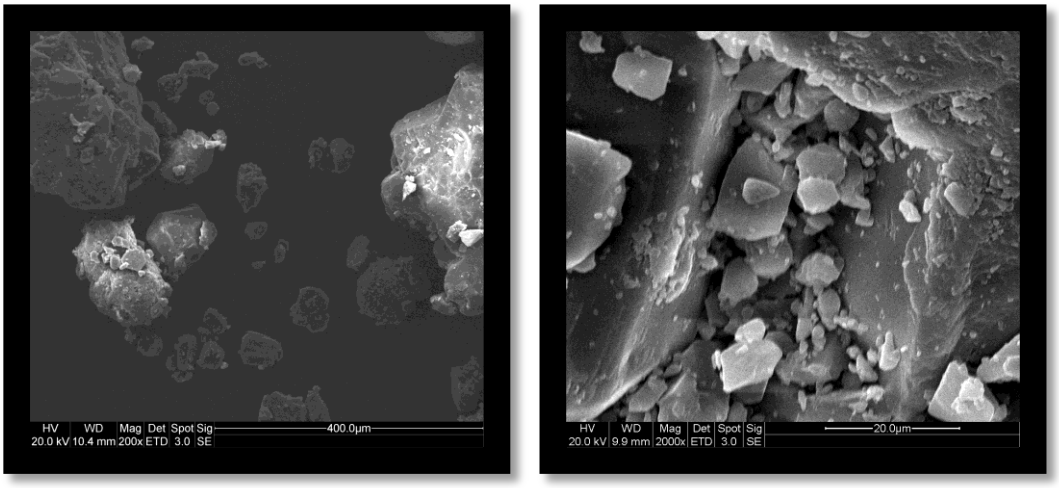

Figure 5.21 SEM images of 1:1 carbamazepine nicotinamide physical mixture at 200X magnification (Left) and 2000X magnification (Right).

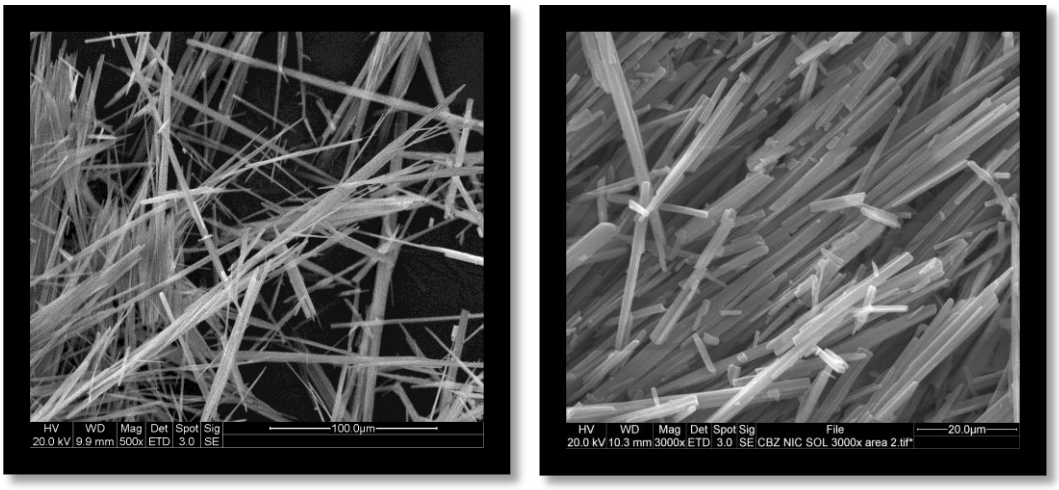

Figure 5.22 SEM images of 1:1 carbamazepine nicotinamide co-crystal (Solvent evaporation method section 3.3) at 500X magnification (Left) and 3000X magnification (Right).

Figure 5.22 displays the SEM images of the 1:1 pure co-crystal made using the solvent evaporation technique described in section 3.3. The co-crystal is shown at 500X and 3000X magnification. In solution, the co-crystals grew

following a needle shaped morphology. The co-crystal needles had a width between 2 µm and 5 µm and a length between 10 µm and 300 µm.

Selected extrusion samples from section 5.2 were analysed using SEM. The images for the extruded sample for the extrusion run carried out under the conditions T135 SGB 20 rpm are shown in figure 5.23. At the magnifications of 500X and 1000X, 1:1 co-crystal needles were observed. The needles had a width between 2 µm and 10 µm and the needle lengths were between 5 µm and 80 µm. The needles were generally shorter than the co-crystal needles produced using solution evaporation in figure 5.22. There was also evidence of hollow co-crystal needles in the 1000X magnification image (Circled in red), the unique conditions of twin screw extrusion could have caused this morphology to occur.

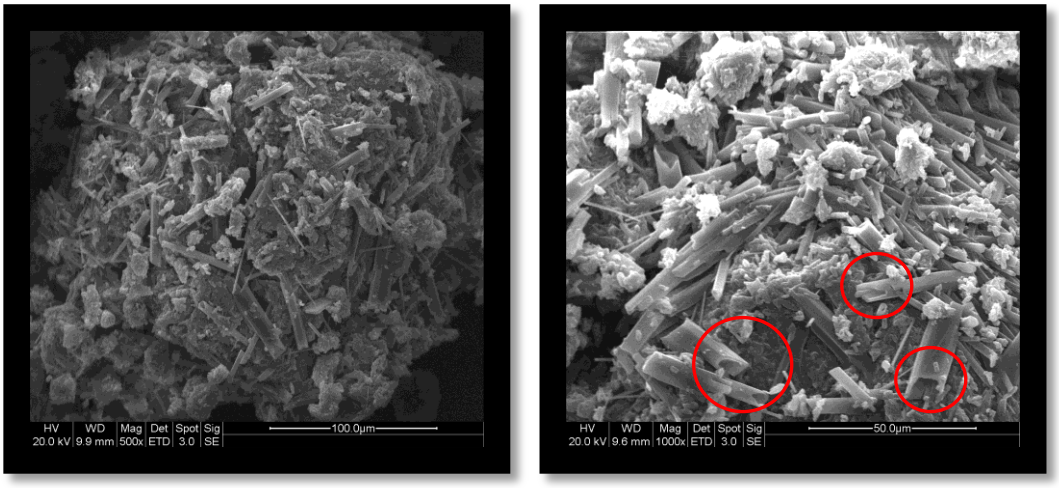

Figure 5.23 SEM images of the carbamazepine nicotinamide extruded sample: T135 SGB 20 rpm at 500X magnification (Left) and 1000X magnification (Right).

SEM images of the extruded sample, using conditions T140 SGB 10 rpm, are shown in figure 5.24. There were no hollow co-crystal needles located in

the section of the sample that was viewed under the microscope. The SEM images do however show co-crystal needles which were slightly shorter than those found in figure 5.23. The image of 3000X magnification was displayed because it exhibited a large co-crystal needle, with a width of approximately 5 µm adjacent to a much thinner co-crystal needle. It was evident, that the unique 'journey' of the material through the extruder barrel had a significant impact on co-crystal morphology. It may also be the case that co-crystals which formed at an early extruder barrel zone, had a longer residence time, and may have experienced more growth than those which formed later along the barrel.

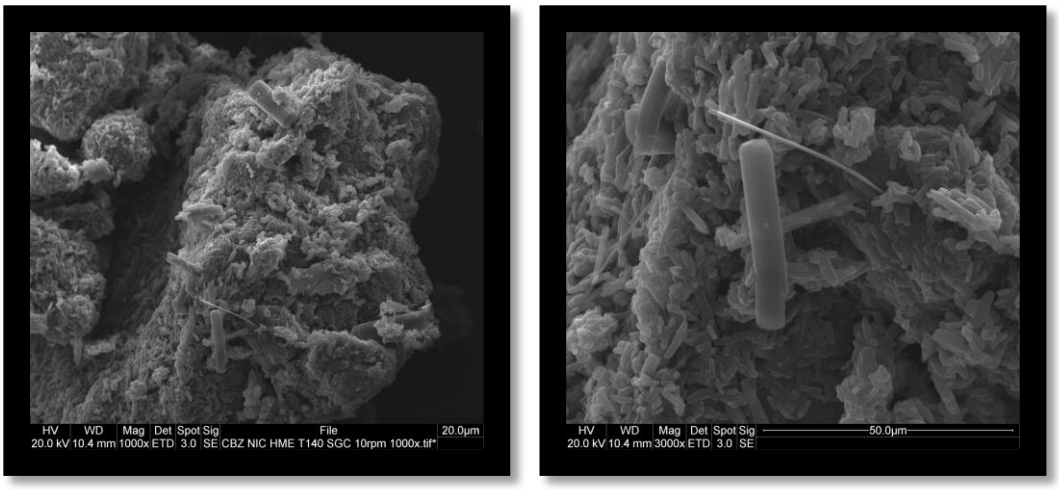

Figure 5.24 SEM images of the carbamazepine nicotinamide extruded sample: T140 SGB 10 rpm at 1000X magnification (Left) and at 3000X magnification (Right).

To investigate observable differences between the samples taken from the extruder barrel zones, SEM images were collected for zone 8 to zone 10 samples for the T140 SGB 10 rpm extrusion run. Figure 5.25 shows the SEM

images for the samples from zones 8 and 9. Figure 5.26 shows SEM images for the samples from zone 10 and a selected image from zone 8.

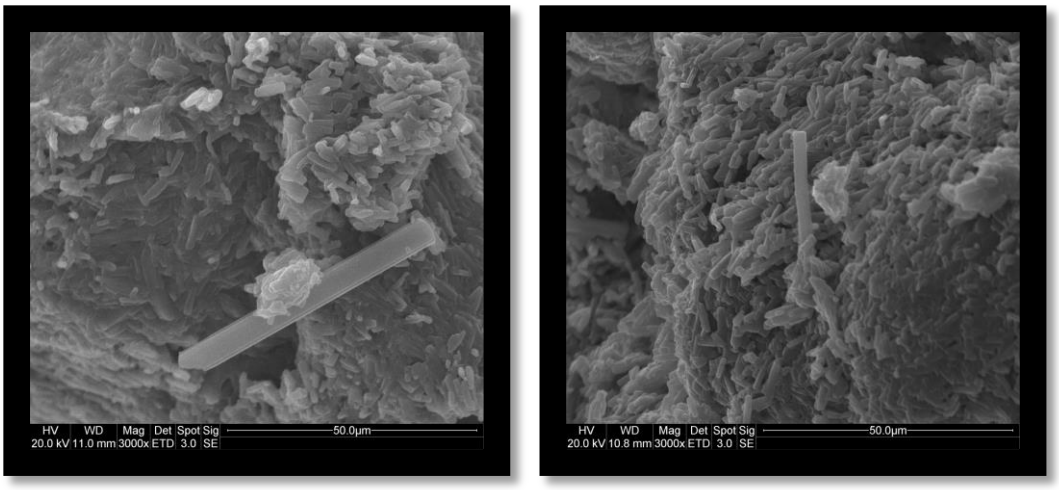

Figure 5.25 SEM images of carbamazepine nicotinamide extruded sample: T140 SGB 10 rpm zone 8 at 3000X magnification (Left) and zone 9 at 3000X magnification (Right).

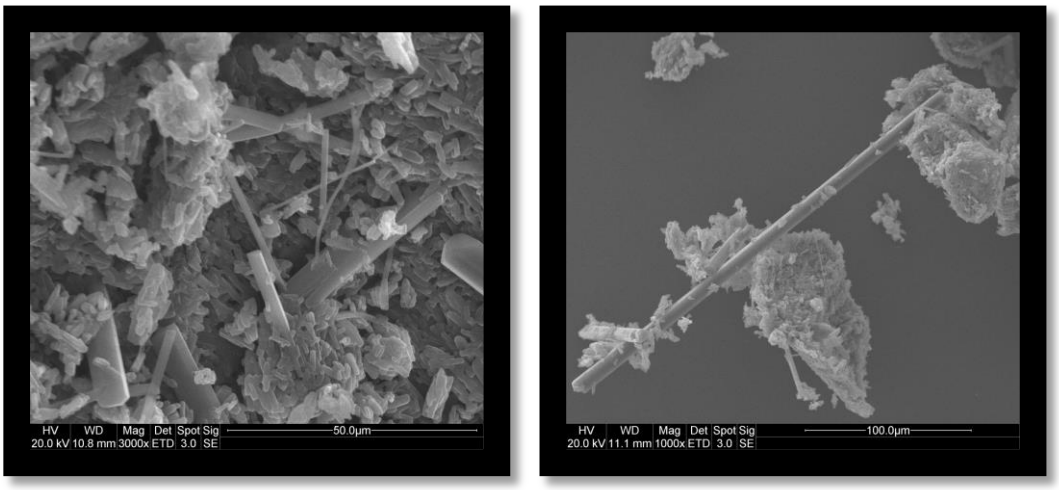

Figure 5.26 SEM images of carbamazepine nicotinamide extruded sample: T140 SGB 10 rpm zone 10 at 3000X magnification (Left) and a selected image from zone 8 at 1000X magnification (Right).

It is difficult to determine co-crystal yield from examining the SEM images in figures 5.25 and 5.26, however there is a clear presence of the co-crystal needles. Many are short, however some of the surface needles appear to have a longer morphology. The number of co-crystal needles with a longer motif on the surface of the agglomerated particles from zone 9 to zone 10 increased. This could indicate that the co-crystals undergo further growth between zones 9 and 10, or alternatively it could suggest that the larger co-crystal needles are formed at zone 10 in the early stages of the extrusion process which are then “picked up” by the agglomerated co-crystal particles when the extrusion process has been running for longer period of time. The image in figure 5.26 from the zone 8 sample shows a particularly long needle that was located with an approximate length of 300 µm, however it must be noted that the majority of the bulk agglomerated co-crystals typically had a length of no longer than 10 µm.

To conclude this section, it was found that the carbamazepine particles had a smaller diameter than the nicotinamide particles. The carbamazepine particles were seen to coat the nicotinamide particles after physical mixing. The co-crystal forms needle shaped crystals which have a small width of 2-5 µm and a length which can vary significantly between 10 µm and 300 µm. The length of the co-crystal needles are restricted more by the extrusion process compared to the solvent evaporation method and more co-crystal needles with a longer length appear at zone 10 of the extruder barrel.

5.3 Degradation study

In this section, the extrusion of pure carbamazepine and nicotinamide was carried out to investigate if any transformations take place when they are extruded at high temperatures. Characterisation and analysis of the extrusion products was conducted. Finally, a HPLC study was carried out to determine the amount of iminostilbene present in samples containing carbamazepine to determine the extent of degradation which can occur during hot melt extrusion.

5.31 Overview

Extrusion was carried out with pure carbamazepine and nicotinamide. It was important to investigate the behaviour and transformations, if any, that the pure materials underwent during extrusion. The materials were extruded using the high shear screw geometry, SGB, 10 rpm screw speed and at high temperatures to exaggerate any polymorphic transformations and to determine if any degradation had occurred.

The extrusion of carbamazepine was carried out under the conditions of T150, SGB 10 rpm. PXRD and DSC techniques were used for sample analysis and characterisation. Firstly, the PXRD spectra in figure 5.27 confirm the extruded carbamazepine had transformed into carbamazepine form I. The peaks at approximately 3.6°, 5.4°, 6.0°, 7.7°, 8.4° and 9.2° (2θ) are good indicators of carbamazepine form I and are present in the extruded carbamazepine spectrum. Upon heating in a DSC chamber at 10°C/min, carbamazepine usually transforms into form I at approximately 179°C. However under the high shear and mixing of screw geometry B used for the

extrusion run, the carbamazepine transformed into form I using a temperature profile with a maximum temperature of 150°C reached along the extruder barrel.

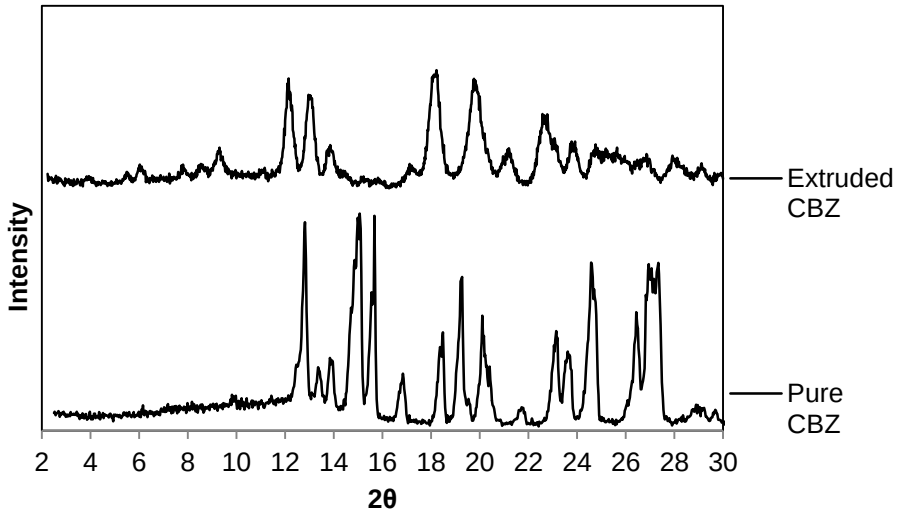

Figure 5.27 PXRD spectra of carbamazepine (Form III) and extruded carbamazepine using screw geometry B, 10 rpm screw speed and temperature profile T150.

The DSC results are shown in figure 5.28. The pure carbamazepine thermogram displays the melting point of carbamazepine form III, the crystallisation of carbamazepine form I and the subsequent melting point of carbamazepine form I. The extruded sample thermogram exhibits an endothermic peak at approximately 154.3°C which could be caused by the melting of some remaining carbamazepine form III and then an endothermic peak at 192.1°C which signifies the melting of carbamazepine form I.

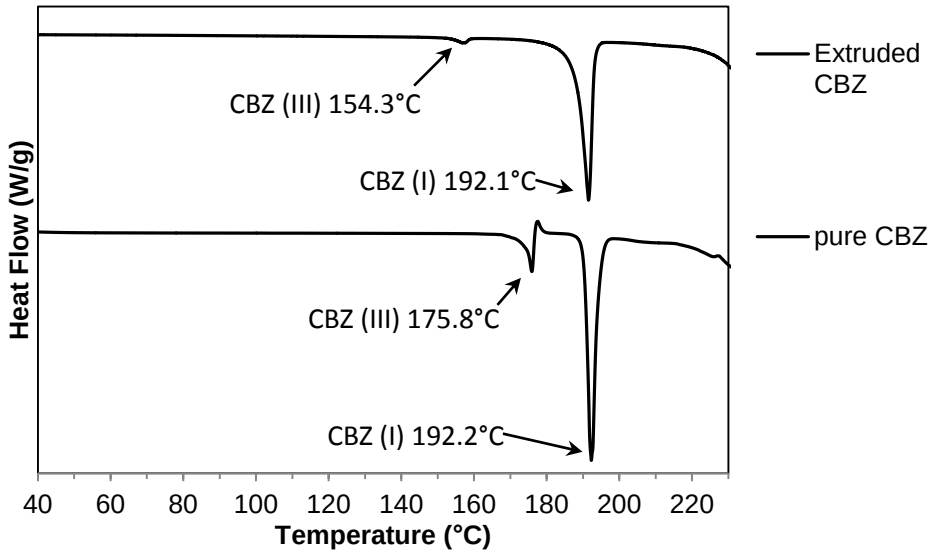

Figure 5.28 DSC thermograms of carbamazepine (Form III) and extruded carbamazepine using screw geometry B, 10 rpm screw speed and temperature profile T150.

Pure nicotinamide was extruded using the screw geometry B, 10 rpm and temperature profiles of T140 and T150. The PXRD spectra are shown in figure 5.29 for the pure nicotinamide and the two extruded samples. Although it appears some shifting has occurred this may have been caused by instrumental error, the powder not being level or by crystal morphological differences. The extruded samples exhibited all of the common XRD peaks associated with nicotinamide; there was no evidence to suggest any transformations had occurred.

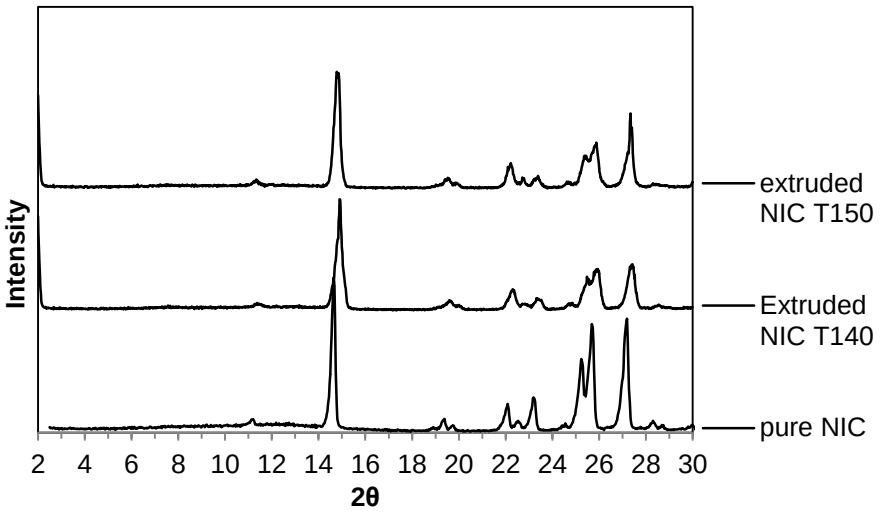

Figure 5.29 PXRD spectra of nicotinamide and extruded nicotinamide using screw geometry B, 10 rpm screw speed and temperature profiles T140 and T150.

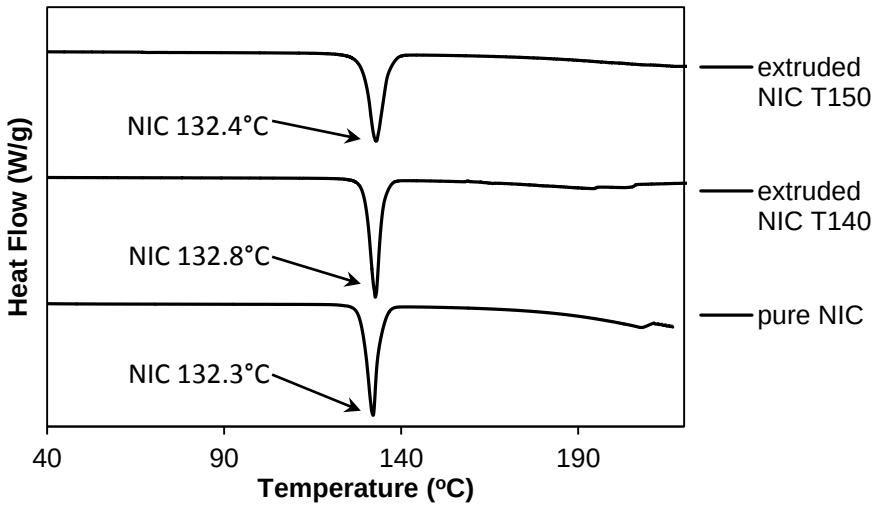

Figure 5.30 DSC thermograms of nicotinamide and extruded nicotinamide using screw geometry B, 10 rpm screw speed and temperature profiles T140 and T150.

The DSC thermograms for pure nicotinamide and the two extruded samples are shown in figure 5.30. The melting peak for nicotinamide is exhibited for

both extruded samples and there was no evidence of any impurities or any transformations which may have occurred.

To conclude this section, carbamazepine transformed into form I after it was extruded using the temperature profile of T150. This was unexpected because the XRD peaks for form I were not present in the extruded samples when carbamazepine was extruded with nicotinamide. The carbamazepine nicotinamide 1:1 co-crystal could be thermodynamically or kinetically favoured to form compared to carbamazepine form I when carbamazepine is extruded in the presence of nicotinamide, even at higher temperatures. The extruded nicotinamide did not indicate any impurities or transformations after it was extruded at high temperature profiles of T140 and T150.

5.32 HPLC results

The analysis of iminostilbene was carried out using HPLC. The results are shown in figure 5.31 for the following extrusion samples: extruded carbamazepine using T130 temperature profile, extruded carbamazepine using T140 temperature profile and extruded carbamazepine nicotinamide using T140 temperature profile.

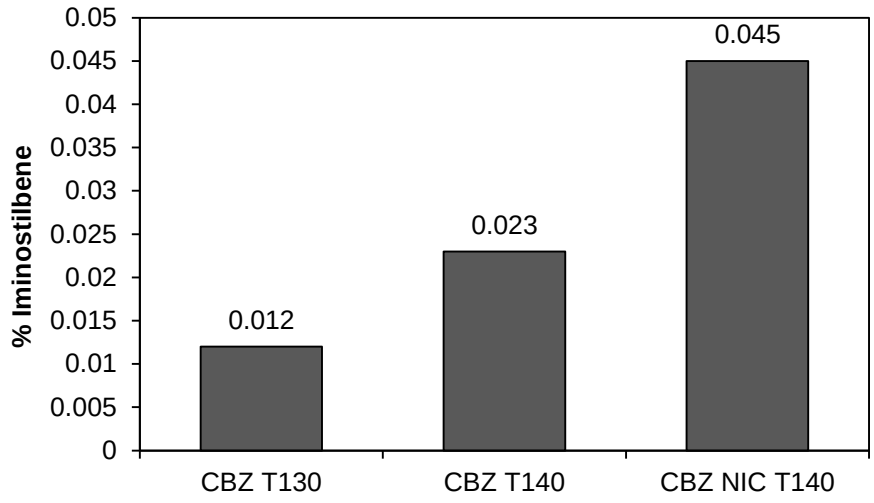

Figure 5.31 HPLC iminostilbene analysis results.

Interestingly, the sample for the extruded carbamazepine nicotinamide physical mixture had the highest amount of iminostilbene present. The presence of iminostilbene indicates the degradation of carbamazepine molecules. Degradation could be caused by the high temperature, high shear conditions within the extruder barrel. The relatively long residence time of the material in the extruder barrel is also a factor which can cause degradation to occur. The presence of nicotinamide may alter the powder flow during the extrusion process, compared to extruding carbamazepine on its own. This difference in powder flow may explain why there is a slightly higher amount of iminostilbene found in the CBZ NIC T140 sample. The presence of nicotinamide also causes a partial melt of the physical mixture at the previously discussed eutectic melting point. This melting event could also be a factor in the degradation of carbamazepine.

Considering the HPLC results in figure 5.31, all of the analysed samples presented a relatively small amount of iminostilbene. The United States Pharmacopeial Convention (USPC) held in 2015 updated the acceptance

criteria for carbamazepine related degradation compounds in carbamazepine tablets (Convention 2015). The revised criteria, for any degradation products of carbamazepine, was a limit of 0.2%. The HPLC results presented iminostilbene concentrations well below this limit.

5.4 Conclusion

Chapter 5 presented a solvent-free hot melt extrusion method for the extrusion of two pharmaceutical co-crystal pairs. The effect of temperature, shear and screw speed on co-crystal yield was investigated. The results directly link up with chapter 4, where the temperature was found to be the most important parameter for cocrystallisation. However, the level of shear (Screw configuration) and the residence time (Screw speed) played important roles in attempting to optimise the co-crystal yield. Temperatures above the physical mixture eutectic points provided higher co-crystal yields, whilst higher shear and reduced residence times improved the co-crystal yield further.

The degradation study conducted for one of the co-crystal pairs provided crucial information and helped to reassure the potential of the solvent-free hot melt extrusion technique. The degradation of carbamazepine was minimal and the extruded samples would meet FDA standards if produced in tablet form.

NIR spectroscopy proved to be an effective characterisation technique which delivered rapid and accurate information for the extruded samples. Its ease of use and its ability to distinguish between small differences in the samples made the technology the favourite choice for material characterisation.

Overall, this chapter showcased the potential of extrusion technology in the pharmaceutical sector. Pharmaceutical co-crystals were successfully manufactured using this technology however it was unclear if 100% co-crystal yield was achieved. Further extrusion experiments are required in order to fully optimise the technology; however this study helped to provide information on the effect of different parameters on cocrystallisation.

CHAPTER 6 A CO-CRYSTAL QUANTIFICATION METHOD

An in-depth investigation of the use of NIR spectroscopy for qualitative and quantitative purposes within the pharmaceutical field was carried out in chapter 2, section 2.92. The literature review revealed NIR spectroscopy was increasingly being used for analysing pharmaceutical materials, including pharmaceutical co-crystals. In chapter 5, it was demonstrated that NIR spectroscopy can distinguish between a co-crystal and its individual components and it was a useful characterisation technique.

In this chapter, NIR spectroscopy was used to predict the concentration of two pharmaceutical co-crystals; 1:1 ibuprofen – nicotinamide (IBU-NIC) and 1:1 carbamazepine – nicotinamide (CBZ-NIC). The mathematical spectral analysis was carried out using partial least squares (PLS) regression. A PLS model was developed for both co-crystal pairs using sets of standard samples to create calibration and validation data sets with which to build and validate the models.

To evaluate each model that was created, the root mean square error of calibration (RMSEC), root mean square error of prediction (RMSEP) and correlation coefficient were used to assess the accuracy and linearity of the models. The objective of this chapter was to create accurate PLS regression models for both co-crystal pairs which can be used to predict the co-crystal concentration in a powder mixture of the co-crystal and the active pharmaceutical ingredient (API). In the following sections, the PLS analysis of each co-crystal pair is discussed along with an in-depth look at the NIR regions and chemometric pre-treatments that were used.

6.1 Ibuprofen – nicotinamide

In this section, the Ibuprofen – nicotinamide pair have been fully analysed and discussed. The NIR regions, chemometric pre-treatments and the results from the PLS analysis are presented in the following sub-sections.

6.11 NIR region selection

To select the NIR regions used for the PLS regression model, the whole spectra was examined in the original state (Figure 6.1). The 1:1 IBU NIC CC spectrum had unique bands at approximately 4794, 5087, 6460, 6676, 8285 and 8393 cm^{-1}, compared to ibuprofen, nicotinamide and their physical mixture.

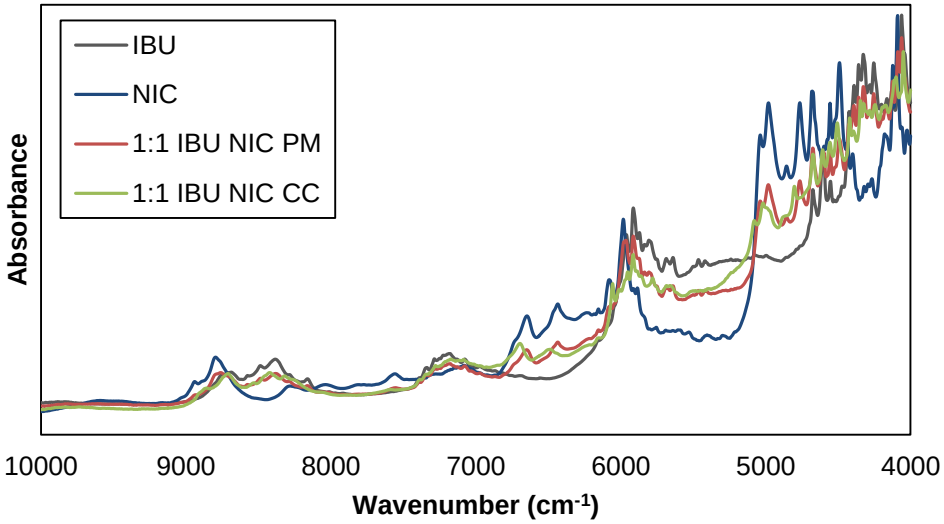

Figure 6.1 NIR spectra for ibuprofen, nicotinamide, IBU-NIC 1:1 physical mixture (PM) and IBU-NIC 1:1 co-crystal (CC) (Microwave method section 3.2). For this figure, the spectra were pre-treated using SNV across the whole region 10000-4000 cm^{-1}.

The spectra were also examined in the second derivative and are shown in figure 6.2. The second derivative was able to extract more detail from the NIR spectra and importantly, it is an effective tool for distinguishing NIR spectra of materials which are very similar to one another at the molecular level.

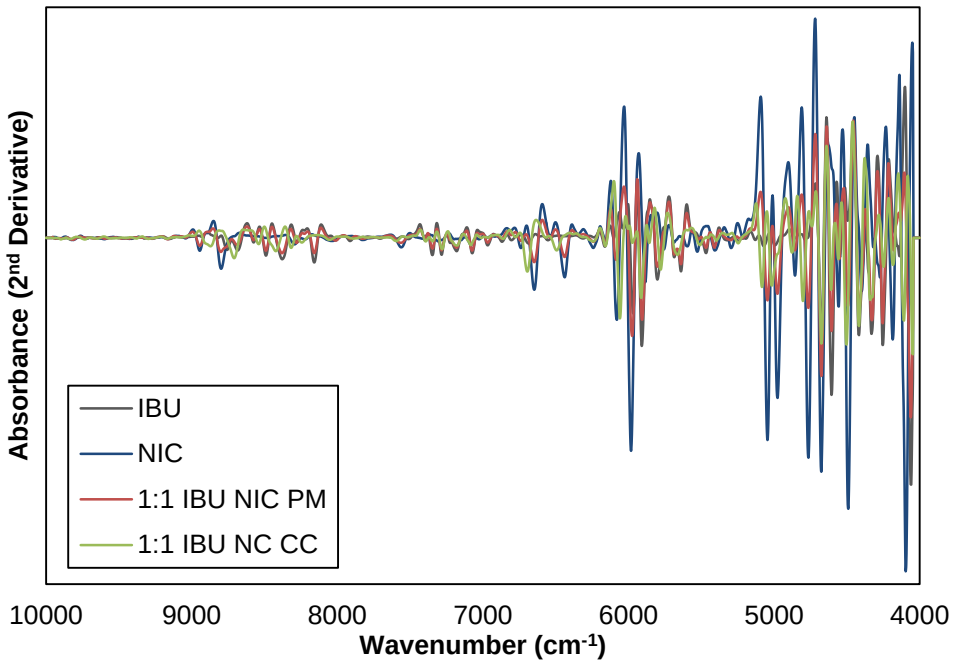

Figure 6.2 Second derivative NIR spectra for ibuprofen, nicotinamide, IBU-NIC 1:1 physical mixture (PM) and IBU-NIC 1:1 co-crystal (CC) (Microwave method section 3.2). For this figure, the spectra were pre-treated using SNV and Norris smoothing across the whole region 10000-4000 cm^{-1}.

We were only able to identify six unique bands when viewing the normal co-crystal spectra in figure 6.1. However, in figure 6.2, there was a much larger number of unique second derivative NIR bands associated with the 1:1 ibuprofen – nicotinamide co-crystal compared to the individual components

and their physical mixture. This ability to differentiate between the materials much more effectively in the second derivative was promising for NIR prediction purposes. This is because the PLS regression uses the spectral data for predicting the co-crystal yield.

Many different NIR regions were evaluated for the ibuprofen – nicotinamide PLS model. The RMSEC, RMSEP and correlation coefficient values were used to determine the performance of each region. The TQ Analyst software which was used to create the PLS models was able to suggest regions according to the covariance of the spectral data. However, when the suggested regions were used for the PLS model, the aforementioned error values were worse than those for the models which used manually selected regions.

The manually selected NIR regions were reviewed, and in total, nine different NIR regions were chosen for further investigation based on their performance. Firstly, the whole NIR region (10000-4000 cm^{-1} wavenumber) was selected, and then relatively large regions to avoid areas that can be affected by noise were chosen. Next, medium sized regions of interest were selected followed by small sized regions which generally covered a small number of bands of interest. The nine NIR regions were as follows: 10000-4000, 10000-5400, 9000-4700, 7450-7000, 6100-5600, 6820-6620, 9000-8000, 6080-6030, 5100-4910 cm^{-1} (Wavenumber).

Standard samples were formulated to make the calibration and validation sets. The samples for the ibuprofen – nicotinamide pair were made by another PhD student, Abdolati Alwati. Refer to section 3.9 for more

information about the standard samples. The NIR spectra for the standard samples were collected. The nine different NIR regions trialled for the PLS models are shown in figure 6.3 in the second derivative for ibuprofen, 25% CC, 50% CC, 75% CC and the pure 1:1 co-crystal (100% CC).

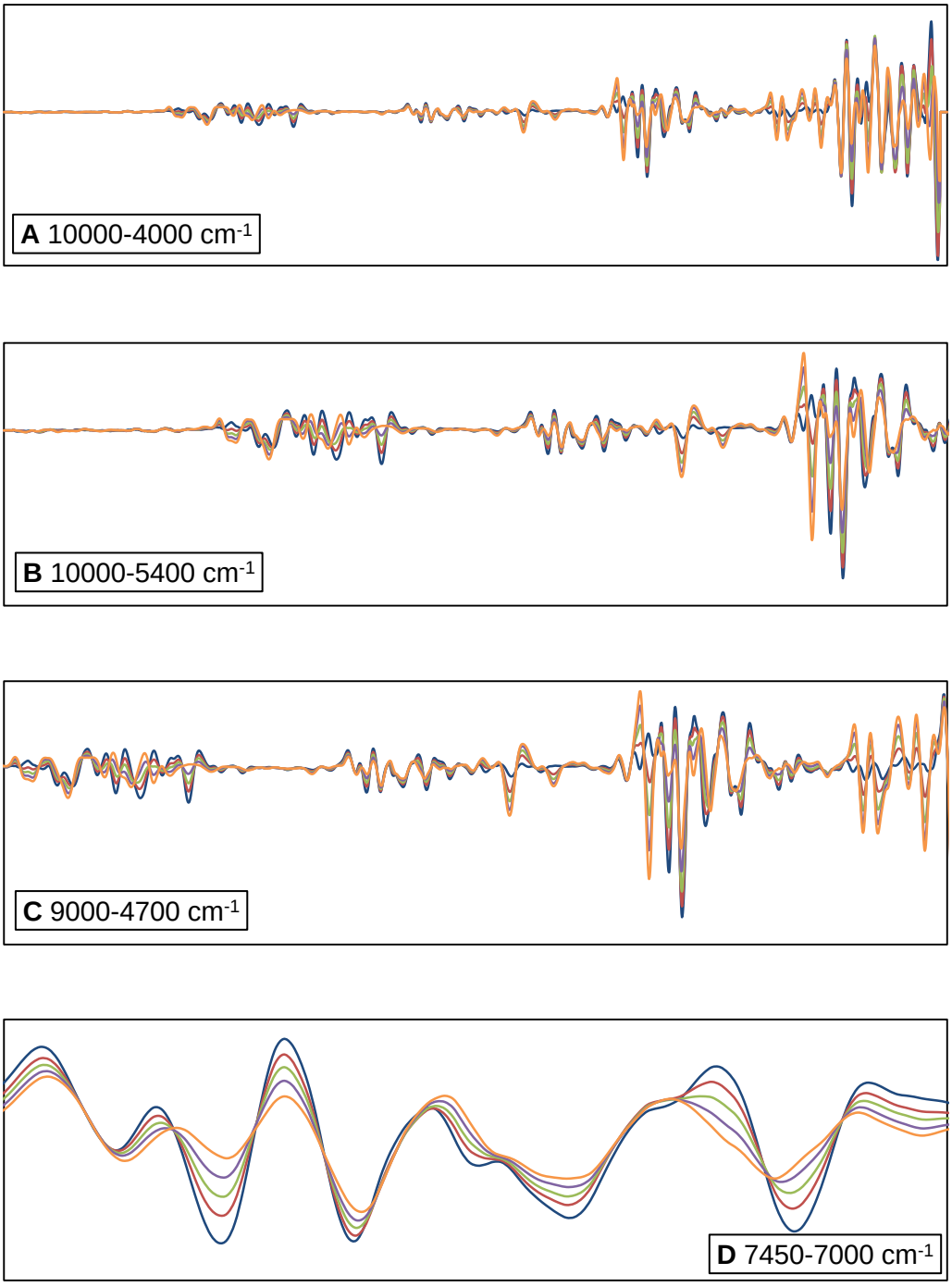

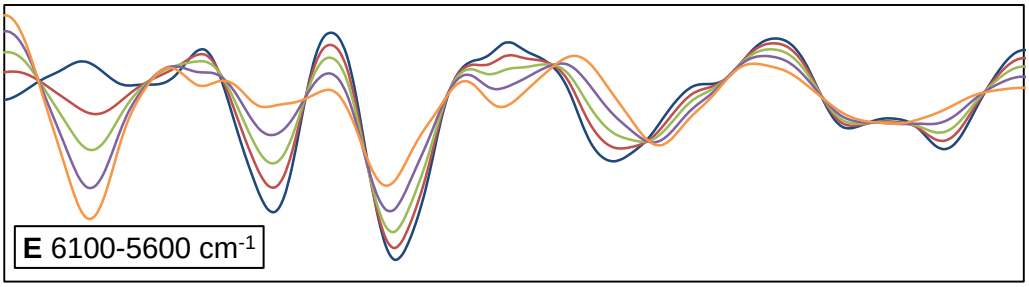
E 6100-5600 cm-1

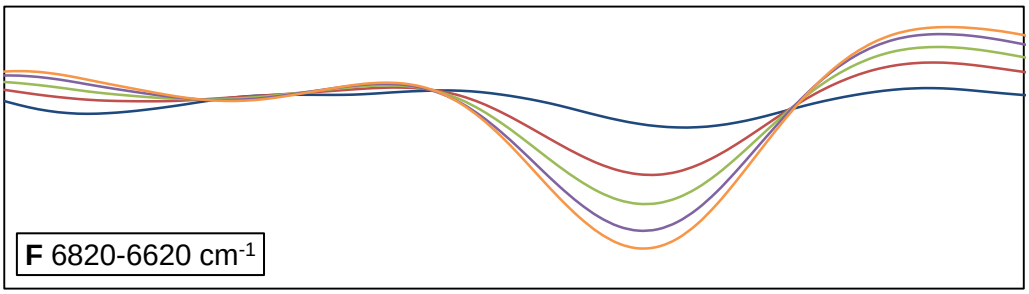
F 6820-6620 cm-1

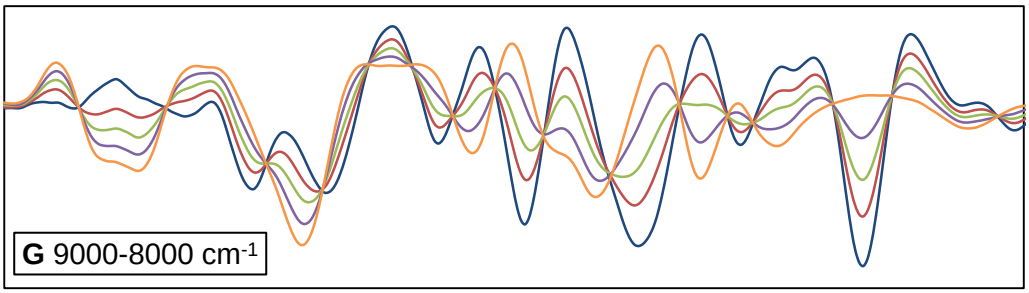
G 9000-8000 cm-1

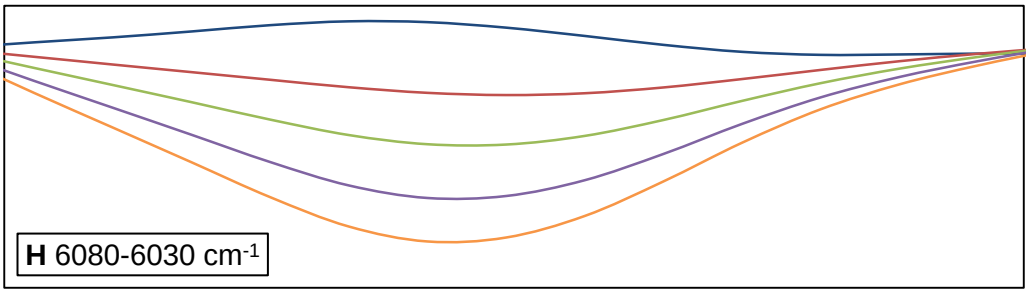
H 6080-6030 cm-1

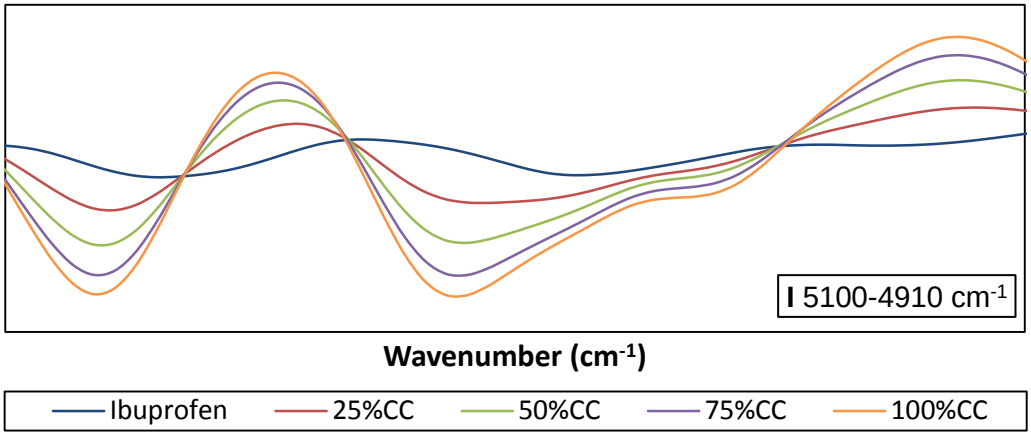

Figure 6.3 A to I show the nine different NIR regions. Second derivative NIR spectra for ibuprofen, 25%CC, 50%CC, 75%CC and 100%CC. All spectra were pre-treated using SNV and Norris smoothing across the whole region 10000-4000 cm^{-1}.

The NIR regions in figure 6.3 are shown in the second derivative for two reasons; it is easier to observe the spectral shifting and the differences in the absorbance intensity are more distinct. As the co-crystal yield is increased in the standard samples, the second derivative NIR bands shift towards the 1:1 co-crystal bands. This was expected because as the co-crystal concentration is increased, the co-crystal NIR bands will have more influence over the resulting spectral pattern.

6.12 Chemometric treatments

For each of the nine NIR regions discussed in section 6.11, different levels of chemometric pre-treatments were carried out to determine their effect on the RMSEP and RMSEC values for the PLS analysis.

Five types of chemometric pre-treatments were used for both co-crystal pairs which included the standard normal variate (SNV) first and second

derivatives, Savitzky-Golay smoothing (SGS) and Norris smoothing (NS) algorithms. SNV pre-treatment was used to compensate for differences in sample pathlength. The SNV was carried out over the full spectral range (4000-10000 cm^{-1} wavenumbers) and effectively minimised any scaling or offset effects which may have occurred.

First and second derivatives were used to improve the resolution of overlapping bands, whilst also acting as a linear baseline correction method. It was also beneficial to view individual spectra in the second derivative as discussed in section 6.11.

Smoothing techniques were applied to reduce noise. SGS was carried out using 7 data points and a polynomial order of 3. NS was carried out using a segment length of 5 and a gap between segments length of 5. Both smoothing techniques can affect the performance of a PLS model.

The RMSEC, RMSEP and correlation coefficient values were recorded for each NIR region. Table 6.1 and table 6.2 display the RMSEC and RMSEP values for each PLS model respectively. The results suggest that the level of chemometrics applied to the spectra had a significant impact on both the calibration and prediction error values. The most significant reduction of the RMSEC and RMSEP values was caused by applying the SNV. The SNV baseline correction algorithm compensates for differences in the pathlength and the PLS regression is heavily influenced by the spectral band intensities in comparison with one another. Therefore, the SNV pre-treatment played a crucial role in improving the model accuracy and prediction capabilities. After applying the SNV, the evaluated regions then reacted differently to the

various levels of other chemometric techniques. The ten models with the lowest RMSEC values in table 6.1 and table 6.2 are in bold text to help visualise their distribution in relation to the different chemometrics that were applied.

Table 6.1 IBU-NIC model: A matrix of RMSEC values of the PLS regression models when using different regions and different levels of chemometrics (Bold text = top ten models).

Region (Wavenumber cm^{-1})	**RMSEC Values (%)**							
	Original	SNV	SNV 1^{st} Dev.	SNV 1^{st} Dev. SGS	SNV 1^{st} Dev. NS	SNV 2^{nd} Dev.	SNV 2^{nd} Dev. SGS	SNV 2^{nd} Dev. NS
10000-5400	7.17	1.20	1.08	1.08	**0.97**	1.11	1.13	1.10
10000-4000	2.21	1.14	1.67	1.67	1.38	1.83	1.79	1.54
9000-8000	6.07	2.60	**0.87**	**0.90**	1.07	**0.89**	**0.96**	1.11
9000-4700	1.96	1.05	1.03	1.03	**0.92**	1.10	**0.96**	1.06
7450-7000	6.17	3.04	1.01	0.99	1.85	1.22	0.99	**0.77**
6820-6620	4.99	2.98	2.93	2.94	3.10	3.22	2.66	2.94
6100-5600	5.12	1.09	1.17	1.17	1.16	1.20	1.19	1.21
6080-6030	3.36	1.96	**0.92**	**0.95**	1.56	1.95	1.41	1.45
5100-4910	2.40	1.47	2.90	2.91	2.82	2.66	2.90	2.81

Table 6.2 IBU-NIC model: A matrix of RMSEP values of the PLS regression models when using different regions and different levels of chemometrics (Bold text = top ten models).

Region (Wavenumber cm^{-1})	RMSEP Values (%)							
	Original	SNV	SNV 1st Dev.	SNV 1st Dev. SGS	SNV 1st Dev. NS	SNV 2nd Dev.	SNV 2nd Dev. SGS	SNV 2nd Dev. NS
10000-5400	11.80	0.91	1.52	1.52	**1.37**	1.88	1.73	1.64
10000-4000	4.61	1.74	3.13	3.12	2.29	3.57	3.38	2.69
9000-8000	12.50	1.84	**1.54**	**1.59**	1.48	**1.60**	**1.80**	1.93
9000-4700	3.57	1.10	1.78	1.78	**1.42**	1.93	**1.74**	1.70
7450-7000	9.82	4.34	1.28	1.26	1.77	1.57	1.52	**0.95**
6820-6620	4.64	2.99	2.18	2.17	2.50	4.72	2.69	2.47
6100-5600	4.58	1.96	1.67	1.68	1.44	1.88	1.80	1.56
6080-6030	3.03	1.52	**0.92**	**0.94**	1.20	1.69	1.62	1.48
5100-4910	2.86	1.60	3.23	3.23	3.33	2.86	2.92	3.00

After examining the RMSEC and RMSEP values it was clear that certain chemometric pre-treatments had significantly different effects on both error values when used on different regions. For example, when applying the first derivative, SNV and Norris smoothing the RMSEC value for the region 9000-4700 cm^{-1} was 0.92%, however for the region 6820-6620 cm^{-1} the RMSEC value was 3.10% under the same conditions. This was expected to be the case because the regions shown in figure 6.3 have different characteristics,

and where one region is greatly affected by a derivative or smoothing technique, another will not necessarily respond in the same way.

The error of calibration was chosen to be a good indicator of the performance of the PLS models. Table 6.3 shows the ten PLS regression models which exhibited the lowest RMSEC values. The correlation coefficient values for the models indicated that they were all well-correlated linear models because they were all 0.999 to three decimal places. Also shown in table 6.3 was the difference between the RMSEC and RMSEP values, this value gave an indication of the variance between the calibration and validation data sets with the optimal value of 0% meaning that the calibration and validation data sets were identical when subjected to PLS regression.

Table 6.3 IBU-NIC model: The top ten PLS regression models in order of RMSEC value. The RMSEP and the difference between RMSEC and RMSEP are also shown along with the regions and chemometrics used.

Model	Region (cm^{-1})	Chemometrics	RMSEC (%)	RMSEP (%)	RMSEC – RMSEP (%)	Corr. Coef.
1	7450-7000	SNV, 2nd Dev., NS	0.77	0.95	-0.18	0.9997
2	9000-8000	SNV, 1st Dev.	0.87	1.54	-0.67	0.9996
3	9000-8000	SNV, 2nd Dev.	0.89	1.60	-0.71	0.9996
4	9000-8000	SNV, 1st Dev., SGS	0.90	1.59	-0.69	0.9996
5	9000-4700	SNV, 1st Dev., NS	0.92	1.42	-0.50	0.9995
6	6080-6030	SNV, 1st Dev.	0.92	0.92	+0.00	0.9995
7	6080-6030	SNV, 1st Dev., SGS	0.95	0.94	+0.01	0.9995
8	9000-8000	SNV, 2nd Dev., SGS	0.96	1.80	-0.84	0.9995
9	9000-4700	SNV, 2nd Dev., SGS	0.96	1.74	-0.78	0.9995
10	10000-5400	SNV, 1st Dev., NS	0.97	1.37	-0.40	0.9995

The wavenumber region of 7450-4700 cm^{-1} provided the smallest calibration error of 0.77%, when the 2nd Dev., SNV and NS algorithms were applied, compared to any other region and level of chemometric pre-treatment used in this study for the ibuprofen – nicotinamide pair. This region provided a model with relatively low error values which can accurately predict the percentage yield of 1:1 IBU-NIC CC in samples where there is a mixture of ibuprofen and the 1:1 IBU-NIC CC. This model (Model 1) exhibited a small RMSEP value of 0.95% and the difference between the RMSEC and RMSEP values was only 0.18%. A small difference was a good indicator of the accuracy and predictability of the model.

6.13 Selected model overview

The selected model shown in table 6.3 (Model 1) is plotted in figure 6.4. The predicted co-crystal yield values for the calibration and validation samples are shown against the measured co-crystal yield. This model had a correlation coefficient of 0.9997 and no outlying points were observed.

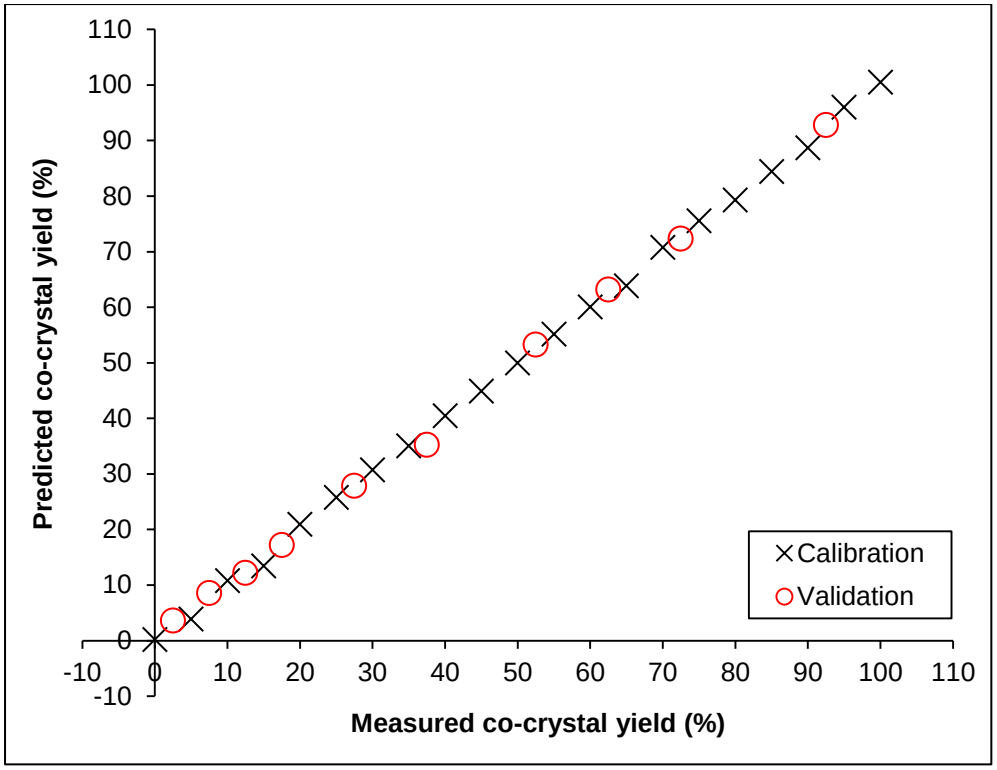

Figure 6.4 IBU-NIC model: PLS regression Model 1. Using the region 7450-7000 cm^{-1} and chemometrics second derivative, SNV and Norris smoothing. Both the calibration and validation data sets are plotted.

In figure 6.5, the cross-validation error for Model 1 was analysed and the RMSECV value did not significantly improve when using more than 2 factors for the PLS regression. Since the models were created using 20 calibration samples, using more than 2 factors could have caused over-fitting of the curves which could have resulted in poor co-crystal yield prediction capabilities.

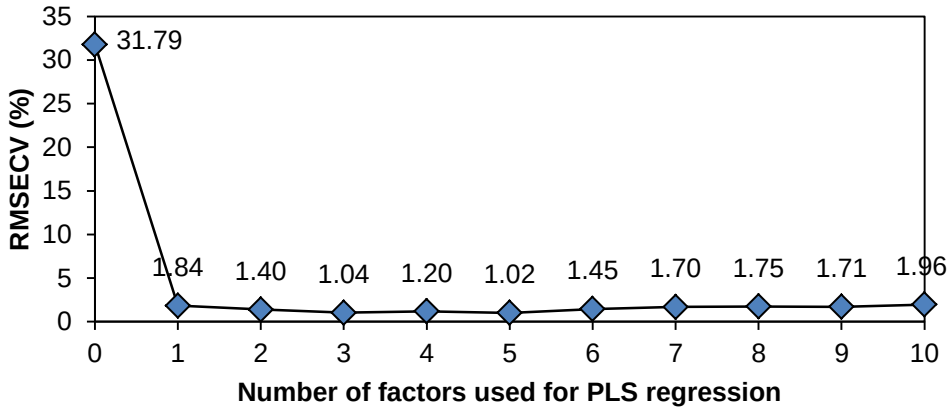

Figure 6.5 IBU-NIC model: PLS regression Model 1. RMSECV values according to the number of factors used in the PLS regression.

The spectral and concentration factor loadings for both PLS factors were calculated and are plotted in figure 6.6. The factor loadings are the numerical loading values for the spectral and concentration contribution of the calibration standards for the selected factor. The first factor describes the majority of the variation in the calibration set, the second factor describes most of the remaining variation. An ideal factor loading will have evenly distributed points along a line that is 45 degrees from both axes. The higher the spectral and concentration loading values are for a given standard, the more significant the standard is to the selected factor.

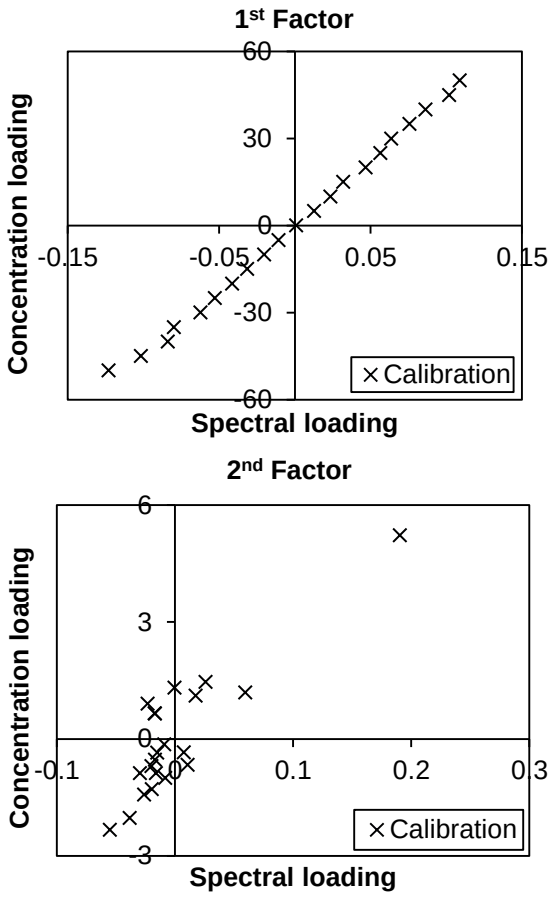

Figure 6.6 IBU-NIC model: PLS regression Model 1. First and second factor loadings for the spectral and concentration contribution of the calibration standards.

The first factor used 99.1% spectral information and 99.7% concentration information. The second factor used 0.5% spectral and 0.2% concentration information. Therefore the total spectral information used was 99.6% and the total concentration information from the calibration set was 99.9%.

The data point observed in figure 6.6 with 0.19 spectral loading and 5.22 concentration loading in the second factor plot was the calibration standard for pure ibuprofen, it was expected that this standard would have some influence to the loading values due to it being pure ibuprofen.

The residual values for Model 1 were plotted against the measured co-crystal yield in figure 6.7. The residuals are the measured co-crystal yield values subtracted from the predicted co-crystal yield values.

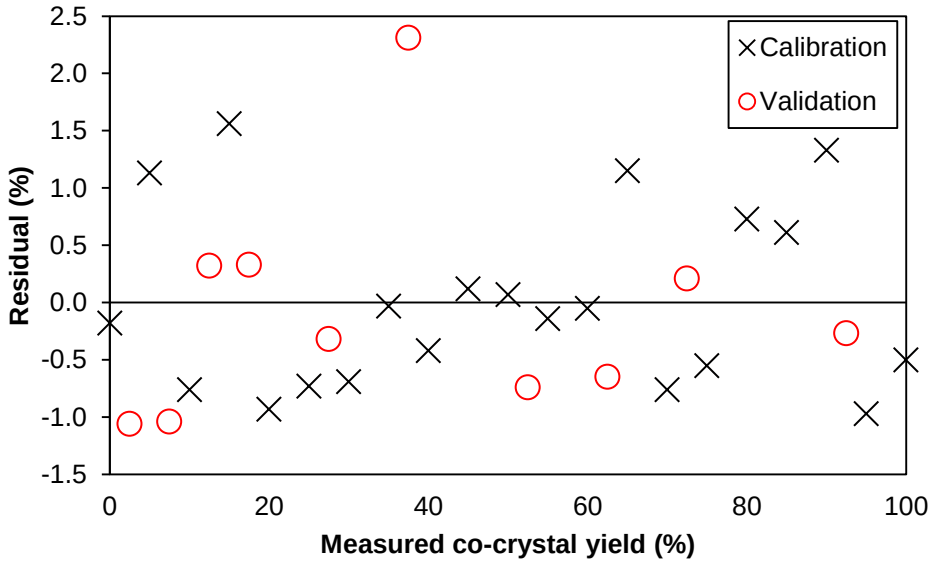

Figure 6.7 IBU-NIC model: Model 1 residuals plot. Using the region 7450-7000 cm^{-1} and chemometrics second derivative, SNV and Norris smoothing.

Upon inspection of the residual plot, the points appear to be randomly dispersed around the horizontal axis for both the calibration and validation sets. This implies that the linear regression model was appropriate for Model 2, as opposed to a non-linear model.

The NIR region, 7450-7000 cm^{-1}, used for Model 1 is shown in figure 6.8 in the second derivative. In this region, the spectra exhibited a clear and predictable trend, with the majority of the second derivative NIR bands increasing in intensity as the 1:1 co-crystal concentration was decreased from 100% co-crystal to 0% (Pure ibuprofen). The only exception to this trend was the band located between 7247 cm^{-1} and 7239 cm^{-1} (Red arrow,

figure 6.8), where the band increased in intensity along with the co-crystal concentration.

It was difficult to identify individual bands within the NIR spectra because most are overtone or combination bands. The hydrogen bonding involved in forming the 1:1 co-crystal may have caused some of the observed band shifting. The most significant shift in this region is from 7108 cm^{-1} to 7128 cm^{-1} (Black arrow, figure 6.8). Two other relatively large shifts are seen from 7070 cm^{-1} to 7081 cm^{-1} and from 7378 cm^{-1} to 7367 cm^{-1} (Black arrows, figure 6.8).

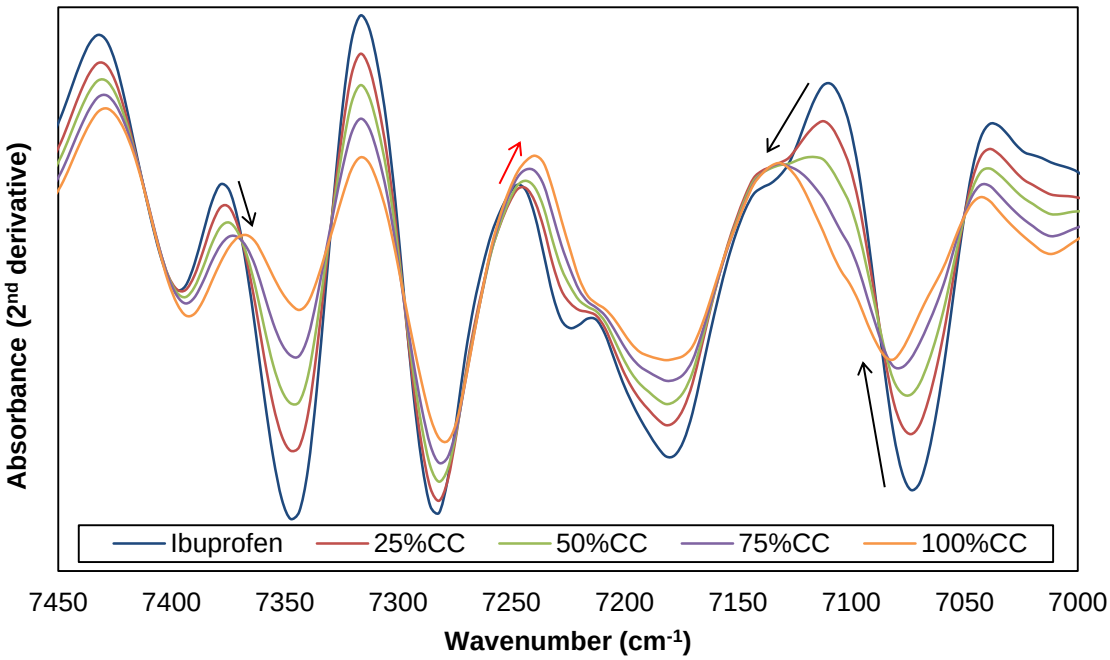

Figure 6.8 IBU-NIC model: second derivative NIR spectra over the region 7450-7000 cm^{-1} with Norris smoothing of ibuprofen and the calibration samples with 25, 50, 75 and 100% 1:1 IBU-NIC CC.

6.2 Carbamazepine – nicotinamide

In this section, the carbamazepine – nicotinamide model has been fully analysed and reviewed. In the same order as the ibuprofen – nicotinamide section, the NIR regions, chemometric pre-treatments and the results from the PLS analysis are presented in the following sub-sections.

6.21 NIR region selection

To select the NIR regions used for the PLS regression model, the whole spectra was observed in the original state (Figure 6.9). The 1:1 CBZ NIC CC spectrum had unique bands at approximately 4636, 5002, 6495 and 6696 cm^{-1}, compared to carbamazepine, nicotinamide and their 1:1 physical mixture.

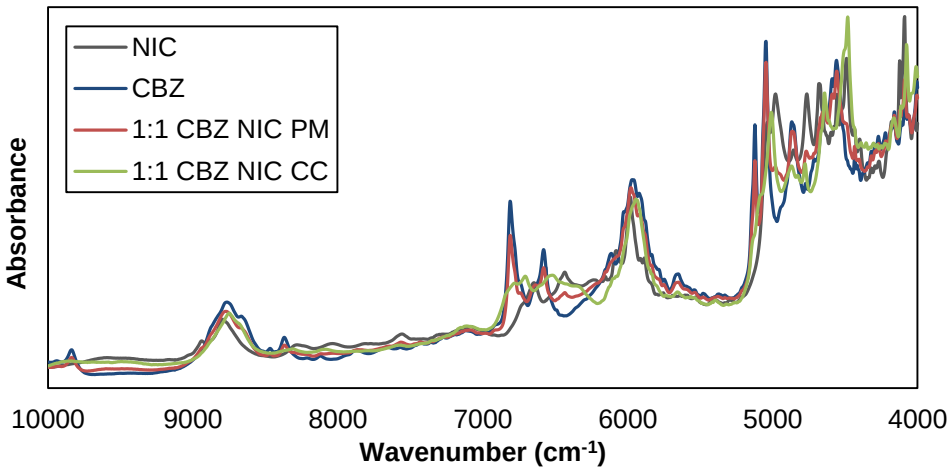

Figure 6.9 NIR spectra for carbamazepine, nicotinamide, CBZ-NIC 1:1 physical mixture and CBZ-NIC 1:1 co-crystal (Solvent evaporation method section 3.3). For this figure, the spectra were pre-treated using SNV across the whole region 10000-4000 cm^{-1}.

The spectra were also viewed in the second derivative and they are shown in figure 6.10. As explained in section 6.8, the second derivative spectra allowed more detail to be extracted and it was an effective tool for distinguishing NIR spectra of materials which are molecularly very similar.

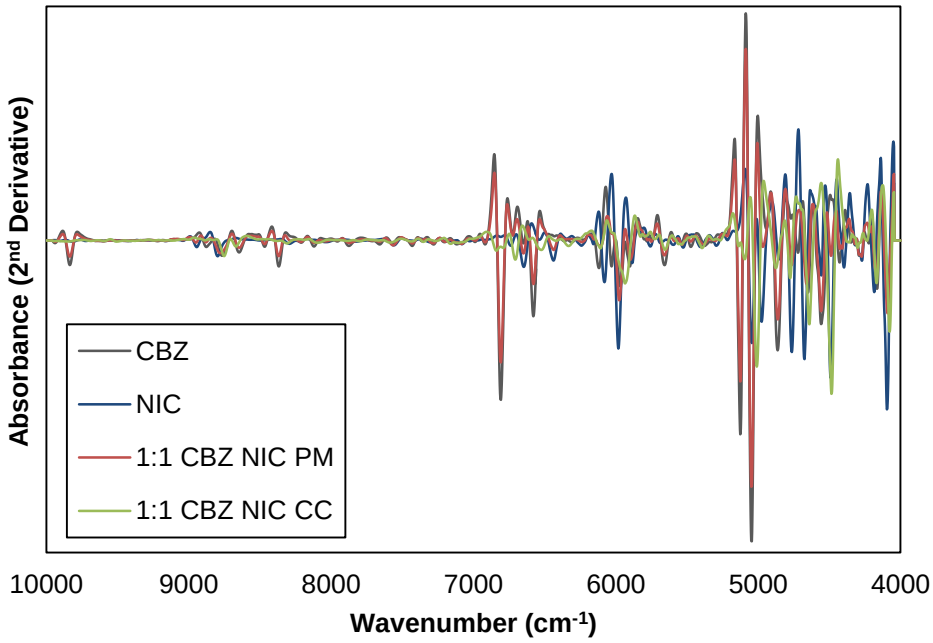

Figure 6.10 Second derivative NIR spectra for carbamazepine, nicotinamide, CBZ-NIC 1:1 physical mixture and CBZ-NIC 1:1 co-crystal (Solvent evaporation method section 3.3). For this figure, the spectra were pre-treated using SNV and Norris smoothing across the whole region 10000-4000 cm^{-1}.

In figure 6.9, we were only able to identify four unique bands when viewing the normal co-crystal spectra. However, in figure 6.10, there are an increased number of unique second derivative NIR bands associated with the 1:1 carbamazepine – nicotinamide co-crystal compared to the individual components and their physical mixture. The second derivative spectra allowed for effective differentiation of the materials, this was promising for

NIR prediction purposes because the PLS regression uses the spectral data for predicting the co-crystal yield.

Just like the ibuprofen – nicotinamide pair, many different NIR regions were evaluated for the carbamazepine – nicotinamide PLS model using the TQ analyst software. The RMSEC, RMSEP and correlation coefficient values were used to determine the performance of each region. The TQ Analyst software suggested regions according to the covariance of the spectral data. However, the PLS model calibration and prediction error values were worse than those for the models which used manually selected regions.

The manually selected NIR regions were reviewed, and in total, nine different NIR regions were selected for further investigation by PLS regression. The whole region (10000-4000 cm^{-1} wavenumber) was selected, and then relatively large regions to avoid areas affected by noise were chosen. Next, medium sized regions of interest were selected followed by small sized regions which generally covered a small number of bands of interest. The nine NIR regions were as follows: 10000-4000, 10000-5400, 9000-5300, 10000-9646, 9000-8500, 7200-5400, 6881-6696, 6684-6457, 6075-5827 cm^{-1} (Wavenumber). It is important to note that only two of the nine regions were used for the ibuprofen – nicotinamide pair; 10000-4000 and 10000-5400 cm^{-1}.

Standard samples were formulated to create the calibration and validation sets (Refer to section 3.9 for more details). The NIR spectra for the standard samples were collected. The nine selected NIR regions used for the PLS

models are shown in figure 6.11 in the second derivative for carbamazepine, 25% CC, 50% CC, 75% CC and the pure 1:1 co-crystal (100% CC).

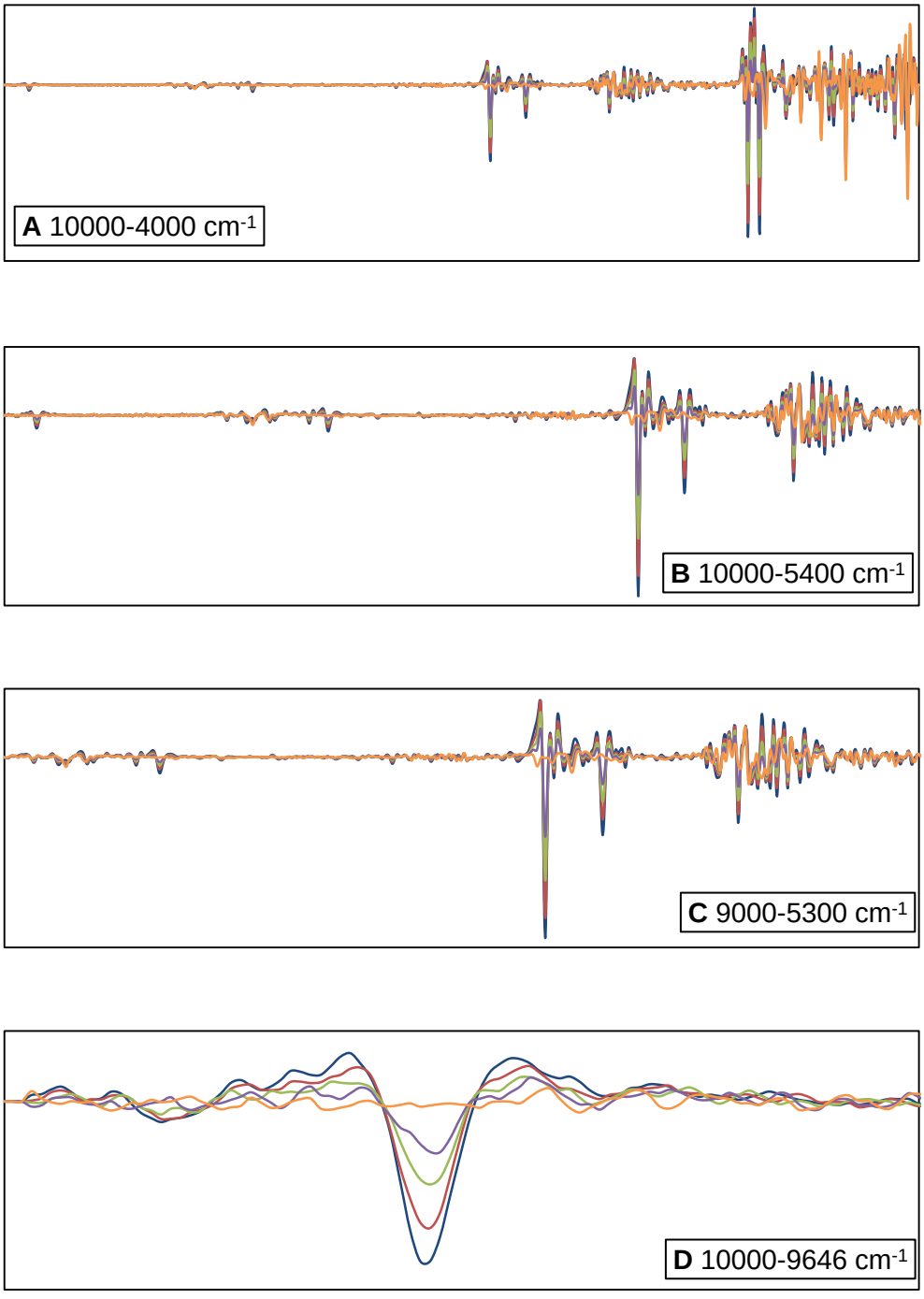

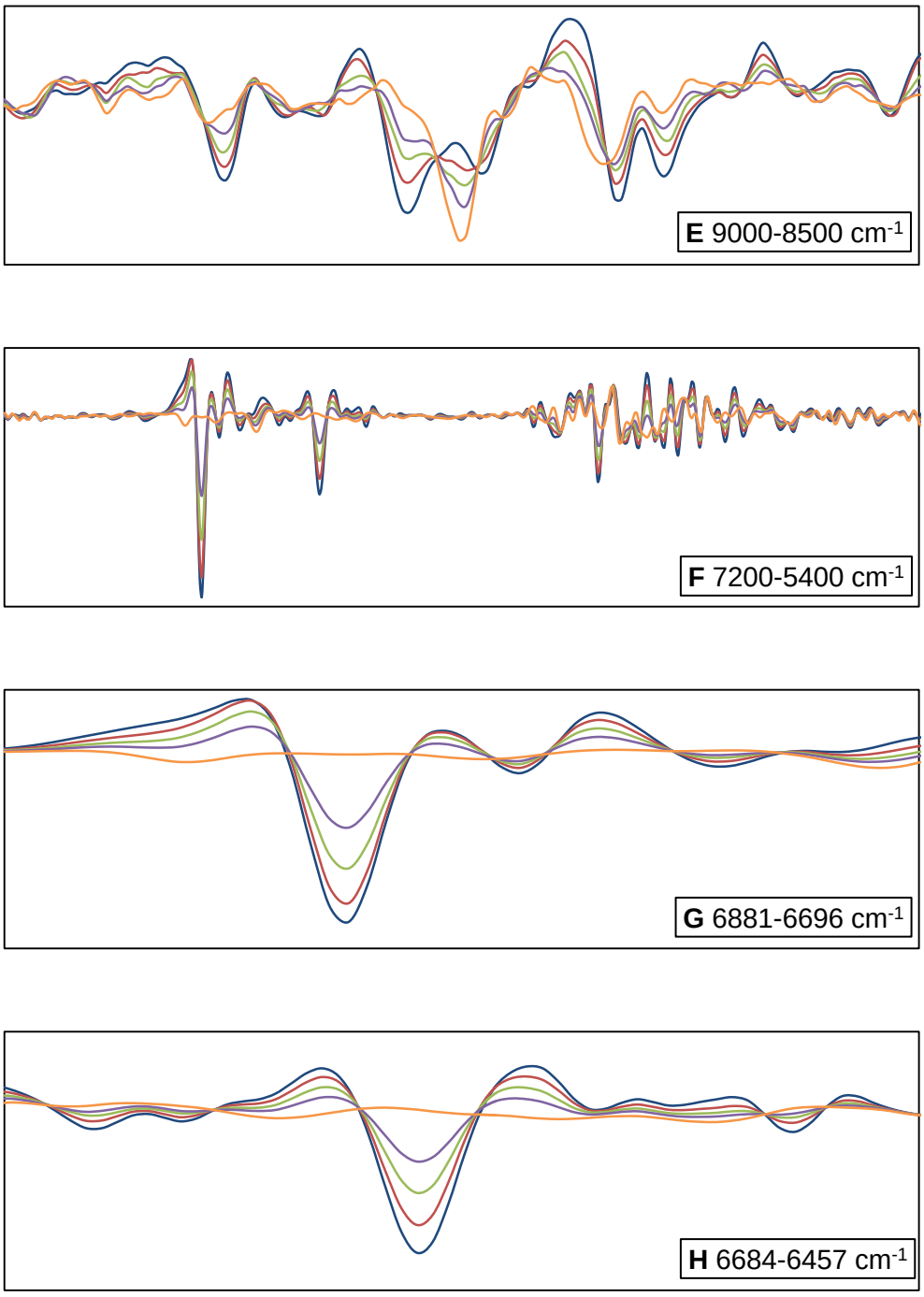
E 9000-8500 cm-1
F 7200-5400 cm-1
G 6881-6696 cm-1
H 6684-6457 cm-1

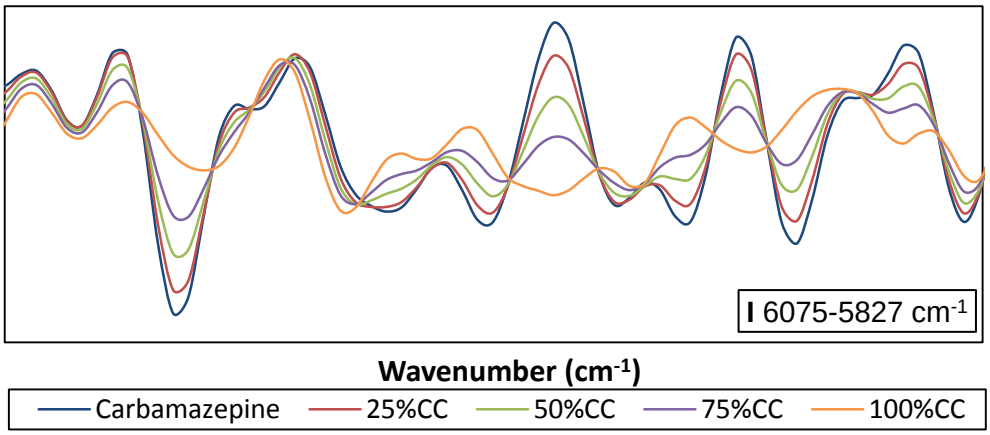

Figure 6.11 A to I show the nine different NIR regions. Second derivative NIR spectra for carbamazepine, 25%CC, 50%CC, 75%CC and 100%CC. All spectra were pre-treated using SNV and Norris smoothing across the whole region 10000-4000 cm^{-1}.

6.22 Chemometric treatments

For each of the nine NIR regions discussed in section 6.21, different levels of chemometric pre-treatments were carried out to determine their effect on the RMSEP and RMSEC values for the PLS analysis. The chemometrics are exactly the same as those described in section 6.11 for the ibuprofen – nicotinamide pair. The chemometric pre-treatments used were the SNV, first and second derivatives, SGS and NS

The RMSEC, RMSEP and correlation coefficient values were calculated for each NIR region. Table 6.4 and table 6.5 display the RMSEC and RMSEP values for each regression model respectively. The results suggested that the level of chemometrics used had a significant impact on both error values; this was the same for the ibuprofen – nicotinamide pair. The most significant reduction of the RMSEC and RMSEP values was caused by applying the

SNV. After using the SNV, the evaluated regions then reacted differently to the various levels of chemometrics. The ten models with the lowest RMSEC values are highlighted in bold text to help visualise their distribution related to the different chemometrics that were applied.

Table 6.4 CBZ-NIC model: A matrix of RMSEC values of the PLS regression models when using different regions and different levels of chemometrics (Bold text = top ten models).

Region (Wavenumber cm^{-1})	**RMSEC Values (%)**							
	Original	SNV	SNV 1^{st} Dev.	SNV 1^{st} Dev. SGS	SNV 1^{st} Dev. NS	SNV 2^{nd} Dev.	SNV 2^{nd} Dev. SGS	SNV 2^{nd} Dev. NS
10000-9646	5.01	3.16	**1.55**	**1.54**	2.37	**1.51**	**1.63**	2.67
10000-5400	6.99	2.40	3.42	2.49	2.49	**2.23**	3.29	2.46
10000-4000	6.46	2.76	2.84	2.84	2.77	2.86	2.94	2.80
9000-8500	7.10	3.28	**2.28**	**2.30**	2.42	**1.18**	**1.23**	**2.32**
9000-5300	6.88	2.60	2.52	2.52	2.51	2.44	2.55	2.49
7200-5400	6.35	2.68	2.58	2.58	2.58	2.59	2.62	2.56
6881-6696	5.26	3.18	2.68	2.68	2.66	2.70	2.68	2.57
6684-6457	5.58	2.52	2.58	2.58	2.58	2.56	2.59	2.60
6075-5827	6.25	3.21	3.26	3.26	3.33	2.82	2.95	3.31

Table 6.5 CBZ-NIC model: A matrix of RMSEP values of the PLS regression models when using different regions and different levels of chemometrics (Bold text = top ten models).

Region (Wavenumber cm^{-1})	RMSEP Values (%)							
	Original	SNV	SNV 1st Dev.	SNV 1st Dev. SGS	SNV 1st Dev. NS	SNV 2nd Dev.	SNV 2nd Dev. SGS	SNV 2nd Dev. NS
10000-9646	3.29	3.59	**3.92**	**4.00**	3.04	**5.49**	**4.73**	3.71
10000-5400	5.03	2.71	4.22	3.09	3.11	**3.07**	4.52	3.00
10000-4000	5.59	3.51	4.20	4.21	3.91	4.58	4.51	4.09
9000-8500	4.26	4.28	**3.32**	**3.32**	3.30	**4.26**	**3.53**	**3.33**
9000-5300	4.97	3.00	3.13	3.13	3.15	3.04	3.08	3.03
7200-5400	4.87	3.12	3.18	3.18	3.20	3.09	3.13	3.10
6881-6696	4.44	3.95	3.41	3.41	3.36	3.41	3.33	3.11
6684-6457	4.08	2.99	3.00	3.00	2.98	3.15	3.07	2.99
6075-5827	5.05	4.23	4.12	4.12	4.34	3.42	3.69	4.34

After examining the RMSEC and RMSEP values it was clear that certain chemometric pre-treatments had significantly different effects on both error values when used on different regions.

The error of calibration was a good indicator of the performance of the PLS models. Table 6.6 shows the ten PLS regression models which exhibited the lowest RMSEC values. The correlation coefficient values for the models were

0.99 to two decimal places and the top two models were 0.999 to three decimal places. This provided evidence that they were all well correlated linear models. Table 6.6 also displays the difference between the RMSEC and RMSEP values to give an indication of the variation between the calibration and validation data sets with the optimal value of 0% for the identical performance of the calibration and validation data sets.

Table 6.6 CBZ-NIC model: The top ten PLS regression models in order of RMSEC value. The RMSEP and the difference between RMSEC and RMSEP are also shown along with the regions and chemometrics used.

Model	Region (cm^{-1})	Chemometrics	RMSEC (%)	RMSEP (%)	RMSEC – RMSEP (%)	Corr. Coef.
1	9000-8500	SNV, 2nd Dev.	1.18	4.26	-3.08	0.9992
2	9000-8500	SNV, 2nd Dev., SGS	1.23	3.53	-2.30	0.9992
3	10000-9646	SNV, 2nd Dev.	1.51	5.49	-3.98	0.9988
4	10000-9646	SNV, 1st Dev., SGS	1.54	4.00	-2.46	0.9987
5	10000-9646	SNV, 1st Dev.	1.55	3.92	-2.37	0.9987
6	10000-9646	SNV, 2nd Dev., SGS	1.63	4.73	-3.10	0.9985
7	10000-5400	SNV, 2nd Dev.	2.23	3.07	-0.84	0.9973
8	9000-8500	SNV, 1st Dev.	2.28	3.32	-1.04	0.9972
9	9000-8500	SNV, 1st Dev., SGS	2.30	3.32	-1.02	0.9971
10	9000-8500	SNV, 2nd Dev., NS	2.32	3.33	-1.01	0.9971

The first and second smallest calibration errors (RMSEC) of 1.18% (Model 1) and 1.23% (Model 2) were found when using the wavenumber region of 9000-8500 cm^{-1}. Therefore, this particular region provided models with relatively low error values which could be used to accurately predict the 1:1 co-crystal yield in samples where there is a mixture of carbamazepine and the 1:1 co-crystal.

The best overall performing model was determined as Model 2. Model 2 was chosen because it exhibited a smaller RMSEP value of 3.53% compared to 4.26% for Model 1. The difference between the RMSEC and RMSEP values were only -2.3% for Model 2 where as it was significantly larger for Model 1, -3.08%.

6.23 Selected model analysis

Model 2 is plotted in figure 6.12 where both the averaged calibration and validation samples are shown to compare the measured co-crystal yield to the PLS regression predicted co-crystal yield. This model had a correlation coefficient of 0.9992.

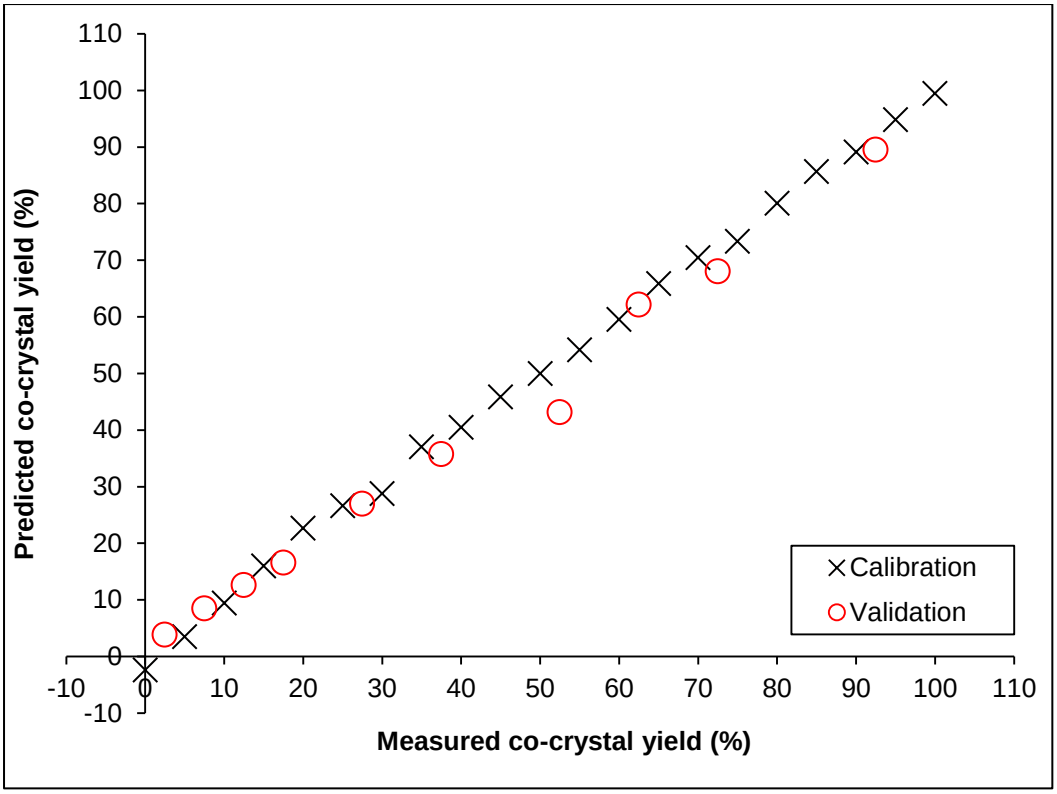

Figure 6.12 CBZ-NIC model: PLS regression Model 2. Using the region 9000-8500 cm^{-1} and chemometrics second derivative, SNV and SG smoothing.

In figure 6.13, the cross-validation error for Model 2 was analysed. The RMSECV value did not significantly improve when using more than 2 factors for the PLS regression. Considering the possibility of curve over-fitting due to the limited number of standard samples, it was decided that the model should only use 2 factors.

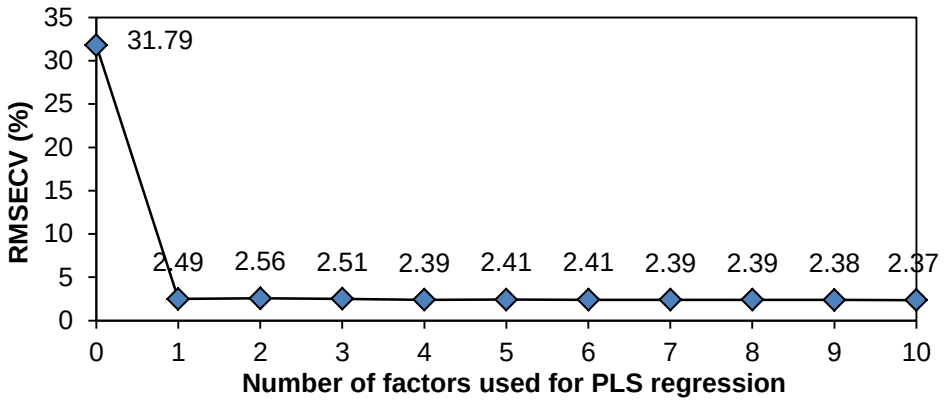

Figure 6.13 CBZ-NIC model: PLS regression Model 2. RMSECV values according to the number of factors used in the PLS regression.

The spectral and concentration factor loadings for both PLS factors were calculated and are plotted in figure 6.14. The factor loadings are the numerical loading values for the spectral and concentration contribution of the calibration standards for the selected factor. The first factor describes the majority of the variation in the calibration set, the second factor describes most of the remaining variation.

The first factor used 95.1% spectral information and 99.4% concentration information. The second factor used 0.6% spectral and 0.4% concentration information. The total spectral information used was 95.6% and the total concentration information gathered was 99.8%.

The factor loadings in figure 6.14 were well-distributed for the first factor. Unlike the ibuprofen – nicotinamide model, the pure carbamazepine calibration standard did not have a strong influence over the second PLS factor for the carbamazepine – nicotinamide model.

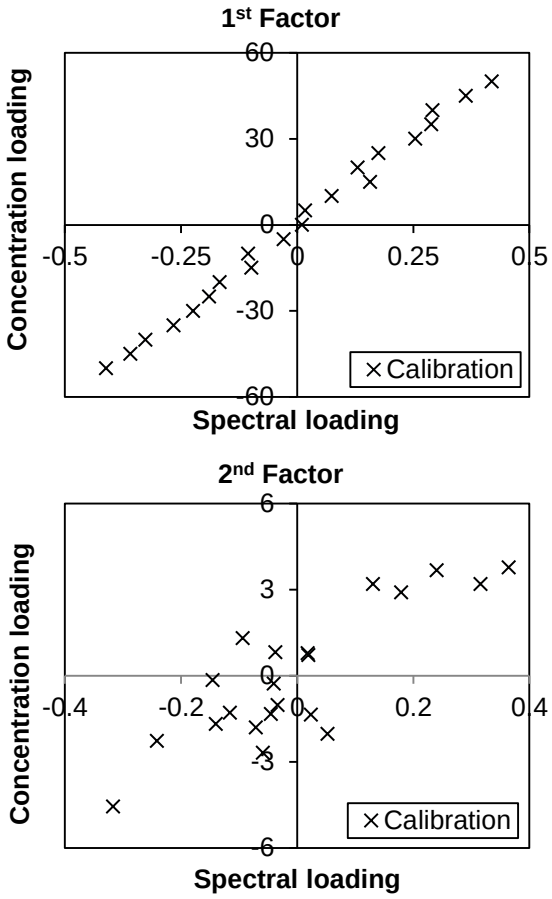

Figure 6.14 CBZ-NIC model: PLS regression Model 2. First and second factor loadings for the spectral and concentration contribution of the calibration standards.

The residual values for Model 2 were plotted against the measured co-crystal yield in figure 6.15. The residuals are the measured co-crystal yield values subtracted from the predicted co-crystal yield values.

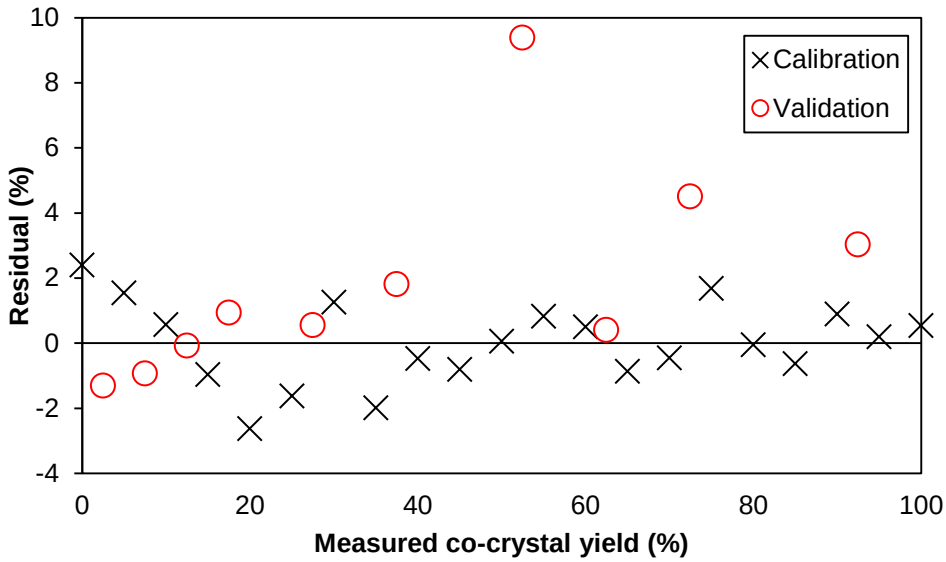

Figure 6.15 CBZ-NIC model: Model 2 residuals plot. Using the region 9000-8500 cm^{-1} and chemometrics second derivative, SNV and SG smoothing.

In the residual plot, the points appear to be randomly dispersed around the horizontal axis, particularly for the calibration set. This indicates that the linear regression model was also appropriate for the carbamazepine – nicotinamide Model 2, as opposed to a non-linear model.

For the carbamazepine – nicotinamide selected model, the validation sample data point with a 52.5% measured co-crystal yield in figures 6.12 and 6.15 could be an outlier as it deviates from the linear model significantly more than any other data point. Table 6.7 shows the SUM of the squared residuals for the calibration set, validation set, and validation set excluding the point at 52.5% measured co-crystal yield.

Table 6.7 CBZ-NIC model: Model 2. The SUM of the squared residuals for the calibration set, validation set and validation set excluding the point at 52.5% measured co-crystal yield.

CBZ-NIC Selected Model (Model 2)	(%)
SUM squared residual calibration	31.59
SUM squared residual validation	124.61
SUM squared residual validation excl. 52.5%	36.62

The squared residual for the point at 52.5% measured co-crystal yield was 87.98%. This was 2.4 times larger than the sum of the squared residuals for the validation set when excluding the outlier (36.62%). If this data point is removed from the validation set, the RMSEP value improves from 3.53% to 2.02% when using all of the same conditions: SNV, second derivative, SGS, NIR region 9000-8500 cm^{-1}. This would bring the carbamazepine – nicotinamide model closer to the 1:1 IBU-NIC model when comparing their prediction error.

The NIR region used for Model 2 of 9000-8500 cm^{-1} is shown in figure 6.16 in the second derivative. The majority of the second derivative NIR bands in this region exhibited an increase in intensity as the 1:1 co-crystal concentration was decreased from 100% to 0% (Pure carbamazepine). However there were two notable exceptions to this rule at 8751 cm^{-1} and 8624 cm^{-1} (Red arrows, figure 6.16), where the bands increased in intensity with an increase in the co-crystal concentration.

It may be possible that the hydrogen bonding involved in forming the 1:1 co-crystal may have caused some of the observed band shifting. The second

derivative NIR spectra for the carbamazepine – nicotinamide pair were more complex compared to the ibuprofen – nicotinamide pair. Some of the more exaggerated band shifting was observed from 8690 cm^{-1} to 8713 cm^{-1}, 8663 cm^{-1} to 8670 cm^{-1} and 8879 cm^{-1} to 8886 cm^{-1} (Black arrows, figure 6.16). The most prominent second derivative band associated with the co-crystal in this region was situated at 8751 cm^{-1}.

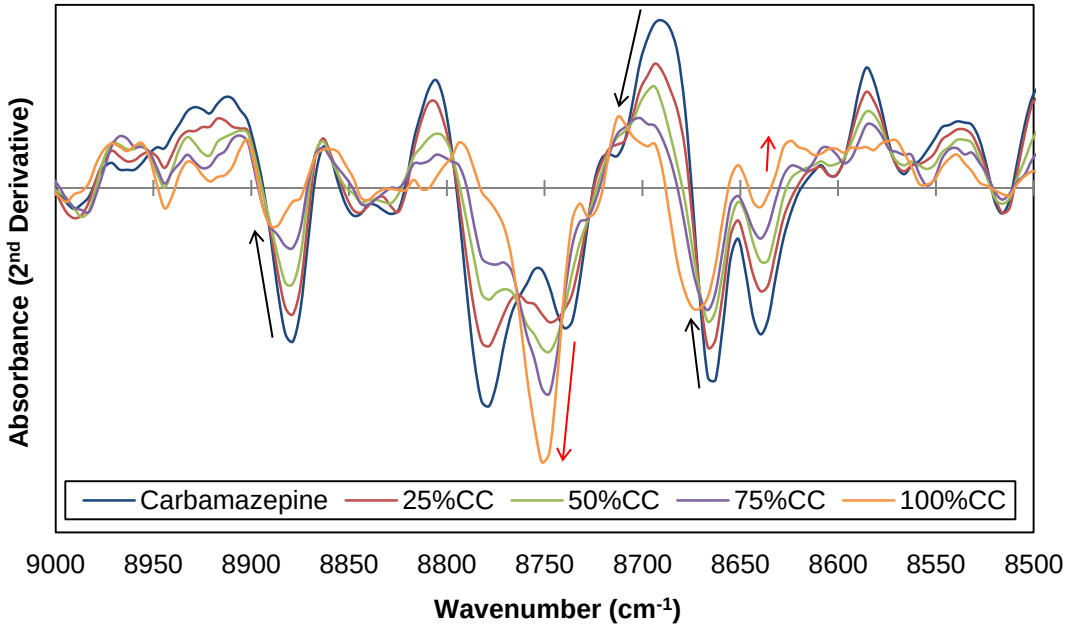

Figure 6.16 CBZ-NIC model: second derivative NIR spectra over the region 9000-8500 cm^{-1} with SG smoothing of carbamazepine and the calibration samples with 25, 50, 75 and 100% 1:1 CBZ-NIC co-crystal.

6.24 Quantification of co-crystal samples

The selected model (Model 2) discussed in section 6.23 was created with the purpose of predicting the co-crystal yield in samples. In this section, several samples from the hot melt extrusion experiments outlined in chapter 5 were selected for 1:1 carbamazepine – nicotinamide co-crystal yield prediction

using this model. The full spectrum fit, measurement region fit, predicted co-crystal concentration and prediction uncertainty were calculated for the extruded samples shown in table 6.8, table 6.9, table 6.10 and table 6.11.

Table 6.8 Hot melt extrusion samples, processed at temperatures T120 to T140, screw geometry B and screw speeds 10 rpm and 20 rpm. Their full spectrum fit, measurement region fit, predicted co-crystal concentration and prediction uncertainty values.

Sample	Full spectrum fit (%)	Measurement region fit (%)	Predicted co-crystal concentration (%)	Prediction uncertainty (%)
T120 SGB 20 rpm	95.6	60.8	81.0	15.7
T125 SGB 20 rpm	91.9	90.9	99.4	9.8
T130 SGB 20 rpm	87.1	72.8	82.4	9.9
T135 SGB 20 rpm	88.2	91.6	84.9	5.5
T140 SGB 20 rpm	85.7	87.4	89.2	7.0
T130 SGB 10 rpm	86.9	90.4	91.6	7.7
T135 SGB 10 rpm	90.5	92.9	95.3	7.7
T140 SGB 10 rpm	87.3	93.2	94.3	6.3

In table 6.8, the full spectrum fit values were relatively high for all extruded samples; this is an indication that the computed predicted co-crystal concentration values were accurate. The predicted co-crystal yield values provided evidence that as the screw speed was reduced from 20 rpm to 10 rpm, the co-crystal yield increased. The predicted value of 99.4% for the T125 SGB 20 rpm sample was unexpected as this result was not supported by the X-ray diffraction and thermal data in chapter 5.

Table 6.9 Hot melt extrusion samples from along the barrel, processed at temperature T135, screw geometry B and screw speed 20 rpm. Their full spectrum fit, measurement region fit, predicted co-crystal concentration and prediction uncertainty values.

T135 SGB 20 rpm sample	Full spectrum fit (%)	Measurement region fit (%)	Predicted co-crystal concentration (%)	Prediction uncertainty (%)
Z2	95.7	46.1	47.4	24.6
Z3	95.1	48.0	49.2	25.1
Z4	97.6	44.6	67.4	23.8
Z5	92.7	47.5	51.6	21.6
Z6	87.6	51.4	57.7	17.4
Z7	89.9	56.9	69.7	12.5
Z8	88.6	89.5	89.8	7.1
Z9	89.6	94.6	91.9	7.1
Z10	98.5	84.4	100.0	10.5
EX	88.2	91.6	84.9	5.5

Table 6.10 Hot melt extrusion samples from along the barrel, processed at temperature T140, screw geometry B and screw speed 20 rpm. Their full spectrum fit, measurement region fit, predicted co-crystal concentration and prediction uncertainty values.

T140 SGB 20 rpm sample	Full spectrum fit (%)	Measurement region fit (%)	Predicted co-crystal concentration (%)	Prediction uncertainty (%)
Z2	97.9	47.1	59.0	24.2
Z3	91.6	50.2	40.8	25.0
Z4	96.9	46.9	50.4	22.9
Z5	90.6	46.5	49.9	21.2
Z6	87.9	58.9	69.6	11.9
Z7	87.8	81.6	88.0	7.3
Z8	89.7	88.3	89.2	8.1
Z9	84.6	92.8	94.7	6.5
Z10	87.2	91.9	92.5	6.2
EX	85.7	87.4	89.2	7.0

Table 6.11 Hot melt extrusion samples from along the barrel, processed at temperature T140, screw geometry B and screw speed 10 rpm. Their full spectrum fit, measurement region fit, predicted co-crystal concentration and prediction uncertainty values.

T140 SGB 10 rpm sample	Full spectrum fit (%)	Measurement region fit (%)	Predicted co-crystal concentration (%)	Prediction uncertainty (%)
Z2	97.3	52.3	48.8	22.7
Z3	95.1	47.1	50.4	25.4
Z4	96.9	51.9	53.0	23.5
Z5	94.1	45.3	63.4	20.1
Z6	85.4	67.8	81.9	9.2
Z7	86.5	85.5	88.3	6.5
Z8	88.7	94.1	94.0	6.2
Z9	85.6	92.7	93.1	6.9
Z10	98.8	85.6	99.1	10.0
EX	87.3	93.2	94.3	6.3

In tables 6.9, 6.10 and 6.11, the full spectrum fit values were relatively high for all samples that were analysed. The predicted co-crystal concentration values indicated that the co-crystal yield increased steadily along the extruder barrel. The reduced co-crystal yield for the extruded samples was expected, as discussed in chapter 5. The prediction uncertainty values were relatively high for the samples Z2 to Z5. Due to these high uncertainty values it is possible the model has over-predicted the co-crystal yield for the samples for the first 4 extruder barrel zones. This scenario would make the most sense because the characterisation techniques used in chapter 5 determined that there were very low levels of co-crystal at these initial zones.

This over-prediction could be caused by the presence of pure nicotinamide in the samples which is not factored into the prediction model.

6.3 Discussion and conclusion

To compare the PLS models for both co-crystal pairs, the selected model details are shown in table 6.12. The correlation coefficient, RMSEC and RMSEP values were compared. Both co-crystal pairs achieved linear models with relatively low error values. In summary, the ibuprofen – nicotinamide model had lower RMSEC and RMSEP values than the carbamazepine – nicotinamide model and a slightly higher correlation coefficient.

Table 6.12 A comparison of the selected 1:1 IBU-NIC model (Model 1) and 1:1 CBZ-NIC model (Model 2), including the region, number of factors, chemometrics, RMSEC, RMSEP and correlation coefficient.

Co-Crystal Pair	Region (cm^{-1})	PLS Factors	Chemo-metrics	RMSEC (%)	RMSEP (%)	Corr. Coef.
IBU-NIC	7450-7000	2	SNV, 2^{nd} Dev., NS	0.77	0.95	0.9997
CBZ-NIC	9000-8500	2	SNV, 2^{nd} Dev., SGS	1.23	3.53	0.9992

The second derivative NIR spectra shown in figures 6.11 and 6.19 for both co-crystal pairs exhibited an increase in the second derivative NIR band intensity for the majority of the NIR bands in the selected model regions, as the co-crystal concentration decreased. This could suggest the PLS models have reduced error values when using a region where the intensity of most second derivative NIR bands directly correlates to a decrease in the co-

crystal concentration. Regarding the size of the NIR regions, there was no clear indication that a particular region size had a large effect on the PLS regression performance.

The second derivative NIR spectra used to create the carbamazepine – nicotinamide model were relatively complex and exhibited less distinct differences between each co-crystal concentration, compared to the ibuprofen – nicotinamide spectra. The complexity of the NIR spectra could be caused by the different arrangement of hydrogen bonding associated with the 1:1 CBZ-NIC co-crystal compared to the 1:1 IBU-NIC co-crystal. The different hydrogen bonding arrangements have been discussed in chapter 4. The complex spectra could have impacted the PLS regression performance and may have been the reason why the error values were higher for the selected carbamazepine – nicotinamide model.

The demonstrated PLS models in this chapter were able to quantify unknown samples from extrusion experiments discussed in chapter 5 with a high accuracy. However, the prediction uncertainty values were relatively high for samples which may have had increased concentrations of pure nicotinamide. This is a downside to the models as they do not take account of pure nicotinamide.

The PLS models presented in this chapter will facilitate future applications of NIR spectroscopy for quantifying pharmaceutical co-crystals. The results suggest that NIR spectroscopy could be used as a PAT tool for many different co-crystal manufacturing methods and could be used to improve the understanding of the cocrystallisation of pharmaceutical materials.

CHAPTER 7 GLOBAL DISCUSSION

Chapter 4 provided evidence of how temperature and shear force effects cocrystallisation and the thermal events involved with forming co-crystals. Key crystal morphology information was also presented for the carbamazepine – nicotinamide pair. The light microscopy images for carbamazepine – nicotinamide pair were useful as the discovered morphologies could be directly compared to the SEM images shown in chapter 5. The thermal data acquired for ibuprofen – nicotinamide and carbamazepine – nicotinamide was also beneficial for designing the extrusion experiments conducted in chapter 5.

In chapters 4 and 5, in figures 4.3 and 5.7, it was found that there was a relatively small endothermic melting peak during DSC heating of carbamazepine – nicotinamide at between 105°C and 109°C. This peak is not observed for nicotinamide on its own or for nicotinamide in the presence of any other material. The light microscopy images in figures 4.9 and 4.10 clearly show a new crystal form appears after this melting event has taken place; however it is still unclear what is causing the initial endothermic peak. In the literature, a nicotinamide polymorph has been reported which is metastable and has been crystallised in solution in the presence of the API isoxyl (Li et al. 2011). This reported polymorph has a melting point of approximately 105°C.

A study by Hino et al. (Hino et al. 2001) discovered four potential nicotinamide polymorphs by DSC. They found the melting points for form III and form IV were between 107-111°C and 101-103°C respectively. Further investigation would be required to characterise the phase which is causing the endothermic peak observed in figures 4.3 and 5.7. However there is a

possibility, that in the presence of carbamazepine, small quantities of nicotinamide form III or form IV are present under heating conditions. The melting of this phase may induce the crystallisation that is observed in the microscope images in figures 4.9 and 4.10.

The model shear experiments in chapter 4 used several techniques to apply small quantities of shear to the selected pharmaceutical pairs. However, a new piece of technology has recently been developed which will help to bridge the gap between the model shear experiments and full scale hot melt extrusion. It is called a mini mixer and has been developed by Anton Paar GmbH (Model: Anton Paar Physica MCR501). It consists of an enclosed chamber which can be loaded to a certain fill factor of the material to be analysed and it also has the capability to heat and cool the material. Inside the chamber is a small scale screw configuration which can be designed to mimic a full scale extruder screw. The mini mixer can then be attached to an Anton Paar rheometer such as the one used in chapter 4. This piece of equipment is able to feedback real-time rheological measurements whilst the chosen material is undergoing shear conditions. This technology has the potential to provide key data for investigating scale-up effects of hot melt extrusion in the near future.

Chapter 5 presented a solvent free continuous cocrystallisation method for ibuprofen – nicotinamide and carbamazepine – nicotinamide co-crystals. NIR spectroscopy was the favoured mode of characterisation which provided detailed insight into where cocrystallisation was occurring along the extruder barrel. The results from the extrusion experiments confirmed that temperature and shear play important roles in cocrystallisation and additional

parameters such as the screw speed can be used to increase the co-crystal yield. SEM analysis provided information about the agglomeration of extruded particles.

The design of the extrusion experiments in chapter 5, with regards to the explored parameters of temperature, screw geometry and screw speed, provided a strong case for the relationship between the parameters and the co-crystal yield. However, the experimental design process itself could be improved using a design of experiment (DoE) methodology. To determine the optimum parameters for extrusion, DoE could have been implemented at the earliest stage of the hot melt extrusion experimental design process (Alagumurthi et al. 2006).

Classical DoE and Taguchi's DoE are common methodologies which can be used to optimise process variables to deliver improved product quality (Roy 2001). In the case of extrusion, these approaches would allow for a multi-dimensional approach to experiment design where each experiment performed is a point on a multi-dimensional axis. This is particularly important for efficiently optimizing a process because each data point or experiment would contribute to the optimisation of all parameters that are being investigated. This is very different to examining one parameter at a time and DoE would benefit future extrusion studies conducted in the pharmaceutical field.

A small degradation study was conducted in chapter 5 which monitored the degradation of carbamazepine. There was a slightly raised amount of iminostilbene found in the extruded sample when carbamazepine was

extruded with nicotinamide compared to when pure carbamazepine was extruded. However, the level of degradation was relatively small and was not considered to be a detrimental factor to the technique due to the measured levels of iminostilbene being well below the recommended limit for carbamazepine tablets of 0.2%.

Chapter 6 presented accurate co-crystal yield prediction models for the 1:1 ibuprofen – nicotinamide and 1:1 carbamazepine – nicotinamide co-crystals, which can predict the 1:1 co-crystal yield in a mixture of the co-crystal and the API. Both models will provide a platform for in-line PAT technologies used in future studies. PAT technology can be used to monitor pharmaceutical manufacturing processes, including hot melt extrusion and can provide vital real-time information about a process. NIR spectroscopy is commonly employed as a PAT tool due to its ease of use, robustness and its ability to rapidly characterise materials. It is a technique which will continue to be developed and implemented as a PAT tool over the forthcoming years, specifically in the pharmaceutical industry, and it is believed that the results presented in chapter 6 have demonstrated the powerful advantages of this technique.

CHAPTER 8 PROJECT CONCLUSION

8.1 Conclusion

The presented project was able to provide important information about pharmaceutical co-crystal formation and behaviour under a variety of conditions using several different techniques. A SFCC technique was successfully explored and NIR spectroscopy was deemed to be an important characterisation technique which provided qualitative and quantitative information about co-crystals and their components. Understanding the behaviour of the materials on the small scale, provided vital knowledge which was subsequently used for designing the large scale hot melt extrusion experiments. NIR spectroscopy was also proven to be an accurate characterisation tool for predicting pharmaceutical co-crystal yields. Two pharmaceutical co-crystal models were created using PLS which can be used to predict co-crystal yield. The models will facilitate future in-line PAT studies of pharmaceutical co-crystals.

8.2 Future work

Future work will include in-line NIR measurements of cocrystallisation of pharmaceutical co-crystals with real-time monitoring during the hot melt extrusion process. This in-line data will provide crucial information about crystallisation events during hot melt extrusion and other techniques.

Mini mixer experiments will be conducted in order to provide small scale rheological data for pharmaceutical co-crystal pairs and the effect of scale on the outcome of hot melt extrusion. This unique technology will deliver data on the mixing properties of materials and the effect of small scale mixing on cocrystallisation.

Synchrotron data will be fully analysed for experiments conducted at Diamond Light Source and ESRF. The data will provide key knowledge on co-crystal formation and will link up with the shear cell data that was presented in chapter 4. Synchrotron X-ray data is more accurate than the conventional PXRD presented in this study and will provide information on the early stages of cocrystallisation of pharmaceutical pairs.

CHAPTER 9 BIBLIOGRAPHY

Aakeröy, C. B., N. C. Schultheiss, A. Rajbanshi, J. Desper and C. Moore (2008). "Supramolecular synthesis based on a combination of hydrogen and halogen bonds." Crystal Growth & Design **9**(1): 432-441.

Afnan, A. (2004). "PAT-A Framework for Innovative Pharmaceutical Development, Manufacturing and Quality Assurance." Guidance for Industry.

Aher, S., R. Dhumal, K. Mahadik, A. Paradkar and P. York (2010). "Ultrasound assisted cocrystallization from solution (USSC) containing a non-congruently soluble cocrystal component pair: caffeine/maleic acid." European Journal of Pharmaceutical Sciences **41**(5): 597-602.

Aitipamula, S., R. Banerjee, A. K. Bansal, K. Biradha, M. L. Cheney, A. R. Choudhury, G. R. Desiraju, A. G. Dikundwar, R. Dubey, N. Duggirala, P. P. Ghogale, S. Ghosh, P. K. Goswami, N. R. Goud, R. R. K. R. Jetti, P. Karpinski, P. Kaushik, D. Kumar, V. Kumar, B. Moulton, A. Mukherjee, G. Mukherjee, A. S. Myerson, V. Puri, A. Ramanan, T. Rajamannar, C. M. Reddy, N. Rodriguez-Hornedo, R. D. Rogers, T. N. G. Row, P. Sanphui, N. Shan, G. Shete, A. Singh, C. C. Sun, J. A. Swift, R. Thaimattam, T. S. Thakur, R. K. Thaper, S. P. Thomas, S. Tothadi, V. R. Vangala, N. Variankaval, P. Vishweshwar, D. R. Weyna and M. J. Zaworotko (2012). "Polymorphs, salts, and cocrystals: what's in a name?" Crystal Growth & Design **12**(5): 2147-2152.

Alagumurthi, N., K. Palaniradja and V. Soundararajan (2006). "Optimization of grinding process through design of experiment (DOE)—A comparative study." Materials and Manufacturing Processes **21**(1): 19-21.

Allen, F. (2002). "The Cambridge Structural Database: a quarter of a million crystal structures and rising." Acta Crystallographica Section B **58**(3 Part 1): 380-388.

Almarsson, Ö., M. L. Peterson and M. Zaworotko (2012). "The A to Z of pharmaceutical cocrystals: a decade of fast-moving new science and patents." Pharmaceutical Patent Analyst **1**(3): 313-327.

Almarsson, Ö. and M. J. Zaworotko (2004). "Crystal engineering of the composition of pharmaceutical phases. Do pharmaceutical co-crystals represent a new path to improved medicines?" Chemical Communications(17): 1889-1896.

Almeida, A., S. Possemiers, M. Boone, T. De Beer, T. Quinten, L. Van Hoorebeke, J. P. Remon and C. Vervaet (2011). "Ethylene vinyl acetate as matrix for oral sustained release dosage forms produced via hot-melt extrusion." European Journal of Pharmaceutics and Biopharmaceutics **77**(2): 297-305.

ASTM (2012). Standard Practices for Infrared Multivariate Quantitative Analysis, ASTM International.

Banerjee, R., P. M. Bhatt, N. V. Ravindra and G. R. Desiraju (2005). "Saccharin salts of active pharmaceutical ingredients, their crystal structures, and increased water solubilities." Crystal Growth & Design **5**(6): 2299-2309.

Berge, S. M., L. D. Bighley and D. C. Monkhouse (1977). "Pharmaceutical salts." Journal of Pharmaceutical Sciences **66**(1): 1-19.

Berry, D. J., C. C. Seaton, W. Clegg, R. W. Harrington, S. J. Coles, P. N. Horton, M. B. Hursthouse, R. Storey, W. Jones and T. Friscic (2008). "Applying hot-stage microscopy to co-crystal screening: a study of

nicotinamide with seven active pharmaceutical ingredients." Crystal Growth & Design **8**(5): 1697-1712.

Bhatt, P. M., N. V. Ravindra, R. Banerjee and G. R. Desiraju (2005). "Saccharin as a salt former. Enhanced solubilities of saccharinates of active pharmaceutical ingredients." Chemical Communications(8): 1073-1075.

Bhattachar, S. N., L. A. Deschenes and J. A. Wesley (2006). "Solubility: it's not just for physical chemists." Drug Discovery Today **11**(21): 1012-1018.

Bialleck, S. and H. Rein (2011). "Preparation of starch-based pellets by hot-melt extrusion." European Journal of Pharmaceutics and Biopharmaceutics **79**(2): 440-448.

Blagden, N., D. J. Berry, A. Parkin, H. Javed, A. Ibrahim, P. T. Gavan, L. L. De Matos and C. C. Seaton (2008). "Current directions in co-crystal growth." New Journal of Chemistry **32**(10): 1659-1672.

Blagden, N., M. De Matas, P. Gavan and P. York (2007). "Crystal engineering of active pharmaceutical ingredients to improve solubility and dissolution rates." Advanced Drug Delivery Reviews **59**(7): 617-630.

Blanco, M., J. Coello, H. Iturriaga, S. Maspoch and C. De La Pezuela (1998). "Near-infrared spectroscopy in the pharmaceutical industry." Royal Society of Chemistry **123**: 135R-150R.

Blanco, M. and I. Villarroya (2002). "NIR spectroscopy: a rapid-response analytical tool." Trends in Analytical Chemistry **21**(4): 240-250.

Bond, A. D. (2006). "Inversion of the melting point alternation in n-alkyl carboxylic acids by co-crystallization with pyrazine." CrystEngComm **8**(4): 333-337.

Bond, A. D. (2007). "What is a co-crystal?" CrystEngComm **9**(9): 833-834.

Breimer, D. (1980). "Towards Better Safety of Drugs and Pharmaceutical Products." Elsevier North-Holland.

Breitenbach, J. (2002). "Melt extrusion: from process to drug delivery technology." European Journal of Pharmaceutics and Biopharmaceutics **54**(2): 107-117.

Brittain, H. G. (2009). Polymorphism in pharmaceutical solids, CRC Press.

Brittain, H. G. (2013). "Pharmaceutical cocrystals: The coming wave of new drug substances." Journal of Pharmaceutical Sciences **102**(2): 311-317.

CDER (2007). "Guidance for Industry, ANDAs: Pharmaceutical Solid Polymorphism, Chemistry, Manufacturing, and Controls Information." Food and Drug Administration.

Chadha, R., P. Arora, A. Saini and D. S. Jain (2010). "Solvated crystalline forms of nevirapine: thermoanalytical and spectroscopic studies." PharmSciTech **11**(3): 1328-1339.

Chadwick, K., R. Davey and W. Cross (2007). "How does grinding produce co-crystals? Insights from the case of benzophenone and diphenylamine." CrystEngComm **9**(9): 732-734.

Chiarella, R. A., R. J. Davey and M. L. Peterson (2007). "Making co-crystals the utility of ternary phase diagrams." Crystal Growth & Design **7**(7): 1223-1226.

Chokshi, R. and H. Zia (2010). "Hot-melt extrusion technique: a review." Iranian Journal of Pharmaceutical Research: 3-16.

Chow, S. F., M. Chen, L. Shi, A. H. Chow and C. C. Sun (2012). "Simultaneously improving the mechanical properties, dissolution performance, and hygroscopicity of ibuprofen and flurbiprofen by

cocrystallization with nicotinamide." Pharmaceutical Research **29**(7): 1854-1865.

Chun, N.-H., M.-J. Lee, G.-H. Song, K.-Y. Chang, C.-S. Kim and G. J. Choi (2014). "Combined anti-solvent and cooling method of manufacturing indomethacin–saccharin (IMC–SAC) co-crystal powders." Journal of Crystal Growth **408**: 112-118.

Convention, U. S. P. (2015). "Carbamazepine tablets monograph." United States Pharmacopeia: 1-4.

Crawford, R. (1981). Progress in Plastics Engineering, Pergamon Press, London.

Crowley, M. M., F. Zhang, M. A. Repka, S. Thumma, S. B. Upadhye, S. Kumar Battu, J. W. McGinity and C. Martin (2007). "Pharmaceutical applications of hot-melt extrusion: part I." Drug Development and Industrial Pharmacy **33**(9): 909-926.

Database, P. S. (2016). "Substance 24896549 Maleic acid." National Centre for Biotechnology Information: https://pubchem.ncbi.nlm.nih.gov/substance/24896549.

Daurio, D., C. Medina, R. Saw, K. Nagapudi and F. Alvarez-Núñez (2011). "Application of twin screw extrusion in the manufacture of cocrystals, part I: four case studies." Pharmaceutics **3**(3): 582-600.

De Armas, H. N., O. M. Peeters, G. Van den Mooter and N. Blaton (2007). "Polymorphism of alprazolam (Xanax®): a review of its crystalline phases and identification, crystallographic characterization, and crystal structure of a new polymorph (form III)." Journal of Pharmaceutical Sciences **96**(5): 1114-1130.

Deshpande, P. P., J. Singh, A. Pullockaran, T. Kissick, B. A. Ellsworth, J. Z. Gougoutas, J. Dimarco, M. Fakes, M. Reyes and C. Lai (2012). "A practical stereoselective synthesis and novel cocrystallizations of an amphiphatic SGLT-2 inhibitor." Organic Process Research & Development **16**(4): 577-585.

Desiraju, G. R. (2003). "Crystal and co-crystal." CrystEngComm **5**(82): 466-467.

Dhumal, R. S., A. L. Kelly, P. York, P. D. Coates and A. Paradkar (2010). "Cocrystalization and simultaneous agglomeration using hot melt extrusion." Pharmaceutical Research **27**(12): 2725-2733.

DiMasi, J. A., H. G. Grabowski and R. W. Hansen (2016). "Innovation in the pharmaceutical industry: new estimates of R&D costs." Journal of Health Economics **47**: 20-33.

Douillet, J., N. Stevenson, M. Lee, F. Mallet, R. Ward, P. Aspin, D. R. Dennehy and L. Camus (2012). "Development of a solvate as an active pharmaceutical ingredient: Developability, crystallisation and isolation challenges." Journal of Crystal Growth **342**(1): 2-8.

Dunitz, J. D. (2003). "Crystal and co-crystal: a second opinion." CrystEngComm **5**(91): 506-506.

Eddleston, M. D., B. Patel, G. M. Day and W. Jones (2013). "Cocrystallization by freeze-drying: Preparation of novel multicomponent crystal forms." Crystal Growth & Design **13**(10): 4599-4606.

Eitzlmayr, A. and J. Khinast (2015). "Co-rotating twin-screw extruders: Detailed analysis of conveying elements based on smoothed particle

hydrodynamics. Part 2: Mixing." Chemical Engineering Science **134**: 880-886.

Eitzlmayr, A., G. Koscher, G. Reynolds, Z. Huang, J. Booth, P. Shering and J. Khinast (2014). "Mechanistic modeling of modular co-rotating twin-screw extruders." International Journal of Pharmaceutics **474**(1): 157-176.

Elbagerma, M., H. Edwards, T. Munshi, M. Hargreaves, P. Matousek and I. Scowen (2010). "Characterization of new cocrystals by Raman spectroscopy, powder X-ray diffraction, differential scanning calorimetry, and transmission Raman spectroscopy." Crystal Growth & Design **10**(5): 2360-2371.

Etter, M. C. (1991). "Hydrogen bonds as design elements in organic chemistry." The Journal of Physical Chemistry **95**(12): 4601-4610.

Evenson, R. E. (1993). "Patents, R&D, and invention potential: International evidence." The American Economic Review **83**(2): 463-468.

Fermi, E. (1931). "Über den Ramaneffekt des kohlendioxyds." Zeitschrift für Physik **71**(3-4): 250-259.

Fleischman, S. G., S. S. Kuduva, J. A. McMahon, B. Moulton, R. D. Bailey Walsh, N. Rodríguez-Hornedo and M. J. Zaworotko (2003). "Crystal engineering of the composition of pharmaceutical phases: multiple-component crystalline solids involving carbamazepine." Crystal Growth & Design **3**(6): 909-919.

Gagniere, E., D. Mangin, F. Puel, A. Rivoire, O. Monnier, E. Garcia and J. Klein (2009). "Formation of co-crystals: kinetic and thermodynamic aspects." Journal of Crystal Growth **311**(9): 2689-2695.

Gardner, C. R., C. T. Walsh and Ö. Almarsson (2004). "Drugs as materials: valuing physical form in drug discovery." Nature Reviews Drug Discovery **3**(11): 926-934.

Ghebre-Selassie, I. and C. Martin (2003). Pharmaceutical extrusion technology, CRC Press.

Giacovazzo, C. (2002). Fundamentals of crystallography, Oxford University Press, USA.

Good, D. J. and N. r. Rodríguez-Hornedo (2009). "Solubility advantage of pharmaceutical cocrystals." Crystal Growth & Design **9**(5): 2252-2264.

Gryczke, A., S. Schminke, M. Maniruzzaman, J. Beck and D. Douroumis (2011). "Development and evaluation of orally disintegrating tablets (ODTs) containing Ibuprofen granules prepared by hot melt extrusion." Colloids and Surfaces B: Biointerfaces **86**(2): 275-284.

Guo, K., G. Sadiq, C. Seaton, R. Davey and Q. Yin (2009). "Co-crystallization in the caffeine/maleic acid system: lessons from phase equilibria." Crystal Growth & Design **10**(1): 268-273.

Haleblian, J. and W. McCrone (1969). "Pharmaceutical applications of polymorphism." Journal of Pharmaceutical Sciences **58**(8): 911-929.

Hasa, D., G. Schneider Rauber, D. Voinovich and W. Jones (2015). "Cocrystal Formation through Mechanochemistry: from Neat and Liquid-Assisted Grinding to Polymer-Assisted Grinding." Angewandte Chemie International Edition **54**(25): 7371-7375.

Hilfiker, R. (2006). Polymorphism: in the pharmaceutical industry, John Wiley & Sons.

Hino, T., J. L. Ford and M. W. Powell (2001). "Assessment of nicotinamide polymorphs by differential scanning calorimetry." Thermochimica Acta **374**(1): 85-92.

ICH (2008a). "Pharmaceutical Development." International Conference on Harmonisation of Technical Requirements for the Registration of Pharmaceuticals for Human Use.

ICH (2008b). "Pharmaceutical Quality System." International Conference on Harmonisation of Technical Requirements for the Registration of Pharmaceuticals for Human Use.

Jayasankar, A., D. J. Good and N. Rodríguez-Hornedo (2007). "Mechanisms by which moisture generates cocrystals." Molecular Pharmaceutics **4**(3): 360-372.

Jones, B. F. (2009). "The burden of knowledge and the “death of the renaissance man”: Is innovation getting harder?" The Review of Economic Studies **76**(1): 283-317.

Kaupp, G. (2003). "Solid-state molecular syntheses: complete reactions without auxiliaries based on the new solid-state mechanism." CrystEngComm **5**(23): 117-133.

Kaur Bhangu, S., M. Ashokkumar and J. Lee (2016). "Ultrasound Assisted Crystallization of Paracetamol: Crystal Size Distribution and Polymorph Control." Crystal Growth & Design **16**(4): 1934-1941.

Kelley, S. P., A. Narita, J. D. Holbrey, K. D. Green, W. M. Reichert and R. D. Rogers (2013). "Understanding the effects of ionicity in salts, solvates, co-crystals, ionic co-crystals, and ionic liquids, rather than nomenclature, is

critical to understanding their behavior." Crystal Growth & Design **13**(3): 965-975.

Kelly, A. L., T. Gough, R. Dhumal, S. Halsey and A. Paradkar (2012). "Monitoring ibuprofen–nicotinamide cocrystal formation during solvent free continuous cocrystallization (SFCC) using near infrared spectroscopy as a PAT tool." International Journal of Pharmaceutics **426**(1): 15-20.

Kelly, R. C. and N. Rodríguez-Hornedo (2009). "Solvent effects on the crystallization and preferential nucleation of carbamazepine anhydrous polymorphs: A molecular recognition perspective." Org. Process Res. Dev **13**(6): 1291-1300.

Kleinebudde, P. (2011). "Pharmazeutisches Produktdesign: Gezielte Freisetzung von Wirkstoffen durch unterschiedliche Extrusionstechniken." Chemie Ingenieur Technik **83**(5): 589-597.

Klug, H. and L. E. Alexander (1974). "X-ray Diffraction." Addision-Wilson Publishing Company Inc, USA **132**.

Krause, J., M. Thommes and J. Breitkreutz (2009). "Immediate release pellets with lipid binders obtained by solvent-free cold extrusion." European Journal of Pharmaceutics and Biopharmaceutics **71**(1): 138-144.

Kulkarni, C., A. Kelly, J. Kendrick, T. Gough and A. Paradkar (2013). "Mechanism for polymorphic transformation of artemisinin during high temperature extrusion." Crystal Growth & Design **13**(12): 5157-5161.

Kulkarni, C., C. Wood, A. L. Kelly, T. Gough, N. Blagden and A. Paradkar (2015). "Stoichiometric control of co-crystal formation by solvent free continuous co-crystallization (SFCC)." Crystal Growth & Design **15**(12): 5648-5651.

Kumar, L., A. Amin and A. K. Bansal (2007). "An overview of automated systems relevant in pharmaceutical salt screening." Drug Discovery Today **12**(23): 1046-1053.

Lara-Ochoa, F. and G. Espinosa-Perez (2007). "Crystals and patents." Crystal Growth & Design **7**(7): 1213-1215.

Lara-Ochoa, F. and G. Espinosa-Pérez (2007). "Cocrystals definitions." Supramolecular Chemistry **19**(8): 553-557.

Lee, M.-J., I.-C. Wang, M.-J. Kim, P. Kim, K.-H. Song, N.-H. Chun, H.-G. Park and G. J. Choi (2015). "Controlling the polymorphism of carbamazepine-saccharin cocrystals formed during antisolvent cocrystallization using kinetic parameters." Korean Journal of Chemical Engineering **32**(9): 1910-1917.

Lehmann, O. (1888). "Molekular Physik, Vol. 1." Engelmann, Leipzig: 193.

Leyssens, T., N. Tumanova, K. Robeyns, N. Candoni and S. Veesler (2014). "Solution cocrystallization, an effective tool to explore the variety of cocrystal systems: caffeine/dicarboxylic acid cocrystals." CrystEngComm **16**(41): 9603-9611.

Li, J., S. A. Bourne and M. R. Caira (2011). "New polymorphs of isonicotinamide and nicotinamide." Chemical Communications **47**(5): 1530-1532.

Lim, S. and J. White (1994). "Flow mechanisms, material distributions and phase morphology development in a modular intermeshing counter-rotating twin screw extruder of Leistritz design." International Polymer Processing **9**(1): 33-45.

Llinàs, A. and J. M. Goodman (2008). "Polymorph control: past, present and future." Drug Discovery Today **13**(5): 198-210.

Long, F. H. (2009). Vibrational spectroscopic methods for quantitative analysis. Handbook of Stability Testing in Pharmaceutical Development, Springer 223-240.

Lu, E., N. Rodríguez-Hornedo and R. Suryanarayanan (2008). "A rapid thermal method for cocrystal screening." CrystEngComm **10**(6): 665-668.

Ma, P. and R. Zemmel (2002). "Value of novelty?" Nature Reviews Drug Discovery **1**(8): 571-572.

Mandic, Z. (2012). Physico Chemical Methods in Drug Discovery and Development, IAPC Publishing.

Maniruzzaman, M., M. Rana, J. Boateng, J. Mitchell and D. Douroumis (2013). "Dissolution enhancement of poorly water-soluble APIs processed by hot-melt extrusion using hydrophilic polymers." Drug Development and Industrial Pharmacy **39**(2): 218-227.

McNamara, D. P., S. L. Childs, J. Giordano, A. Iarriccio, J. Cassidy, M. S. Shet, R. Mannion, E. O'Donnell and A. Park (2006). "Use of a glutaric acid cocrystal to improve oral bioavailability of a low solubility API." Pharmaceutical Research **23**(8): 1888-1897.

Medina, C., D. Daurio, K. Nagapudi and F. Alvarez-Nunez (2010). "Manufacture of pharmaceutical co-crystals using twin screw extrusion: A solvent-less and scalable process." Journal of Pharmaceutical Sciences **99**(4): 1693-1696.

Miroshnyk, I., S. Mirza and N. Sandler (2009). "Pharmaceutical co-crystals–an opportunity for drug product enhancement." Expert Opinion on Drug Delivery **6**(4): 333-341.

Moradiya, H. G., M. T. Islam, S. Halsey, M. Maniruzzaman, B. Z. Chowdhry, M. J. Snowden and D. Douroumis (2014). "Continuous cocrystallisation of carbamazepine and trans-cinnamic acid via melt extrusion processing." CrystEngComm **16**(17): 3573-3583.

Nehm, S. J., B. Rodríguez-Spong and N. Rodríguez-Hornedo (2006). "Phase solubility diagrams of cocrystals are explained by solubility product and solution complexation." Crystal Growth & Design **6**(2): 592-600.

Nordström, F. L. and Å. C. Rasmuson (2006). "Solubility and melting properties of salicylic acid." Journal of Chemical & Engineering Data **51**(5): 1668-1671.

Pammolli, F., L. Magazzini and M. Riccaboni (2011). "The productivity crisis in pharmaceutical R&D." Nature Reviews Drug Discovery **10**(6): 428-438.

Patil, S. P., S. R. Modi and A. K. Bansal (2014). "Generation of 1: 1 carbamazepine: nicotinamide cocrystals by spray drying." European Journal of Pharmaceutical Sciences **62**: 251-257.

Perissutti, B., J. M. Newton, F. Podczeck and F. Rubessa (2002). "Preparation of extruded carbamazepine and PEG 4000 as a potential rapid release dosage form." European Journal of Pharmaceutics and Biopharmaceutics **53**(1): 125-132.

Peterson, M. L., M. B. Hickey, M. J. Zaworotko and Ö. Almarsson (2006). "Expanding the scope of crystal form evaluation in pharmaceutical science." J Pharm Pharm Sci **9**(3): 317-326.

Pinto, S. S. and H. P. Diogo (2006). "Thermochemical study of two anhydrous polymorphs of caffeine." The Journal of Chemical Thermodynamics **38**(12): 1515-1522.

Porter III, W. W., S. C. Elie and A. J. Matzger (2008). "Polymorphism in carbamazepine cocrystals." Crystal Growth & Design **8**(1): 14-16.

Qiao, N., K. Wang, W. Schlindwein, A. Davies and M. Li (2013). "In situ monitoring of carbamazepine–nicotinamide cocrystal intrinsic dissolution behaviour." European Journal of Pharmaceutics and Biopharmaceutics **83**(3): 415-426.

Rastogi, R., P. S. Bassi and S. Chadha (1962). "Kinetics of reaction between naphthalene and picric acid in the solid state." The Journal of Physical Chemistry **66**(12): 2707-2708.

Read, E., J. Park, R. Shah, B. Riley, K. Brorson and A. Rathore (2010). "Process analytical technology (PAT) for biopharmaceutical products: part I. Concepts and applications." Biotechnology and Bioengineering **105**(2): 276-284.

Reading, M., A. Luget and R. Wilson (1994). "Modulated differential scanning calorimetry." Thermochimica Acta **238**: 295-307.

Reich, G. (2005). "Near-infrared spectroscopy and imaging: basic principles and pharmaceutical applications." Advanced Drug Delivery Reviews **57**(8): 1109-1143.

Richardson, M. and E. Charsley (1998). Handbook of Thermal Analysis and Calorimetry, Elsevier Amsterdam.

Roblegg, E., E. Jäger, A. Hodzic, G. Koscher, S. Mohr, A. Zimmer and J. Khinast (2011). "Development of sustained-release lipophilic calcium

stearate pellets via hot melt extrusion." European Journal of Pharmaceutics and Biopharmaceutics **79**(3): 635-645.

Rodríguez-Hornedo, N., S. J. Nehm, K. F. Seefeldt, Y. Pagan-Torres and C. J. Falkiewicz (2006). "Reaction crystallization of pharmaceutical molecular complexes." Molecular Pharmaceutics **3**(3): 362-367.

Rodríguez-Spong, B., C. P. Price, A. Jayasankar, A. J. Matzger and N. r. Rodríguez-Hornedo (2004). "General principles of pharmaceutical solid polymorphism: a supramolecular perspective." Advanced Drug Delivery Reviews **56**(3): 241-274.

Roy, R. K. (2001). Design of experiments using the Taguchi approach: 16 steps to product and process improvement, John Wiley & Sons.

Saal, C. and A. Becker (2013). "Pharmaceutical salts: A summary on doses of salt formers from the Orange Book." European Journal of Pharmaceutical Sciences **49**(4): 614-623.

Sanphui, P., S. S. Kumar and A. Nangia (2012). "Pharmaceutical cocrystals of niclosamide." Crystal Growth & Design **12**(9): 4588-4599.

Sarraguça, M. C., M. Paisana, J. Pinto and J. A. Lopes (2015). "Real-time monitoring of cocrystallization processes by solvent evaporation: A near infrared study." European Journal of Pharmaceutical Sciences.

Sarraguça, M. C., P. R. Ribeiro, A. O. Santos, M. C. Silva and J. A. Lopes (2014). "A PAT approach for the on-line monitoring of pharmaceutical co-crystals formation with near infrared spectroscopy." International Journal of Pharmaceutics **471**(1): 478-484.

Sarraguça, M. C., P. R. Ribeiro, A. O. D. Santos and J. A. Lopes (2015). "Batch Statistical Process Monitoring Approach to a Cocrystallization Process." Journal of Pharmaceutical Sciences **104**(12): 4099-4108.

Schultheiss, N. and A. Newman (2009). "Pharmaceutical cocrystals and their physicochemical properties." Crystal Growth & Design **9**(6): 2950-2967.

Seefeldt, K., J. Miller, F. Alvarez-Nunez and N. Rodriguez-Hornedo (2007). "Crystallization pathways and kinetics of carbamazepine–nicotinamide cocrystals from the amorphous state by in situ thermomicroscopy, spectroscopy, and calorimetry studies." Journal of Pharmaceutical Sciences **96**(5): 1147-1158.

Shan, N., F. Toda and W. Jones (2002). "Mechanochemistry and co-crystal formation: effect of solvent on reaction kinetics." Chemical Communications(20): 2372-2373.

Shan, N. and M. J. Zaworotko (2008). "The role of cocrystals in pharmaceutical science." Drug Discovery Today **13**(9): 440-446.

Shayanfar, A., S. Velaga and A. Jouyban (2014). "Solubility of carbamazepine, nicotinamide and carbamazepine–nicotinamide cocrystal in ethanol–water mixtures." Fluid Phase Equilibria **363**: 97-105.

Sheth, A. R. and D. J. Grant (2005). "Relationship between the structure and properties of pharmaceutical crystals." KONA Powder and Particle Journal **23**(0): 36-48.

Siesler, H. W. (2008). "Basic principles of near-infrared spectroscopy." Practical Spectroscopy Series **35**: 7.

Stahly, G. P. (2007). "Diversity in single-and multiple-component crystals. The search for and prevalence of polymorphs and cocrystals." Crystal Growth & Design **7**(6): 1007-1026.

Stieger, N. and W. Liebenberg (2012). Recrystallization of Active Pharmaceutical Ingredients, INTECH Open Access Publisher Rijeka, Croatia.

Takata, N., K. Shiraki, R. Takano, Y. Hayashi and K. Terada (2008). "Cocrystal screening of stanolone and mestanolone using slurry crystallization." Crystal Growth & Design **8**(8): 3032-3037.

Tayeb, J., B. Vergnes and G. D. VALLE (1989). "A basic model for a twin-screw extruder." Journal of Food Science **54**(4): 1047-1056.

Thakuria, R., A. Delori, W. Jones, M. P. Lipert, L. Roy and N. Rodríguez-Hornedo (2013). "Pharmaceutical cocrystals and poorly soluble drugs." International Journal of Pharmaceutics **453**(1): 101-125.

Thayer, A. M. (2010). "FINDING SOLUTIONS." Chemical & Engineering News Archive **88**(22): 13-18.

Trask, A. V., W. S. Motherwell and W. Jones (2004). "Solvent-drop grinding: green polymorph control of cocrystallisation." Chemical Communications(7): 890-891.

Trask, A. V., W. S. Motherwell and W. Jones (2005). "Pharmaceutical cocrystallization: Engineering a remedy for caffeine hydration." Crystal Growth & Design **5**(3): 1013-1021.

Vishweshwar, P., J. A. Mcmahon, J. A. Bis and M. J. Zaworotko (2006). "Pharmaceutical co-crystals." Journal of Pharmaceutical Sciences **95**(3): 499-516.

Vishweshwar, P., A. Nangia and V. M. Lynch (2003). "Molecular complexes of homologous alkanedicarboxylic acids with isonicotinamide: X-ray crystal structures, hydrogen bond synthons, and melting point alternation." Crystal Growth & Design **3**(5): 783-790.

Vithani, K., M. Maniruzzaman, I. Slipper, S. Mostafa, C. Miolane, Y. Cuppok, D. Marchaud and D. Douroumis (2013). "Sustained release solid lipid matrices processed by hot-melt extrusion (HME)." Colloids and Surfaces B: Biointerfaces **110**: 403-410.

Weyna, D. R., T. Shattock, P. Vishweshwar and M. J. Zaworotko (2009). "Synthesis and structural characterization of cocrystals and pharmaceutical cocrystals: mechanochemistry vs slow evaporation from solution." Crystal Growth & Design **9**(2): 1106-1123.

Whelan, T. and D. Dunning (1988). The Dynisco Extrusion Processors Handbook, Dynisco Incorporated.

White, J. L., H. Potente and U. Berghaus (2003). Screw extrusion: science and technology, Hanser Verlag.

Williams, P. A., C. E. Hughes and K. D. Harris (2012). "New insights into the preparation of the low-melting polymorph of racemic ibuprofen." Crystal Growth & Design **12**(12): 5839-5845.

Wood, P. A., N. Feeder, M. Furlow, P. T. Galek, C. R. Groom and E. Pidcock (2014). "Knowledge-based approaches to co-crystal design." CrystEngComm **16**(26): 5839-5848.

Yan, Y., J.-M. Chen, N. Geng and T.-B. Lu (2012). "Improving the solubility of agomelatine via cocrystals." Crystal Growth & Design **12**(5): 2226-2233.

Yu, L. (2001). "Amorphous pharmaceutical solids: preparation, characterization and stabilization." Advanced Drug Delivery Reviews **48**(1): 27-42.

Zukerman-Schpector, J. and E. R. Tiekink (2008). "What is a co-crystal?" Zeitschrift für Kristallographie **223**(3/2008): 233-234.

APPENDIX A

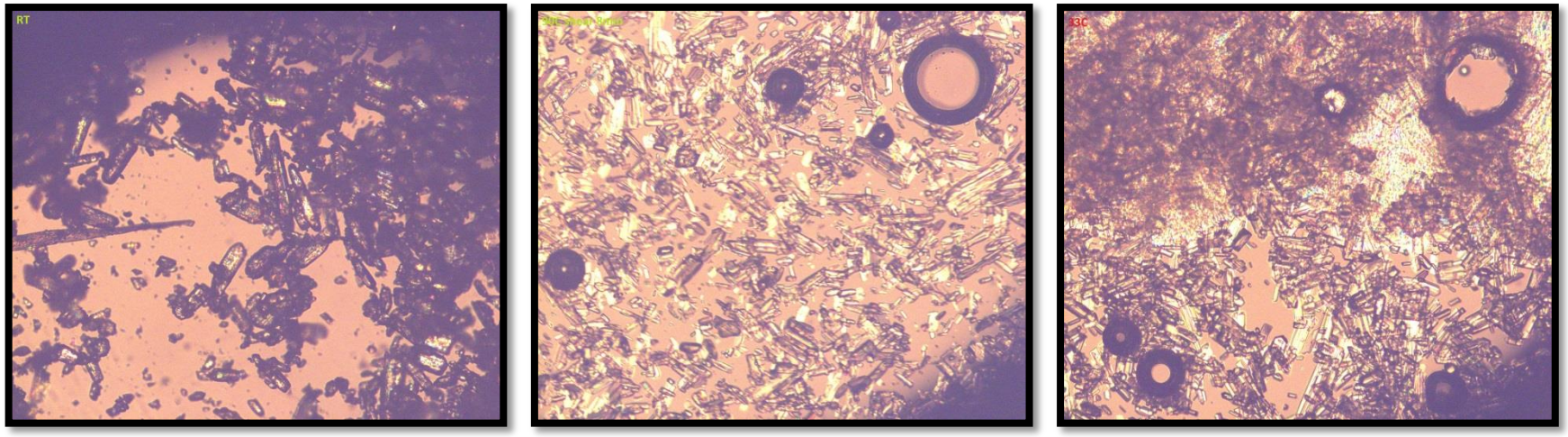

Figure A.1 Light microscopy images of 1:1 ibuprofen – nicotinamide physical mixture shear cell run 1. Showing the starting material (Left), after 8 minutes of shear (Centre) and post shear 33°C (Right).

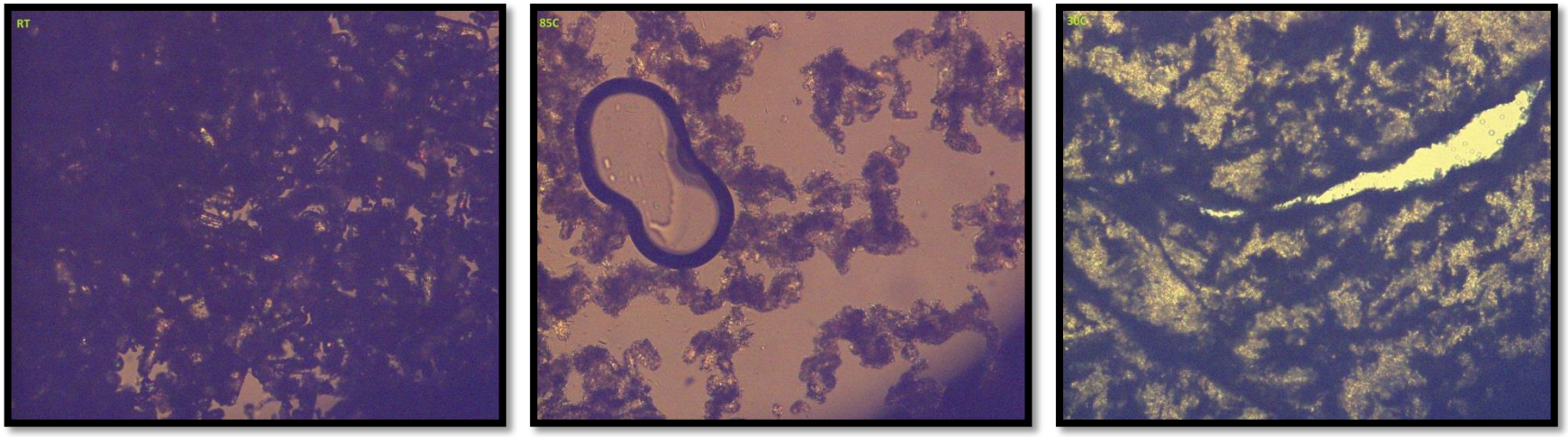

Figure A.2 Light microscopy images of 1:1 ibuprofen – nicotinamide physical mixture shear cell run 2. Showing the starting material (Left), the material at 85°C pre shear (Centre) and post shear 30°C (Right).

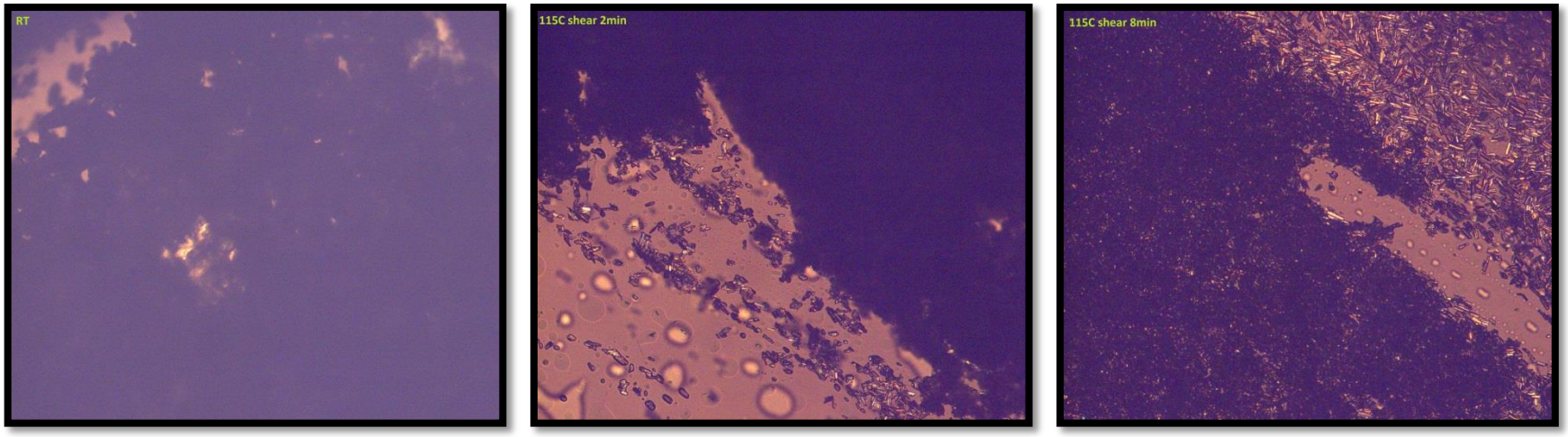

Figure A.3 Light microscopy images of 1:1 nicotinamide – salicylic acid physical mixture shear cell run 1. Showing the starting material (Left), after 2 minutes of shear (Centre) and after 8 minutes of shear (Right).

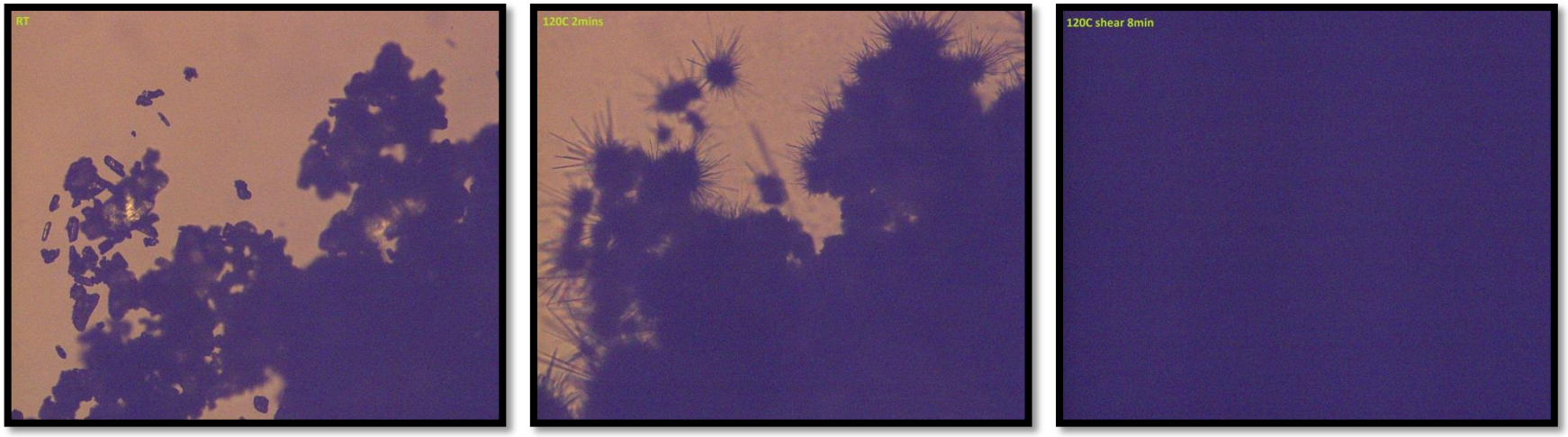

Figure A.4 Light microscopy images of 1:1 nicotinamide – salicylic acid physical mixture shear cell run 2. Showing the starting material (Left), after 2 minutes isothermal at 120°C (Centre) and after 8 minutes of shear (Right).

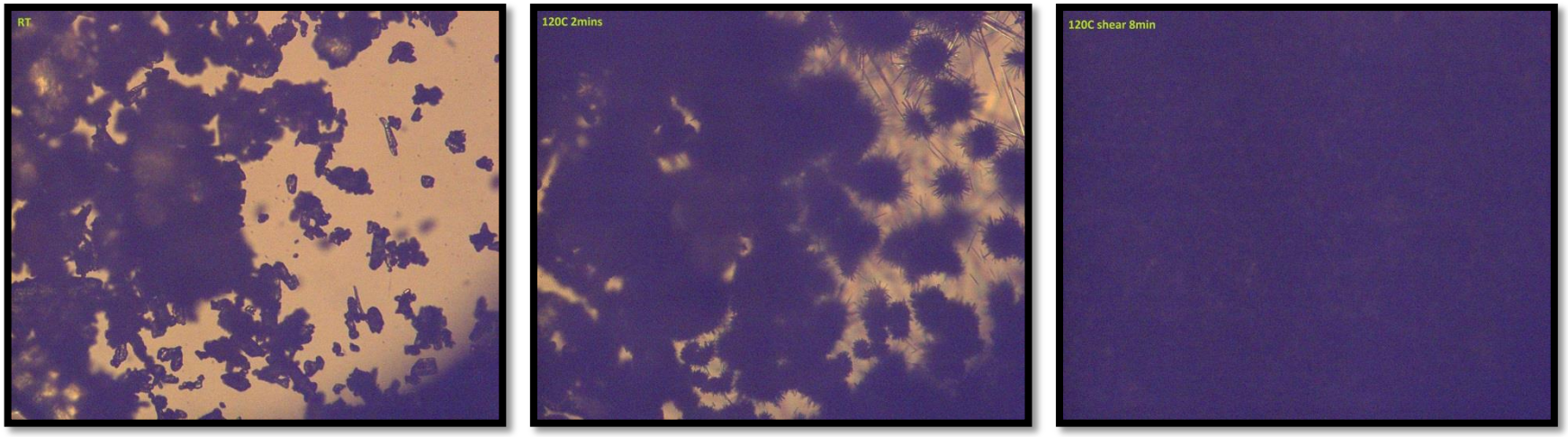

Figure A.5 Light microscopy images of 1:1 nicotinamide – salicylic acid physical mixture shear cell run 3. Showing the starting material (Left), after 2 minutes isothermal at 120°C (Centre) and after 8 minutes of shear (Right).

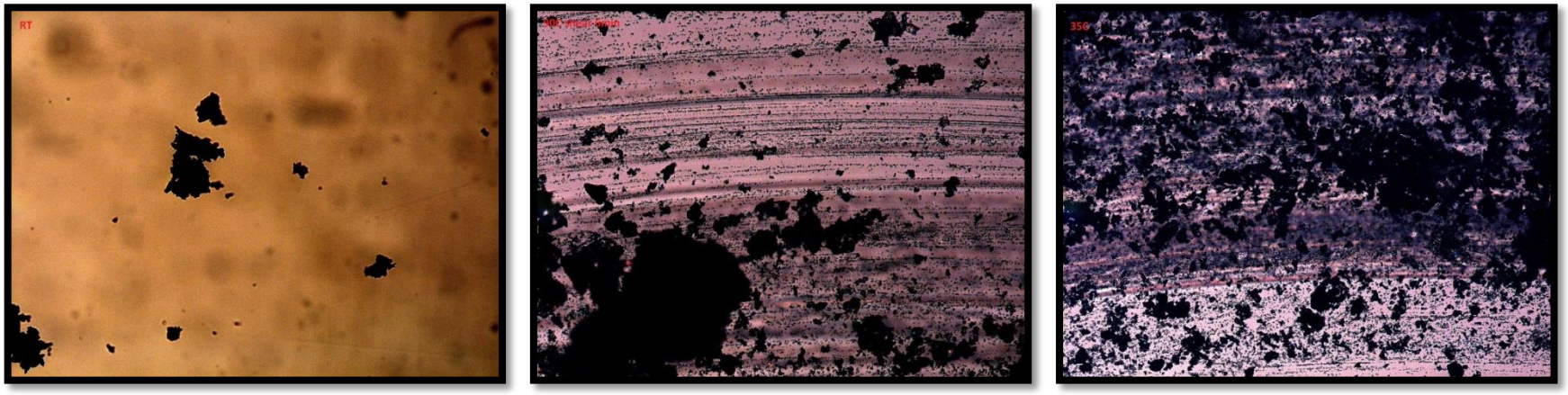

Figure A.6 Light microscopy images of 1:1 caffeine - maleic acid physical mixture shear cell run 1. Showing the starting material (Left), after 6 minutes of shear (Centre) and post shear 35°C (Right).

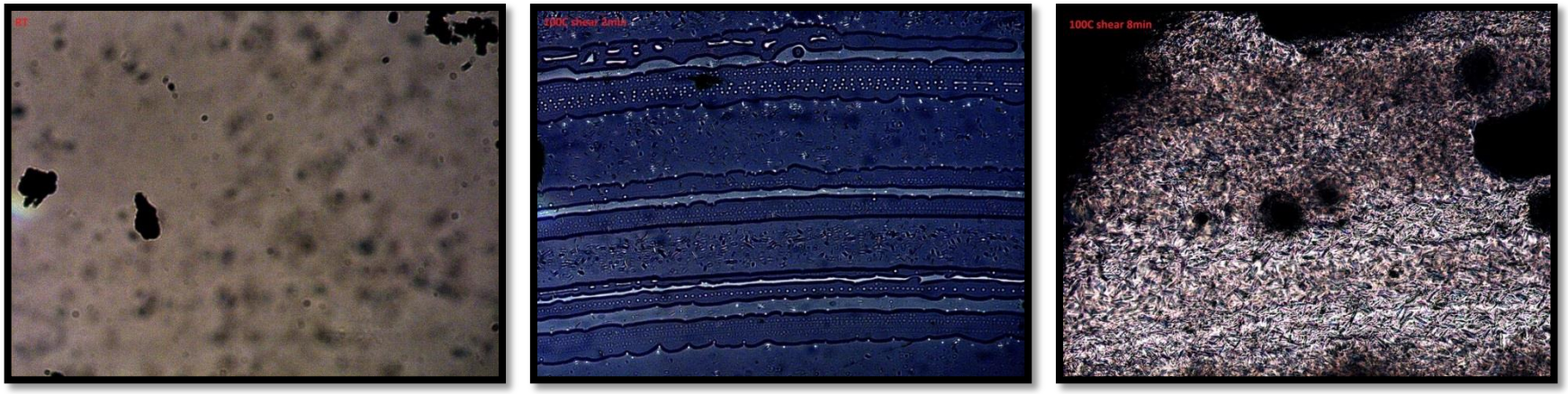

Figure A.7 Light microscopy images of 1:1 caffeine - maleic acid physical mixture shear cell run 2. Showing the starting material (Left), after 2 minutes of shear (Centre) and after 8 minutes of shear (Right).

Figure A.8 Light microscopy images of 1:1 caffeine - maleic acid physical mixture shear cell run 3. Showing the starting material (Left), after 2 minutes of shear (Centre) and after 8 minutes of shear (Right).

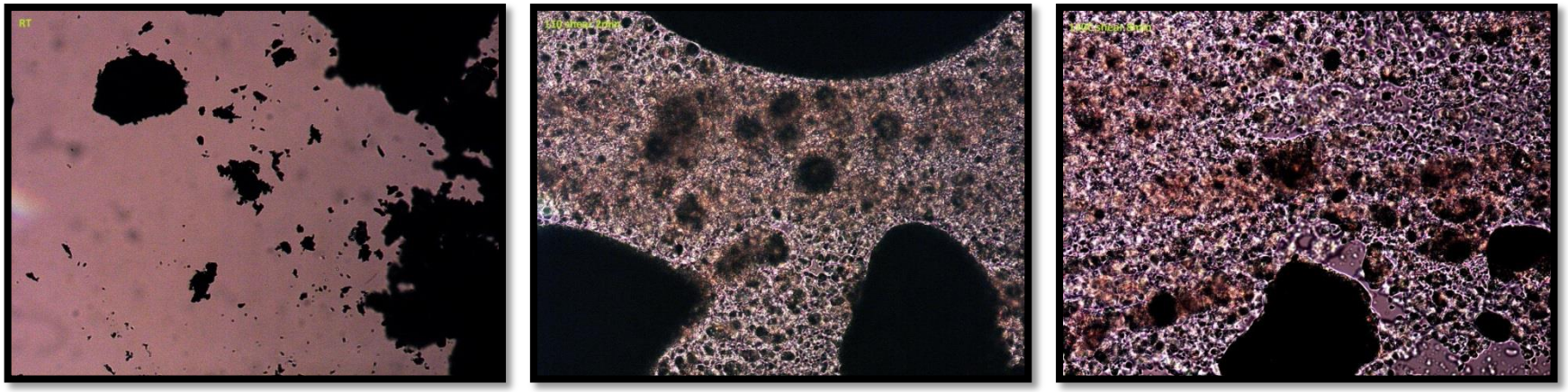

Figure A.9 Light microscopy images of 1:1 caffeine - maleic acid physical mixture shear cell run 4. Showing the starting material (Left), after 2 minutes of shear (Centre) and after 8 minutes of shear (Right).

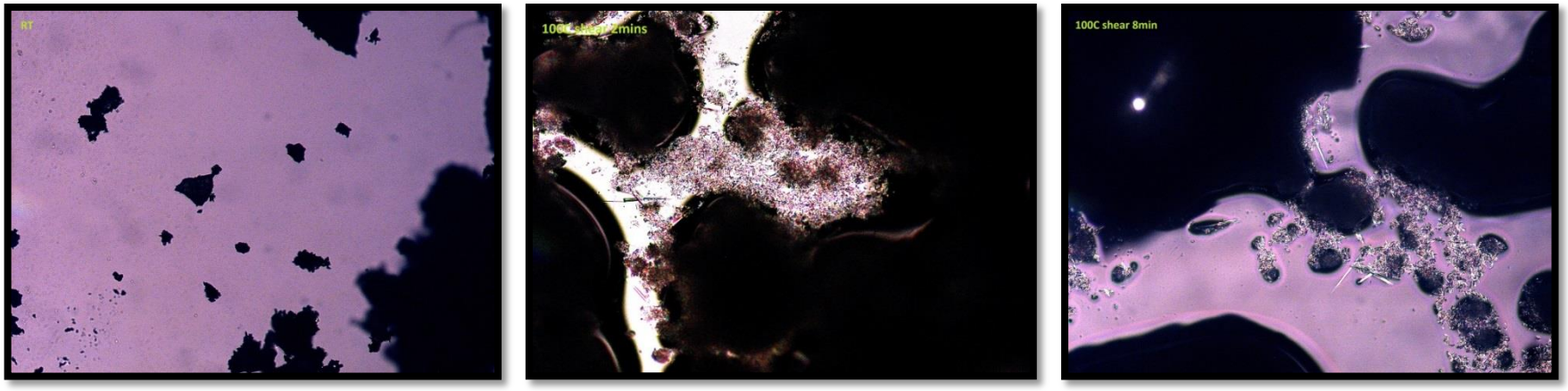

Figure A.10 Light microscopy images of 2:1 caffeine - maleic acid physical mixture shear cell run 5. Showing the starting material (Left), after 2 minutes of shear (Centre) and after 8 minutes of shear (Right).